UNIVERSITY OF SOUTHAMPTON

Temporal, spatial, spectral and polarisation characteristics of the SAR backscatter from regenerating tropical forests

Tatiana Mora Kuplich

A thesis submitted for the degree of Doctor of Philosophy

Department of Geography
Faculty of Science

December 2001

For Isabela and the setting of new priorities.

This thesis is the result of work done wholly while I was in registered postgraduate candidature at the University of Southampton.

Tatiana Mora Kuplich
December 2001

UNIVERSITY OF SOUTHAMPTON

ABSTRACT

FACULTY OF SCIENCE
GEOGRAPHY

Doctor of Philosophy

TEMPORAL, SPATIAL, SPECTRAL AND POLARISATION CHARACTERISTICS OF THE SAR BACKSCATTER FROM REGENERATING TROPICAL FORESTS

by Tatiana Mora Kuplich

The establishment of an accurate global carbon budget and the consequent ability to understand and predict future environmental change is dependent on knowing the strength of terrestrial sinks and sources of carbon. Regenerating tropical forests are one of the major terrestrial carbon sinks as they are found growing quickly and are sequestering carbon from the atmosphere. Total forest biomass (which includes above and below ground living mass of plants and litter) is a measure of terrestrial vegetation carbon content. It follows that to determine the strength of terrestrial carbon sinks we require information on the location, extent, biomass and biomass change of regenerating tropical forests. Near-constant cloud cover over the tropics and an insensitivity to biomass change at relatively low levels of biomass has limited the use of optical imagery but not Synthetic Aperture Radar (SAR) imagery for the provision of such information. The biophysical properties of regenerating tropical forests are related to the temporal, spatial, spectral and polarisation characteristics of SAR backscatter (σ°) and this formed the framework for this thesis. The objectives were to (i) detect biomass accumulation using the temporal characteristics of σ°, (ii) use the spatial characteristics of σ° (texture) to increase the strength of the σ°/biomass relationship and (iii) use the spectral and polarisation characteristics of σ° to classify a surrogate for biomass in regenerating tropical forests (optical Landsat TM data were also included to widen the spectral analysis).

Although no biomass change was detectable using temporal σ°, a seasonal pattern in σ° for young regenerating forest was detected, as a result of changing water content in both vegetation and soil. The influence of recent rainfall was confirmed to be an important source of variation in σ°, suggesting the use of SAR data from the dry season only.

Using simulated data, seven texture measures showed potential for strengthening the σ°/biomass relationship. However, when applied to real SAR data only GLCM (Grey Level Co-occurrence Matrix) derived contrast strengthened the σ°/biomass relationship. The addition of GLCM-derived contrast to σ° potentially increases the accuracy of biomass estimation and mapping.

Neural networks can be used for the classification of land cover in tropical forest regions. Classification accuracy of around 80% was achieved using combined multiwavelength and multipolarisation SAR and Landsat TM bands for 4 land cover classes (pasture, mature forest, 0-5 years old regenerating forests and 6-18 years old regenerating forest).

These results demonstrated that multiwavelength and multipolarisation SAR data could provide information on the location, and extent of regenerating tropical forests. However an increase in the accuracy of biomass estimation relies on the optimal use of additional information that resides within the spatial, spectral and polarisation domains of SAR data.

LIST OF CONTENTS

LIST OF FIGURES

LIST OF TABLES

ACKNOWLEDGEMENTS

Although a PhD is an extremely lonely job, it would never be possible without the sharing of knowledge, data, thoughts and ideas with many people. Always first in my heart and mind come my husband Ronald Buss de Souza, who faced the challenge without fear and believed in me above all. Without him and my daughter Isabela this thesis would not exist.

This research was funded by CAPES (Fundação Coordenação de Aperfeiçoamento de Pessoal de Nível Superior) from Brazil. I am deeply grateful for the opportunity and assistance they have given to me. I thank NASDA (National Space Development Agency of Japan) for providing SAR data as part of the Global Rain Forest Mapping (GRFM) project, particularly Masanobu Shimada and Osamu Tanaka. The ground data used was from the British Terrestrial Initiative in Global Environmental Research (TIGER) project, funded by the Natural Environment Research Council's (NERC). I thank Richard Lucas and team for collecting data at Manaus study area and Adrian Luckman and team (which luckily I made part of) for collecting data at Tapajós study area.

My eternal gratitude for all help, support, ideas and encouragement goes to Paul Curran, always a source of inspiration and knowledge. Peter Atkinson deserves a special thanks for helping me with spatial tasks and other puzzles. I thank also Giles Foody for helping to understand Manaus data and my first attempt at running a neural network. I thank Ted Milton for support and the use of EPFS facilities. I am grateful for Charlie Kerr and Jim Milne for computing assistance and the staff of the Cartographic Unit for their help and friendship. Adrian Luckman (University of Wales, Swansea), Robert Green, Philip Bailey (Nobility Systems – Canada) and Lourdes Rico (Kew Gardens) also helped with data and ideas.

The Brazilian front, mainly represented by friends from INPE (Brazilian Institute for Space Research) was always ready to share views and data: Camilo Rennó, Corina Freitas, Luciano Dutra, Sidnei Sant'Anna, Evlyn Novo, Thelma Krug, Dalton Valeriano, Helena França, Sergio Donizeti Faria, Marisa da Motta, José Eduardo Mantovani, Lúbia Vinhas, João Roberto dos Santos, Lélio Walter, Getúlio Batista, Diógenes Alves, Yosio Shimabukuro and always Fernando Ii. Still INPE but from

Cachoeira Paulista: Luciano Ponzi Pezzi, José Antonio Marengo, Luiz Gonzaga and Alessandra Pereira. A big thanks for Alejandro Frery (UFPE - Recife), Lilian Eggers (PUC – Porto Alegre) and Regina R. Rodrigues (University of Rhode Island, US).

To friends who provided me joy and sometimes shared with Ronald and me the care of Isabela I am very grateful: Márcia Ide and Flávio Bergamaschi, Ana Lopez and Peter de Groot, Marisa da Motta and Luciano Ponzi Pezzi, Luciane Veeck and Antonio Caltabiano, Valeria Quaresma and Alex Bastos, Frideriki and Tom Papenbrock, Roberta and Erik Muxagata. Fernando and Cacilda II, Silvia Lucato, Oliver Hadeler, Luca Centurioni and Cristina Belpassi, Gilberto Fillmann, Elisa Fernandes, Alexandre Cabral, Dhesiree e Rodrigo Maggioni, Ana Paula and Hervé Teles, Philippe and Liz Guyard, David Cromwell and Foske Twiest, Boris and Tamaris Kelly-Gerreyn, Marcos Salas and Tati Santander, Jaime Rojas and Claudia Haensel were also part of the "caring-net".

I thank my fellow Geography postgrads, past and present, as supportive partners of daily life, particularly Kate Delaney, Süha Berberoglu, Andrew Ford, Toby Wicks, Valeria Salvatori, Reno Choi, Eman Ghoneim, Paul Aplin, Chris Lloyd, Anjana Khatwa, Luciano Cau, Sarah Edwards, Gary Llewellyn, Matt Wilson, Richard Jeffries, Michael Riedmann, Isabel Sargent, Marco van de Wiel, Sally Priest and Marie Cribb.

The support, understanding and love of my sisters Nadia and Vanessa, grandad Arno and family in Porto Alegre were essential. My parents Sergio and Lettilia were always close to inspire me with love and protection.

CHAPTER ONE

Introduction

Regenerating tropical forests are a major terrestrial sink of atmospheric carbon dioxide (CO_2) that can be located, mapped and monitored using Synthetic Aperture Radar (SAR) data. In this thesis the temporal, spatial, spectral and polarisation characteristics of SAR backscatter were investigated for regenerating tropical forests in Brazilian Amazonia. This introductory chapter explains the rationale and objectives behind the research and gives a description of the thesis outline.

1.1. Global carbon budget

> *"Humans are altering the global environment, driving changes in crucial characteristics at rates largely unprecedented in the history of the Earth... CO_2 concentrations have varied widely over geological time, but current rates of change have not been matched" (Aber and Melillo 2001, p.533).*

Carbon (C) is a key element linked to the transfer of energy through ecosystems. Concentration of atmospheric CO_2 in many environments and situations controls the rates of photosynthesis and thus ecosystem productivity (Aber and Melillo 2001). The link between rising atmospheric CO_2 concentration and global climatic change is related to the role of CO_2 as a greenhouse gas (GHG) as it traps thermal radiation and reduces Earth-space release of energy (Royal Society 2001).

The establishment of an accurate global carbon budget and the consequent ability to predict future environmental change relies upon the identification and quantification of all sinks and sources of atmospheric CO_2 (Tremberth *et al.* 1996). This is because

the relationship between emissions of CO_2 and its atmospheric concentration is dependent upon the uptake and release of CO_2 from the ocean and terrestrial ecosystems (Schimel *et al.* 2001). The partition of atmospheric CO_2 uptake between oceans and land is made with increased confidence (Schimel *et al.* 2001).

The rise in atmospheric CO_2 concentration from approximately 280 parts per million (ppm) in 1880 to a current value of around 370 ppm was caused mainly by burning of fossil fuels but also by deforestation (IPCC 2001). The warming of the global mean surface temperature by 0.6° C over the 19th and 20th centuries has led to an international effort aimed at reducing anthropogenic emissions of CO_2 and other GHG. The 1997 Kyoto Protocol is the ultimate commitment of developed nations to reduce their emissions of GHG by 2008-2012 by 5.2% below their emissions in 1990 (Royal Society 2001). At the present, the ratification of the Kyoto protocol is very close and delegates from more than 160 countries agreed an official rulebook in the 10th November meeting in Marrakech, Morocco (Schiermeier 2001). The ratification of the protocol is still dependent on the leading role played by the United States of America as the world's largest CO_2 emitter, which refuses to ratify the protocol. The Kyoto Protocol is expected to come into force before the next World Summit on Sustainable development, to be held in September 2002 in South Africa (Schiermeier 2001).

Estimates of global carbon budgets with natural and human-induced fluxes for the 1990s are shown in figure 1.1. Uncertainties associated with these budgets are related to differences in measurement methods. 1 PgC = 1 Gt of C (1 Gt = 1 million tonnes) (Royal Society 2001).

Terrestrial ecosystems are currently acting as a major sink for carbon despite large releases of carbon due to fossil fuel combustion and deforestation (figure 1.1). The estimates in figure 1.1 show a land carbon sink of 3.2 PgC, although the partition of fluxes between natural and human-induced as well as between sinks in tropical and temperate regions is uncertain (IPCC 2001, Schimel *et al.* 2001). The balance of the terrestrial carbon cycle requires detailed information on land use change and ecosystem processes, particularly for the tropics (Schimel *et al.* 2001)

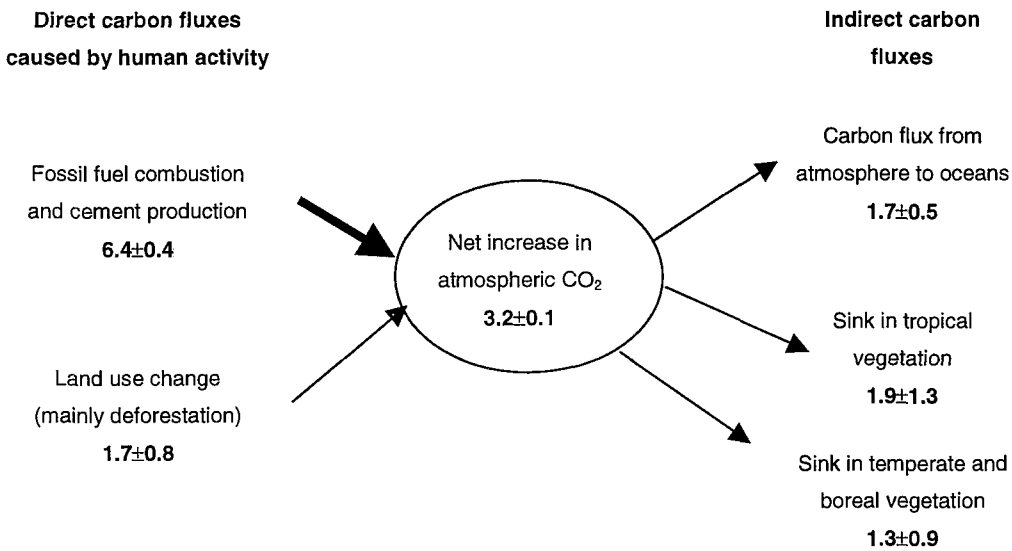

Figure 1.1: Estimate of the carbon budget in the 1990s (in $PgCyr^{-1}$). Error bars denote ±1 standard deviation (Royal Society 2001).

The role of land carbon sinks was highlighted by the Kyoto Protocol. Each country has to meet net emission targets to mitigate the warming threat and climate change. However, the gross carbon release can be reduced by a limited amount by taking into account forestry activities such as 'reforestation, afforestation and deforestation' carried out since 1990 (Grace and Malhi 1999). The operation of these land carbon sinks into the future, however, is likely to diminish as a result of, among other factors, forest maturation (Schimel *et al.* 2001).

1.2. Tropical forests and the carbon budget

Terrestrial carbon stocks are partitioned between vegetation (550 ± 100 PgC) and soils (1750 ± 250 PgC) and together they contain three times as much carbon as the atmosphere (which contains around 760 PgC) (Royal Society 2001). Figure 1.2 shows the relative proportions of carbon in different terrestrial ecosystems and the clear dominance of forests as the main carbon pools.

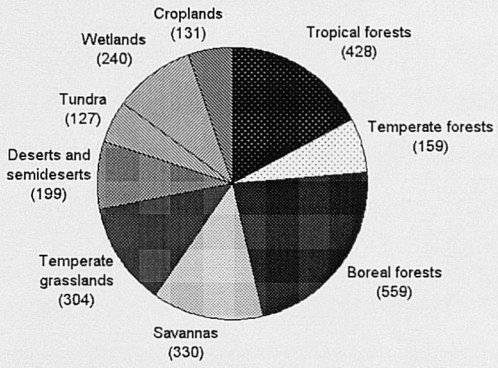

Figure 1.2. Estimate of relative proportions of carbon in terrestrial ecosystems (carbon stock x total area of ecosystem). To note forests as the main carbon pools. In brackets are estimates of total carbon stock in PgC (Royal Society 2001).

Forests cover around 31% of the Earth's land surface and of these around 42% are in low latitudes with more than half in South America. Forests contain around 80% of all aboveground carbon and around 40% of all belowground (soil, litter and roots) carbon (Dixon *et al.* 1994).

The carbon content of forests can be derived directly from forest biomass estimates and this enables quantification of the amount of carbon released to the atmosphere (Brown and Lugo 1992). Forest biomass is defined as the total aboveground and belowground living mass of all vegetation components (as well as the dead mass of litter) and so integrates measures of volume and wood density (Brown and Lugo 1990, 1992).

Tropical forests are a major terrestrial carbon sink. There is much uncertainty and controversy about (i) the amount of carbon they currently hold (following different estimation methods and a poor global data base) and (ii) the balance in space and time between their joint roles as sources/sinks of carbon (Lugo and Brown 1992, Grace and Malhi 1999, Schimel *et al.* 2001). Nevertheless, climatic modelling experiments have shown evidence of climatic change following replacement of tropical forest by pasture in Brazilian Amazonia (Shukla *et al.* 1990, Gash *et al.* 1996).

Tropical forest deforestation is responsible for the release of carbon to the atmosphere via burning of the vegetation, decay of biomass and from soils (Fearnside 2000). The timing of carbon release depends on the type of land use change. If burning follows deforestation, CO_2 will be released immediately, while decay of remaining vegetation and organic matter in soils can be a source of CO_2 for many years (Detwiller and Hall 1988).

Brazil contained, in 1990, around 41% of all remaining areas of tropical forest in the world (Fearnside 2000). Agriculture, ranching, hydroelectric dams and selective logging (building of roads and forest clearance) are the main reasons for deforestation in that country. The dynamics of the deforestation in Brazil will be discussed in chapter 4. Annual deforestation rates in Brazilian Amazonia have been estimated by the Brazilian Institute for Space Research (INPE) since 1988 using Landsat MSS (Multi Spectral Scanner) and TM (Thematic Mapper) images (table 1.1) as part of the Deforestation Project (PRODES).

Table 1.1. Mean rate of gross deforestation in Brazilian Amazonia ($km^2\ y^{-1}$) from 1978 to 2000 (INPE 2000).

78/88	88/89	89/90	90/91	91/92	92/94	94/95	95/96	96/97	97/98	98/99	99/00*
21130	17860	13810	11130	13786	14896	29059	18161	13227	17383	17259	19836

*The mean rate for 1999/2000 was based on linear projection of data from 49 Landsat TM scenes.

Estimating global carbon budgets requires detailed information about the net tropical forest flux, including deforestation rates and carbon sequestration (as a result of forest regrowth or growth by CO_2 fertilisation) (Melillo *et al.* 1996).

Regenerating tropical forests in Brazil increased in extent during the 1970s and 1980s and are known to be sequestering CO_2 from the atmosphere (Curran *et al.* 1995, Houghton *et al.* 2000). Regenerating tropical forests are mainly a result of farming practices such as slash-and-burn of forest, shifting cultivation or pasture creation and eventually abandonment followed by forest regrowth (Fearnside 2000).

To determine the total strength of terrestrial carbon sinks in Brazilian Amazonia information on the location, extent, biomass and biomass change of regenerating tropical forests is required.

1.3. The need for remotely sensed information about regenerating tropical forests

Remote sensing is a tool used to collect information on and better understand the environment (Curran *et al.* 1998). Information from remote sensing can be used to map, estimate and monitor environmental variables (e.g. vegetation biomass, leaf area index - LAI) from the ecosystems they represent (e.g. tropical forest). Information on the location, extent, biomass and biomass change of regenerating tropical forests is needed for the global carbon budget (Curran and Foody 1994) and also to help in the struggle to maintain the biodiversity of the remaining forested areas (Viana 1998).

Depending on the region, regenerating forests at different successional stages and biomass levels cover between around 6% to 60% of the deforested areas in Brazilian Amazonia (Batista 1999). Remote sensing data in optical wavelengths has been used for the assessment and quantification of deforestation in Amazonia (e.g. INPE 2000) and for the characterisation of regenerating forest stages (Lucas *et al.* 1993, Curran and Foody 1994, Foody *et al.* 1996, Lucas *et al.* 2000). The major limitations of the use of optical data for regenerating tropical forest studies are (i) near-constant tropical cloud cover and (ii) an insensitivity of reflectance to biomass change at relatively low levels of biomass.

The use of synthetic aperture radar (SAR) data can overcome these limitations as SAR data are independent of cloud cover and there is a known positive relationship between SAR backscatter and biomass up to relatively high levels of biomass.

The framework for this research is based upon the influence of biophysical properties of regenerating tropical forests on the temporal, spatial, spectral and polarisation characteristics of SAR backscatter (σ), represented as follows:

$$\sigma = f(t, x, \lambda, p) \qquad [1.1]$$

where t refers to the temporal, x to the spatial, λ to the spectral and p to the polarisation characteristics of SAR backscatter.

1. 4. Research aim and thesis objectives

Taking the known positive relationship between SAR backscatter and forest biomass as a starting point, the aim of this research was to:

- Understand the information content of the temporal, spatial, spectral and polarisation domain of SAR backscatter as a precursor to determining the accuracy with which SAR backscatter can be used to derive biophysical properties of regenerating tropical forests.

Inventory data from two study areas were used. These study areas were located close to Manaus City, Amazonas State and Tapajós National Forest, Pará State, Brazil, where forest inventories had already been conducted as part of the Terrestrial Initiative in Global Environmental Research (TIGER) programme of the Natural Environment Research Council (NERC). These forest inventory data were used to describe, among other things, biomass and floristic composition of the regenerating forest plots and to relate them to SAR backscatter. The JERS-1 SAR dataset were made available to this research as part of the Global Rain Forest Mapping (GRFM) project of NASDA, the Japanese Space Agency.

Within the framework discussed in section 1.3 the three specific objectives of this thesis were:

- Detect biomass accumulation using the temporal characteristics of SAR backscatter.
- Use the spatial characteristics of SAR backscatter to increase the strength of the backscatter/biomass relationship.
- Use the spectral and polarisation characteristics of SAR backscatter to classify a surrogate for biomass of regenerating tropical forests. (Optical data were also included to widen the spectral analysis.)

The first and second objectives were achieved by relating temporal and spatial (texture) SAR data of both study areas to regenerating tropical forest biomass. The third objective was achieved by classifying regenerating forest stages in multiwavelength and multipolarisation SAR data of the Manaus study area.

1.5. Thesis outline

The outline of the thesis is illustrated in figure 1.3. In chapters 1, 2 and 3 the rationale behind the research and basic information that underpins the three objectives are covered. Chapter 2 and 3 present a review of radar fundamentals and the use of radar data for regenerating tropical forests studies, respectively, establishing the theoretical framework for the research. Chapter 4 presents the study areas along with general information about Brazilian Amazonia. The collection of forest inventory data and the forest regrowth map used as the ground data for chapter 7 are also described in chapter 4. The regenerating tropical forests are studied using temporal, spatial, spectral and polarisation characteristics of SAR backscatter in chapters 5, 6 and 7, respectively. Research findings are discussed in each chapter. Finally, the conclusions for this research are drawn in chapter 8.

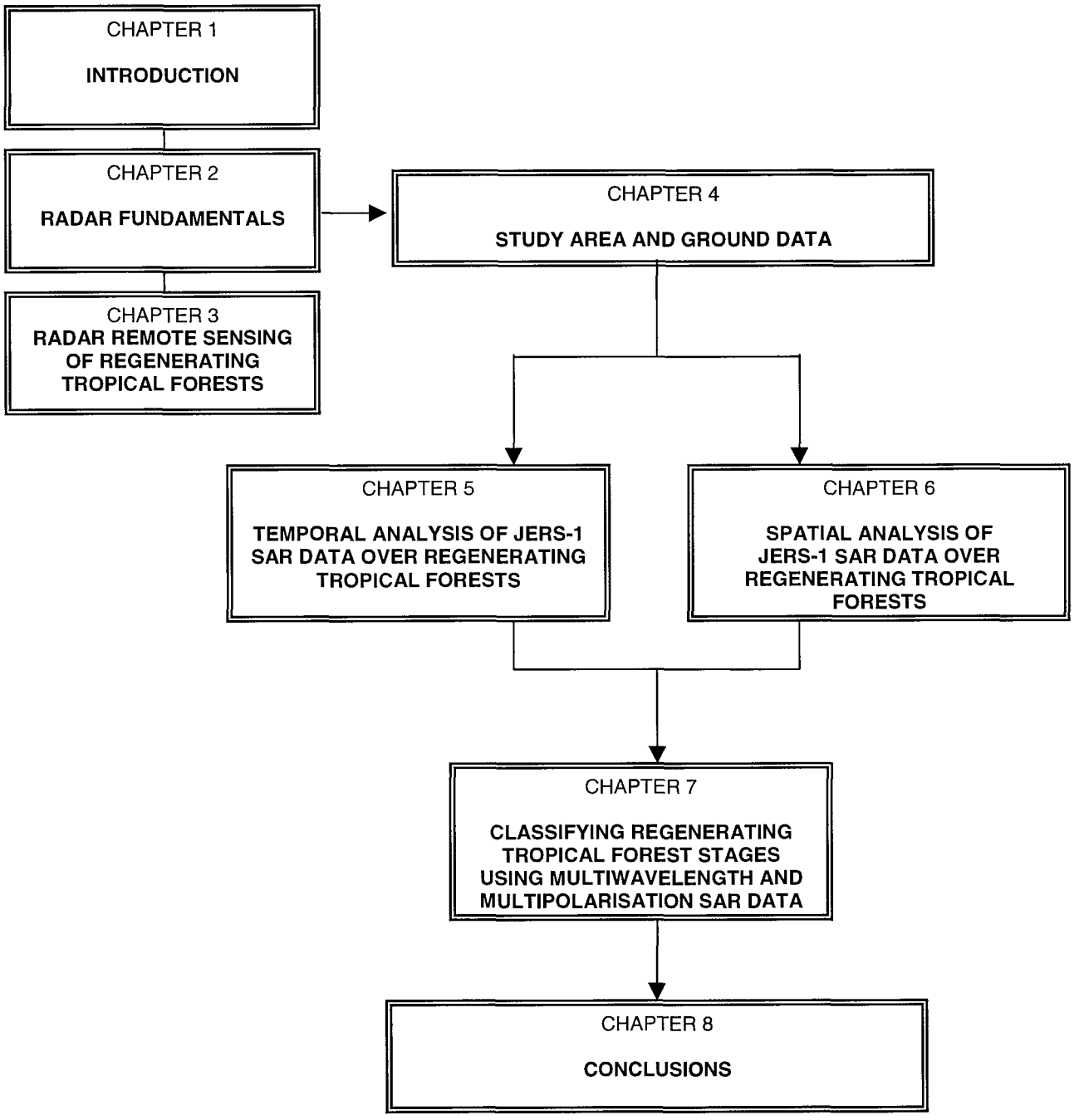

Figure 1.3. Structure of thesis by chapter.

CHAPTER TWO

Radar fundamentals

RADAR, an acronym for "Radio Detection And Ranging", is an active device that transmits and receives electromagnetic energy in microwave wavelengths. The majority of current operational imaging radars use wavelengths between 1 mm to 1 m. Two distinctive features characterise microwave wavelengths from a remote sensing point of view: (i) microwaves are capable of penetrating the atmosphere under virtually all conditions, and (ii) microwave reflections or emissions from surface materials bear no direct relationship to reflectance in the visible or thermal portions of the spectrum (Lillesand and Kiefer 2000).

The launch of orbital civil radar systems since the 1970s made possible the acquisition of a unique view of natural resources over the Earth's surface. Although much progress has been made in the fields of both active and passive microwave remote sensing, they are still important research areas for the environmental sciences, engineering and the military (Lewis and Henderson 1998).

This chapter introduces some of the concepts of imaging radar remote sensing considered important for understanding their applications to the study of regenerating tropical forests.

2.1. Radar operation

Radar remote sensing of the land is made possible by the high atmospheric transmission in the microwave region of the electromagnetic spectrum (figure 2.1).

As an active sensor, a radar transmits pulses of energy that illuminates the terrain. It then records the response returned from the objects or targets on the terrain towards the sensor (Lewis and Henderson 1998). In a radar system, a transmitter sends out an amplified pulse of energy (a signal), set by a frequency synthesiser and made a pulse by a modulator. The pulse is sent to the antenna via a transmit/receive switch, which also converts the antenna to receive the pulses back (for monostatic radars). When the pulse is received back (called an echo) after being reflected from the targets, it is amplified, converted to an intermediate frequency, detected and processed to generate the final radar product (Kingsley and Quegan 1992).

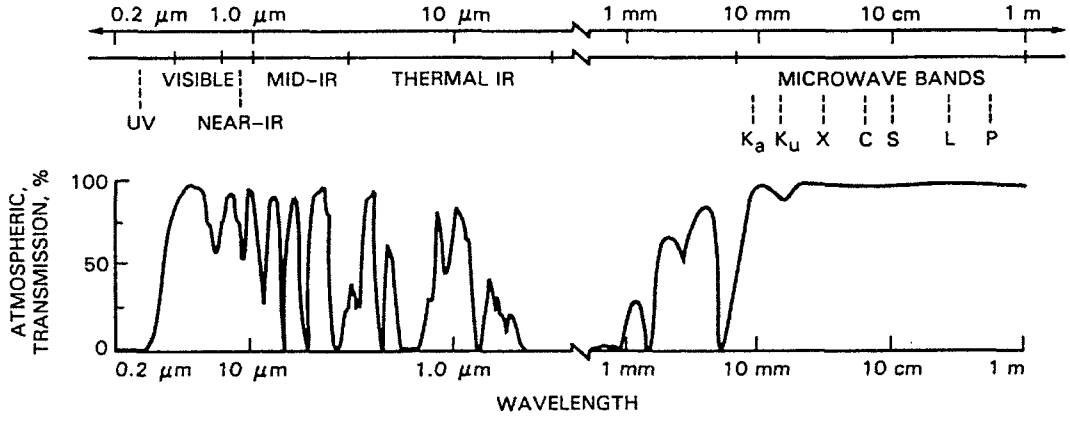

Figure 2.1. Electromagnetic spectrum showing atmospheric windows in the visible, near, middle and thermal infrared and the microwave regions (Lewis and Henderson 1998).

The signal strength and the time delay between transmission and reception are the main elements of the radar signal (Trevett 1986). The principles of image formation are assured by the motion of an aircraft or satellite and the recording of these incoming signals.

The differences between the many imaging radars used in remote sensing are due primarily to the antenna which determines the spatial resolution in the azimuth (or travel) direction (Raney 1998). Imaging radars can be divided in two main categories, depending on the imaging technique used: Real Aperture Radar (RAR) also called Side Looking Airborne Radar (SLAR) and the Synthetic Aperture Radar (SAR). For both radar types the side-looking imaging geometry applies. The radar antenna illuminates a surface strip (footprint) to one side of the nadir track.

The area continuously imaged from the radar beam is called the swath and can be divided into near range (the part nearer to the ground track) and far range. Each transmitted wave front hits the target surface at near range and sweeps across the swath to far range. The spatial resolution of a radar system can be defined as the minimum distance between two targets for them to produce separate backscatter or to be resolved as individual features (Lewis and Anderson 1998). For imaging radars the spatial resolution is defined according to the flight direction. Azimuth spatial resolution is parallel to the flight direction and range spatial resolution is perpendicular to the flight direction.

Real Aperture Radars transmit pulses from a side-looking antenna and are airborne rather than satellite borne. The azimuth spatial resolution is dependent on the antenna footprint and is linearly proportional to the distance between the sensor and the surface. For high spatial resolution requirements in spaceborne platforms this technique is not viable because the antenna would need to be impractically large (Elachi 1988).

The synthetic aperture imaging technique in a SAR uses the movement of the sensor to simulate a much larger antenna than its actual size. A single antenna moving along the flight line acquires the data and the effect is similar to using an array of antennas. The target is illuminated several times from different locations generating numerous echoes that are recorded coherently (i.e., amplitude and phase as a function of time) and subsequently combined to synthesise a linear array. A higher spatial resolution is achieved independently of the distance between sensor and target and by a small antenna (Elachi 1988). SAR systems can be either airborne or spaceborne and are much more complex than the RAR systems.

2.2. System parameters

Interpreting radar data depends on an understanding of the interaction between system parameters and target characteristics. Both RAR and SAR systems have specific operational parameters which will influence the interaction between the pulses transmitted and the targets on the Earth's surface. System parameters are explained in the next section.

2.2.1. Wavelength

The electromagnetic spectrum (figure 2.1) illustrates the wide range of microwave wavelengths/frequencies in comparison to visible wavelengths/frequencies. Most of imaging radars operate in a single band, defined either by its frequency (preferred by engineers) or wavelength (preferred by geoscientists) (Lewis and Anderson 1998). The main reason for a single band operation is the limiting power supply, as radar systems rely upon their own energy source. The antenna design must be specific for transmitting and receiving a defined wavelength, which can be a limitation for operation in multi-band mode. Short wavebands or high frequency transmission require a large amount of power, precluding their use in spaceborne systems (Trevett 1986). Table 2.1 lists some of the common radar bands along with the equation that relates wavelength and frequency.

Table 2.1: Common wavelength/frequency bands for radar systems (Modified from Trevett 1986).

Radar band	Wavelength - λ (cm)	Frequency - f (MHz)
P	136-77	220-390
UHF	100-30	300-1000
L	30-15	1000-2000
S	15-7.5	2000-4000
C	7.5-3.75	4000-8000
X	3.75-2.40	8000-12500
Ku	2.40-1.67	12500-18000
K	1.67-1.18	18000-26500
Ka	1.18-0.75	26500-40000

$$\lambda(cm) = \frac{c}{f} = \frac{30000}{f(MHz)} = \frac{30}{f(GHz)}$$

1 Hertz = 1 cycle s^{-1}
1 MegaHertz = 10^6 Hertz
1 GigaHertz = 10^9 Hertz

The interaction of microwaves and targets on Earth's land surface is dependent on the wavelength used. Penetration depth increases with the wavelength (Elachi 1988). The roughness of a surface on a SAR image is also influenced by the wavelength used.

2.2.2. Polarisation

Microwaves are transversal waves, i.e., in the direction of propagation the electric and magnetic fields are mutually orthogonal. In addition, the electric field vector defines the polarisation component. Linear (or planar) polarisation refers to the vibration of the electric field vector in a parallel direction to the propagating wave. There are also elliptical and circular polarisations, characterised by the rotation of the electric field vector in corresponding fashions and these in turn define different polarisation planes (Lewis and Anderson 1988).

Most of the radar systems use linear polarisation, operating using vertically or horizontally polarised microwave radiation. As the microwaves are transmitted and received, the polarisation is defined for the outgoing and incoming radiation and the antenna design must account for that. Table 2.2 lists the four polarisation types.

Table 2.2: Linear polarisation options (Lewis and Anderson 1998).

Like-polarised
HH Horizontal transmit; Horizontal receive
VV Vertical transmit; Vertical receive
Cross-polarised
VH Vertical transmit; Horizontal receive
HV Horizontal transmit; Vertical receive

Targets on the Earth's surface scatter microwave radiation differently depending on the polarisation of the wave transmitted. If the plane of polarisation of the transmitted wave is parallel to the main line of polarisation of the target being sensed the like-polarised backscatter is stronger. For instance, a wheat field has a dominant vertical

component, so the interaction and backscatter with a VV polarised wave is much stronger than that with a HH wave (Lewis and Anderson 1998).

The cross-polarisation or depolarisation of the transmitted wave is also a function of the amount of multiple volumetric scattering taking place at the targets. SAR systems with cross-polarised receiving capabilities can provide additional information for the image interpretation and understanding the target/wave interaction (Lewis and Anderson 1998).

2.2.3. Incident angle

The incident angle (θ) is a major factor influencing the radar backscatter and the appearance of the targets in the images. This angle is defined between the radar pulse and a line perpendicular to the Earth's land surface. Figure 2.2 illustrates the system and local incident angles. In a flat surface, θ is the complement of the depression angle (γ) (Jensen 2000).

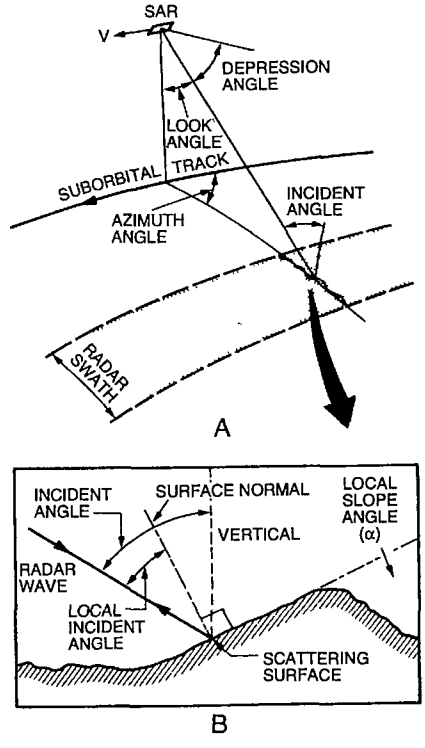

Figure 2.2. Schematic diagrams of system (A) and local (B) incident angles (Lewis and Anderson 1998).

In general, smaller θ results in more backscatter, although for very rough surfaces the backscatter is independent of θ. Surface roughness, as discussed later in this chapter, changes as a function of the local incident angle (Lewis and Anderson 1998). This parameter can be used to emphasise the roughness of particular features on the Earth's surface.

2.3. Target characteristics

Radar backscatter is the result of the interaction between system parameters and the characteristics of the target, such as geometry (and associated roughness) and moisture content (and associated dielectric constant). First the backscattering coefficient is introduced, as it is a quantitative measure of backscatter intensity from a specific region on the Earth's land surface. Surface roughness and electrical characteristics of the targets are examined next.

2.3.1. Backscatter coefficient

The targets scatter the energy transmitted by the radar in all directions. The energy scattered in the backward direction is what the radar records. The intensity of each pixel in a radar image is proportional to the ratio between the density of energy scattered and the density of energy transmitted from the targets in the Earth's land surface (Waring *et al.* 1995).

The energy backscattered is related to the variable to referred as radar cross-section (σ), and is the amount of transmitted power absorbed and reflected by the target. The backscatter coefficient (σ°) is the amount of radar cross-section per unit area (A) on the ground (Jensen 2000). σ° is a characteristic of the scattering behaviour of all targets within a pixel and because it varies over several orders of magnitude is expressed as a logarithm with decibel units (Waring *et al.* 1995).

Backscatter coefficient is a function of wavelength, polarisation and incidence angle, as well as target characteristics such as roughness, geometry and dielectric

properties. The targets will be distinguishable in radar images if their backscatter components are different and the radar spatial resolution is adequate to discriminate between targets (Trevett 1986).

The backscatter is measured as a complex number, which contains information about the amplitude (easily converted to σ° by specific equations) and the phase of the backscatter (Baltzer 2001). For SAR applications other than interferometry and polarimetry, however, the phase carries no useful information and can be discarded (Oliver and Quegan 1998). The information that remains when the phase is discarded is related to the amplitude of the backscatter. After linear detection and processing, amplitude SAR data are converted to an amplitude (or magnitude) image. After square-law detection and processing, amplitude SAR data are converted to an intensity (or power) image (Kingsley and Quegan 1992).

All SAR images contain speckle, an interference phenomenon produced between backscatter coming from many random targets within a pixel. The speckle represents true electromagnetic scattering and influences the interpretation of SAR images (Oliver and Quegan 1998). In chapter 6 speckle will be discussed as part of spatial properties of backscatter.

2.3.2. Surface roughness

Surface roughness is one of the important target characteristics that influences the strength of backscatter and must be considered in relation to the scale at which the target is being observed. Three scales are often described: microscale roughness, mesoscale roughness and macroscale roughness, associated respectively with image tone, image texture and topographic effects (Lewis and Henderson 1998).

Microscale roughness refers to the scale of small components (targets) within an individual pixel such as leaves and branches of trees or stones. Microscale is measured in centimetres and is a function of wavelength, the depression angle and the height of target or component of target. The modified Rayleigh criteria can be used to express this relationship (Jensen 2000):

$$h < \frac{\lambda}{25 \sin \gamma} \qquad [2.1]$$

where h is the local height of target or component of target, λ is the wavelength in cm and γ is the depression angle in degrees. Computing h using this criteria for λ = 3 cm (X band) and γ= 45°, results in h < 0.17 cm. If the local height of target is < 0.17 cm the target's surface is considered smooth and a near-perfect specular reflector. Therefore it will produce a dark tone in the image as no radiation will be backscattered to the sensor.

Table 2.3 shows the modified Rayleigh criteria for radars with different parameters. Owing to intrinsic variations of depression angle from far range to near range, the image tone will also vary across the image (Lewis and Henderson 1998).

Table 2.3: Surface roughness categories and the local height (h) above which the surface appears rough on three different SAR systems (Jensen 2000). This is calculated using a modified Rayleigh criteria.

Surface roughness category	Aircraft K_a band λ = 0.86 cm, γ= 45°	Aircraft X band λ = 3 cm, γ= 45°	Seasat L band λ = 23.5 cm, γ= 70°
Smooth, cm	h < 0.048	h < 0.17	h < 1
Intermediate, cm	h = 0.048 to 0.276	h = 0.17 to 0.96	h = 1 to 5.68
Rough, cm	h > 0.276	h > 0.96	h > 5.68

Mesoscale surface roughness is related to image texture and is a function of the characteristics of numerous pixels covering a single target, for instance, an entire forest canopy. With the same λ and γ, a forest canopy will present a coarser roughness (texture) than a grassland (Jensen 2000). SAR image texture will be discussed in detail in chapter 6.

Macroscale surface roughness is influenced by shadow caused by topographic slope and the aspect of the terrain. The macro-texture patterns created by shadow are often many times larger than an individual pixel (Lewis and Henderson 1998).

Particular types of strong scattering occur when two or three smooth surfaces are adjacent, causing double or triple reflection. In this case the surfaces are known as dihedral or trihedral corner reflectors (Trevett 1986).

2.3.3. Electrical characteristics

The electrical characteristics of targets also determine the intensity of backscatter. The complex dielectric constant is a measure of the electrical characteristics of objects, indicating the reflectivity and conductivity of various materials (Lillesand and Kiefer 2000). The moisture content within materials has a direct influence on the dielectric constant and reflectivity. The more liquid water within a material the more reflectivity/backscatter is produced (Waring *et al.* 1995)

Most materials have a dielectric constant ranging from 3 to 8 when dry, while water has a dielectric constant of around 80. Forest canopies are excellent reflectors because of the leaves high moisture content, while dry soils absorb the radar signal and produce very low (or no) backscatter (Jensen 2000).

2.4. SAR images characteristics

SAR images are configured in either slant range or ground range format. Slant range is the direct distance from the antenna to an object on the ground, measured using the time delay from transmission of the signal to the reception of its echo (Raney 1998). The spacing between return signals on slant range imagery is directly proportional to the time interval between echoes from adjacent terrain features. The spacing between pixels on ground range imagery is approximately proportional to the horizontal ground distance between terrain features (Lillesand and Kiefer 2000). In this latter case, a correction at each data point for local terrain slope and elevation is required.

Slant range data are the natural result of radar range measurements. Because of the side-looking geometry, radar images inherently contain geometric distortions, such as (i) *layover* or the reverse ordering of surface elements on the radar image as a

result of the tops of objects or slopes being imaged before their bases (most severe on the near range); (ii) *shadow* caused by a slope away from the radar illumination with an angle that is steeper than the radar depression angle and (iii) *foreshortening*, that is the effect by which foreslopes appear to be compressed (Trevett 1986).

In general, images acquired at small incident angles (less than 30°) emphasise variations in surface slope, and geometric distortions due to layover and foreshortening in mountainous regions can be severe. Images with large incident angles have reduced geometric distortion and emphasise variations in surface roughness, although radar shadows increase (Lillesand and Kiefer 2000).

2.5. A new trend: SAR interferometry

SAR interferometry is a technique that uses information on phase derived by recording the phase difference between two SAR images acquired from slightly different sensor positions (Wegmüller and Werner 1995). Different sensor positions, called the baseline, can be achieved by a temporal shift (repeat-pass interferometry) or spatial shift (single-pass interferometry) (Baltzer 2001). The phases of the backscatter from the two positions interfere in a characteristic pattern and are sensitive to change in the scattering elements of targets. The phase difference between the two positions indicates the average three-dimensional position of the scattering elements (Baltzer 2001). The phase difference, under certain conditions, allows the height of scatterers to be inferred and a Digital Elevation Model (DEM) can be constructed (Oliver and Quegan 1998).

The interferometric coherence/correlation is a measure of the phase properties of SAR image pairs and indicates displacement and change of the scattering elements within the scene (Wegmüller and Werner 1995). It also can be seen as the accuracy in the estimation of the interferometric phase: more accurate phase estimates means less phase interference and change. Coherence decreases with increasing time delay and temporal changes in the targets. For forested areas, coherence diminishes with increase in vegetation density, as the volumetric scattering increases with movement (wind) and forest growth (Luckman *et al.* 2000).

Interferometric data have been used recently to map water level changes in the Amazon River Basin (Alsdorf *et al.* 2000). In addition, interferometric data have been used to derive topographic maps and estimate forest height (Wegmüller and Werner 1995). As tree biomass and age are a function of tree height, interferometric coherence has been related to tropical forest biomass and age of regenerating tropical forest plots (Luckman *et al.* 2000).

SAR interferometry can provide information on the three-dimensional structure of vegetation and therefore support estimates of forest biophysical variables and forest mapping and monitoring, including deforestation assessment.

2.6. Available and future SAR systems

The SAR data used in this thesis come primarily from the SAR onboard the Japanese Earth Resources Satellite JERS-1, launched in February 1992 and operational until October 1998. More detailed information about JERS-1 characteristics and parameters will be given in chapter 5, along with the analysis of a temporal series of JERS-1 SAR data. The Spaceborne Imaging Radar – C/X band Synthetic Aperture Radar (SIR-C/XSAR) onboard the U.S. Space Shuttle Endeavour that flew in 1994 provided data for the spectral analysis performed in chapter 7 and details about these sensors will be given there. This section gives some information about the satellite systems planned for launch in the near future, such as ASAR on Envisat-1, SAR on Radarsat-2 and PALSAR on ALOS.

In January 2002, the European Space Agency will launch Envisat, a polar-orbiting Earth observation satellite, carrying an Advanced Synthetic Aperture Radar (ASAR). The ASAR sensor has been designed to provide continuity to the ERS SAR, but also to extend the range of measurements through exploitation of its various operating modes. These modes will enable varied capability in terms of swath width (58 to 405 km), range of incidence angles (from 14° to 45°), spatial resolution (30 to 1000 m) and polarisation (HH, VV, VH and HV) (http://envisat.esa/int).

Radarsat-2 satellite is scheduled for launch in 2003. It will carry a C-band SAR with multi-polarisation capability able of imaging at swath widths ranging from 10 to 500

km, spatial resolutions from 3 to 100 m and incidence angles from 10° to 59° (http://www.space.gc.ca/csa_sectors/earth_environment/radarsat2/).

NASDA plans to launch an Advanced Land Observing Satellite (ALOS) in summer 2004, following the JERS-1 mission. Among the systems onboard this satellite is a Phased Array L-band Synthetic Aperture Radar (PALSAR) system. PALSAR will be multi-polarised and include look angles ranging from 18° to 55°. In its fine spatial resolution mode, PALSAR will use an HH or VV single polarisation, although a dual polarisation of HH and HV or VV and VH can be used. Range spatial resolution will be 10 m for single polarisation operation and 20 m for dual polarisation mode (at a look angle of 35°) and an azimuth resolution of 10 to 20 m, depending on the number of looks. PALSAR will also have the ScanSAR mode, which will have a swath width of 250 to 350 km, with a spatial resolution of about 100 m in both azimuth and range directions, and a polarisation of either HH or VV (http://alos.nasda.go.jp).

Some characteristics of past, present and future spaceborne imaging radar systems are shown in table 2.4. Additional information on the systems can be found in the web sites cited above.

Table 2.4. Characteristics of spaceborne image SAR systems (modified from Lillesand and Kiefer 2000).

Satellite/sensor	Launch	Band	Polarisation	Spatial resolution (m)
Seasat/SAR	1978	L	HH	25
Shuttle/SIR-A	1981	L	HH	40
Shuttle/SIR-B	1984	L	HH	17-58
Almaz-1/SAR	1991	S	HH	10-30
ERS1/2/SAR	1991/95	C	VV	30
JERS-1/SAR	1992	L	HH	18
SIR-C/XSAR	1994	C-L-X	multi	15-45
Radarsat/SAR	1995	C	HH	8-100
Envisat/ASAR	2002	C	multi	30-1000
Radarsat-2/SAR	2003	C	multi	3-100
ALOS/PALSAR	2004	L	multi	10-100

Note: 1) The wide range of values of some parameters is because these systems all have several operating modes. Not all of the above values are available in every mode. 2) multi = multi-polarisation (HH, HV, VV, VH).

Besides reinforcing a global effort in increasing large-scale environmental research, these future satellites manifest the need for high quality SAR data. The SIR-C/X-SAR mission demonstrated the advantages of multi-parameter SAR systems in space. Although multi-band in a single SAR was not planned for the next orbital systems, the combination between data of different systems is common and means expanding the effective use of SAR data in scientific applications.

CHAPTER THREE

Radar remote sensing of regenerating tropical forests

The framework for the research presented in this thesis is the interaction of SAR backscatter, depending on its temporal, spatial, spectral and polarisation characteristics, with regenerating tropical forests. This chapter reviews the use of SAR images to estimate forest properties (such as biomass) and classify forest types (such as regenerating forests) within this framework.

This chapter outlines how SAR backscatter has been related successfully to forest biophysical variables and used for biomass estimation and classification, with emphasis on regenerating tropical forests.

3.1. Radar remote sensing of forests

Our current understanding of the interaction of microwave radiation with forest canopies has been obtained primarily from temperate and northern forest ecosystems (e.g. Sader 1987, Le Toan *et al.* 1992). Limited species diversity coupled with spatially and structurally homogeneous stands made the backscatter from these formations easier to understand and model, therefore, a great amount of research has been devoted to them (Leckie and Ranson 1998).

Although there are major differences between temperate, northern and tropical forests, the main findings of radar remote sensing of temperate and northern forests also apply to tropical forests.

Since the 1960s radar systems have been recognised as particularly useful for military applications in tropical regions (such as in Vietnam), where cloud cover is persistent. In the 1970s radar data were declassified and airborne high frequency radar systems were used for mapping natural resources at continental scales. For example, the Brazilian RADAM (Radar Amazon) Project, one of the largest accomplishments in resources surveys by SAR data (Azevedo 1971, Leckie and Ranson 1998). During 1980s and 1990s there was a significant growth in research focused on developing approaches for using SAR in ecosystem studies (Kasischke *et al.* 1997). This was due to the launching of many spaceborne SAR systems (such as the SAR onboard the Japanese Earth Resources Satellite (JERS-1) in 1992) and the increasing need to understand global environmental processes.

To date, the progress made in the study of SAR data from tropical forests has been in the assessment of the potential of radar sensors for the discrimination of land cover types. The ultimate aims being that of (i) monitoring tropical land cover change (Nezry *et al.* 1993, Saatchi *et al.* 1997, Grover *et al.* 1999, van der Sanden and Hoekman 1999) and (ii) mapping forest biomass (Luckman *et al.* 1997a, 1998). These aims are generally included in a broader context intended to assess the contribution of radar to global environmental monitoring and ecosystem modelling (Leckie and Ranson 1998).

3.1.3. Forest backscatter

The main components and scattering mechanisms of the total backscatter from forests comprise backscatter from (1) crown surface and volume, (2) trunks, (3) direct from the ground, (4) crown-ground scattering and (5) double-bounce scattering from trunk and ground (Leckie and Ranson 1998). Figure 3.1 shows these components and the interaction of the main wavelengths used in operational radar remote of forests. Le Toan *et al.* (1992) also included multiple scattering from the branches and canopy attenuated trunk-ground scattering as influencing the total forest backscatter.

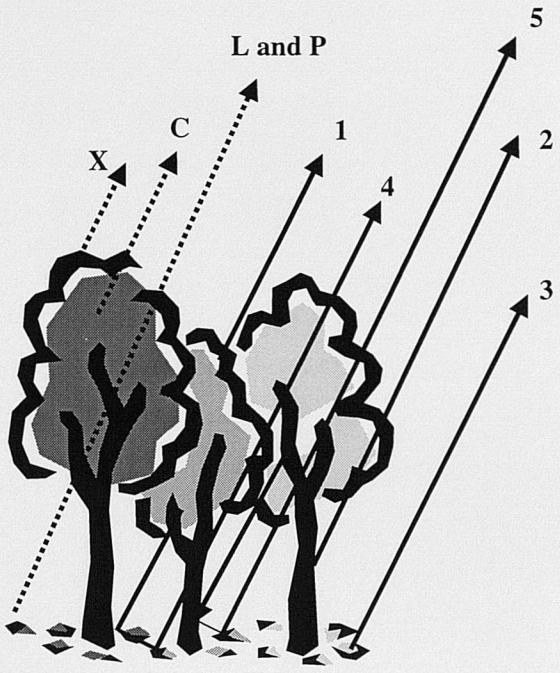

Figure 3.1. Main components and scattering mechanisms that influence the total backscatter from forests: (1) backscatter from crown surface and volume, (2) backscatter from trunks, (3) backscatter direct from the ground, (4) crown-ground scattering and (5) double-bounce scattering from trunk and ground (Leckie and Ranson 1998). Also, the interaction of the main wavelengths (bands X, C, L and P) used in SAR remote sensing is shown.

The magnitude of the scattering mechanisms and the importance of the different components are dependent on geometric factors (e.g., structural attributes of trees, canopy and soil surface roughness) and dielectric properties of vegetation and underlying surface (e.g., moisture content of vegetation and soil) (Dobson *et al.* 1995). Wavelength, polarisation and incidence angle of radiation control these scattering mechanisms (Leckie and Ranson 1998) and the final backscatter as a result of surface and/or volume scattering.

At X band, which is a short wavelength, the backscatter results mainly from the upper part of the canopy (Le Toan *et al.* 1992) and the leaves, twigs and small branches (Leckie and Ranson 1998). There is little penetration of the radiation into the canopy, therefore, volumetric scattering and soil contribution to the final backscatter are weak.

At C band, which is a intermediate wavelength, greater penetration of the radiation into the canopy enables further sources of scattering to be active and so there is some volumetric scattering. Typical sources of scattering at C band are secondary branches and leaves (Ranson and Sun 1994, Leckie and Ranson 1998). The penetration of crown thickness by the radiation is normally not exceeded (Le Toan *et al.* 1992).

At longer L and P band wavelengths, the penetration of the radiation into the canopy is deeper and components from the lower parts of the canopy are included in the scattering (Le Toan *et al.* 1992), as well as the major woody biomass components (trunks and branches) (Dobson *et al.* 1992). Trunk-ground and crown-ground interactions are important at these wavelengths (Leckie and Ranson 1998) and are mainly dependent on the canopy structure and openness. Foliage and small branches act as attenuators of the radiation at these wavelengths (Kasischke *et al.* 1997).

The incidence angle of the SAR sensor determines the amount of vegetation illuminated by the radar beam. The angular dependence is stronger for surface scattering mechanisms, when higher scattering is observed for small incidence angles (Leckie and Ranson 1998). Volumetric scattering mechanisms in the canopy will dominate for high incidence angles, as a large amount of the canopy is illuminated. For incidence angles close to nadir, depending on the wavelength and forest type, the ground will contribute to the scattering mechanisms.

The polarisation of the radiation determines the type of interaction with the forest components. Co-(or like) polarised radiation interact with structures with a similar orientation, so vertical stalks will interact strongly with VV (Vertical transmit and receive) polarisation. Horizontal branches or the soil surface interact strongly with HH (Horizontal transmit and receive) polarisation. HH can also be a result of trunk-ground scattering interactions (Dobson *et al.* 1992) and VV is more sensitive to canopy attributes (Dobson *et al.* 1995). Cross-polarised backscatter (HV - horizontal transmit and vertical receive and/or VH) is related to volumetric scattering, as the canopy is a medium capable of depolarisation (Saatchi and Rignot 1997). In general, double bounce trunk-ground, when not as a result of a perfect corner reflector situation (Leckie and Ranson 1998), is more likely to produce backscatter in a distinct polarisation than the received one (Waring *et al.* 1995).

3.2. Modelling forest backscatter

Interpretation of radar imagery relies on knowledge about backscatter process and the relative importance of various scattering mechanisms that contribute to the final backscatter (Richards 1990). When trying to establish links between backscatter, scattering mechanisms and vegetation components, energy-matter interaction models have been used. Many types of models are available to predict the backscatter for a given target and SAR parameters. Comparison with real SAR data allows various mechanisms and the contribution of each vegetation component in the final backscatter to be understood. For backscatter modelling purposes, the forest canopy has two main characteristics: the gross structure of the scattering medium and the geometry and electromagnetic properties of the individual vegetation components (Saatchi and McDonald 1997).

There are several types of backscatter models. When based on electromagnetic theory and known expressions for backscatter coefficients, these models are called radiative transfer (RT) models, and their 'order' is determined by the complexity of scattering taken place at the target (Richards 1990). First order RT models take into account only volume, surface and double-bounce (from trunk and ground and foliage or branches and ground) scattering mechanisms. Backscatter involving two or more scattering events is thought to be attenuated inside the canopy and are considered in the second order RT models (Richards 1990). There are several examples of first order radiative transfer in the literature, but by far the most utilised is the Michigan microwave canopy scattering model (MIMICS) (Ulaby *et al.* 1990). This model considers the canopy as two distinct homogeneous layers over a ground surface. The first order solution consist of a sum of the scattering mechanisms occurring between these three layers (McDonald *et al.* 1991).

Other types of backscatter models are the index or regression models, which are based on preconceived mathematical expressions and the model parameters are found by regressions (Richards 1990). The disadvantages of these models are the dependence of model parameters (where a change would preclude application on other situation) and little information provided on the physics of the scattering events involved (Richards 1990). A third type of model is called functional or conceptual, but could be called

phenomenological because of their ability to explain phenomena rather than energy-matter interactions (Richards 1990).

Few situations, such as the specular reflection from a water surface, can be modelled exactly. The complexity of a forest ecosystem may require a combination of different models (Richards 1990). Also, the straightforward inversion of the models to obtain the required output is unlikely and connecting models are often needed (Kasischke and Christensen 1990).

Backscatter models are evolving to be more complex and realistic (Leckie and Ranson 1998). Recently, Castel *et al.* (2001) presented the Architectural Plant Model (AMAP), which relies on both qualitative and quantitative architectural plant growth descriptions. The AMAP model provides a more realistic 3-D view of trees and allows differentiating vertical profiles of ageing canopies. A RT model was modified, fed by canopy parameters derived by using AMAP model and successfully tested using data from pine stands in Southern France (Castel *et al.* 2001).

For tropical forest environments, the available current backscatter models would require adaptations to take into account a large number of vegetation variables. The difficulties in obtaining data required as input for the available models also hamper their application for such environments. However, some authors have used existing models such as MIMICS (Grover *et al.* 1999) and a model based on the one devised by Attema and Ulaby (1978) (Luckman *et al.* 1998) to try to understand scattering mechanisms over tropical forests.

To date, few attempts have been made to construct backscatter models that are applicable exclusively to tropical ecosystem variables (Leysen, pers. comm. 1998).

3.3. Biomass estimation and mapping

The study of radar remote sensing of forests has been aided by theoretical models, which have helped researchers to understand the causative factors for the backscatter coming from forests (Dobson *et al.* 1995). The dependency of backscatter on above ground biomass was observed and related to the penetration of the radiation into the

canopy and interaction with the trunk, where most of the volume, therefore, biomass of the vegetation is concentrated (Sader 1987, Le Toan *et al.* 1992, Dobson *et al.* 1992).

HV polarisation in longer wavelengths (L or P band) is the most sensitive to biomass (Sader 1987, Le Toan *et al.* 1992, Ranson *et al.* 1997a) because it originates mainly from canopy volume scattering (Wang *et al.* 1995), trunk scattering (Le Toan *et al.* 1992) and is less affected by the ground surface (Ranson and Sun 1994). The sensitivity of backscatter to biomass is, however, limited by an asymptotic response of backscatter beyond certain levels of biomass, a phenomenon which is wavelength dependent (Dobson *et al.* 1995, Kasischke *et al.*1997). This 'saturation' of the backscatter is considered the limit for an accurate estimation of biomass from SAR data (Imhoff 1995a) and normally corresponds to backscatter coming from biomass of mature forest or dense forest vegetation (table 3.1).

Table 3.1. Saturation levels for backscatter/biomass relationship

Author	Type of forest	Band	Biomass (T ha^{-1})
Sader (1987)	Temperate broadleaf and pine	L	100
Dobson *et al.* (1992)	Two species of pine	P L	100-200
Rauste *et al.* (1994)	Temperate coniferous	L	100
Imhoff (1995a)	Combined data from conifer and broadleaf evergreen	C L P	20 40 100
Rignot *et al.* (1997)	Tropical	L	Likely close to 100
Luckman *et al.* (1997a)	Tropical	L	60
Araújo *et al.* (1999)	Tropical	L	100

The lack of a backscatter/biomass relationship does not necessarily indicate the lack of sensitivity of backscatter to vegetation. For example, a structural descriptor described as a ratio between vegetation surface area and volume (SA/V) was found by Imhoff (1995b) to have an influence on backscatter

Some approaches have been proposed to minimise the influence of the asymptote or extend the range of estimated biomass from SAR data. Most of these relate to polarisation and bands ratios, meant to isolate the contribution of biomass to the backscatter and reduce the effect of forest structure (Ranson and Sun 1994, Foody *et al.* 1997). As forest backscatter in different wavelengths and polarisations originate from separate layers of a canopy, the use of multiple channels or multistep approaches (e.g., Dobson *et al.* 1995) could be used to estimate total above-ground biomass (Kasischke *et al.* 1997). For example, the ratio P_{HV} and C_{HV} was used successfully by Ranson and Sun (1994) to estimate biomass up to 250 T ha^{-1} in a mixed conifer/ deciduous temperate forest.

Dobson *et al.* (1995) consider these band ratios too simplistic, although effective in extending the range of estimable biomass. Their argument is that the biomass estimate can hide a variety of structural factors, as same biomass values can represent few tall trees or many short trees. The corresponding backscatter will be much higher for the few tall trees than for the many short ones (Dobson *et al.* 1995). In spite of this, a combination of bands and polarisations in a multistep approach made possible the mapping of biomass in a mixed temperate forest up to 250 T ha^{-1} (Dobson *et al.* 1995). Saatchi *et al.* (1997) found an early asymptote on the backscatter in regenerating tropical forest and attributed it to the lack of the contribution of fresh biomass components (like lianas and leafy vegetation understory and overstory) in the calculation of (woody) biomass.

The backscatter/biomass issue must be treated with care, as a lot of variation exists not only on the ecosystems themselves, but also in the way their biomass are estimated.

Establishing a strong link between backscatter and forest variables is an important part of the successful estimation of forest biomass from backscatter. As already mentioned, models are often used to explain the relationship between forest variables, scattering mechanisms and SAR configuration parameters (Richards 1990, Kasischke and Christensen 1990). Another approach is the use of statistical analysis, where forest variables are related to SAR backscatter by regression models (Sader 1987, Le Toan *et al.* 1992, Rauste *et al.* 1994). Some authors used the combination of the two approaches, in most cases to assess the results of the predicted biomass or backscatter via regression (Ranson and Sun 1994, Ferrazzoli *et al.* 1997, Franson and Israelson 1999). Statistical procedures such as stepwise regression were also used to determine

the best set of bands and polarisations to discriminate biomass levels (Ranson *et al.* 1997a).

The mapping of biomass in Northern Michigan forest was achieved successfully by Dobson *et al.* (1995) using a three-step process: (1) forest classification into structural categories, (2) estimation of structural variables (basal area, height and crown biomass) from polarimetric SAR data and (3) estimation of total biomass based on a simple biophysical model. Accuracy assessment was performed based on available land cover maps and was accurate up to a biomass of at least 250 T ha^{-1}. Modelled backscatter and ratio images of multitemporal polarimetric SAR data were also used successfully to map biomass in a Northern forest of Maine (Ranson and Sun 1994). PHV data were used for estimating stem volume of forests in Finland (Rauste *et al.* 1994), as were pine forests biomass estimated and mapped (Beaudoin *et al.* 1994). A procedure devised by Ranson *et al.* (1997a) combined simulated variables of a forest growth model to AIRSAR data based backscatter model and the result was a third model relating all variables. The final map underestimated biomass and the backscatter asymptote was at biomass levels of 150 T ha^{-1} (Ranson *et al.* 1997a). For boreal forests, however, another procedure based on combined SAR and Landsat Thematic Mapper (TM) data allowed the estimation of biomass up to 150 T ha^{-1}, with RMS (root mean square) errors around 37 T ha^{-1} (Ranson *et al.*1997b).

The mapping of biomass for a large area in Brazilian Amazonia used JERS-1 SAR mosaic data (Luckman *et al.* 1998) and the biomass categories mapped were from 6 T ha^{-1} to 13 T ha^{-1}, 14 T ha^{-1} to 31 T ha^{-1} and above 31 T ha^{-1}. The limitation of the rôle of SAR data on biomass estimation was attributed to the asymptote in the backscatter/biomass relationship (Imhoff 1995a, Luckman *et al.* 1998), although no alternatives were considered.

3.4. Forest classification

Classification of a remote sensing image is a process that recognises one or several categories of real-world objects in pixels (Mather 1999). Normally spectral patterns present within the images are used as a numerical basis for categorisation, due to objects inherent reflectance, emittance or scattering properties (Lillesand and Kiefer 2000).

Classification can use also spatial and temporal information as a basis for categorisation. Spatial classifiers categorise image pixels based on their spatial relationships with the surrounding pixels and texture is a commonly used measure of these relationships (Lillesand and Kiefer 2000). The temporal domain can be used as an aid to the categorisation of spectral and spatial features present in remote sensing images. Some features can be identified only when, for instance, a particular season or phenological stage is reached. The classification process will then use combined information from the spectral and spatial domains in a temporal series of data (Lillesand and Kiefer 2000).

The study of forest ecosystems usually requires their differentiation from the remaining land covers and the classification of specific vegetation communities (Kasischke *et al.* 1997). Regenerating tropical forests, for instance, are normally found close to mature forest but also close to agricultural crops, pastures and urban settlements, making their differentiation from the remaining land cover very useful.

Two main approaches used to classify SAR data have been (1) maximum likelihood classification (MLE) including supervised and unsupervised cluster analysis and (2) knowledge-based hierarchical decision trees (Kasischke *et al.* 1997). The extendibility of MLE classification results to global scales is usually impaired by the need for localised training (Kasischke *et al.* 1997). Knowledge-based approaches have been proposed to overcome this limitation by using explicit relationships between backscatter and vegetation structure and then reclassification based on these links and floristic community (Dobson *et al.* 1995, Kasischke *et al.* 1997, Bergen *et al.* 1998).

Maximum-a-posteriori (MAP) Bayesian classifier was developed for the classification of multifrequency polarimetric SAR data and differed to the MLE approach because of the revisions on the decision rules about the classes nature (Saatchi and Rignot 1997).

Recent research has shown promising results using segmentation methods (Oliver 1998, Frery *et al.* 1999, Grover *et al.* 1999). These methods consist of aggregation of pixels with similar properties and limits defined by the borders of the segments (Yanasse *et al.* 1997). The segment labelling is performed afterwards in a classification procedure.

Artificial Neural Network (ANN) based classifiers are also a promising approach. Among ANN advantages are facilitated incorporation of different types of data which do not have to fit any particular statistical distribution (Atkinson and Tatnall 1997).

The advantages of each approach depend on the suitability of the classification estimator to the available data set, which will determine a high accuracy on the classification process. Good field knowledge, field data and adequate maps make far easier algorithm training (when needed) and accuracy assessment of the final classification.

Temperate and boreal forest types have been classified with radar data (Saatchi and Rignot 1997, Bergen *et al.* 1998, Williams *et al.* 1999). For management inventory purposes, however, radar data does not provide detailed enough information (Leckie and Ranson 1998). Nevertheless, radar data can provide complementary information to aerial photographs (Leckie and Ranson 1998) and forest biophysical parameters have been estimated (Ranson and Sun 1994, Dobson *et al.* 1995, Ranson *et al.* 1997b). When radar data are combined with optical data, forest mapping capabilities are usually increased.

Manual interpretation of radar images played an important rôle on the mapping of tropical forest types in Brazil and Colombia (RADAM Project) (Kasischke *et al.* 1997) and today is still considered an important technique for discriminating forest types (Leckie and Ranson 1998, Kuntz and Siegert 1999).

Accurate automatic classification of radar data for tropical forest is still under development and some of the achievements are showed in table 3.2. Merging classification techniques (Rignot *et al.* 1997), the use of estimators adapted to radar data (Nezry *et al.* 1993, Saatchi *et al.* 1997, Saatchi *et al.* 2000) and the use of texture measures derived from SAR images (Oliver 1998, Saatchi *et al.* 2000) seem to be the trends for the high classification accuracy of the vegetation on the tropics. Some authors, however, found the use of a minimum of two SAR C, L and/or P channels essential to discriminate between regenerating forest and selectively logged forest (van der Sanden and Hoekman 1999). Similarly to temperate forests, SAR for tropical forests has promising but yet complementary capabilities (van der Sanden and Hoekman 1999).

Optical sensor data are commonly combined with SAR images when studying tropical forests (Nezry *et al.* 1993, Rignot *et al.* 1997, Araújo *et al.* 1999). Time series of optical

images have been used as a reference in the field or prior to field work to establish the age of clearings and land cover history (Foody *et al.* 1997, Luckman *et al.* 1997a, Yanasse *et al.* 1997, Salas and Skole 1998). Thematic maps reflecting age-related areas were created from classified TM images in a pixel-to-pixel Boolean basis (Sant'Anna *et al.* 1995). This procedure, however, is still not possible with SAR images, due to the much poorer classification performances in tropical forest classes.

3.4.1. Spatial characteristics of backscatter - texture

Texture can be defined as the variation of the grey level of a single pixel (tone) within a neighbourhood (Mather 1999). This variability can be structured and reflects the spatial relationships among grey levels of pixels (Mather 1999). Texture is dependent on (i) the scale of the variation to be defined and (ii) on the scale of observation, limited by the spatial resolution of remotely sensed data (Mather 1999). For backscatter, textural attributes quantify the pattern of spatial variations in the strength of backscatter (van der Sanden and Hoekman 1999). An optimised texture measure depends on the statistical properties of the backscatter (Oliver and Quegan 1998) and is based on the statistical dependence between pixels within a region (Kurvonen and Hallikainen 1999).

Many texture measures in remotely sensed data are referenced as important tools in vegetation and land cover classification. Local statistics texture measures are statistical moments (such as mean, skewness, kurtosis and coefficient of variation (CV)), of the window from which the texture of the image is extracted (Kurvonen and Hallikainen 1999). Second-order texture measures (such as entropy, energy, contrast, etc.) relate to statistical dependence between pixels in a given distance and direction and are calculated from the grey-level co-occurrence matrix (GLCM) (Kurvonen and Hallikainen 1999, Mather 1999). Another approach for texture analysis includes the variogram that provides a concise description of the scale and pattern of spatial variability in remotely sensed data (Curran *et al.* 1998). These texture measures will be discussed in detail in chapter 6.

In general, there is an unclear utilisation of the spatial domain in the analysis of remotely sensed data (Curran *et al.* 1998). While recent forest discrimination research has shown

interest on the textural approach, results are difficult to extrapolate because of the variety of physical environments and techniques used.

For temperate forests in Finland, texture measures (CV and four measures derived from GLCM) from a multitemporal set of SAR images were found to increase the accuracy of classification results, even though the final accuracy was around 65% (Kurvonen and Hallikainen 1999).

Table 3.3 shows some recent results using SAR textural information for tropical forest discrimination. Low discrimination accuracy results and absence of a texture measure that works with all or certain forest types are the main conclusions that can be draw from table 3.3. Also, the use of a simple texture measure (such as the mean) can result in accurate discrimination between forest types (Yanasse *et al.* 1997, Podest and Saatchi 1999).

Despite low accuracy in the discrimination of forest types, some authors report encouraging representation of classes with distinctive texture signatures (Miranda *et al.* 1996, 1998, van der Sanden and Hoekman 1999). Perhaps the gap in texture modelling (Oliver and Quegan 1998) will be resolved with a better understanding of the physics that governs backscatter and associated texture, given that texture is still a promising approach.

3.4.2. Temporal characteristics of backscatter

The dielectric characteristics of vegetation and soils have a strong effect on backscatter and are important sources of variation in σ°. Varying weather conditions are related to changes in water content of vegetation and soils, therefore, impact directly on backscatter (Gates 1991). In addition to rainfall, air temperature and wind speed can induce physiological and/or geometric changes in the vegetation components and influence backscatter (Leckie and Ranson 1998). The monitoring of seasonal phenological development is a substantial part of forest ecosystem studies and justifies the study of temporal backscatter.

Table 3.2. Examples of classification approaches using radar imagery in tropical ecosystems (adapted from Kasischke *et al.* 1997).

Ecosystem	Purpose	Classifier[a]	Data source	No of classes and types[b]	Accuracy[c]	Radar band/ polarisation	Reference
Tropical forest and adjacent areas	Vegetation mapping	Supervised MLE adapted to radar	SIR-B SPOT-HRV	6 and 8 W,B,A,F,U,Aru plus rF, C	Medium on SIR-B High on SIR-B +HRV (8 classes)	L_{HH}	Nezry *et al.* 1993
Subtropical forest and wetlands	Ecosystem mapping	MLE cluster	AIRSAR	7 W,B,A,H,S, F(2)	Medium	P,L,C, all polarisations	Pope *et al.* 1994
Tropical floodplain forest	Map forest flooding	Decision tree	SIR-C	5 W,fH,H,F,fF	High	L_{HH},L_{HV}, C_{HH}	Hess *et al.* 1995
Tropical forest and adjacent areas	Map deforestation and regeneration	Supervised on TM, after MAP on SIR-C	SIR-C Landsat TM	6 and 7 W,F,fdF,yrF,B, Ct	High on SIR-C Higher on SIR-C +TM (7 classes)	L_{HH}, L_{HV}, C_{HH},C_{HV}	Rignot *et al.* 1997
Tropical forest and adjacent areas	Map deforestation and land use	MAP supervised	SIR-C	5 F,rF,A,Ct,dF	Medium	L_{HH}, L_{HV}, C_{HH},C_{HV}	Saatchi *et al.* 1997
Tropical forest and adjacent areas	Map forest and non forest	Annealed segmentation	CCRS airborne SAR	2 F, nF	High with texture (from parameters of K-distribution)	C_{HH}	Oliver 1998
Amazon Basin	Map land cover types in the Amazon Basin	MAP and hierarchical decision based on texture measures	JERS-1 SAR 100 m resolution image mosaic	14 W, r, F, nF and 10 vegetation types	Medium with first order texture measures	L_{HH}	Saatchi *et al.* 2000

[a]Classification approaches: Maximum likelihood estimator (MLE), Maximum-a-posteriori Bayesian (MAP).

[b]Agriculture (A), water (W), bare soil (B), clearings (c), urban (U), forest (F), flooded (f), young (y), regenerating (r), trunks (t), rubber (ru), disturbed (d), non(n), dead (d).

[c]High indicates >90% classification accuracy, medium indicates 70-90% classification accuracy.

Table 3.3. Examples of the use of texture measures in SAR imagery of tropical forests (adapted from Kasischke *et al.* 1997).

Ecosystem	Purpose	Texture measure. Result assessment	Data source	No of classes and types[b]	Discrimination accuracy[c]	Band/ polarisation	Reference
Tropical forest and adjacent areas	Vegetation mapping	Semivariogram texture classifier. Confusion matrix.	JERS-1	4 W,F, oF, fF	Low	L_{HH}	Miranda *et al.* 1996
Tropical forest and adjacent areas	Discriminate regenerating stages	Tonal mean, CV (Coefficient of Variation). BD and ED.	SIR-C, Landsat TM age map	7 RA, (0,2], (2,4], (4,6], (6,8], >=9 years old, F	Good for the mean in L band (L_{HV} better) Poor with CV, better with L band	L,C, all polari-sations	Yanasse *et al.* 1997
Tropical forest and adjacent areas	Discriminate regenerating stages	K-distribution α parameter, CV, GLCM contrast. CV.	CCRS airborne SAR, Landsat TM age map	5 B, 1-3, 4-6, >6 years old, F	Low and only between F and other classes Better with CV	C_{HH},C_{VV},	Luckman *et al.* 1997b
Tropical forest and adjacent areas	Map major land cover types	CV,mean,variance, entropy,energy, skewness,kurtosis, contrast. MLE and BD.	JERS-1 SAR 100 m spatial resolution	8 W, F, rF, nF, fF, fnF, wS, nwS	Medium with mean, variance and entropy. Mean best for overall separability	L_{HH}	Podest and Saatchi 1999
Tropical forest and adjacent areas	Map detailed land cover types	GLCM derived texture measures. TD_{ij}, MLE, Kappa statistics.	CCRS airborne SAR	8 F (5 types), IF, rF, nF	Low, better measures contrast and correlation	X,C all polari-sations	van der Sanden and Hoekman 1999

[a]Result assessment approaches: Maximum likelihood estimator (MLE), Bhattacharyya distance (BD), Euclidean distance (ED), transformed divergence (TD_{ij}).

[b]Agriculture (A), water (W), bare soil (B), clearings (C), forest (F), recent activities (RA), savanna (S), flooded (f), logged (l), regenerating (r), open (o), woody (w), disturbed (d), non(n).

[c]High indicates >90% classification accuracy, medium indicates 70-90% classification accuracy, low indicates <70% classification accuracy..

Results from studies on the seasonal forest backscatter indicated that soil frost and snow can reduce relative backscatter values and be detected at L and C bands (Pulliainen *et al.* 1999). Also, the absence of leaves in deciduous forest trees lowered the backscatter at C band, raising the assumption of leaves as highly forward scatterers (Ahern *et al.* 1993). Other authors, however, found a very weak correlation between ERS-1 SAR C band backscatter and seasonal changing variables, as foliage dynamics (Mougin *et al.* 1998). Weather related variables (rainfall, wind speed and air temperature) were reported as not being clearly related to backscatter from a deciduous-coniferous forest (Mougin *et al.* 1998).

Seasonal effects were observed in a walnut orchard backscatter at X and L bands. Changes at X band backscatter were attributed to changing water content of branches and leaves, while at L band to both soil and vegetation water content variation (McDonald *et al.* 1991).

For tropical environments, seasonal L band backscatter was detected by Rosenqvist (1996a) from oil palm stands. The seasonal behaviour corresponded to high backscatter coinciding with the two annual dry seasons in the area and was attributed to changing water content of leaves and fronds. For rubber tree plantations, however, even after shedding their leaves, little variation of backscatter with time was detected (Rosenqvist 1996a). In Brazilian Amazonia, a backscatter seasonal cycle, corresponding roughly with low backscatter for dry season and high backscatter for wet season, was detected in low biomass regenerating forest plots and attributed to the changing water content of vegetation and soils (Kuplich and Curran 1999).

A general consensus among researchers is that data from the dry season in the tropics are the most useful when differentiating vegetation classes (Rignot *et al.* 1997, Luckman *et al.* 1998, Grover *et al.* 1999, Kuntz and Siegert 1999). In addition, backscatter/biomass relationships are stronger during the dry season, because the influence of water and consequent increase on backscatter are minimised (Luckman *et al.* 1998, Kuplich and Curran 1999).

For Amazonian forest, the influence of the season on the backscatter is not restricted to the effect of water, but also to land cover dynamics, which determines, in addition to the increased soil moisture in wet seasons, the availability of some temporary

crops (Saatchi *et al.* 1997). Moreover, the dry season is the preferable time for logging, forest clearing and pasture burning, thus care must be taken when analysing dynamic tropical environments (Saatchi *et al.* 1997).

3.5. Summary

The study of backscatter of regenerating tropical forests is a relatively new topic (Foody *et al.* 1997, Luckman *et al.* 1997a, 1998, Yanasse *et al.* 1997, Salas and Skole 1998). When describing tropical land cover types the diversity of logging and agricultural practices in areas surrounding tropical forest is revealed. Potential sources of forest regeneration are added to the ones following slash and burn cycles. Disturbed forests as a result of selective logging (by hand or machine) are also common land cover types described for the tropics (Saatchi *et al.* 1997, van der Sanden and Hoekman 1999, Kuntz and Siegert 1999, Kuplich *et al.* 2000b). Different practices trigger forest regeneration and most of the works concerning backscatter of tropical had at least one land cover type or class labelled either as regrowth forest (Nezry *et al.* 1993, Pope *et al.* 1994, Rignot *et al.* 1997), secondary forest (Kuntz and Siegert 1999, van der Sanden and Hoekman 1999) or regenerating forest (Foody *et al.* 1997, Yanasse *et al.* 1997, Luckman *et al.* 1997a,b, 1998, Grover *et al.* 1999).

As part of the regenerating forest process, deforested areas are usually present in tropical environments and its discrimination from mature forest assessed. Discrimination between these areas is a function of the contrast offered by the backscatter of the deforested areas (Ribbes *et al.* 1997). The type of logging seems to determine the intensity of radar backscatter, as woody debris can be removed or not. If removed and the soil is left bare, the radar response will be of the soils, therefore, the rules about roughness and soil moisture apply, with stronger backscatter for rougher and wetter soils (Ulaby *et al.* 1974).

The presence of residual biomass after logging produces high horizontally polarised returns, as this polarisation interacted strongly with the remaining trunks (Rignot *et al.* 1997). When some trees are left standing, double-bounce scattering occurs between trees and clear forest floor and LHH returns are higher than others bands in SIR-C configuration (Saatchi *et al.* 1997). If the wavelength penetrates the forest canopy,

horizontal co-polarised radiation will also give information about the underlying soil and canopy- and trunk-ground interactions (Hess *et al.* 1995).

Some recent studies have suggested limitations on the use of C band in tropical forest area discrimination (Pope *et al.* 1994, Luckman *et al.* 1997b, Rignot *et al.* 1997, Saatchi *et al.* 1997, Yanasse *et al.* 1997, Grover *et al.* 1999). The reason for that is the backscatter asymptote at low levels of biomass and consequent C band insensitivity to even young regenerating forest areas (Saatchi *et al.* 1997). The shallow penetration of the C band into forest canopies restricts its use for the differentiation between deforested areas and forest when the soil is dry and the influence of water is minimised (Luckman *et al.* 1997a, Grover *et al.* 1999). Kuntz and Siegert (1999), however, found some discrimination power on the texture extracted from ERS-1 SAR images (CVV band) for Indonesian forests.

L band has proved some success in tropical vegetation studies, owing to its deeper penetration and volumetric interactions into the canopy (Grover *et al.* 1999). When configured as LHV its sensitivity to forest biomass and structure allowed some discrimination between regenerating stages (Yanasse *et al.* 1997) and between regenerating and mature forest (Saatchi *et al.* 1997). The backscatter asymptote was found to be the reason for the low separability between regenerating areas and L band with at least two different polarisations was suggested to perform this task (Rignot *et al.* 1997).

Regenerating forest backscatter will approach that of the surrounding mature forest as the forest grows, so the differentiation between regenerating and mature forest can become difficult (Leckie and Ranson 1998, Salas and Skole 1998).

Reliable assessment of various forest types including regenerating, selectively-logged and mature tropical forest required SAR data on C, L and/or P bands (van der Sanden and Hoekman 1999). Four biophysical indices derived from fully-polarimetric SAR data were used successfully to discriminate vegetation types (called landscape units) in the tropics (Pope *et al.* 1994).

The great variety of tropical forest ecosystems still did not allow the finding of an ideal radar configuration capable of identification and discrimination at the desired level. A multitemporal approach along with texture analysis (Saatchi *et al.* 1997) can help clarify backscatter/tropical forest relationships.

The influence of regenerating tropical forest characteristics (e.g. species composition, their structures and canopy properties) on the backscatter is still not fully understood. An initial attempt to group regenerating forests by their dominant species (therefore, reducing structural variability) was made and some encouraging results obtained (Foody *et al.* 1997). Variation in biomass was secondary to canopy spatial variability (canopy closure and homogeneity) in the backscatter of tropical forest in Belize (Pope *et al.* 1994). These highlight the limitations of approaches used to study tropical regenerating forests until now and the amount of work still to do.

CHAPTER FOUR

Study areas and ground data

This chapter presents background information on the study areas and the ground data available for them. Brazilian Amazonia is introduced in the context of tropical rain forests, the Amazon Basin and the Legal Amazon, with general descriptions of climate, soil and vegetation. This is followed by an outline of the two study areas, Manaus and Tapajós, where details on the way biophysical properties were estimated are given. Finally, rainfall and cloudiness data are listed.

4.1. Brazilian Amazonia

American or neotropical rain forests of the permanently wet tropics are the most extensive block of tropical rain forests, covering one-sixth of the total broad-leaf forest of the world (Whitmore 1997). The Amazon Basin covers around 6.4 million km^2 (7 million km^2 including the Tocantins-Araguaia Basin) (Ribeiro *et al.* 1996) and it is where the Brazilian Amazonia lies. 'Brazil is the country with more rain forests than any other' (Whitmore 1997, p.10).

The Legal Amazon, an administrative region created by the Brazilian government in 1953, covers 9 Brazilian States: Acre, Amapá, Amazonas, Maranhão, Mato Grosso, Pará, Rondônia, Roraima and Tocantins and comprises around 5 million km^2 (Diegues 1992).

The Amazon river's mouth was first reached from the Andes, in the Cinnamon expedition by Spanish Francisco de Orellana in 1542 (Gheerbrant 1992).

Since the 16th century, the exploration of Amazonia by European conquistadors had mainly a commercial character (Whitmore 1997). In the last 40 years, however, human disturbances in Amazonia have increased dramatically as a consequence of its opening for international exploitation and the failure of some Brazilian government policies (Diegues 1992, Ab'Sáber 1996). Amazonia has a critical importance for Brazil and for the rest of the world, as the 'single richest region of the tropical biome' (Myers 1984) and as an ecosystem that is still not fully understood (Ab'Sáber 1996).

4.1.1. Climate

Tropical rain forest climates are characterised by monthly mean temperatures of 18°C or more and annual rainfall of at least 1700 mm (Walsh 1996). Variations of less than 5°C in the mean monthly temperatures are expected in the humid tropics (Sanchez *et al.* 1982) and average midday temperatures for the Amazon Basin are in the range 27°C - 32°C (Pearce and Smith 1993).

Climatic types associated with tropical rain forests are based on, among other things, the presence or absence of a dry season or periods with a monthly rainfall less than 100 mm (Walsh 1996). Table 4.1 shows these climatic types in general terms and its associated potential natural vegetation. Tropical montane climates and vegetation are not considered due to their small coverage in Brazilian Amazonia.

Rainfall averages 2000 mm annually in the central Amazon Basin (Salati and Vose 1984). Superwet climates occupy a small area in upper and western parts of the Amazon Basin, within Colombia and Peru. Both study areas in the Brazilian Amazon are typical of the tropical wet seasonal climatic type, with a long wet but also a significant dry season that lasts from 3 to 5 months (Walsh 1996). Vegetation types assigned to these climatic types will be discussed later.

Table 4.1: Climatic types and associated potential natural vegetation for South American tropical rain forests. Adapted from Walsh (1996).

Climatic type	Dry periods	Annual rainfall (mm)	Potential natural vegetation
Tropical superwet	Periods> 1 month absent or rare	>3000	Lowland and Lower montane rain forest
Tropical wet	Relatively frequent short dry periods or very short dry season	> 2000	Lowland and Lower montane rain forest
Tropical wet seasonal	Significant dry season of up to 4 months < 100 mm rainfall	> 1700	Evergreen seasonal rain forest

Evidence of past environmental conditions, deduced from palynology and direct physical traces, lead to the assumption that fluctuations in climate (associated with glacial and interglacial periods) were coupled with fluctuations in vegetation (Whitmore 1990, Ab'Sáber 1996). Changes in rainfall and temperature patterns throughout the Quaternary are among the most important environmental factors to which tropical rain forests had to adapt (Richards 1996).

4.1.2. Soils

Most of the Amazon Basin lies below 300 meters with gentle topography (Ab'Sáber 1996). Tropical soil types normally have low fertility (Sanchez *et al.* 1982) as a result of intensive and prolonged leaching. Heavy rainfall, high temperatures and stability of land surfaces in the humid tropics have resulted in a high proportion of old and intensively weathered soils. These soils are deep (2 metres or more), porous and suffer from rapid water infiltration (Baillie 1996).

Dominating around 75% of the Amazon Basin (Sanchez *et al.* 1982) are the main soil groups of Brazilian Amazonia (RADAMBRASIL 1976): the Latosols (Ferralsols (FAO 1971), Oxisols (USDA 1975)) and the Podzols (Acrisol (FAO 1971), Ultisols (USDA

1975)). These soils are acid, infertile and normally well drained with colours varying from red to yellow, indicative of the presence of iron oxides (Sanchez *et al.* 1982). These soils have coarse to medium topsoil textures and subsoils of medium texture, as the clay content generally increases with depth (Baillie 1996). Next on the distribution of soils in the Amazon Basin are the poorly-drained alluvial soils (14%) followed by moderately fertile well-drained soils (8%) and finally, sandy infertile soils (3%) (Sanchez *et al.* 1982).

The main constraints imposed by these types of soils are on agricultural cultivation. The constraints are chemical rather than physical, like phosphorus deficiency in around 90% and aluminium toxicity in around 73% of Amazonian soils (Sanchez *et al.* 1982). The logging of native vegetation and the consequent soil exposition alter the ecosystem equilibrium and induce physical and chemical soil change as well as an increase in the susceptibility to soil erosion (Baillie 1996).

4.1.3. Vegetation

In this section characteristics of mature and regenerating Amazonian forest are given, after general features of both forest types have been described. After that an overview of biomass (i.e., the carbon content) of tropical vegetation is presented, as this is a critical component of the global carbon cycle.

4.1.3.1. Mature forests in Amazonia

Around 94% of the Brazilian Amazon *terra firme* (i.e., areas not permanently or seasonally flooded) are covered with forests (Ab'Sáber 1996). Distribution patterns of Amazon forests were a result of tropical humid climate generalisation allied with forest expansion from refugia (Ab'Sáber 1996). As mentioned before, glacial and interglacial periods were associated with dry and wet periods, respectively. Refuge theory or the fragmentation of the vegetation in islands or refuges during dry periods in the late Pleistocene was first used to explain the diversity and endemism of animal species in Amazonian forests (Richards 1996). Evidence supporting this theory was

found when analysing distributional patterns of trees from certain families in Amazonia (Prance 1987).

Even though no agreement was reached in the scientific community to support the refuge theory, the idea of continual adjustment of tropical rain forests in response to changing environmental conditions has been accepted (Whitmore 1990, Richards 1996, Ab'Sáber 1996). In this context, the concept of climax plant community as a final successional stage in a climatic climax (Hartshorn 1980) seems questionable.

Budowsky (1965, p.42) defined a climax community as 'the end product of a successional sere when a relatively stable, although certainly not static, community has been reached and when changes of floristic composition, structure and physiognomy over the age span of the dominants become significant'. Jacobs (1988, p.97) related climax tropical vegetation to unchanging environmental conditions stating that 'climax vegetation is one which has reached its maximum development, i.e., it consists of the maximum number of species able to survive under the existing conditions, and one whose composition, if undisturbed, will not change if climate and soil conditions remain the same'.

More recently it was found that undisturbed tropical forests increase biomass production under enhanced CO_2 conditions (Chambers *et al.* 2001). For a 25% increase in atmospheric CO_2 scenario, model simulations showed that carbon accumulation continue for over a century when the enhanced carbon availability finishes (Chambers *et al.* 2001). These authors calculated a new dynamic equilibrium in carbon storage once a tree has reached its full growth (around 175 years) under enhanced productivity conditions.

Adjectives as undisturbed, old growth, primary, mature and virgin have been used to refer to climax communities (Hartshorn 1980). Nowadays, however, growing human pressure over forests made very unlikely the identity of undisturbed tropical forests. The term mature forest will be used in this work along with the concept of tropical mature forest as a mosaic of successional stages (Hartshorn 1980).

The vegetation of tropical mature forests has a more elaborate structure and is richer in species than any other plant community. The majority of tropical plants are woody species and of the dimensions of trees. Mixed forests present numerous dominant tree species and are the mainly type of formation in the tropics (Richards 1996).

Terra firme dense forests are the dominant mature forest type formation in Amazonia and present an irregular canopy surface with 25-35 m high trees and emergent trees that can exceed 40 m. Generally there are 500-700 trees per hectare and 100-280 different tree species per hectare (Nelson 1996). Four to five layers (or strata) are found and many tree species with small diameters are concentrated in the lower storeys. Tree trunks are slender and straight and branches appear near the top of the tree, barks are thin and smooth and vines and epiphytes are abundant. Most of the trees are evergreen but some large trees in seasonal forests (usually associated with a tropical wet seasonal climate) can be leafless for periods of few days or weeks. The amount of leaf-fall depends on the moisture conditions and varies from year to year, being also a response to severe droughts. For some classification schemes, leaf-fall is seen just as a leaf-exchange process, not as a part of a deciduous nature (Richards 1996).

Forest types in Amazonia can be divided by climatic type and elevation (table 3.1) or based on geomorphological information (RADAMBRASIL 1976). Other approaches include physiognomic (as closed and open forests classes) and human induced features (as fragmented forest, deforested or forest converted classes) (Nelson 1996, Saatchi *et al.* 2000). The enormous diversity of plant forms and the huge variability in species composition of mixed Amazonian forests were reflected in the forest classification schemes proposed until today.

4.1.3.2. Regenerating forests in Amazonia

The germination of plant species in a newly formed forest gap, resulting from a large tree fall, for instance, is an initial stage of the succession process. These 'coloniser' or pioneer species can grow up together with older mature tree species, in a mosaic of successional stages.

The impacts of human pressure in the tropics have altered some natural cycles and various areas of mature forest have been cleared completely, mainly for agricultural purposes. The vegetation communities that replace mature forests are called secondary forests, secondary growth or simply regenerating forests. In Brazil they are called *capoeiras.*

The structure and species richness of regenerating forests are dependent upon the type of disturbance and the history of the previous use (Uhl *et al.* 1987, Richards 1996, Whitmore 1997). Common features to all regenerating forests are light-demanding species with (i) a high leaf area index and total stem density, (ii) low density of trees having more than 10 cm diameter at breast height (dbh) and woody density and basal area (Brown and Lugo 1990). A canopy in regenerating forests has a tendency to be mono-layered with no emergent trees. 'After a few years, particularly on abandoned cultivated ground, even-aged stands of trees of remarkably regular structure often grow up. These may consist of a single fast-growing species such as *Cecropia* sp. (American Tropics)...'(Richards 1996, p.460). Table 4.2 lists the main characteristics of tropical pioneer and mature ('climax') tree species, the latter ones are included for ease of comparison.

Pioneer species are very aggressive, producing a large amount of low density wood in slender trunks rapidly (Whitmore 1997). The main differences between pioneer and mature species presented in table 4.2 refer to this strategy based on a fast life but 'unable to occupy any site permanently' (Richards 1996). Eventually, pioneer species create the environment for the establishment of mature forest tree species. The number of species in a regenerating forest is regulated by the type of disturbance to which the area has been subject and a rich species composition in the early phases of succession indicates high opportunities for species establishment (Brown and Lugo 1990).

Changes in species composition, from pioneer to early and late regenerating species (Budowski 1965) and associated change in structure are a sign of growing and maturation of the forest. After 60-80 years regenerating forests are often indistinguishable from mature forests (Brown and Lugo 1990).

Biomass allocation in tropical regenerating trees varies little in relation to mature trees, with large amount of biomass concentrated in woody components. The accumulation of biomass in the different components of trees is a function of age of the regenerating forest. Figure 4.1 shows the biomass accumulation in wood and leaves of tropical regenerating forest trees. Woody biomass increases rapidly in the first years, followed by a slower rate towards maturity. Leaves and roots present a different pattern, but in initial stages biomass is accumulated more rapidly (Brown and Lugo 1990).

Biomass accumulation rates for regenerating forests are dependent upon the history of previous use and vary in response to environmental conditions (Uhl *et al.* 1988, Alves *et al.* 1997, Lucas *et al.* 2000). These rates are not commonly reported due to a lack of comprehensive temporal biomass estimates for regenerating forests in Brazilian Amazonia (Lucas *et al.* 2000).

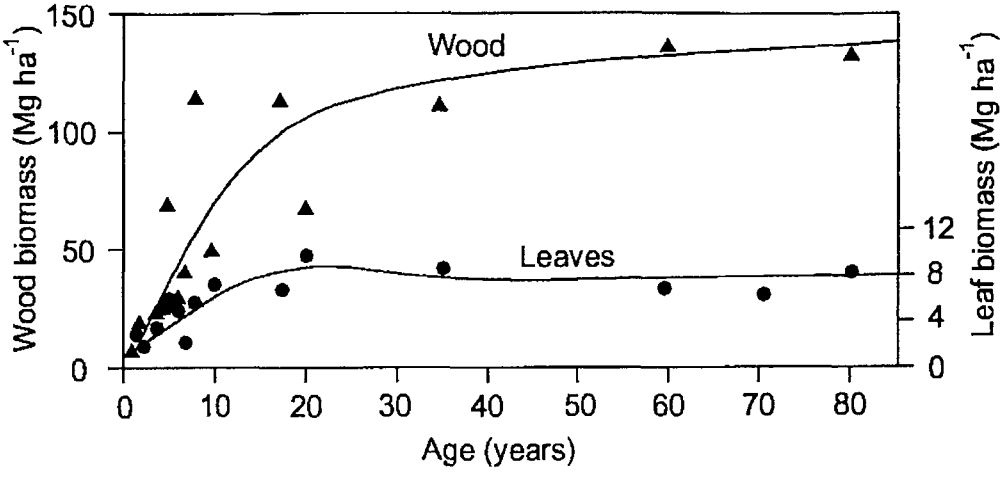

Figure 4.1. Biomass of leaves and wood (from twigs, branches and stems) of different aged tropical regenerating forests (modified from Brown and Lugo 1990).

The more frequent pioneer species in Brazilian Amazonia are from *Cecropia* and *Vismia* genera. They differ in structure and in colonisation strategies, being characteristic of successional pathways dictated by the land use history of the site they colonise (Williamson *et al.* 1998, Lucas *et al.* 2000). *Cecropia* usually develop in sites with no heavy use prior to being left fallow. Conversely, *Vismia* frequently dominate sites where pastures were abandoned after heavy use, possibly including burning. *Vismia* have higher wood density than *Cecropia*, in shorter and stronger trunks (Williamson *et al.* 1998).

Table 4.2. Main characteristics of pioneer and mature tree species of tropical forests (adapted from Whitmore 1997).

	Pioneer	Mature
Common names	Light-demander, (shade-)intolerant, secondary	Shade-bearer, (shade-)tolerant, primary
Germination	Only in canopy gaps open to the sky with full sunlight	Usually below canopy
Seedlings	Cannot survive below canopy in shade, never found there	Can survive below canopy, forming a 'seedling bank'
Seeds	Small, produced copiously and more or less continuously and from early in life	Often large, not copious, often produced annually or less frequently and only in trees that have (almost) reached full height
Soil seed bank	Many species	Few species
Dispersal	By wind or animals, often for a considerable distance	By diverse means, sometimes only a short distance
Dormancy	Capable of dormancy, commonly abundant in forest soils as a seed bank	Often with no capacity for dormancy, seldom found in soil seed bank
Growth rate	Carbon fixation rate, unit leaf rate and relative growth rates high	These rates lower
Height growth	Fast	Often slow
Branching	Sparse, few orders	Often copious, often several orders
Leaf life	Short, one generation present, viz. high turn-over rate	Long, sometimes several generations present, slow turn-over rate
Herbivory	Leaves susceptible, soft, little chemical defence	Leaves sometimes less susceptible due to mechanical toughness or toxic chemicals
Wood	Usually pale, low density, not siliceous	Variable, pale to very dark, low to high density, sometimes siliceous
Ecological range	Wide	Sometimes narrow
Stand table	Negative (no small individuals, no regeneration *in situ)*	Positive (young individuals, regeneration *in situ)*
Longevity	Often short	Sometimes very long

4.1.3.3. Biomass of tropical forests

Biomass can be defined as the total aboveground and belowground living mass of all vegetation components as well as the dead mass of litter and integrates volume and wood density information (Brown and Lugo 1990, 1992). Recalling chapter 1, the carbon content of forests can be derived directly from forest biomass estimates (1 T biomass ≅ 0.5 T carbon) (Brown and Lugo 1992).

Different approaches can be used for biomass estimation in tropical forests. The first is the intensive weighing of all vegetation components, a very laborious approach particularly for roots and large trunks. The second approach is the use of allometric regression equations derived from the weighing of a subset of trees. These equations use measurements of diameter and sometimes height and wood densities of trees as independent variables (Brown *et al.* 1992).

Considerable variation exists in estimates of tropical forest biomass, mainly due to (i) confusion about what fraction of total biomass is being considered, (ii) few biomass estimates derive from real intensive forest measurements and (iii) allometric equations consider forest variables which are often not available for all tree species involved (Brown *et al.* 1992). The use of data derived from forest volume inventories are supposedly more accurate as they are generally collected from larger sample areas and 'the scale of sampling must match the scale of the subject to be measured' (Brown and Lugo 1992, p.9). The problem is the scarcity and the variability in such large tropical forest inventories.

Accurate estimates of tropical forest biomass are essential parts of carbon flux models (Brown and Lugo 1992, Houghton *et al.* 2000). The need for accuracy is emphasised today by the large amount of change that biomass and associated carbon have been subject to, whenever forest conversion and forest regeneration take place.

4.1.3.4. Deforestation dynamics in Brazilian Amazonia

Many actors are behind Amazonian deforestation and it is difficult to draw a list of causes and factors involved. The only real consensus is that deforestation is a result of human disturbances. The first records of deforestation coincide with records of human occupation in the area, the indigenous population along the major river floodplains (várzeas) was believed to be around 6 million before contact with the first European colonisers in the 16th century (Anderson 1990). The Portuguese brought the first non-indian settlements along the várzeas for commercial purposes, as they looked for spices and drugs. In the 19th century up to 1910, rubber (latex) extraction led to an economic boom in the region, migrating people from the drought-affected areas of the North-east of Brazil and increasing human-disturbance in the forest (Diegues 1992).

Large-scale deforestation began in 1958 with the construction of the first Amazonian highway, the Belém-Brasilia (BR364). Large governmental projects of "national integration" started in the 1960s with the main objective of colonising the remote borders of Brazil and sustaining the national integrity over the very extense Brazilian territory. Although fewer people than initially intended were settled, roads were built (e.g. the Transamazonia) and government started financial incentives to agricultural and ranching activities (Moran *et al.* 1994). Until the 1980s, however, deforestation rates were about 1.5 % of the Legal Amazon and the annual increase was a mere 0.33 % (Tardin *et al.* 1980).

Since 1980 deforestation rates increased mainly as a result of government supported projects, for example subsides for large cattle ranchers that converted forest to pasture (Anderson 1990, Moran *et al.* 1994). Large-scale agricultural and cattle raising schemes were responsible for most of deforestation in despite of the removal of most fiscal incentives in 1987 (Diegues 1992). Currently pasture is the dominant land use in forest-converted areas (Ceccon and Miramontes 1999).

Selective logging of commercial timber affected 50-90 % of the total area deforested in 1996 and is largely underestimated because of its difficult detection. Surface fires initiated by the logging process also increase forest loss (Nepstad *et al.* 1999).

In addition to agriculture, cattle ranching and logging, mineral exploitation is a major cause of deforestation. The world's largest iron deposits are extracted in the Carajás Province, southern Pará State. The increasing demand for energy in the area has resulted in the building of hydroelectric dams and forest cut for charcoal production, with substantial environmental impact (Diegues 1992).

More recently occupation and colonisation of the Brazilian Amazonia is under private control and new small-scale settlements are seldom responsible for large deforestation actions. Around 60 % of arable land is concentrated in the hands of around 2 % of agricultural landowners, a socially unstable land tenure system division that calls for agrarian reform (Diegues 1992). The "unequal distribution of resources" (Anderson 1990) highlights the social dimension of the deforestation problem. Brazil's external debt (and the use of forest to pay it), inflation and other economic factors promote land speculation also, indirectly, cause deforestation (Diegues 1992).

International companies and multinational capital from, among others, Canada, Japan, Taiwan, United Kingdom and USA, associated with national corporations, own great expanses of land in Brazilian Amazonia also promoting deforestation through logging, cattle raising, agricultural and mining (Diegues 1992, Ceccon and Miramontes 1999).

Alternative use of the forest, such as agroforestry and new-extractivism, can be combined with implementation of biodiversity reserves in an effort to decrease deforestation rates, whilst maintaining economic activities in the forest. The challenge for Brazil and developed nations is to manage forest exploitation and balance environmental concerns with economic development.

4.2. Study areas

Two areas in Brazilian Amazonia were studied near Manaus and Santarém cities (Amazonas and Pará States, respectively). They were selected as part of British Terrestrial Initiative in Global Environmental Research (TIGER) project, part of the Natural Environment Research Council's (NERC) community program to study global environmental change. These were the study areas described next.

4.2.1. Manaus study area

The Manaus study area is located around 70 km north of Manaus City, the capital of Amazonas State (figure 4.2). It comprises several experimental forest reserves that are part of the Biological Dynamics of Forest Fragments Project (BDFFP) of the Brazilian National Institute for Amazonian Research (INPA) and the Smithsonian Institute in Washington, D.C.. The BR-174 Highway linking Manaus to Boa Vista (capital of Roraima State) crosses the study area.

The origins of the BDFFP go back to 1979, when INPA and WWF (World Wildlife Fund) agreed to study the effects of forest fragmentation on different species. Taking advantage of a Brazilian Law that required the land owners to leave undisturbed half of the land under development, mature forest reserves were delineated within cattle ranches. Clearcut areas were used as pastures for cattle grazing. With the Brazilian economic crisis of the 1980s and the removal of incentives for cattle ranching, most of the pastures were abandoned and colonised by secondary vegetation. These reserves have been the subject of several studies and forest regeneration is an important issue of the BDFFP (Bierregaard and Stouffer 1997).

The Manaus study area is located in moderately rugged terrain, with a maximum elevation of 142 m above sea level. The main soils within this region are Latosols that are nutrient-poor and yellow with a high clay content and porosity (RADAMBRASIL 1976).

The dry season is from June until the beginning of October. The annual rainfall is around 2290 mm and the mean temperature is around 27° C (data for Manaus station - coordinates 03.08° S, 60.01° W - and the climatological mean is from 1961-1990, DNM 1992).

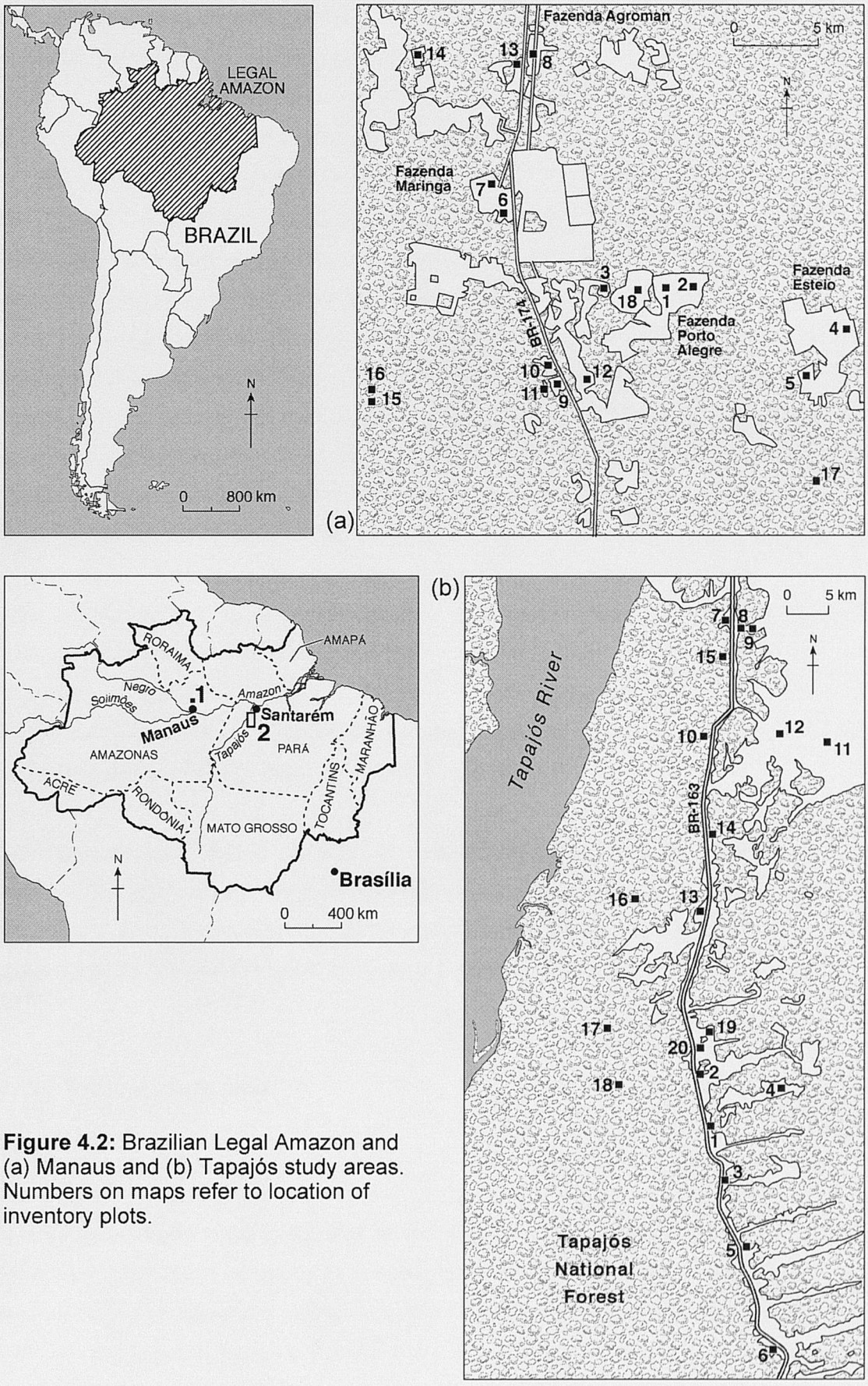

Figure 4.2: Brazilian Legal Amazon and (a) Manaus and (b) Tapajós study areas. Numbers on maps refer to location of inventory plots.

In July and August 1993 and 1995 field data were collected at the Manaus study area. It was part of the NERC TIGER 1.4 Consortium, which involved the Universities of Wales, Swansea and Southampton (Honzák 1997).

In 1993 fifteen 10x100 m plots and one 15x20 m plot were established in some of the BDFFP reserves. To locate the plots within a range of regenerating forests biomass, the approximate age of the plots was determined from a time-series of Landsat TM data following a post-classification comparison (Lucas *et al.* 1993). The inventory was conducted in structurally and floristically homogenous plots, ranging in age from 4 to 16 years (Honzák *et al.* 1996). Within each plot, the diameter at breast height (dbh) for all trees greater than 3 cm in diameter were measured, along with the record of the tree's genus (and species, when possible). The height of a random sample of trees (270 individuals) was estimated using an inclinometer (Honzák *et al.* 1996). The total height was estimated using allometric regressions relating dbh and height for all species measured in the plots (Honzák *et al.* 1996). Global Positioning System (GPS) readings were also taken at each plot. In 1995 some of the 1993 plots were resampled and fourteen additional plots were established in forests younger than 18 years (Lucas *et al.* 2000).

These data were used to generate, via allometric equations, an estimate of total above-ground biomass (T ha $^{-1}$) and density (tree ha^{-1}).

Estimates of biomass of mature forest and pasture plots were required in order to provide an adequate biomass/backscatter range for this study. However, mature forest and pasture plots were not inventoried for Manaus study area and were located only in the satellite sensor imagery described later.

4.2.2. Tapajós study area

The Tapajós study area is located in the South of the Amazon River port/city of Santarém, Pará State (figure 4.2). It comprises the Tapajós National Forest, a large reserve of dense tropical forest (around 200 km^2). The Tapajós River is located at the west of the Tapajós National Forest. East of the Tapajós National Forest and the study area is the Cuiabá-Santarém highway (BR-163) and a mixture of mature and

regenerating forest covers. The regenerating forests found there are on abandoned farmlands and were formerly areas of pasture or crops. The usual agricultural practice in the area is block-logging, burning of forest, agriculture and a resting period of five years or more when the area is left to regenerate. Some of these cleared areas have since been abandoned thus they present regenerating forest at different successional stages (Shimabukuro *et al.* 1997). Whenever agricultural areas are still active, they are mainly used to grow pepper or manioc (cassava).

Tapajós study area is also located in relatively flat terrain with maximum elevation at 280 m above sea level (inside the Tapajós National Forest). The soils are also Latosol type that are deep, highly weathered and porous, with textures varying from sandy clay loam to heavy clay (Hernandez Filho *et al.* 1993).

The dry season is from July until the beginning of December, the annual rainfall is around 1911.2 mm and the mean temperature 24.8° C (data for Belterra station - coordinates 02.38° S, 54.57° W - DNM 1992).

From 24th August to 15th September 1994 a field data collection campaign was carried out at the Tapajós study area. It was part of TIGER joint project between what was the Remote Sensing Applications Development Unit (RSADU) of the British National Space Centre (BNSC), the Brazilian Institute for Space Research (INPE), what was the Institute of Terrestrial Ecology (ITE) of the NERC and the Sheffield Centre for Earth Observation Science (SCEOS) of Sheffield University.

With the aid of an age map, derived from a time-series of Landsat TM data in a post-classification comparison (Luckman *et al.* 1995, Sant'Anna *et al.* 1995), fifteen 10x50m plots in forest were selected. The age map indicated the regenerating stage and size of the area such as to give sufficiently large regions to be averaged within SAR images. Forest areas greater than one hectare were considered suitable for inventory (Luckman *et al.* 1995) and plots were established in forests aged between 2 and around 25 years. The diameter at breast height (dbh) of each tree greater than 3 cm in diameter for young regenerating plots and greater than 15 cm for mature forest plots were measured using a girth tape. Approximately every eighth tree was measured for height using an inclinometer and the remaining tree's height was estimated using a regression technique relating height and dbh (Luckman *et al.* 1997a). Global Positioning System (GPS) readings were also taken at each plot.

These data were used to generate, via allometric equations, an estimate of total above-ground biomass (T ha $^{-1}$) and density (tree ha^{-1}) as described below.

Estimates of biomass of mature forest and pasture plots were required in order to provide an adequate biomass/backscatter range. Pasture plots were not inventoried and were located only in the satellite sensor imagery described later.

4.3. Ground data

In this section the study areas and forest plots described above are presented in relation to their biomass and rainfall data.

4.3.1. Biomass estimates

Total above-ground biomass (T ha $^{-1}$), herein called *biomass,* was estimated for the plots inventoried in Manaus and Tapajós study areas. Allometric regression equations that use the relationship among dbh, height (h), in some cases wood density (S, g cm^{-3}) and biomass (B) were used (Luckman *et al.* 1997a). When available, single species regressions were used, as for *Vismia* and *Cecropia* (equations (1) and (2)). General regressions were used for the rest of secondary and mature forest species (equations (3) and (4)). Wood density values were found for most species in Reyes *et al.* (1992). These equations are shown below, with the authors and for which genus/type of species they were applied to.

- Uhl *et al.* (1988) for *Vismia*:

$$B = 0.0290 \times (dbh^2)^{1.13} \times h^{0.77} \qquad (1)$$

- Uhl *et al.* (1988) for *Cecropia*:

$$B = 0.0298 \times (dbh^2)^{0.950} \times h \quad (2)$$

- Deans *et al.* (1995) for secondary species:

$$B = 0.40 + 0.0406 \times (dbh^2) \times h \times S \quad (3)$$

- Brown *et al.* (1989) for mature species:

$$B = 0.0899 \times (dbh^2 \times h \times S)^{0.9522} \quad (4)$$

All of the mature forest plots (10, 15, 16, 17, 18) for Tapajós study area were located inside the Tapajós National Forest, although only plots 10 and 15 were inventoried.

For Manaus study area, inventory data from 1995 were considered. Biomass estimates for mature forest plots not visited in the field (plot 17 for Manaus and plots 16, 17 and 18 for Tapajós study area) were taken as those estimated for mature forest plot (15) in the Tapajós study area. Pasture plots (plot 18 for Manaus and 19 and 20 for Tapajós study area) were located inside known cattle ranching areas, and the biomass assigned to them was the one associated with established pasture grasses (Eggers, pers. comm. 1999).

Tables 4.3 and 4.4 show plot numbers and coordinates, land cover, biomass, density and basal area estimates for the Manaus and Tapajós study areas, respectively.

Table 4.3: Field data for the Manaus study area. NA refers to not available, NV refers to not visited.

Plot number	Long, Lat coordinates	Land cover	Biomass (T ha^{-1})	Density (trees ha^{-1})	Basal area (m^2 ha^{-1})
1	-59.964,-2.358	Regenerating forest	144.1	2580	25.8
2	-59.953,-2.360	Regenerating forest	131.3	3270	23.9
3	-59.999,-2.352	Regenerating forest	140.3	6880	26.5
4	-59.857,-2.391	Regenerating forest	144.8	2520	26.9
5	-59.888,-2.419	Regenerating forest	134.7	3820	24.3
6	-60.049,-2.291	Regenerating forest	124.3	2590	21.4
7	-60.051,-2.277	Regenerating forest	130.3	2960	24.8
8	-60.0.3,-2.201	Regenerating forest	143.9	2940	24.4
9	-60.041,-2.396	Regenerating forest	91	3460	20.1
10	-60.042,-2.393	Regenerating forest	127	2850	22.6
11	-60.048,-2.403	Regenerating forest	126.1	2680	24.6
12	-60.018,-2.405	Regenerating forest	131.5	7140	27
13	-60.020,-2.207	Regenerating forest	156.6	3830	25.8
14	-60.080,-2.195	Regenerating forest	117.4	3660	20.7
15	-60.174,-2.434	Regenerating forest	116.3	2630	20
16	-60.171,-2.432	Regenerating forest	32.6	5140	15
17	-59.898,-2.483	Mature forest (NV)	387	NA	NA
18	-59.979,-2.354	Pasture (NV)	2	NA	NA

Table 4.4: Field data for the Tapajós study area. NA refers to not available, NV refers to not visited.

Plot number	UTM coordinates	Land cover	Biomass (T ha $^{-1}$)	Density (tree ha^{-1})	Basal area (m^2 ha^{-1})
1	730017, 9632303	Regenerating forest	62	1120	16.8
2	728753, 9637184	Regenerating forest	15	9720	9
3	731555, 9626650	Regenerating forest	62	4400	17
4	740214, 9635587	Regenerating forest	8	10400	4.8
5	733267, 9618849	Regenerating forest	54	1580	11
6	737409, 9605512	Regenerating forest	82	2440	18.3
7	723404, 9693411	Regenerating forest	78	900	16.3
8	734483, 9693376	Regenerating forest	104	1140	20.8
9	735870, 9691362	Regenerating forest	75	1540	18.9
10	731789, 9680134	Mature forest	181	560	17.9
11	742950, 9682087	Regenerating forest	101	1920	17.5
12	739006, 9681246	Regenerating forest	42	3640	19.3
13	729637, 9668093	Regenerating forest	89	2160	17.9
14	729886, 9661866	Regenerating forest	25	3000	7.8
15	733331, 9691809	Mature forest	387	720	37.5
16	720838, 9646571	Mature forest (NV)	387	NA	NA
17	718826, 9636379	Mature forest (NV)	387	NA	NA
18	717528, 9621642	Mature forest (NV)	387	NA	NA
19	729889,9642786	Pasture (NV)	2	NA	NA
20	730614,9641298	Pasture (NV)	2	NA	NA

Biomass estimates for both study areas present a considerable degree of variability, which was expected as the literature reports wide ranges for the biomass of tropical mature and regenerating forests. In addition, it is difficult to account for all potential sources of errors when measuring forest variables, starting with the selection and

assumption of homogeneity of a certain forest plot and as a result, no error assessment was performed. Moreover, there are no error margins associated with the allometric equations used for biomass estimates in this research (Luckman *et al.* 1997a).

Estimates of biomass for dense mature forests varied from 166 to 397 T ha $^{-1}$ as reported by Brown and Lugo (1992) in a comprehensive summary of biomass inventories in Brazilian Amazonia. This research found 387 T ha^{-1} for mature forest in Tapajós, which was consistent with previous findings and suitable for assigning to further known mature forest plots in Tapajós and Manaus study areas.

Regenerating tropical forests biomass values reported in the literature are difficult to extrapolate, as they are age-dependent and a function of previous use (Uhl *et al.* 1988). Estimates of biomass for eight year old regenerating forests varied from 5 T ha $^{-1}$ to 87.1 T ha $^{-1}$, following light, moderate and heavy use of abandoned pastures (Uhl *et al.* 1988). This research found variation between 8 T ha $^{-1}$ and 156.6 T ha $^{-1}$ for regenerating forests in Manaus and Tapajós study areas. Although not considered here, the biomass variation between 8 T ha $^{-1}$ and 156.6 T ha $^{-1}$ reflects the variety of ages and previous land uses of the regenerating forest plots.

4.3.2. Forest regrowth maps

For both study areas, forest age maps were produced and used as a guide in the location of the regenerating forest plots in the ground (Lucas *et al.* 1993 for Manaus age map and Sant'Anna *et al.* 1995 for Tapajós age map). The method for the production of these maps included analysis and classification of TM sensor bands in broad classes such as mature forest, regenerating forest and agricultural land. With each temporal TM sensor band classified, the pixels were traced according to the classes they belonged and a model of changes in land cover was devised (Lucas *et al.* 1993).

For Manaus study area seven classes were mapped: mature forest, pasture and five different ages of regenerating forest (i) <2 years, (ii) 2-3 years, (iii) 3-6 years regenerating from forest, (iv) 3-6 years regenerating from pasture and (v) 6-14 years.

This chronology of forest regrowth for Manaus study area is an additional source of information about the area.

The updated Manaus forest regrowth map was used in chapter 7 as the ground data. Multifrequency and multipolarisation SAR data, along with the 1991 Landsat TM bands 3, 4 and 5, were tested for the discrimination of mature forest, pasture and age classes in a classification approach.

4.3.3. Biomass accumulation simulation

The remote sensing data described in the next chapter cover a period from 1992 to 1997 and the ground data described above are from inventories that represent the biomass for a single date. That was the reason for a biomass accumulation simulation, which results were used later in conjunction with backscatter.

Dividing biomass by the estimated age of the regenerating forest is usually how biomass accumulation rates are estimated (Alves *et al.* 1997, Lucas *et al.* 2000). This procedure, however, was not applicable in Tapajós data, as the age of the regenerating forest plots was not available.

Seven plots in Manaus study area had their measurements taken in two field campaigns, in 1993 and in 1995. An increase in biomass was observed for all plots over the two years period, although rates were variable. The biomass estimates were grouped and subtracted (biomass data from 1995 minus biomass data from 1993), producing an averaged monthly rate of biomass of 0.6 T ha^{-1} (annual increase of 7.2 T ha^{-1}). This value was added or subtracted from the biomass estimates for the regenerating forest plots depending on the dates of their inventory.

Biomass accumulation rate of 7.2 T ha^{-1} $year^{-1}$ is within the range already found for Manaus study area plots (Lucas e*t al.* 2000). Assuming a linear rate of growth, however, may not be a valid assumption, mainly when dealing with forests younger than 10 years (Lucas *et al.* 2000). These authors also found different biomass accumulation rates depending on the successional pathway that regenerating forests follow, which was determined by, among other things, the differences in previous land use intensity.

4.3.4. Floristic composition

When describing the nature of vegetation communities, some techniques are proposed to rank species in relation to others (Krebs 1978). The Importance Value Index (IVI) is used to define the relative dominance of species of a certain community and enables the comparison among different communities (Krebs 1978). IVI was derived for Manaus and Tapajós regenerating forest plots (tables 4.5 and 4.6).

For Manaus study area a comprehensive study on the plots has been undertaken. With the help of IVI and historical data, the age of the plots and their successional pathway could be traced. The floristic composition of the regenerating forest plots was analysed using TWINSPAN classifier (Lucas *et al.* 2000). The plots were classified according to their species composition and tree basal area (m^2 ha^{-1}). Three levels and eight groups were defined, differing basically by the dominant species (table 4.7).

Table 4.5: Dominant genera for the Manaus regenerating forest plots.

Plot number	Dominant genera
1	*Cecropia*
2	*Vismia, Cecropia*
3	*Vismia, Goupia*
4	*Cecropia, Guatteria*
5	*Vismia, Bellutia*
6	*Vismia, Cecropia*
7	*Cecropia, Laetia*
8	*Cecropia*
9	*Cecropia*
10	*Cecropia*
11	*Cecropia, Laetia*
12	*Vismia*
13	*Laetia, Vismia*
14	*Vismia, Miconia*
15	*Goupia, Vismia*
16	*Goupia, Vismia*

Table 4.6: Dominant genera for the Tapajós regenerating forest plots. NA refers to not available.

Plot number	Dominant genera
1	*Cecropia*
2	NA
3	*Poecilanthe, Cecropia*
4	*Poecilanthe, Vismia*
5	*Vismia*
6	*Vismia*
7	*Mangifera*
8	*Guatteria*
9	*Orbignya*
10	*Couratari*
11	*Sloanea*
12	*Orbignya, Poecilanthe*
13	*Vismia, Guatteria*
14	*Vismia*
15	*Orbignya*

Table 4.7: Classification of floristic composition of the Manaus regenerating forest plots (Lucas *et al.* 2000).

Level	Group	Classification
Vismia-dominated	1	*Vismia*-dominate (pasture)
Cecropia	2	*Cecropia*-mixed
	3	*Cecropia*-dominated (<10 years)
	4	*Cecropia*-dominated (>10 years)
	5	*Cecropia-Bellucia*
Mixed species	6	*Vismia*-mixed (non-pasture)
	7	*Goupia*-mixed
	8	Mixed (>20 years)

All plots were dominated by pioneer species and the common genera *Cecropia* and *Vismia* were present in almost all forest regeneration categories in table 4.7. *Vismia*-dominated forests occurred where pastures had been used previously for moderate to long periods. In contrast, *Cecropia* dominated both pasture and non-pasture sites that had been used for less than two years. Both levels could have been submitted to fire, although in some plots this was not certain. Mixed forests were found in smaller clearances and its history was uncertain with previous use ranging from short to long periods (Lucas *et al.* 2000).

The forest plots inventoried at Manaus study area may be typical of regeneration following low intensity of previous use and therefore their biomass and succession pathways varied accordingly (Lucas *et al.* 2000).

For the Tapajós study area, however, historical information was not fully available and the floristic composition of its regenerating forest plots did not seem to provide evidence of their successional pathway. Only two plots were dominated by *Cecropia* and four plots dominated by *Vismia* genera, which could lead to the assumption that the previous use of the regenerating forests plots were heavier that the plots at Manaus study area. Most of the plots were previously cleared and burned to be used as agricultural land for a variety of crops (excluding pasture) (Shimabukuro *et al.* 1997). Floristic composition (table 4.6) varied in relation to Manaus plots, but was also representative of regenerating forests in Brazilian Amazonia.

4.3.5. Rainfall and cloudiness data

Rainfall data for both study areas were available on a daily basis, but for Tapajós the weather station from Brazilian Meteorological Office (Barragem Curuá-Una Station, coordinates 2°47'00"S, 54°16'16"W) was situated around 50 km from the regenerating forest plots. As the rain in equatorial climates occurs in localised cells (convective type), these rainfall data may not be representative of the Tapajós study area. Therefore meteorological images such as from GOES (Geostationary Operational Environmental Satellite) and Meteosat sensor satellites were checked to confirm the cloudiness and rainfall. The meteorological images were chosen to be the closest possible to the time of the JERS-1 satellite overpass, which was usually

around 15:00 GMT. Figure 4.3 shows both study areas in a cloud-free GOES-8 sensor image.

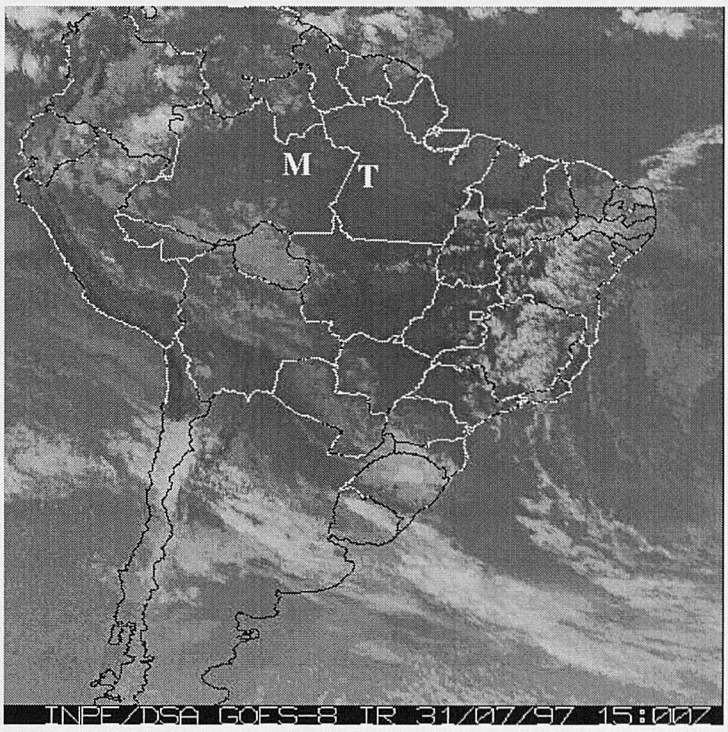

Figure 4.3: GOES-8 image for 31/07/1997, showing no cloudiness for (M) Manaus and (T) Tapajós study areas.

For the Manaus study area, data on rainfall were gathered from the LBA website (Large Scale Biosphere-Atmosphere Experiment in Amazonia, from Brazil). The actual site where the rainfall measurements were taken is Fazenda Dimona, one of the reserves of the BDFFP (coordinates 02°19'S, 60°19'W). The data were available on a daily basis for 1994, 1995 and for part of 1996. For 1993 rainfall data were from the Brazilian Meteorological Office (Balsa do Rio Urubu Station, coordinates 2°54'47"S, 59°2'2"W) around 100 km away from the study area and without GOES sensor data available to confirm them. Table 4.8 and 4.9 show the rainfall totals for the day before the JERS-1 overpass, the total for ten days before the satellite overpass and cloudiness conditions when GOES or Meteosat sensor images were available.

Table 4.8: Rainfall totals (mm) and cloudiness conditions over the Manaus study area. NA refers to not available.

JERS-1 overpass	Day before	Ten days before	Cloudiness
23/02/93	16.3	80.9	Yes
01/10/93	0	25.4	No
10/02/94	1.2	108.6*	NA
05/08/94	0	5.4	No
28/01/95	10.6	102.2	Yes
02/12/95	1.8	49.8	Yes
12/04/96	NA	NA	Yes
22/08/96	0	0	No

* 7 days before the satellite overpass.

Table 4.9: Rainfall totals (mm) and cloudiness conditions over the Tapajós study area. NA refers to not available.

JERS-1 overpass	Day before	Ten days before	Cloudiness
22/08/92	0	29.4	NA
14/02/93	0	44.8	NA
30/03/93	83.8	154.1	Yes
26/06/93	0	17	No
27/07/94	0	11	No
19/01/95	0	39.3	No
10/10/95	0	0.2	No
17/05/96	0	51.5	No
13/08/96	0	2.2	No
31/07/97	0	7.4	No

There was a remarkable agreement between the rainfall totals and the cloud conditions in the meteorological satellite sensor images over the study areas. The rainfall data seemed to be suitable for inferring the water content of the regenerating forest plots.

CHAPTER FIVE

Temporal analysis of JERS-1 SAR data for regenerating tropical forests

In this chapter, the temporal behaviour of regenerating tropical forests on JERS-1/SAR images was investigated. Following a phase of data pre-processing, which involved geometric correction and registration, the Digital Number (DN) of regenerating forest plots were collected. The regenerating forest plots are located in Manaus and Tapajós study areas, as described in the previous chapter. GPS coordinates taken at the plots on the ground and TM images from the study areas allowed the collection of the DN. The DN were later converted to backscatter coefficient (σ°), herein called backscatter.

SAR images for both the wet and dry seasons and some rainfall data for the study areas were available for this research. That allowed an investigation of the influence of seasonally changing variables in σ°. As possible sources of temporal variation on σ°, the variables investigated were biomass and rainfall. The objective of this analysis was to assess the utility of a temporal series of JERS-1/SAR images to detect changes in σ° (or $\Delta\sigma^\circ$). The ultimate goal was to detect biomass accumulation in regenerating forests in two study areas in Brazilian Amazonia based on $\Delta\sigma^\circ$.

5.1. JERS-1 satellite

The NASDA (National Space Development Agency of Japan) and MITI (Ministry of International Trade and Industry of Japan) launched the Japanese Earth Resources (JERS-1) satellite in 11 February 1992. The satellite carried a Synthetic Aperture Radar (SAR) and an Optical Sensor (OPS). Despite its two years designed lifetime the

SAR and some of the bands of the optical sensor were able to observe the Earth for more than six years, until October 1998. Table 5.1 shows the main characteristics of the JERS-1 satellite and its SAR.

Table 5.1. Main characteristics of JERS-1 and its SAR (RESTEC leaflet).

Altitude	568 km
Orbit	Sun synchronous
Recurrent period	44 days
Antenna size	11.9 m x 2.4 m
SAR frequency and wavelength	1.275 GHz, 23.5 cm (L band)
SAR polarisation	HH
SAR incident angle	38.5° (to the centre of swath)
SAR swath width	75 km
SAR ground resolution	18 m x 18 m (3 looks)

Of the SAR parameters cited above, the band and polarisation (L and HH) make this sensor suitable for the study of regenerating tropical forests. L_{HH} is able to penetrate into the vegetation canopy and discrimination between biomass levels is possible (Pope *et al.* 1994, Luckman *et al.* 1998). Coupled with that, the all-weather capabilities of a L band SAR sensor and the recurrent period of 44 days for the JERS-1 further increase its utility (Rosenqvist *et al.* 2000).

5.2. The GRFM project

The Global Rain Forest Mapping (GRFM) project is a joint effort led by NASDA to acquire a cloud-free data set of the major rain forest areas on Earth. The project, started in 1995, covered an area of about 40000 km^2, from the Amazon Basin to South-East Asia (Rosenqvist *et al.* 2000). As a major aim of the project, SAR image

mosaics at 100 m resolution were generated for Africa, South America and South-East Asia (Rosenqvist *et al.* 2000). The GRFM project involved 29 technical studies at local to global scales, led by researchers in universities and scientific organisations worldwide. These studies were generally supported by ground campaigns and aimed the assessment of the state of forest and associated flood plains, as can be seen in Shimada (1999).

As one of the British counterparts of the GRFM project, the present research was provided with a series of JERS-1/SAR images, enumerated in the next section.

5.3. JERS-1 SAR data

The original JERS-1/SAR images were processed by NASDA and available for this research at level 2.1. This level corresponds to standard georeferenced amplitude images resampled to Universal Transverse Mercator (UTM) projection and with pixel size of 12.5 m. The GRFM SAR data were corrected using corner reflectors deployed in non-forested areas in Japan, USA, Alaska and Brazil. For correcting the antenna pattern related radiometric errors (range and azimuth dependent), large areas of tropical rainforest were used as references. According to Chapman *et al.* (1999), multi-temporal studies can be undertaken on JERS-1 SAR data. In equation (5.1) the "calibration" factor of (-68.5) is set to compensate for absolute errors and is accurate to around 1 dB. NASDA image products are quantified to 16 bits and the minimum DN (corresponding to low σ° of around –20 dB) is around 265 (Chapman *et al.* 1999).

The study areas in Manaus and Tapajós were extended over two JERS-1 SAR scenes hence two images were obtained for each of the dates. Data on eight dates were obtained for the Manaus study area, while the Tapajós study area was covered in ten dates. The overall period of study covered 60 months and for ease of analysis each of the dates was coded by month from August 1992 to July 1997. Tables 5.2 and 5.3 present the characteristics of the SAR images for each study area. A total of 16 images (8 dates) were obtained for the Manaus study area and 20 images (10 dates) were obtained for the Tapajós study area. Table 5.4 shows the SAR data for both study areas plus new codes for months used in a joint analysis in section 5.5.5.

Table 5.2. JERS-1/SAR images for the Manaus study area.

Path/Row	Path/Row	Date	Season	Month
414/304	414/305	23/02/93	wet	1
414/304	414/305	01/10/93	dry	9
414/304	414/305	10/02/94	wet	13
414/304	414/305	05/08/94	dry	19
414/304	414/305	28/01/95	wet	24
414/304	414/305	02/12/95	wet	35
414/304	414/305	12/04/96	wet	39
414/304	414/305	22/08/96	dry	43

Note: Approximate central coordinates for path/rows 414/304 are 2°05'S, 59°4'W and for 414/305 are 2°41'S, 59°50'W.

Table 5.3. JERS-1/SAR data for the Tapajós study area

Path/Row	Path/Row	Date	Season	Month
405/305	405/306	22/08/92	dry	1
405/305	405/306	14/02/93	wet	7
405/305	405/306	30/03/93	wet	8
405/305	405/306	26/06/93	dry	11
405/305	405/306	27/07/94	dry	24
405/305	405/306	19/01/95	wet	30
405/305	405/306	10/10/95	dry	39
405/305	405/306	17/05/96	wet	46
405/305	405/306	13/08/96	dry	49
405/305	405/306	31/07/97	dry	60

Note: Approximate central coordinates for path/rows 405/305 are 2°24'S, 54° 34'W and for 405/306 are 3°10'S, 55°03'W.

Table 5.4. JERS-1/SAR images dates for the Tapajós (T) and the Manaus (M) study areas and their month codes.

Location-Date	Season	Month	Location-Date	Season	Month
T-22/08/92	dry	1	T-19/01/95	wet	30
T-14/02/93	wet	7	M-28/01/95	wet	30
M-23/02/93	wet	7	T-10/10/95	dry	39
T-30/03/93	wet	8	M-02/12/95	wet	41
T-26/06/93	wet	11	M-12/04/96	wet	45
M-01/10/93	dry	15	T-17/05/96	wet	46
M-10/02/94	wet	19	T-13/08/96	dry	49
T-27/07/94	dry	24	M-22/08/96	dry	49
M-05/08/94	dry	25	T-31/07/97	dry	60

5.4. Methods

The images were pre-processed using geometric corrections before the extraction of the pixel DNs and conversion to backscatter. These backscatter values were then analysed with the ground data by the steps described next.

5.4.1. Geometric correction and registration

Very often remotely sensed images need to be transformed to a product with properties similar to a map, with a known scale and projection. The sources of distortions in remotely sensed images are linked to sensor and satellite instabilities, as well as the Earth's rotation. The location of the study area, the overlay of temporal sequences and the generation of maps are some of the circumstances where the geometric correction of the images are required. The fitting of coordinates between two images of the same area is called registration (Mather 1999). The geometric correction process includes the determination of a common coordinate system between images and maps by the establishment of a set of ground control points. A map-to-image coordinate transformation is achieved using polynomial functions from

first to third-order. A first-order polynomial function can accomplish the geometric correction of images with no strong "bending" effects. A higher order polynomial function will be selected to achieve the correction of large distortions on satellite sensor imagery (Mather 1999).

The assignment of the DN associated with the new corrected pixels is done by means of a resampling. The nearest neighbour resampling preserves the original DN, as it takes the closest pixel value to be the new output pixel value. Other methods of resampling such as bilinear and cubic convolution involve spatial interpolations that produce new DNs out of the original ones (Mather 1999).

In the case of this research, both Manaus and Tapajós study areas contain few natural or anthropogenic features suitable for use as ground control points. The geographic position of those ground control points was taken from topographical maps of the study areas. However, the ground features chosen as control points were much easier to locate on optical than on SAR images. For that reason the SAR images were registered to geometrically corrected Landsat Thematic Mapper (TM) images of the same area.

For the Manaus study area a Landsat TM image (orbit 231/62 of 08/08/1991) was geometrically corrected to a UTM projection using ground control points from a topographic map. A first-order polynomial was used for the mapping and a nearest neighbour resampling was performed. The final pixel size of the TM image was 25 metres. The SAR image from February 1993 was registered to the TM image and the fifteen remaining SAR images were subsequently co-registered. The number of ground control points used for the registering between images was around 18 and the total RMS errors were of less than one pixel.

Prior to the registration with the TM image, sets 2x2 pixels on the SAR images were averaged spatially, generating a nominal spatial resolution of 25 metres. Averaging the pixels before resampling reduced the speckle, but retained the statistical properties of the SAR images (Luckman *et al.* 1998).

The procedure applied for the Tapajós study area was nearly the same as described above. A Landsat TM image (orbit 227/62 of 29/07/1992) was corrected geometrically to a UTM projection using ground control points from a topographic map. The SAR image from June 1993 was registered to the TM image and then the nineteen

remaining SAR images were co-registered. The number of ground control points used for the registering between images was around 18 and the total root-mean-square (RMS) errors of the registration were of less than one pixel.

5.4.2. DN to σ° conversion

Pixel Digital Numbers (DN) of the SAR images were converted to backscatter coefficient (σ°) in decibels (dB) via equation:

$$\sigma^{0} = 10 \times \log_{10}\left[\sum (DN)^{2} / n\right] + CF \qquad [5.1]$$

where n is the number of pixels extracted from the images and CF is the "calibration" factor of –68.5 (Rosenqvist 1996a).

Equation (5.1) was applied in two steps. Firstly, to obtain backscatter in linear units and prepare the data for the fitting of a model as explained in next section, the images were squared and divided by ($10^{6.85}$). To correlate backscatter with the ground data, a mean value of backscatter was derived from the plots located on the images. Twenty plots were located on the Tapajós images and eighteen plots on Manaus images, using their GPS coordinates, knowledge of the area and Landsat TM images. The smallest polygon used for the estimation of the mean backscatter was composed of 14 pixels or 8750 m^2, following the recommendation of Luckman *et al.* (1997a). The polygons were located in large homogeneous areas where the biomass was assumed to be the same as the one measured on the ground. Standard deviation of backscatter was also computed for each polygon representing the plots in the different images. Linear units of mean and standard deviation of backscatter were converted to decibels by multiplying by a 10 x $\log_{10}$ factor.

The images from January 1995 (North portion) for Tapajós and from October 1995 for Manaus contained a stripe with noisy data in the North-South direction and these data were discarded. To replace the missing data for Manaus, NASDA provided a pair of images from December 1995 (table 5.2).

5.4.3. Principal Components Analysis (PCA)

Principal Component (PC) analysis is a statistical technique used to (i) identify groups of interrelated variables, (ii) reduce the redundancy of variables by reducing the number of variables and (iii) rewrite the variables in an alternative form (Johnston 1980).

For remotely sensed data, PCA is used to generate new images which are often more interpretable than the original data. It is also used to compress the information content of a series of images (such as different bands of the same image or temporal sequences of images over the same scene) into a reduced number of images, called the principal component images (Jensen 1986). The PC transformation reduces the spectral redundancy of data and generates uncorrelated multispectral data that has ordered variance properties (Jensen 1986). PC translates the original data axes so that they are reprojected onto a new set of axes or dimensions. The first of this new set of axes is associated with the maximum amount of variance found in the original data set. This is the first principal component or eigenvalue (PC1) and represents the variance of the particular PC mode 1. The second principal component (PC2) is orthogonal to the first and comprises the second largest amount of variance found in the data set. The third, fourth, fifth, and so on, principal components contain decreasing amounts of variance.

The eigenvectors are a set of coordinates defining the direction of the associated eigenvalue. The length and direction of the PCs are described by the eigenvalues and eigenvectors (Mather 1999). The eigenvectors can also be interpreted as the correlation between the original images and the new generated principal components (Mather 1999). In practical terms, this correlation (or factor loading) informs what image, out of the original set, contributed more to each of the PC modes.

In this work PCA was used to provide additional information about the change in the spatial time series SAR data for both study areas. Standardised PCs were obtained based on the correlation matrices (Eastman and Fulk 1993) of 8 SAR images for the Manaus study area and 10 SAR images for the Tapajós study area

5.4.4. Exploratory statistical analysis

An exploratory statistical analysis was undertaken on the mean backscatter for each plot and date. Normality tests were undertaken as normality is a pre-requisite for the Analysis of Variance (ANOVA) performed later. The objective of this statistical analysis was to detect significant differences in σ° between SAR dates.

For the Manaus study area, the distribution of the data were normal (*Kolmogorov-Smirnov* test, $p>0.0001$) so the mean backscatter could be considered. ANOVA indicated that the differences in the mean backscatter values among the dates were statistically significant at the 95% level of confidence ($F=5.61$, d.f.=7, $p<0.05$).

For the Tapajós study area, the distribution of the data were non-normal (*Kolmogorov-Smirnov* test, $p<0.0001$). In this case, the median of the mean backscatter was considered. The median of the mean backscatter values for each SAR date differed significantly at the 95% level of confidence (*Kruskall-Wallis* ANOVA, $H=20.4$, d.f.=9, $p<0.05$).

The variability in the mean backscatter for Manaus data and in the median of the mean backscatter for Tapajós data were a pointer to the temporal component explored.

5.4.5. Modelling backscatter/biomass relationship

From the trend observed in the data when plotting backscatter against biomass, it was observed that using a logarithmic (log) function of biomass would resulted in a stronger correlation between these data than if using a linear function (Dobson *et al.* 1992; Ranson and Sun 1994). That was probably because of the log function used to convert DN to σ°. Consequently, a model with a log fitting (equation 5.2) was applied to describe the relationship between backscatter and biomass. The model is as follows:

$$\sigma^0 = a_0 + a_1 \times \log(\text{biomass}) \qquad [5.2]$$

where σ° is the backscatter in dB and a_0 and a_1 are the coefficients of the log fitting. Biomass was in units of T ha^{-1}.

The log fitting, however, did not allow quantification of the asymptotic region where backscatter is insensitive to biomass (Le Toan *et al.* 1992, Dobson *et al.* 1992, Ranson and Sun 1994, Imhoff 1995a, Luckman *et al.* 1997a).

To assess the asymptote in the backscatter/biomass relationship, a second model (equation 5.3) was fitted to the data (Luckman *et al.* 1998, Fransson and Israelsson 1999). This model was based on a water cloud model designed by Attema and Ulaby (1978) which represents the extinction of microwaves as they pass through a layer of vegetation made up of elements containing water (Luckman *et al.* 1998). The parameter *a* corresponds to the saturation point of σ° (in linear units) or when the asymptote in the relationship backscatter/biomass is reached. *B* refers to biomass in units of T ha^{-1}.

$$\sigma^0 = a - e^{(bB+c)} \qquad [5.3]$$

To get a better fitting of the model, pasture plots in both study areas were included in the analysis. Although not visited on the ground, these plots were assigned a biomass of 2 T ha^{-1} (Eggers, pers. communication, 2000).

For the Manaus study area the fitting of equation (5.3) was compromised by the lack of low biomass values for regenerating forest plots. For this reason the data for the two study areas were combined.

The relationship between backscatter and biomass was determined and subsequently the temporal behaviour of σ° was examined. Different types of analyses allowed some potential sources of variation in σ° to be investigated. The main points were:

- The *temporal behaviour of DN* was assessed through PCA to provide information about change in the spatial time series of SAR data for both study areas.

- The *temporal behaviour of* σ^o was assessed through plotting the mean σ^o for each regenerating forest plot against time. Three-dimensional graphs were also produced to visualise the influence of different biomass levels in the long term distribution of σ^o. In addition to that, residuals from the mean backscatter for each plot were plotted to detect any existing anomaly in the data.

- The influence of the *biomass accumulation* on the behaviour of σ^o was also determined. Seven plots in Manaus study area had their measurements taken in two field campaigns, in 1993 an in 1995. Their biomass estimates were grouped and subtracted, producing an averaged monthly increase of biomass of 0.6 T ha^{-1}. This value was added or subtracted from the biomass estimates for the regenerating forest plots depending on the dates of their inventory. This biomass accumulation was simulated regardless the history of disturbance and age of vegetation in the regenerating forest plots.

- To investigate the *influence of rainfall* on SAR data, rainfall measurements were plotted alongside the mean backscatter of some regenerating and mature forest plots for both study areas.

5.5. Results and discussion

This section presents the results of investigations conducted on some of the possible sources of temporal variation in σ^o. Backscatter/biomass relationships for both study areas are presented, along with an attempt to describe the temporal behaviour of σ^o for regenerating and mature forest plots. An investigation of a possible cyclical pattern of σ^o is presented as well as a simulation of the biomass accumulation during the time span studied. Finally, the potential influence of rainfall on SAR data is discussed.

5.5.1. PCA

SAR images from 8 dates were used for the Manaus study area (table 5.5) and SAR images from 10 dates (referred as bands) were used for the Tapajós study area (table 5.6). Month code was used to ease the identification of trends in the graphs.

Generally the correlation between SAR bands was low. The maximum correlation coefficient of 0.55 was found between bands 4 (June 1993) and 8 (May 1996) for Tapajós study area data. The first four principal components of both study areas concentrated around 70 % of the variance of the original SAR bands (table 5.5 and 5.6). As a result of decreasing information content of PCs with the decline in variance, the last PCs are likely to contain mainly the noise of the original SAR bands (Kuplich *et al.* 2000a).

For both study areas, the first principal component image was the only to depict the land covers (e.g. pasture and regenerating forest plots) or features seen in the original SAR bands from where they were derived. In addition, those features were exceptionally enhanced and contrasted from the mature forest that is the major land cover for both study areas images. The remaining components did not depict any feature visually interpretable. They seemed to be variations around different levels of fine texture and tone.

For the Manaus study area, band 1 (February 1993) and band 6 (December 1995) contributed with positive eigenvectors (table 5.5 and figure 5.1) suggesting positive correlation of these bands with the features seen in PC1. Similarly, those bands could contain unapparent spatial patterns very alike to the ones depicted in PC1 (Eastman and Fulk 1993).

For Tapajós study area band 1 (August 1992), band 2 (February 1993) and band 4 (June 1993) presented significant positive eigenvectors (table 5.6 and figure 5.2) suggesting positive correlation of these bands with the features seen in PC1.

Table 5.5. Principal components coefficients (eigenvectors in columns and eigenvalues in bottom row as the percentage of variance) for the Manaus study area SAR images. Cum. Perc. refers to the cumulative percentage of variance.

Date (Month)	PC1	PC2	PC3	PC4	PC5	PC6	PC7	PC8
02/93 (1)	0.336	0.319	0.317	0.406	0.391	0.358	0.318	0.372
10/93 (9)	-0.386	-0.422	-0.375	0.065	0.410	0.139	0.576	-0.096
02/94(13)	-0.386	-0.438	0.486	-0.186	-0.184	0.319	-0.107	0.491
08/94(19)	-0.066	0.050	0.549	-0.217	0.095	-0.653	0.453	-0.073
01/95(24)	-0.578	0.715	-0.048	-0.243	-0.111	0.243	0.148	-0.029
12/95(35)	0.461	-0.084	0.074	-0.570	-0.209	0.445	0.351	-0.293
04/96(39)	-0.195	-0.076	0.462	0.327	0.117	0.260	-0.189	-0.720
08/96(43)	-0.023	-0.044	-0.031	0.509	-0.753	-0.018	0.413	-0.015
Percentage variance	34.04	12.84	11.34	9.37	8.66	8.55	7.99	7.21
Cum.Perc..	34.04	46.88	58.22	67.59	76.25	84.80	92.79	100

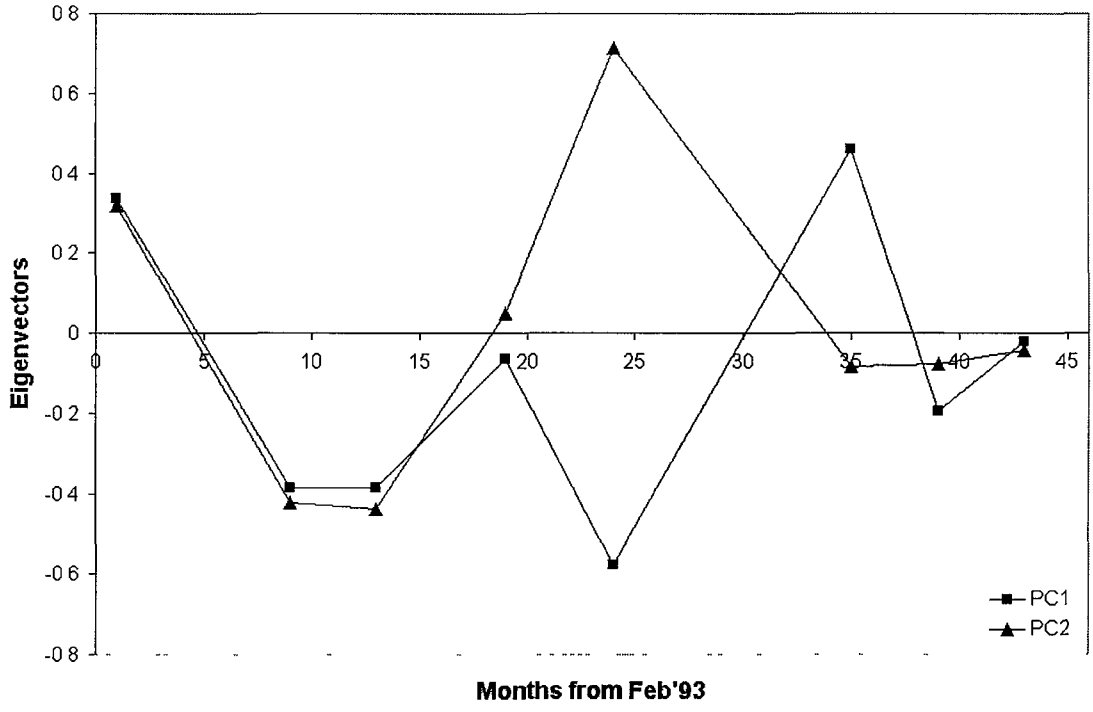

Figure 5.1. Eigenvectors for the first and second principal component from Manaus study area SAR images. Dates corresponding to month codes are in table 5.5.

Table 5.6. Principal components coefficients (eigenvectors in columns and eigenvalues in bottom row as the percentage of variance) for the Tapajós study area SAR images. Cum. Perc. refers to the cumulative percentage of variance.

Date (Month)	PC1	PC2	PC3	PC4	PC5	PC6	PC7	PC8	PC9	PC10
08/92(1)	0.264	0.327	0.318	0.315	0.328	0.316	0.320	0.329	0.317	0.323
02/93(7)	0.640	-0.217	0.214	0.342	-0.206	-0.203	-0.306	0.307	-0.281	-0.175
03/93(8)	-0.254	0.365	0.460	0.164	0.370	-0.478	-0.107	-0.221	-0.371	0.015
06/93(11)	0.648	0.266	-0.205	-0.499	0.248	-0.171	0.192	-0.294	-0.071	-0.018
07/94(24)	0.023	-0.139	-0.321	0.129	-0.088	-0.345	-0.023	0.014	-0.104	0.850
01/95(30)	-0.052	-0.095	-0.299	0.385	0.000	-0.347	0.722	0.067	-0.072	-0.316
10/95(39)	-0.040	0.019	-0.066	-0.036	0.016	0.528	0.204	0.066	-0.810	0.106
05/96(46)	0.018	0.256	-0.608	0.419	0.390	0.152	-0.431	-0.048	0.010	-0.160
08/96(49)	-0.013	0.729	-0.092	0.061	-0.673	-0.035	-0.002	0.045	-0.012	-0.011
07/97(60)	-0.177	0.130	-0.156	-0.405	0.198	-0.242	-0.075	0.806	-0.075	-0.074
Percentage variance	51.88	8.48	6.54	5.59	5.05	4.87	4.75	4.55	4.36	3.93
Cum.Perc.	51.88	60.36	66.90	72.49	77.54	82.41	87.16	91.71	96.07	100

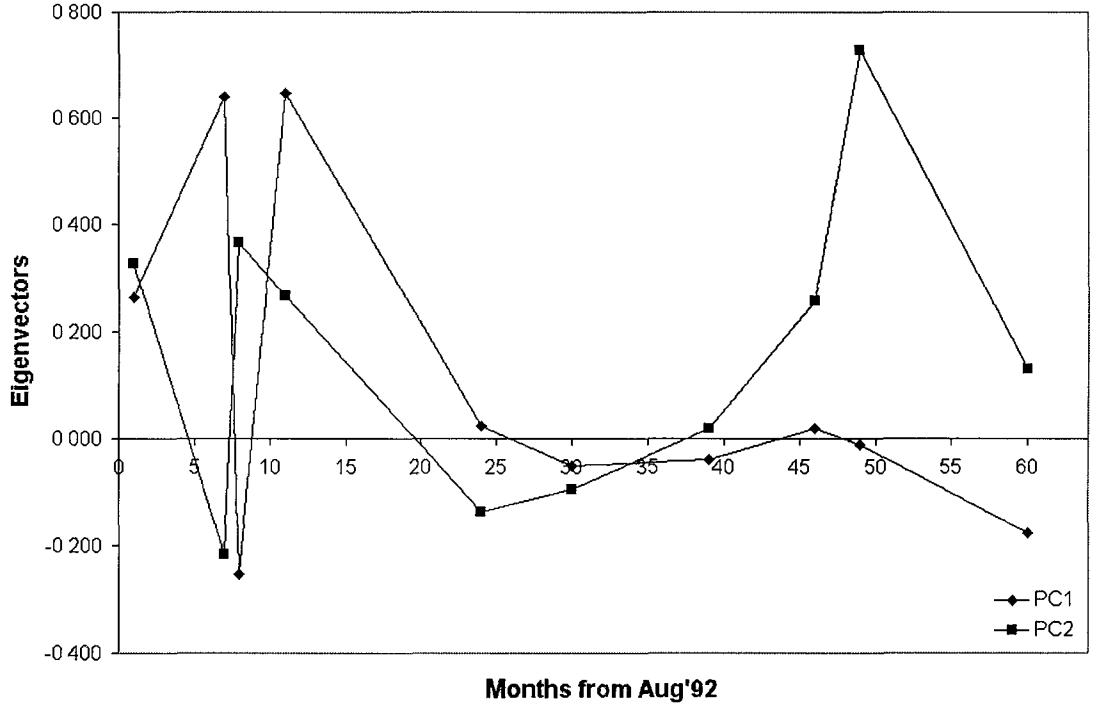

Figure 5.2. Eigenvectors for the first and second principal component from Tapajós study area SAR images. Dates corresponding to month codes are in table 5.6.

SAR image time series can enable assessment of land cover variation whether due to seasonality or disturbance. For the images studied here, however, the main land cover – mature forest - has not been submitted to any dramatic change, either seasonal or as a result of disturbance. Therefore the results of PCA demonstrated that the DN variability in the SAR time series was high but not particularly spatially related. PC1 for both study areas summarised the features potential to change in a spatial/temporal perspective: the relative small areas covered by agricultural/pasture activities and the regenerating forests. The remaining PCs presented features not interpretable in terms of spatial variations. Nevertheless, the PCA did not show any particular temporal or sensor derived anomaly that could hinder the analysis to be performed next. In addition, the weather conditions during the dates of SAR images acquisition and biomass status of the vegetation may prove useful for understanding the variability shown during the PCA.

5.5.2. Backscatter and biomass

The relationship between backscatter and biomass was positive for both study areas. The resulting correlation coefficient (*r*) for Manaus data was 0.68 (figure 5.3) and 0.77 for Tapajós data (figure 5.4). The biomass range was not so wide in Manaus as it was in Tapajós study area. Perhaps this was the reason why the correlation between backscatter and biomass was lower for Manaus data.

Figures 5.5 and 5.6 display the results of regressions using the mean backscatter values for each of the plots in the Manaus and Tapajós study areas, respectively. Both regressions showed a stronger relationship between backscatter and biomass, with correlation coefficients of 0.8 (Manaus) and 0.87 (Tapajós).

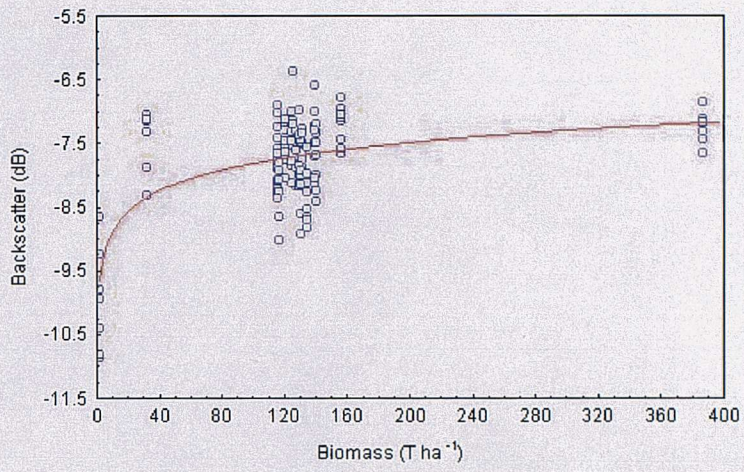

Figure 5.3: Relationship between backscatter and biomass for pasture, regenerating and mature forest plots at the Manaus study area where all data for individual dates were plotted (r=0.68, σ° = -9.99+0.47*log (biomass), 46% variance accounted for).

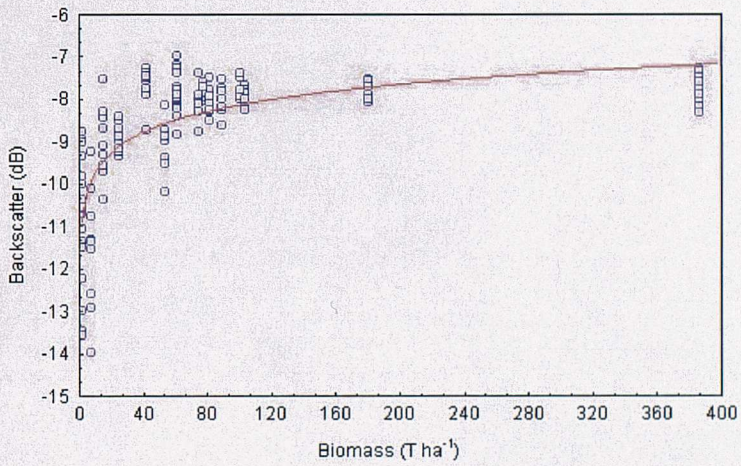

Figure 5.4. Relationship between backscatter and biomass for pasture, regenerating and mature forest plots at the Tapajós study area where all data for individual dates were plotted (r=0.77, σ° = -11.38+0.7031*log (biomass), 59% variance accounted for).

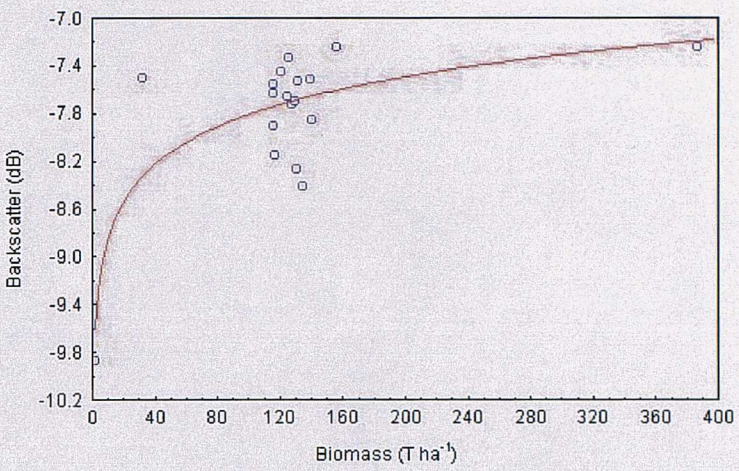

Figure 5.5: Relationship between backscatter and biomass for pasture, regenerating and mature forest plots at the Manaus study area where averaged data were plotted (r=0.80, σ° = -9.92+0.46*log (biomass), 64% variance accounted for).

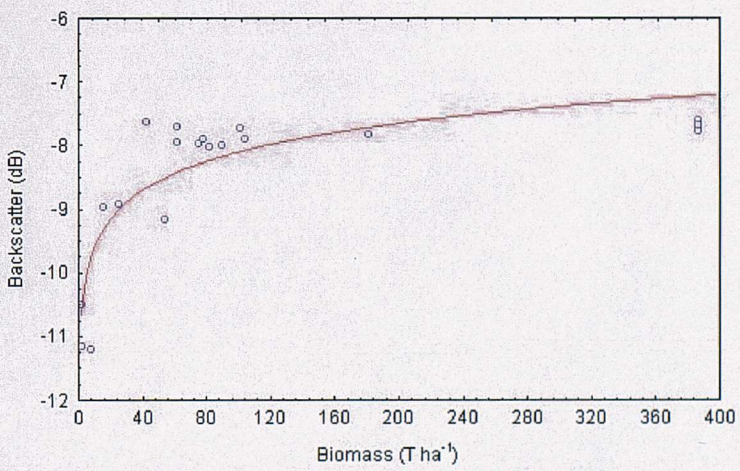

Figure 5.6. Relationship between backscatter and biomass for pasture, regenerating and mature forest plots at the Tapajós study area where the mean backscatter for each plot was used. (r=0.87, σ°=-11.12+0.65*log(biomass), 76% variance accounted for).

The log model (equation 5.2) utilised here indicated the strength of the backscatter/biomass relationship. It did not allow, however, to set a limit for the estimation of biomass from backscatter, as the log does not converge to an asymptote. Figure 5.7 shows the results of fitting the second model (equation 5.3), from which it was possible to predict the location of the asymptote and up to what extent backscatter is sensitive to biomass.

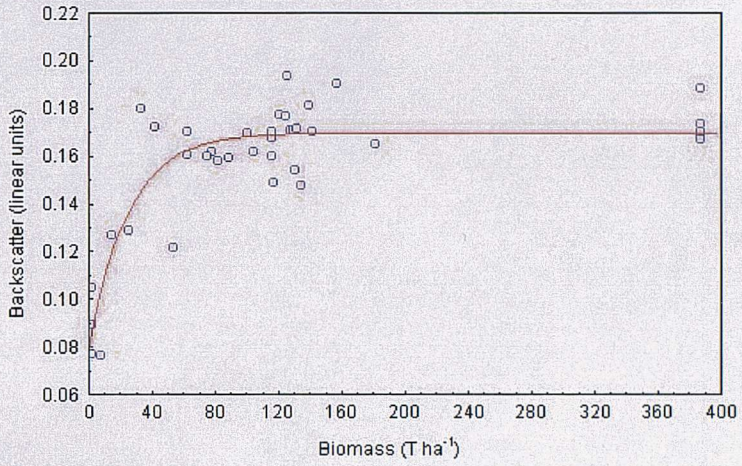

Figure 5.7: Relationship between backscatter/biomass for pasture, regenerating and mature forest plots at the Tapajós and Manaus study areas. The curve represents the fitted model (Luckman *et al.* 1998) with r=0.87 and 76% of the variance accounted for. The parameters of the fitted model were a=0.17, b=0.04 and c=2.4.

Using equation (5.3) (figure 5.7), the relationship between backscatter and biomass was found to be stronger (r=0.87) than in the other fittings (figures 5.1 to 5.4). The asymptote was reached at backscatter of 0.17 (–7.70 dB), which corresponds to biomass of around 90 T ha^{-1}. These values are consistent with previous works (Le Toan *et al.* 1992, Dobson *et al.* 1992, Imhoff 1995a, Wang *et al.* 1995). For tropical regenerating forests, it is reported that L band backscatter saturated at biomass levels of between 40 T ha^{-1} and 100 T ha^{-1} (Imhoff 1995a, Luckman *et al.* 1997a, Araújo *et al.* 1999). These biomass saturation levels would limit the detection and estimation of biomass for regenerating forests under 13 years old (Uhl *et al.* 1987, Brown and Lugo 1990).

5.5.3. Biomass accumulation simulation

Considering the simulation of the biomass accumulation, the model described in equation (5.3) was applied to Manaus and Tapajós data. The resulting correlation coefficient (*r*) was 0.77 (figure 5.8). The parameter from which the asymptote can be defined was 0.17, corresponding to –7.64 dB or biomass values of around 100 T ha^{-1}. The biomass accumulation was simulated in a simplistic way, but the correlation coefficient between backscatter and biomass indicated consistency in the new biomass values. Nevertheless, the correlation coefficient was lower than the one obtained with constant biomass values for the time span analysed (figure 5.7). The biomass simulation performed here might have created a variety of biomass values not actually present in the field and therefore not followed by comparable backscatter responses. The apparent backscatter saturation from biomass values around 100 T ha^{-1} have probably limited the correlation analysis up to this biomass value.

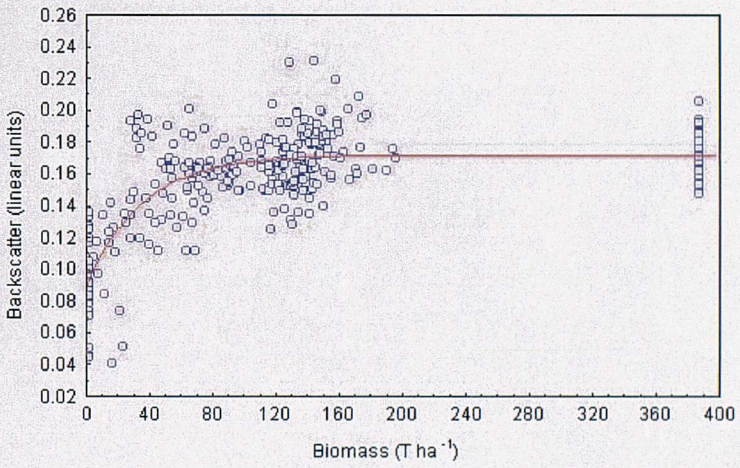

Figure 5.8. Relationship between backscatter and simulated biomass for pasture, regenerating and mature forest plots at the Manaus and Tapajós and study areas. The curve represents the fitted model (Luckman *et al.* 1998) with *r*=0.77 and 59% of the variance accounted for. The parameters of the fitted model are *a*=0.17, *b*=0.03 and *c*=2.49.

5.5.4. Temporal behaviour of backscatter

When analysing the backscatter/biomass behaviour with time, different responses were found for younger and intermediate regenerating forests. In most cases, younger regenerating forest plots (below the backscatter/biomass asymptote) had a backscatter that changed with seasons and over time. Intermediate and mature forest plots (above the backscatter/biomass asymptote) had a temporally stable σ°. However, this behaviour was more evident for regenerating forest plots in the Tapajós study area, as they presented a wider range of biomass. A less dynamic σ° behaviour for intermediate and old forest stages was also observed by Quegan *et al.* (2000) in pine forest plots in UK.

For regenerating forest plots at the Manaus study area, σ° ranged between –6.5 dB and -9 dB (figure 5.9). Most of the plots presented biomass around 130 T ha^{-1} and the behaviour of σ° did not show any marked trend. Figure 5.9 (a), (b) and (c) show the σ° behaviour of plots ranging in biomass from 91 T ha^{-1} to 156.6 T ha^{-1}. Some coincidence among troughs and peaks from different plots were noticed, but not consistently. In figure 5.9 (a), for instance, decreasing σ° occurred from February 1993 to October 1993 for all plots, except for plot 5, which exhibit a distinct behaviour. In some dates, as in April 1996 (figure 5.9 (b)), σ° seem to be restricted to a narrow range of values.

Plot 16, with low biomass (32 T ha^{-1}) and the only plot below the backscatter/biomass asymptote, had few variations in σ° (figure 5.9(d)) if compared to plots with similar biomass in the Tapajós study area. The mature forest plot (figure 5.9(d) plot 17), with a biomass above the backscatter/biomass asymptote, presented a nearly stable σ° of around –7.5 dB.

For the Tapajós study area σ° ranged between -7 and -9 dB (figure 5.10) for all plots in regenerating and mature forest.

Plots 2,4,5 (biomass of 15, 8 and 54 T ha^{-1} respectively), illustrated in figure 5.10(a), had lower backscatter than plots 1 and 3 (both 62 T ha^{-1}). Plot 4 (figure 5.10(a)) had the lowest biomass amongst all plots as well as the widest range of σ°. The extremes values of σ° for plot 4 corresponded to the wet season (March 1993) with the highest

backscatter and dry season (October 1995) with the lowest backscatter for the time span analysed here. Plot 14 (figure 5.10(c)), however, although presenting low biomass (25 T ha^{-1}), had a very variable behaviour of σ°, without correspondence between peaks and troughs and wet and dry season data, respectively.

The temporal variation found in plots 4 and 14 may have been due to the large variability in the data arising from the calculation of mean σ° from relatively few pixels.

With the exception of plot 6, the plots with biomass close or above the asymptote presented approximately the same trends of increasing and decreasing σ° (figure 5.10(b)).

Mature forest plots (plots 10, 15, 16, 17 and 18) presented the more stable behaviour, with similar trends of increasing or decreasing backscatter (figure 5.10 (b) and (d)). The six mature forest plots were above the saturation on the sensitivity of radar to biomass. Mature tropical forest is known to have small variations in σ°, being often chosen as a radiometric correction site (Hashimoto *et al.* 1996, Chapman *et al.* 1999).

Although the backscatter/biomass relationship was showed in the previous section, it was not expected that it would explain all variation in σ°. The temporal analysis enabled the effect of biomass on σ° to be isolated as plots above the backscatter/biomass asymptote were considered and presented similar trends of increasing and decreasing σ° with time (Quegan *et al.* 2000). High biomass plots such as mature forest presented a high σ° that indicated the contribution of another biophysical variables (McDonald *et al.* 1991, Imhoff 1995b, Dobson *et al.* 1995, Foody *et al.* 1997) and scattering mechanisms (Wang *et al.* 1995) rather than only biomass to the final backscatter values.

When temporal variations in σ° coincided with dry (low backscatter) and rainy season (high backscatter), the importance of soil moisture contribution and the penetration of LHH band in young regenerating forest could have been demonstrated (Hess *et al.* 1995, Saatchi *et al.* 1997). However, the small number of young regenerating forest plots that followed this behaviour did not seem to confirm this affirmation.

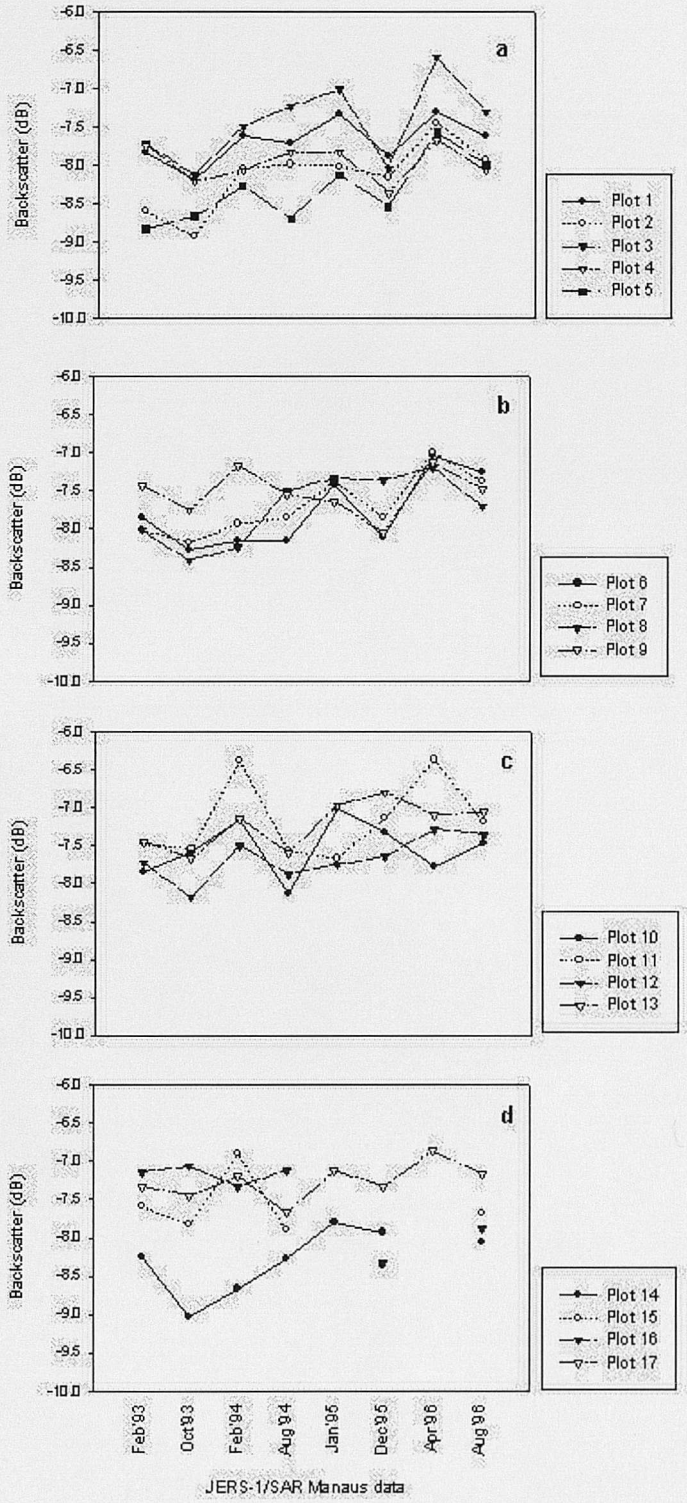

Figure 5.9. Temporal behaviour of σ° from regenerating and mature forest plots in Manaus study area.

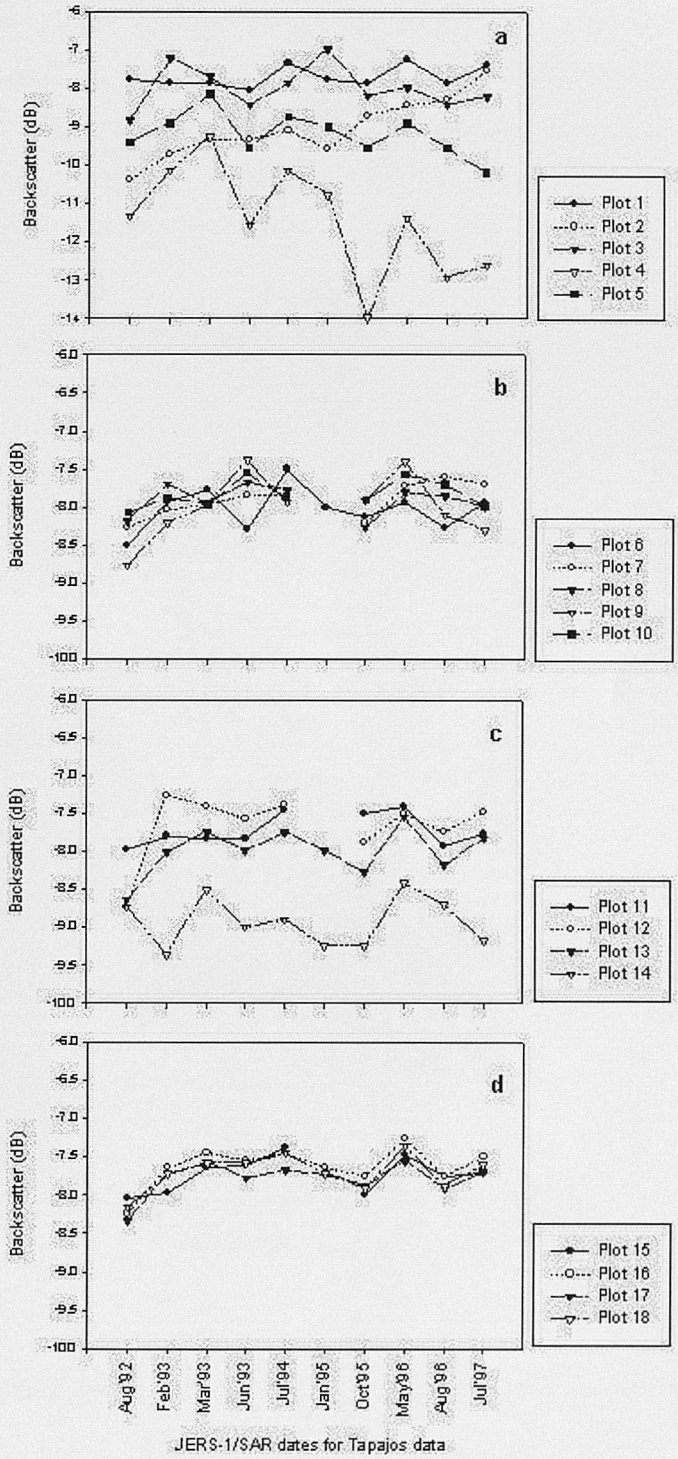

Figure 5.10. Temporal behaviour of σ° from regenerating and mature forest plots in Tapajós study area.

Figures 5.11 and 5.12 illustrate the residuals (or deviations from the mean) of the mean backscatter for selected plots in regenerating and mature forest plots in Manaus and Tapajós. The analysis of these residuals did not allow the observation of any particular anomaly of σ° with time. The tendencies are similar to the ones noticed in figures 5.9 and 5.10. Young regenerating forest plots (54 T ha^{-1},25 T ha^{-1} and 33 T ha^{-1} – figures 5.11 and 5.12) had more variable backscatter behaviour, with higher deviations from the mean. Mature and intermediate regenerating forest plots residuals were much smaller than those of young regenerating forest plots, indicating a greater stability due to saturation of the backscatter/biomass relationship.

Both the Manaus and Tapajós and study areas (figures 5.9 to 5.13) indicated no consistent trend of increasing σ° with time.

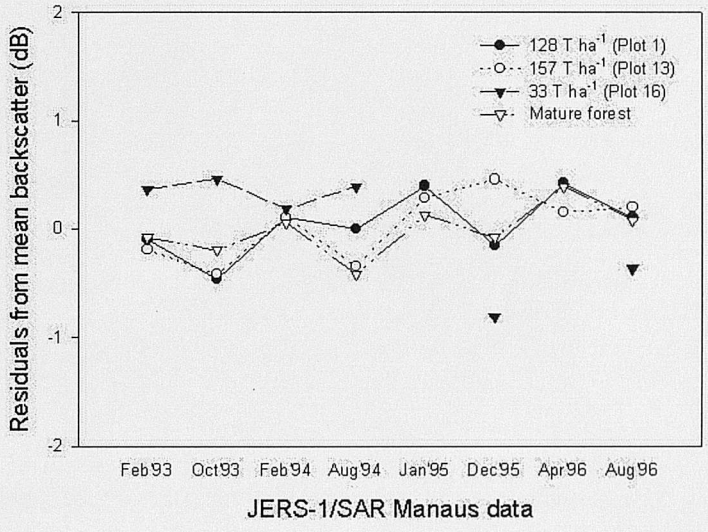

Figure 5.11. Residuals from mean backscatter of regenerating and mature forest plots in Manaus study area.

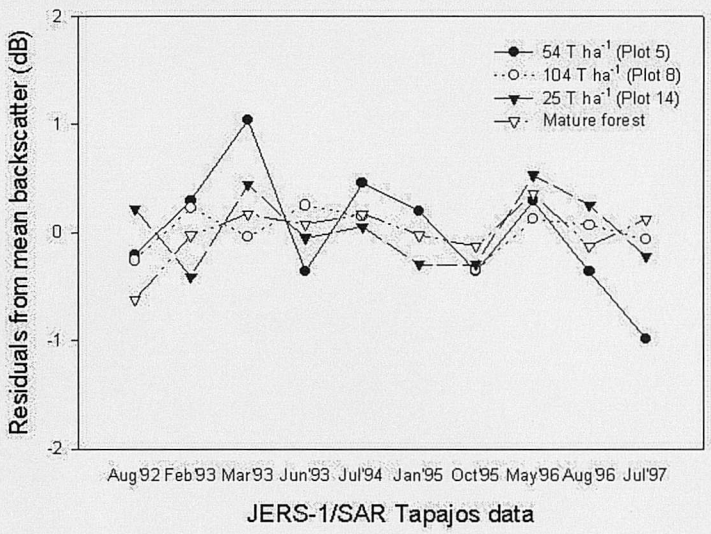

Figure 5.12. Residuals from mean backscatter of regenerating and mature forest plots in Tapajós study area.

5.5.5. Temporal behaviour of backscatter and biomass

For the Manaus data, the tri-dimensional relation of backscatter/biomass/time seen in figure 5.13 indicated a cyclical pattern. The peaks were concentrated on the region of intermediate biomass, where most of the data were from. The highest peaks in backscatter (months 1, 24, 35, 39) corresponded to wet seasons (December to June). The peak around month 9 (October 1993) corresponded to an unusual high backscatter in the dry season (July to November) and could not be explained.

The low biomass region, represented only by data from plot 16 (32.6 T ha^{-1}), presented a trough around month 35 (December 1995) which was probably caused by the absence of data for months 24 and 39 (January 1995 and April 1996) and a low backscatter value in December 1995.

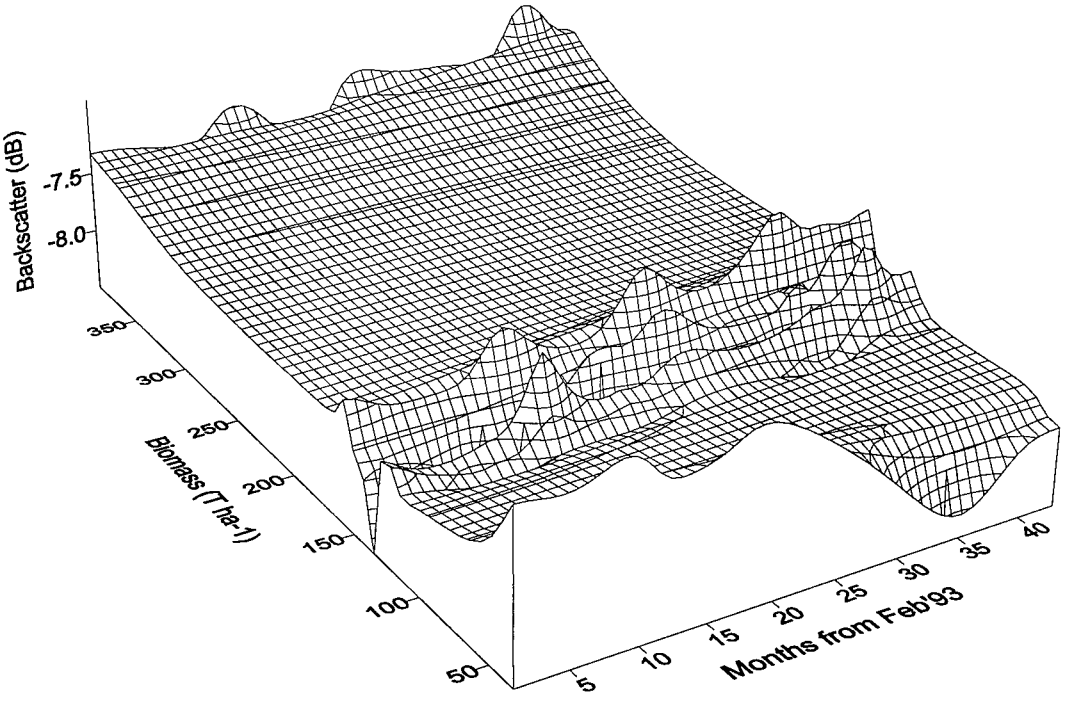

Figure 5.13. Biomass and backscatter as a function of time for Manaus data. The dates relating to months on the x-axis are in table 5.2.

For the Tapajós study area (figure 5.14) a cyclical pattern of backscatter for low biomass was observed. Except from month 24 (July 1994) the dry season was represented by sharp troughs. Similarly, the peaks corresponded roughly to wet season.

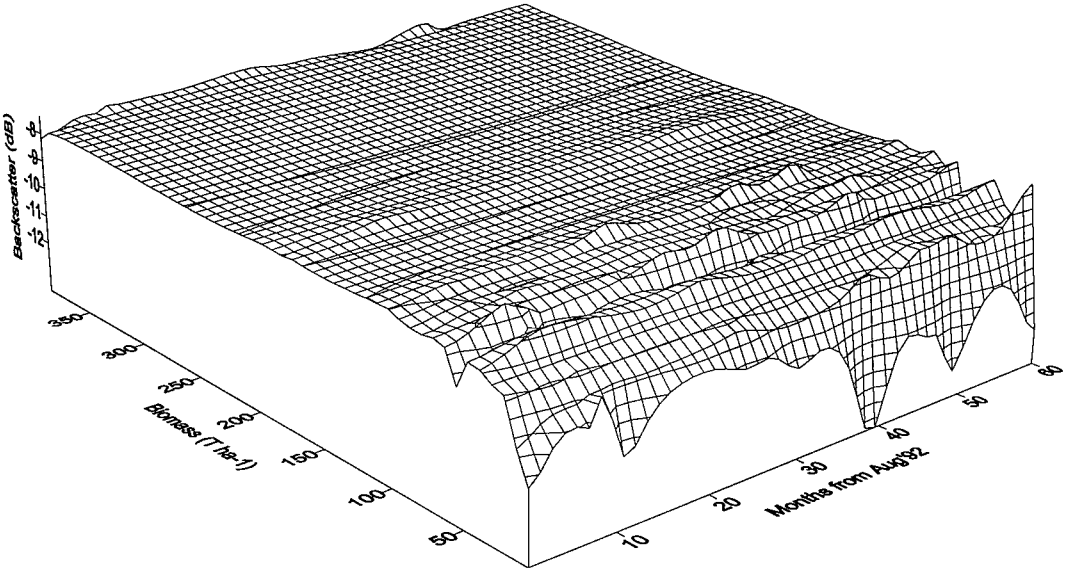

Figure 5.14. Biomass and backscatter as a function of time for Tapajós data. The dates relating to months on the x-axis are in table 5.3.

The water content of vegetation varies seasonally and diurnally (McDonald *et al.* 1991, Gates 1991). The saturation on the SAR response to biomass can hide, depending on a series of factors including vegetation and canopy structure, the water content influence on σ^o. Forests above 90 T ha^{-1} are certainly high and dense enough to prevent further penetration of L band. Therefore, if soil moisture contribution can not be accounted for, the varying water content of vegetation parts can play a rôle in the temporal behaviour of σ^o (Ahern *et al.*1993).

It has been noted by other authors that SAR imagery acquired during a dry season provides the backscatter range needed to develop robust backscatter/biomass relationships (Rignot *et al.* 1997, Luckman *et al.* 1997a, Saatchi *et al.* 1997, Grover *et*

al. 1999). In a temporal analysis, data from the dry season only would reduce the influence of water content of vegetation and soils in the backscatter/biomass relationship.

Figure 5.15 presents a 3D plot of backscatter/biomass/time using simulated biomass values for Manaus data (see section 5.5.3). The fluctuations in σ° over time for intermediate biomass remained, but less consistently. For the low biomass region there is a negative relationship of decreasing backscatter with time.

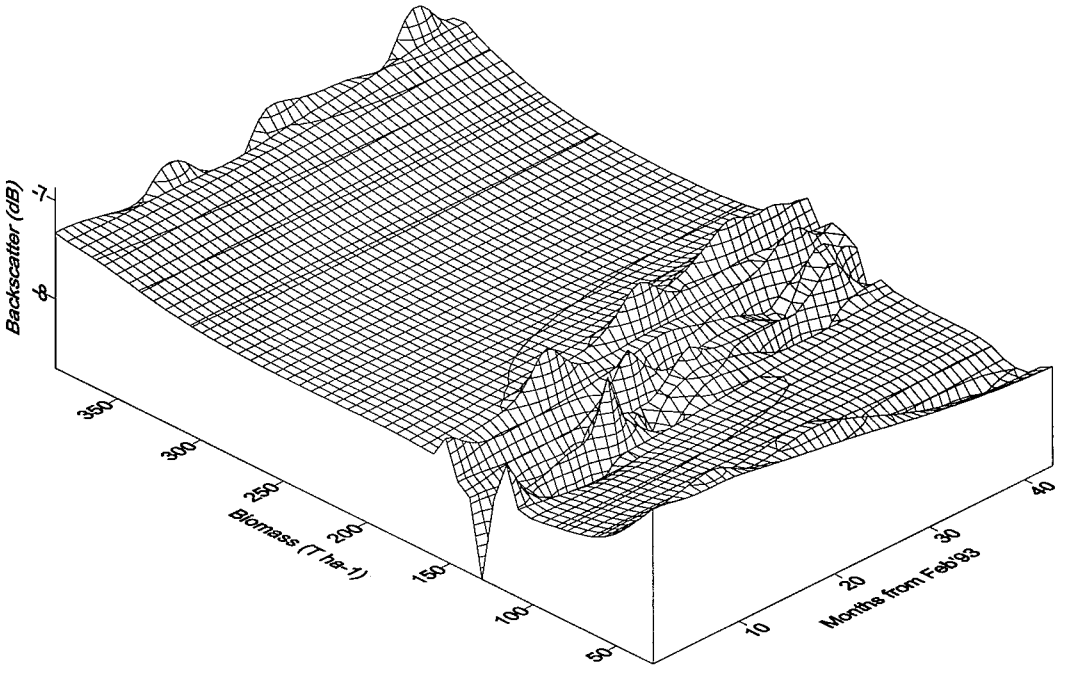

Figure 5.15. Simulated biomass and backscatter as a function of time for Manaus data. The dates relating to months on the x-axis are in table 5.2.

For Tapajós data, one of the effects of using simulated biomass accumulation was the fading of the cyclical pattern for low biomass (figure 5.16). In addition, the graph highlighted the absence of any increasing tendency for σ°, even in the light of biomass accumulation.

The adequacy of simulating biomass accumulation needs to be assessed. However, the rate of biomass accumulation in regenerating tropical forests is still an object of investigation (Chapman and Chapman 1999). Errors could have been introduced by not accounting for the age and rapid biomass accumulation on the first years of development (Brown and Lugo 1990).

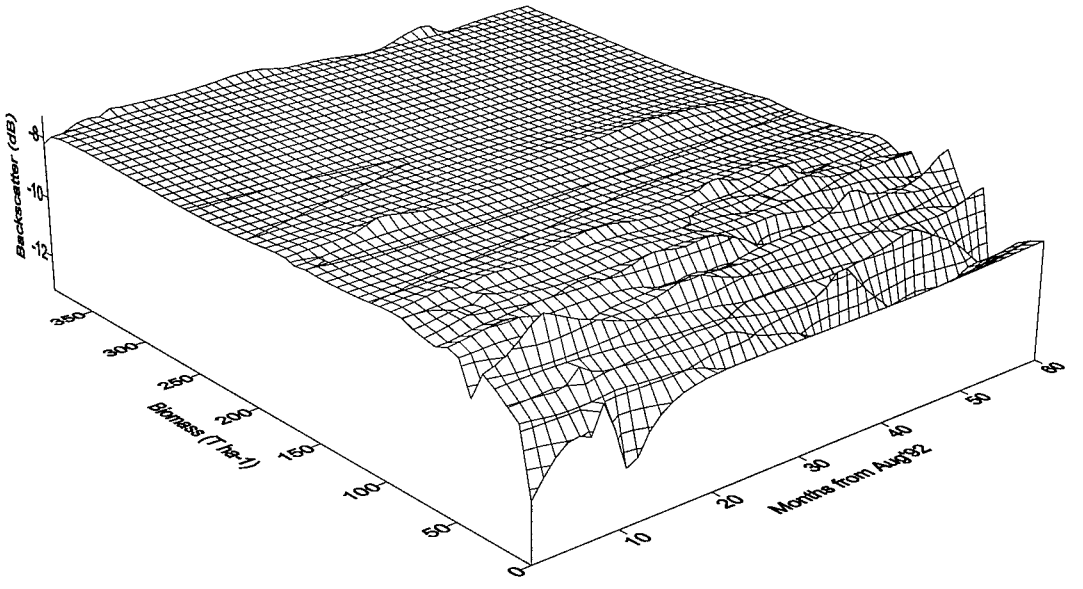

Figure 5.16. Simulated biomass and backscatter as a function of time for Tapajós data. The dates relating to months on the x-axis are in table 5.3.

When plotting Tapajós and Manaus data altogether (figure 5.17) no added features were present. However, there were more data points in the region of low and intermediate biomass. The seasonal cycle in low biomass was kept. Fluctuations of σ° for plots with intermediate biomass were not always consistent and there was no single response for similar biomass levels. This was expected after the known saturation of SAR response to forest vegetation. Also, variables other than biomass and water content certainly play a role in the backscatter response of regenerating and mature tropical forests (Imhoff 1995b, Foody *et al.* 1997).

It was not possible to detect biomass accumulation with temporal variation in σ°.

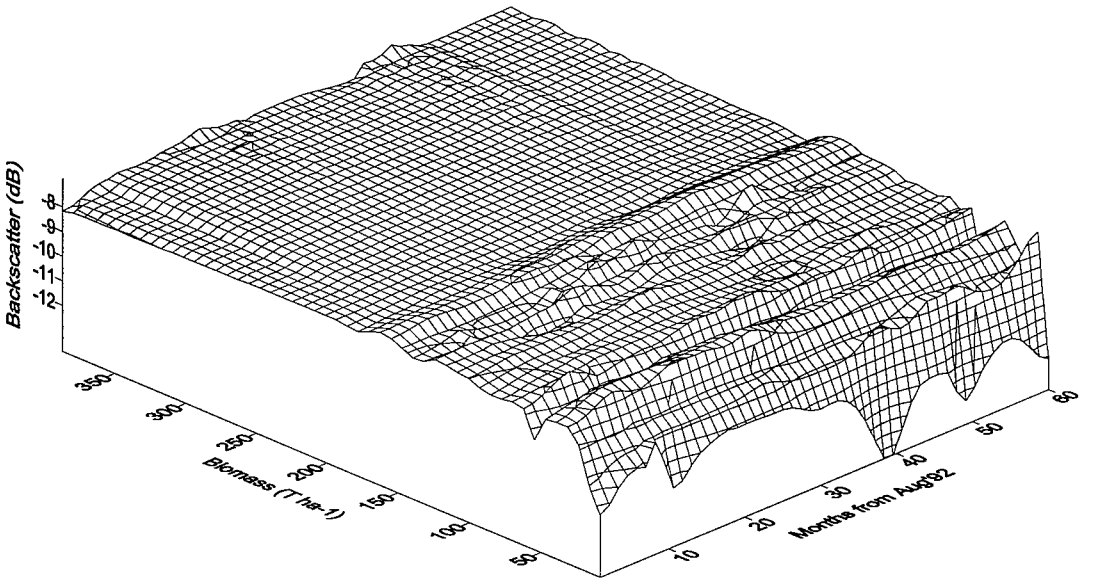

Figure 5.17. Biomass and backscatter as a function of time for Tapajós and Manaus data. The dates relating to months on the x-axis are in table 5.4.

5.5.6. Rainfall and backscatter

The seasonality of the backscatter in radar images is a function of the water content in the vegetation components, the amount of water in the soil and the amount of rainfall intercepted by vegetation surfaces. The moisture holding capacities of the soils is a function of the topography and drainage characteristics of the study areas (Grover *et al.* 1999).

The water content of soils, leaves and woody vegetation components was not measured in any of the regenerating and mature forest plots. Thus, the sensitivity of radar to water content and season was investigated by analysing rainfall data with support from GOES and Meteosat sensor's images used to infer cloud conditions and therefore rainfall occurring in the study areas. As rainfall is convective and occurs in

localised cells in the study areas, no comprehensive conclusions can be drawn from this research.

Figures 5.18 and 5.19 display the total rainfall for the previous day and for the cumulative amount of rain for the ten previous days to the date of SAR image acquisition. Backscatter from three different biomass stages (young, intermediate and mature forest plots) were plotted alongside rainfall data, as they represent different behaviour in the backscatter/biomass relationship.

Figure 5.18 indicated that there was not much coincidence between high rainfall and peaks in backscatter for the three forest plots in the Manaus study area. The expected higher backscatter for wetter periods did not occur for the three forest plots in all dates studied. The available regenerating forest plot with biomass below the backscatter/biomass asymptote was not included in all eight SAR scenes analysed, being missed in two dates (months 24 and 39). As a result, the backscatter/rainfall relationship could not be investigated for January 1995 and April 1996. The influence of the ten days cumulative rainfall was not remarkable in the Manaus study area data.

Figure 5.19 indicated that there was some coincidence between high rainfall and peaks in backscatter for the three forest plots in Tapajós study area. The younger regenerating forest plot (54 T ha^{-1}) appeared to parallel closer the rainfall values. This plot had a biomass below the backscatter/biomass asymptote. The two remaining plots in figure 5.17 showed a less marked coincidence between rainfall and backscatter distribution. These plots presented biomass values close or above the saturation point. Month 60 (July 1997) records showed no rainfall data whatsoever, but two plots had a high backscatter. The minimum backscatter occurred for the driest month (Month 60) and the maximum backscatter occurred for the wettest month (Month 8).

An interesting feature to note in figure 5.19 is the importance of the rainfall records of up to ten days before the SAR image acquisition date. These 10 days rainfall values seemed to have an influence in backscatter from the three forest plots. Although Tapajós study area is in a relatively flat terrain and presenting soils well drained, the water from rainfall might be held in soils for days, depending on the local topography. Drainage characteristics of the Tapajós study area were already seen as a dramatic influence on temporal backscatter (Grover *et al.* 1999).

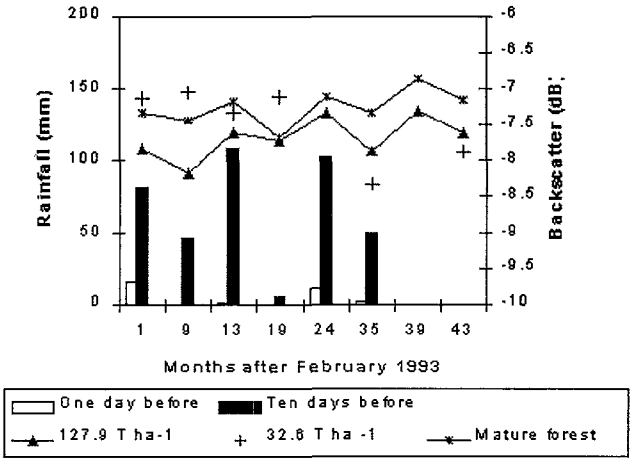

Figure 5.18. Rainfall data of one day before the JERS-1 satellite overpass, total cumulative rainfall data of ten days before the satellite overpass and backscatter over mature and two regenerating forest plots for the Manaus study area. The dates relating to months on the x-axis are table 5.2.

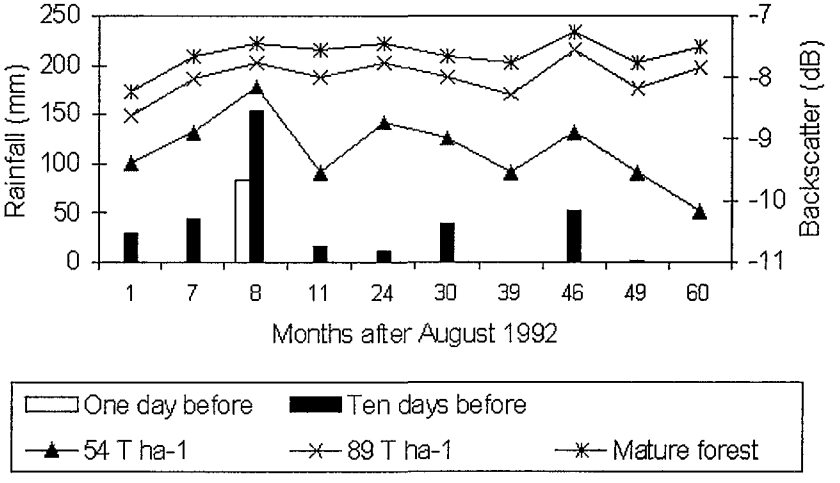

Figure 5.19. Rainfall data of one day before the JERS-1 satellite overpass, total cumulative rainfall data of ten days before the satellite overpass and backscatter over mature and two regenerating forest plots for the Tapajós study area. The dates relating to months on the x-axis are in table 5.3.

5.6. Summary

The backscattering properties of thirty regenerating forest plots, six mature forest plots and three pasture plots were studied at Manaus and Tapajós study areas in Brazilian Amazonia using a time series of around four years of JERS-1 SAR images.

There was a positive backscatter/biomass relationship at both study areas. The correlation between the mean backscatter (σ°) and biomass for each plot over time were r=0.80 for Manaus and r=0.87 for Tapajós data. A model was fitted to the data in order to quantify the location of the asymptote in the σ°/biomass relationship. The resulting correlation was r around 0.87, with saturation in σ° at biomass levels of around 90 T ha^{-1}. That would limit the detection and estimation of biomass for regenerating forests under approximately 13 years old (Uhl *et al.* 1987, Brown and Lugo 1990).

The σ°/biomass/time plots indicated a cyclical pattern in σ° for young regenerating forest plots. The pattern was seasonal with the dry season corresponding to lower σ° and the wet season corresponding to higher σ°. This pattern pointed to the influence of water content in vegetation and soil on σ°. Rainfall was another important source of variation in σ° and regenerating forest plots below the σ°asymptote showed corresponding high rainfall rates and high σ° and vice-versa.

The σ° varied most strongly with time for those regenerating forest plots that had biomass levels below the σ° asymptote. A similar temporal σ° behaviour for intermediate biomass regenerating plots and mature forest plots indicated properties other than biomass (i.e. water) influenced the backscatter from tropical forests.

Biomass accumulation was not detected by change in backscatter over time. The information in the σ° temporal domain was not related to biomass but primarily to water content of vegetation and soil.

SAR data from the dry season is recommended for forest studies in order to eliminate the influence of varying water content of vegetation and soil in backscatter.

CHAPTER SIX

Spatial analysis of JERS-1 SAR data for regenerating tropical forests

As tropical forest matures, the structure of the canopy changes due to progressive replacement of pioneer species by early and late regenerating species. Some of the physical changes in the canopy through time are related to an increase in height (tree growth), a decrease in canopy surface homogeneity (as emergent trees start to break through the canopy) and an increase in canopy thickness (related to more branches in trees and differentiation into strata) (Richards 1996). All of these changes influence the spatial characteristics of SAR radiation and consequently the texture of SAR images.

In this chapter, the texture of regenerating forests and mature forest canopies on JERS-1 SAR images was investigated. The objective was to assess if spatial (texture) information derived from SAR imagery could be used to increase the correlation between backscatter and the log of biomass (logbio).

6.1. Spatial analysis and texture

The spatial analysis of remotely sensed data exploits the relations between pixels in the images. Texture measures quantify relations between pixels and are therefore an important tool in the spatial analysis of remotely sensed data.

Texture is an intrinsic property of virtually all surfaces and is visible in, for instance, a satellite sensor image of the Earth's surface and a microscopic image of cell cultures. It is related to the structural arrangements of surfaces and their relationship to the

surrounding environment as "...*an organised area phenomena*" (Haralick 1979). Despite its importance in image data there is no precise definition or standard mathematical formulation for texture (Haralick 1979, Soares *et al.* 1997).

When interpreting aerial photographs or satellite sensor images the tone and texture of objects are among the most important features in their visual recognition. While tone refers to the grey level of a resolution cell (pixel in digital images), texture refers to the spatial distribution of tonal variations at the neighbourhood of the resolution cell (Haralick *et al.* 1973, Mather 1999).

Texture is dependent on the scale of observation and is a function of the spatial resolution (Mather 1999). Local and regional contrast along with scale and preferred orientation of the texture elements are the components of the texture of a digital image (Rubin 1990).

6.2. Overview of texture models

Texture analysis is based mainly on structural and statistical approaches (Haralick 1979). The structural approach models texture as a set of primitives that repeat with a certain periodicity. A primitive is a connected set of pixels characterised, for instance, by a list of attributes such as its grey levels (Haralick 1979). Texture is determined by the selection of different types of primitives, the extraction of a set of features describing these primitives (e.g., size and shape) and the definition of a placement rule (He and Wang 1990). The identification of primitives and definition of a placement rule for land covers usually found in remote sensing images can hinder the application of the structural approach for textural analysis (He and Wang 1990).

More commonly used for remote sensing data is the statistical approach, which describes texture as a set of local statistical measures based on the spatial distribution of grey levels of an image. First- and second-order statistical measures are computed over regions or distances of pixels within the images, respectively. Several methods and techniques for describing texture based in statistical models have been developed and these include the variogram, the grey level co-occurrence matrices (GLCM) and local statistics derivation, which were all used in this work and are described below.

6.3. Texture of radar images

Visual interpretation of radar images is based largely on texture (Rubin 1990, Raney 1998). Terms such as rough, smooth, coarse and fine are usually employed for describing radar image texture (Lewis and Henderson 1998).

Texture analysis is relatively straightforward in images from optical sensor (incoherent) systems as they contain primarily scene texture. For radar images, however, texture comprises scene texture and image texture as a result of the dominating inherent image noise called speckle (Raney 1998).

The presence of speckle in radar data increases the variability of both spatial and radiometric information. As a result, some image classifiers based on tone alone classify land cover with low accuracy in radar images (Ulaby *et al.* 1986). Speckle also hinders the visual discrimination of land cover in radar images.

Speckle is commonly assumed to be a multiplicative factor to the SAR scene texture (Ulaby *et al.* 1986, Soares *et al.* 1997). The following model combines variability due to texture and speckle in SAR images (Ulaby *et al.* 1986):

$$I_i(j) = \mu_{Ii} T_i(j) F_N(j) \qquad [6.1]$$

where $I_i(j)=I_{ij}$ is the intensity of pixel j in field I, μ_{Ii} is the mean intensity of field i, $T_i(j)$ represents texture as a random within-field variability and $F_N(j)$ represents speckle as a fading random variable with a normalised χ^2 (chi-square) distribution.

Image pre-processing techniques such as the use of speckle filters or multilook averaging of the data can increase the discrimination of land cover in SAR images. However, these techniques also reduce local variation and therefore partially remove image texture. Although speckle information is present in image texture, the spatial variability attributable to intrinsic scene texture is not related to the variability attributable to speckle (Ulaby *et al.* 1986). It follows that the intrinsic scene variability causing the image texture can be detected even in the presence of speckle. This hypothesis has been corroborated by recent results (as described in section 3.4.1).

Figure 6.1 shows a subset of a JERS-1/SAR image of the Tapajós study area with the main land covers and types of texture indicated. Water can be considered "textureless". The remaining dark, small local contrast surfaces in the image subset are examples of recent human activity such as crops, pasture and forest clearings. Mature forest is characterised by a fine texture, where, at larger spatial resolutions, a close inspection would reveal bright and dark areas as a result of scattering from emergent trees and shadowing. Regenerating forests, depending on a series of factors (e.g., dominant species, regenerating stage, etc), exhibit less texture than mature forest and are generally darker, although are not always discriminated visually from mature forest. The absence of emergent trees and a thinner canopy (less volume scattering) would partially explain the darker appearance of regenerating forests in radar images. Speckle (although reduced by 3-look processing and pixel averaging) is also responsible for the fine texture exhibited over the image that is usually referred as grainy or "salt-and-pepper" (Lewis and Henderson 1998).

6.4. Texture measures

Image data recorded on the closest date to the fieldwork were used. JERS-1 SAR data from July 1994 (fieldwork August/September 1994) was chosen for the Tapajós study area and SAR data from December 1995 (fieldwork September 1995) were chosen for the Manaus study area.

In chapter 5, the mean backscatter for regenerating forest, mature forest and pasture plots were estimated from within polygons located in the amplitude images. In this chapter, the same polygons were used but this time as subsets of the images. These subsets were used as input either as images or as text files for the implementation of texture methods described below. The images were not converted to linear units and backscatter and the information used was pixel DN. In this chapter, the designation GL (grey level) is also used for DN as most of the literature in texture analysis uses pixel values as tonal information.

The statistical texture measures investigated are described next.

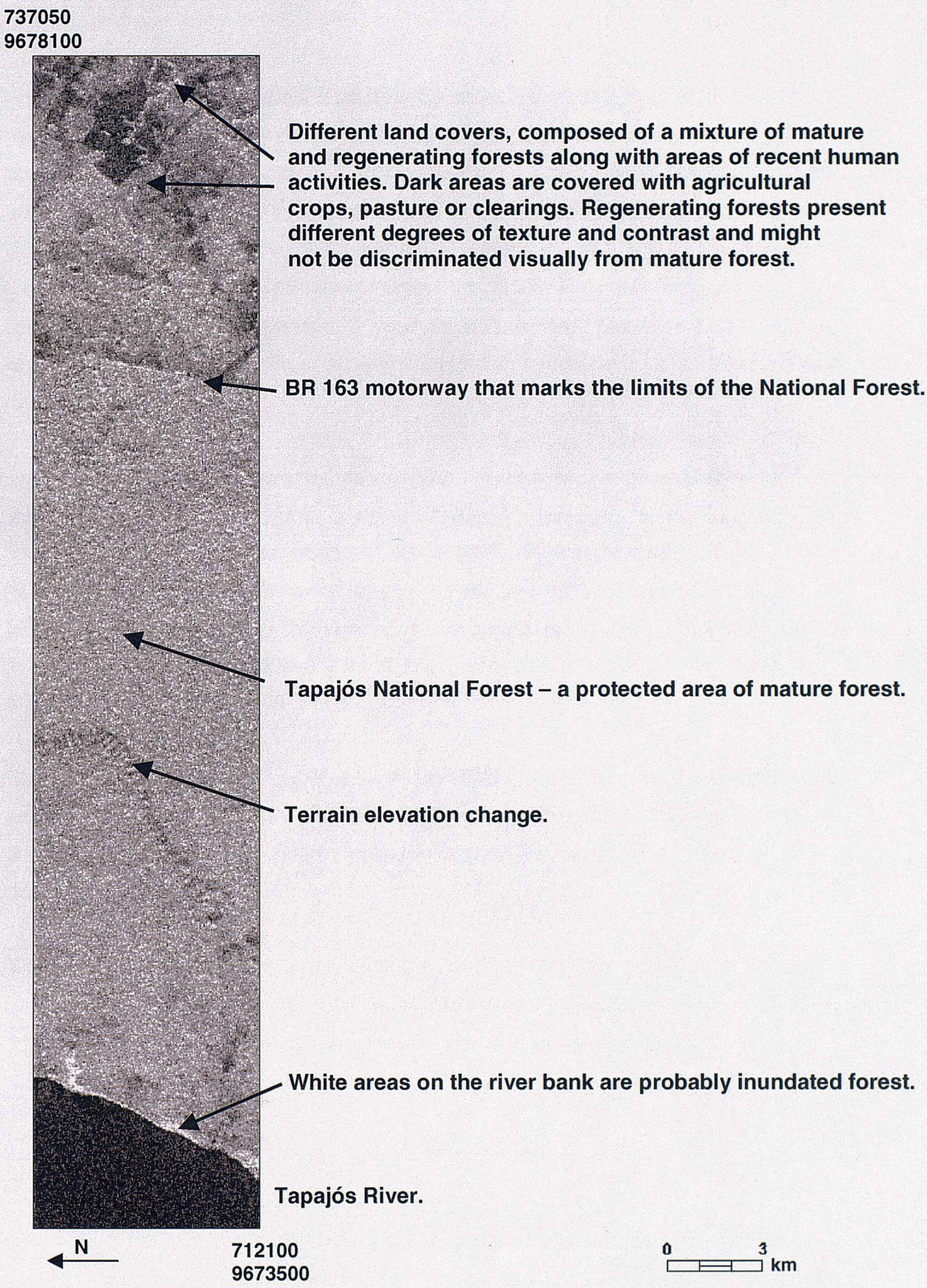

Figure 6.1. Subset of JERS-1/SAR image of Tapajós study area and its main land covers. Corners display UTM coordinates.

6.4.1. Texture measures derived from the variogram

Geostatistics is a set of statistical techniques used to describe the spatial variation of variables within a region of interest (Atkinson 1999). These variables are assumed to be spatially correlated, that is, in a remote sensing context, pixels close together are more likely to have similar values of a property than pixels further apart (Curran and Atkinson 1998). The theory of regionalised variables is the framework within which geostatistical techniques are based (Matheron 1965). A regionalised variable has properties intermediate between a random and a deterministic variable, mainly because it presents continuity in space although this continuity is not easily described by a function (Davis 1986).

The variogram (or semivariogram as it is also called) is a core geostatistical tool and was first described for remote sensing studies in the late 1980s (Curran 1988, Woodcock *et al.* 1988a, Curran and Atkinson 1998). Variograms were mainly used as pre-requisites for interpolation (or kriging) in mapping and cartographical modelling (Burrough 1996). Recently, however, the use of variograms for analysis of spatial information in remotely sensed images has been widely referenced (Miranda *et al.* 1998, Berberoglu *et al.* 2000, Chica-Olmo and Hernández 2000).

The variogram relates the variance of pixels to its spatial location and describes the scale and patterns of spatial variability (Curran and Atkinson 1998). Pixel's GL can be interpreted as a regionalised variable and spatially characterised by a variogram function.

The variogram is derived by calculating half the average squared difference – *semivariance* - between pairs of pixels separated by a distance h – the lag distance (Curran 1988). An estimate of the average semivariance (γ) is given by:

$$\hat{\gamma}(\mathbf{h}) = \frac{1}{2m(\mathbf{h})} \sum_{i=1}^{m(\mathbf{h})} [Z(\mathbf{x}_i) - Z(\mathbf{x}_i + \mathbf{h})]^2 \qquad [6.1]$$

where m is the number of pairs of pixels, $\mathbf{x}$ is a pixel location, $\mathbf{h}$ is the lag distance and $Z(x_i)$ is the pixel value at location $\mathbf{x}$. The larger γ the less similar are the pixels (Curran 1988).

The resulting variogram is used for the fit of a model with known mathematical properties. These properties allow the variogram values and descriptors to be used for the estimation at unsampled locations (Wallace *et al.* 2000) or texture analysis (Chica-Olmo and Abarca-Hernández 2000).

The descriptors of a modelled variogram include information on (i) the distance over which pixels are correlated (the range), (ii) the level of random variation within pixels (the nugget variance) and (iii) the total variation present in the data (the sill) (Wallace *et al.* 2000). The sill is the summation of the spatially related (structured) and uncorrelated (nugget) variance.

Uses of the variogram and its descriptors in spatial analysis also include their connection with scene class properties (for digital classification purposes) and with continuous scene variables (for understanding spatial relations between and within variables) (Atkinson and Lewis 2000). Figure 6.2 shows an example of a typical variogram and its main descriptors.

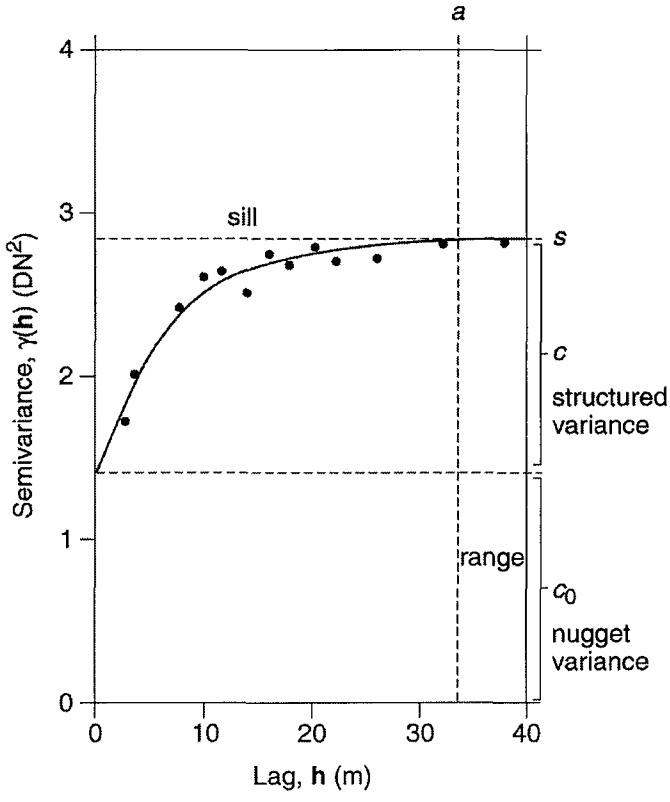

Figure 6.2. A variogram and its main descriptors (from Curran and Atkinson 1998).

The models more commonly fitted to experimental variograms are the spherical, exponential, Gaussian and power models (Atkinson 1999). The nugget and spherical

models have a defined sill, although the exponential and Gaussian models only approach the sill asymptotically. These types of model are called bounded. The power model (of which the linear is a special case) does not present a sill and is called unbounded (Atkinson 1999).

Variograms were computed for each plot located within the SAR images using the software GSTAT (Pebesma and Wesseling 1998). Transects of pixels were used as the regenerating and mature forest plots presented different shapes and sizes. This software allows the definition of lag spacing and the maximum distance for which semivariance is calculated. The settings were 25 metres for lag spacing (equal to pixel size) and 250 m (or 10 pixels) for maximum distance. The plots were assumed to be isotropic (with the same variation for any direction) and so the transects were taken with the largest number possible of pixels in any direction. Subsequently variograms were fitted using nugget and spherical models.

6.4.2. Texture measures derived from the grey level co-occurrence matrix (GLCM) and sum and difference histogram (SADH)

The application of a set of textural measurements to remotely sensed data began with the second-order textural measures based on Haralick's grey level co-occurrence matrix (GLCM) (Haralick *et al.* 1973). Distance and angular spatial relationships among grey levels are summarised in a GLCM, as it is a measure of the probability of occurrence of two grey levels separated by a given distance in a given direction (Mather 1999). GLCM has been used successfully in a variety of SAR applications, including land-cover mapping (Kurosu *et al.* 1999, van der Sanden and Hoekman 1999, Wu and Linders 1999), crop discrimination (Soares *et al.* 1997) and forest studies (Luckman *et al.* 1997, Kurvonen *et al.* 1999, van der Sanden and Hoekman 1999).

To determine the spatial information present in a digital image, a co-occurrence matrix is computed on a pixel neighbourhood delimited by a moving window of a given size. Each element $P(i,j,d,\theta)$ of the co-occurrence matrix represents the relative frequency with which two neighbouring pixels (separated by a distance d and having an angular relationship θ) occur on the image, one with grey level i and the other with grey level j. Subsequently, statistics are computed from the grey level co-

occurrence matrix and they describe the spatial information according to the relative position of the matrix elements (Mather 1999).

Figure 6.3 illustrates the construction of a four-directional co-occurrence matrix. Figure 6.3(a) displays a 3 x 3 window from an image ranging from 0 to 3 grey levels, (b) shows the general form of any grey level co-occurrence matrix obtained from (a). Pairs of neighbour pixels are considered in orientation and the grey level of these pixels forms the index for incrementing an entry of the matrix. Figures 6.3(c) to 6.3(f) represent the co-occurrence matrices derived for four angular orientations using distance of one pixel between two neighbouring pixels.

0	1	3
0	0	1
2	0	1

(a)

Gr	0	1	2	3
0	#(0,0)	#(0,1)	#(0,2)	#(0,3)
1	#(1,0)	#(1,1)	#(1,2)	#(1,3)
2	#(2,0)	#(2,1)	#(2,2)	#(2,3)
3	#(3,0)	#(3,1)	#(3,2)	#(3,3)

(b)

Horizontal

$$P_{0^o} = \begin{bmatrix} 2 & 3 & 1 & 0 \\ 3 & 0 & 0 & 1 \\ 1 & 0 & 0 & 0 \\ 0 & 1 & 0 & 0 \end{bmatrix}$$

(c)

Vertical

$$P_{90^o} = \begin{bmatrix} 4 & 1 & 1 & 0 \\ 1 & 2 & 0 & 1 \\ 1 & 0 & 0 & 0 \\ 0 & 1 & 0 & 0 \end{bmatrix}$$

(d)

Left diagonal

$$P_{135^o} = \begin{bmatrix} 4 & 1 & 0 & 0 \\ 1 & 2 & 0 & 0 \\ 0 & 0 & 0 & 0 \\ 0 & 0 & 0 & 0 \end{bmatrix}$$

(e)

Right diagonal

$$P_{45^o} = \begin{bmatrix} 0 & 2 & 1 & 1 \\ 2 & 0 & 0 & 0 \\ 1 & 0 & 0 & 0 \\ 1 & 0 & 0 & 0 \end{bmatrix}$$

(f)

Figure 6.3. An example of the construction of the co-occurrence matrices. (a) 3 x 3 image quantised to four grey levels (0-3). (b) general form of any spatial co-occurrence matrix for an image quantised to four grey levels (0-3). *#(i,j)* represents the number of times grey levels *i* and *j* have been neighbours. (c)-(f) spatial co-occurrence matrices derived for four angular orientations using distance 1.

The greater the number found in the diagonal of the GLCM the more homogeneous is the texture for that part of the image. Several statistical measures can be extracted from the GLCM to describe specific textural characteristics of the image (Haralick *et al.* 1973).

The texture measures analysed in this work are presented below. A short description is included for the six best known. A more complete theoretical description of the most commonly used co-occurrence measures can be found elsewhere (Haralick *et al.* 1973, Baraldi and Parmiggiani 1995, Soares *et al.* 1997). Each element $P(i,j)_{\Delta x \Delta y}$ represents the relative frequency with which two neighbouring pixels separated by a distance of Δx columns and Δy lines occur (Soares *et al.* 1997).

Entropy (enth):

$$ENTH_{\Delta x \Delta y} = -\sum_i \sum_j P(i,j)_{\Delta x \Delta y} \log P(i,j)_{\Delta x \Delta y} \qquad [6.2]$$

Entropy is a measure of the degree of disorder in an image. Entropy is larger when the image is texturally non-uniform or heterogeneous and approaches its maximum when all GLCM entries have similar contents, indicating an image with completely random pixel values. Entropy and energy are inversely correlated.

Energy (eneh):

$$ENEH_{\Delta x \Delta y} = \sum_i \sum_j P(i,j)^2_{\Delta x \Delta y} \qquad [6.3]$$

Also called angular second moment and uniformity, energy is a measure of textural uniformity or pixels pairs repetitions. When the pixels of the image window under consideration have similar grey levels, energy reaches its maximum (equal or close to 1). Therefore, constant or periodic distribution of grey levels over the window will produce high values for energy.

Contrast (cont):

$$CONT_{\Delta x\Delta y} = \sum_i \sum_j P(i-j)^2_{\Delta x\Delta y} P(i,j)_{\Delta x\Delta y} \quad [6.4]$$

Contrast is a measure of the degree of spread of the grey levels or the average grey level difference between neighbouring pixels. The contrast values will be higher for regions exhibiting large local variations. The GLCM associated with these regions will display more elements distant from the main diagonal, than regions with low contrast. Local statistics contrast and GLCM contrast are strongly correlated.

Homogeneity (hom):

$$HOM_{\Delta x\Delta y} = \sum_i \sum_j \frac{P(i-j)^2_{\Delta x\Delta y}}{1+(i-j)^2} \quad [6.5]$$

Also called inverse difference moment, homogeneity is a measure of lack of variability or the amount of local similarity in the scene. High homogeneity values suggest small grey tone differences in pair elements. In this case, the associated GLCM will present elements around the main diagonal. Contrast and homogeneity are inversely correlated.

Correlation (cor):

$$COR_{\Delta x,\Delta y} = \frac{\sum_i \sum_j ijP(i,j)_{\Delta x\Delta y} - \mu l \mu c}{\sigma l \sigma c} \quad [6.6]$$

Correlation is a measure of grey level linear dependencies in the image. High correlation values denote a linear relationship between the grey levels of pixel pairs. A completely homogeneous area is a limiting case of linear-dependency, for which correlation reaches its maximum (equal to 1). Correlation is uncorrelated to entropy and energy, i.e., to pixel pair repetitions.

Chi-square (chi):

$$CHI_{\Delta x,\Delta y} = \sum_i \sum_j \frac{P(i,j)^2{}_{\Delta x,\Delta y}}{P(i,*)_{\Delta x,\Delta y} P(*,j)_{\Delta x,\Delta y}} \qquad [6.7]$$

Chi-square is a normalisation of the scene energy to the grey levels linear dependencies of the image. It is correlated to energy.

An alternative to the GLCM method is the replacement of the co-occurrence matrix by estimates of first order probability functions in its principal axes, namely the sum and difference histograms (SADH) (Unser, 1986). New variables defining the sum and difference of grey levels *i* and *j* are created and from them a new reduced matrix. Each element of the sum vector is defined as

$$P^s(k)_{\Delta x,\Delta y} = \sum_i \sum_j P(i,j)_{\Delta x,\Delta y} \qquad \forall i+j=k$$

and each element of the difference vector is defined as

$$P^D(l)_{\Delta x,\Delta y} = \sum_i \sum_j P(i,j)_{\Delta x,\Delta y} \qquad \forall |i-j| = l\,.$$

Although derived from a "reduced GLCM", the measures described next have the same characteristics as mean and variance (section 6.4.3) and as GLCM derived entropy and energy (shown above). The following measures were extracted using SADH technique (Soares *et al.* 1997):

Mean of the sum vector (sme):

$$SME_{\Delta x,\Delta y} = \sum_k k P^s(k)_{\Delta x,\Delta y} \qquad [6.9]$$

Variance of the sum vector (sva):

$$SVA_{\Delta x,\Delta y} = \sum_{k} (k - MS_{\Delta x,\Delta y})^2 P^s(k)_{\Delta x,\Delta y} \quad [6.10]$$

Energy of the sum vector (sene):

$$SENE_{\Delta x,\Delta y} = \sum_{k} P^s(k)^2{}_{\Delta x,\Delta y} \quad [6.11]$$

Entropy of the sum vector (sent):

$$SENT_{\Delta x,\Delta y} = \sum_{k} P^s(k)_{\Delta x,\Delta y} \log P^s(k)_{\Delta x,\Delta y} \quad [6.12]$$

Mean of the difference vector (dme):

$$DME_{\Delta x,\Delta y} = \sum_{l} lP^D(l)_{\Delta x,\Delta y} \quad [6.13]$$

Variance of the difference vector (dva):

$$DVA_{\Delta x,\Delta y} = \sum_{l} (l - DME_{\Delta x,\Delta y})^2 P^D(l)_{\Delta x,\Delta y} \quad [6.14]$$

Energy of the difference vector (dene):

$$DENE_{\Delta x,\Delta y} = \sum_{l} P^D(l)^2{}_{\Delta x,\Delta y} \quad [6.15]$$

Entropy of the difference vector (dent):

$$DENT_{\Delta x,\Delta y} = -\sum_{l} P^D(l)_{\Delta x,\Delta y} \log P^D(l)_{\Delta x,\Delta y} \quad [6.16]$$

The extraction of the texture measures based on the GLCM were performed using a code developed using IDL (Interactive Data Language) and ENVI (Environment for Visualising Images) functions (Rennó *et al.* 1998). Regenerating and mature forest and pasture plots were used as image subsets and the GLCM measures were calculated within a moving window of a given size.

An optimal window size for calculating GLCM texture measures is a compromise between providing enough spatial information to characterise the land cover and limiting overlapping textures between different land covers (Ulaby *et al.* 1986). Window sizes of 3 x 3 and 5 x 5 pixels (corresponding to areas of 75 m x 75 m and 125 m x 125 m respectively) were chosen based on (i) the variogram for each plot and (ii) prior knowledge of the small size of some regenerating forest plots.

One drawback of the GLCM approach is a requirement for relatively large computational resources and the production of a sparse matrix, depending on the quantisation level of the image studied. For a 256 grey level image (8-bit) the GLCM has 65536 entries, which can result in a very sparse matrix, depending on the region studied (Soares *et al.* 1997). Diminishing the quantisation levels of an image, as long as the textural properties of the image are preserved, can reduce GLCM complexity and sparseness (Dutra and Huber 1999).

Methods for reducing the grey level range of an image include uniform and equal probability quantisation. In the uniform quantisation method grey levels are quantised into separate bins with uniform spaces, without taking into consideration the grey level distribution of the image. By contrast, in the equal probability quantisation method each bin has a similar probability, thus producing a near uniform histogram (Mather 1999).

Although the equal probability quantisation method is generally recommended for texture analysis (Mather 1999), some authors found no difference when analysing texture in images reduced by both methods (Ii, pers. comm. 2000). Following Rennó *et al.* (1998) this work used the method of uniform quantisation.

Table 6.1 illustrates the window sizes and quantisation levels which were tested when deriving GLCM textures measures:

Table 6.1: Window sizes and quantisation levels used in the calculation of GLCM and SADH derived texture measures.

Bits	Grey levels	Window siz
2	4	5x5 pixels
4	16	5x5 pixels
6	64	5x5 pixels
8	256	5x5 pixels
2	4	3x3 pixels
4	16	3x3 pixels
6	64	3x3 pixels
8	256	3x3 pixels

6.4.3. Texture measures derived from local statistics

Local statistics characterise the moments of a neighbourhood of individual pixels in a particular segment or region of an image. Local statistics have been used extensively to quantify texture in SAR images (Soares *et al.* 1997, Kurvonen and Hallikainen 1999, Haack and Bechdol 2000, Saatchi *et al.* 2000).

The local statistics measures derived from the regenerating forest, mature forest and pasture plots were analysed in this work. They are presented below:

Notation:

$P(i)$ = $F(i) / n$
$F(i)$ = frequency for grey level (GL) i
n = number of pixels
M = $M = \sum_i iP(i)$ (mean)
V = $V = \sum_i [i - M]^2 P(i)$ (variance)

Mean Absolute Deviation (mad):

$$MAD = \frac{\sum_i |i - M|}{n} \quad [6.17]$$

Mean absolute deviation is a measure of heterogeneity similar to the variance, increasing with greater DN differences from the mean.

Median (med):

The median divides a frequency distribution into two halves: half the scores are above the median and half are below the median. When n is even, the median is calculated as the midpoint between the (n/2)th and the [(n/2) + 1]th pixel. The median is less sensitive to extreme scores than the mean and this makes it a more suitable measure than the mean for image data with highly skewed distributions (Sokal and Rohlf 1995).

Entropy (ent):

$$ENT = -\sum_i P(i) \log[P(i)] \quad [6.18]$$

The meaning of local entropy is the same as GLCM derived entropy: a measure of the amount of disorder in an image.

Energy (ene):

$$ENE = \sum_i [P(i)]^2 \quad [6.19]$$

Correlated to GLCM energy as a measure of image homogeneity and is at a maximum when DNs are constant spatially (Saatchi *et al.* 2000).

Skewness (ske):

$$SKE = \frac{\sum_i (i - M)^3 P(i)}{V^2} \qquad [6.20]$$

Skewness is a measure of the asymmetry of the DN distribution in an image. A normal DN distribution is symmetric and therefore has no skew (Lane 2000).

Kurtosis (kur):

$$KUR = \frac{\sum_i (i - M)^4 P(i)}{V^2} \qquad [6.21]$$

Kurtosis is a measure of the relative peakedness (platykurtic) or flatness (leptokurtic) of the DN distribution. DN distribution with same kurtosis as the normal distribution is called "mesokurtic" (Saatchi *et al.* 2000, Lane 2000).

Coefficient of Variation (CV):

$$CV = \frac{\sqrt{V}}{M} \qquad [6.22]$$

CV is also a measure used to characterise the inhomogeneity of a DN distribution and it is particularly useful to compare relative amounts of variation in distributions with different means (Sokal and Rohlf 1995).

Local statistics texture measures were extracted using the same code IDL/ENVI (Rennó *et al.* 1998). Regenerating forest, mature forest and pasture plots were used as image subsets and the texture measures were calculated for all whole subsets.

6.5. An experiment using simulated images

Prior to analysing relationships between texture measures, logbio and backscatter, an investigation of the texture measures reviewed in section 6.4 was performed. The objective was to identify those texture measures that maximised the discrimination of textural information independently of image contrast i.e., backscatter. Different levels of "contrast" (tonal information) and "clumpiness" (textural information) were created by means of nine matrices. These matrices were conceived as simulated digital "images", with DN varying from 1 to 9, representing areas covered with vegetation disposed in big clumps, small clumps and randomly. Inside these three basic types of spatial arrangement (or texture), the contrast of these images was simulated as high, medium and low. The controlling factors were (i) mean ($\overline{X}$), which was kept constant in the images and (ii) standard deviation (S), which was adjusted by changing DN according to the intended contrast. The design of simulated images is summarised in table 6.2.

Table 6.2. Simulated images, with varying degrees of clumpiness and contrast. Standard deviations (S) defining contrast level are also shown: b refers to big clumps, s refers to small clumps and r refers to random, while contrast is defined as high, medium (med) and low.

		CLUMPINESS		
		Big clumps	**Small clumps**	**Random**
CONTRAST	**High ($S \geq 2.5$)**	bhigh	shigh	rhigh
	Medium ($S \cong 1.5$)	bmed	smed	rmed
	Low ($S \leq 1$)	blow	slow	rlow

This experiment involved a small illustrative data set, which provided an indication of algorithm sensitivity to different textures and contrast but did not account for all possible textural variation in real SAR data. The simulation of real SAR images would include a wider DN range and the inclusion of noise (to account for speckle) although that was not contemplated here. The nine matrices along with their representation as simulated digital images (in which minimum and maximum DNs were represented as black and white, respectively), are shown in figure 6.4. The random arrangement (figures 6.4.g,h,i) of the simulated images is visually similar to the real SAR images of tropical vegetation (compare with figure 6.1).

9	9	9	1	1	1	1	1	1	1
9	9	9	1	1	1	1	1	1	1
9	9	9	1	1	1	1	1	1	1
9	9	9	1	9	9	9	1	1	1
1	1	1	1	9	9	9	1	1	1
1	1	1	1	9	9	9	1	1	1
1	1	1	1	9	9	9	1	9	9
1	1	1	1	1	1	1	1	9	9
1	1	1	1	1	1	1	1	9	9
1	1	1	1	1	1	1	1	9	9

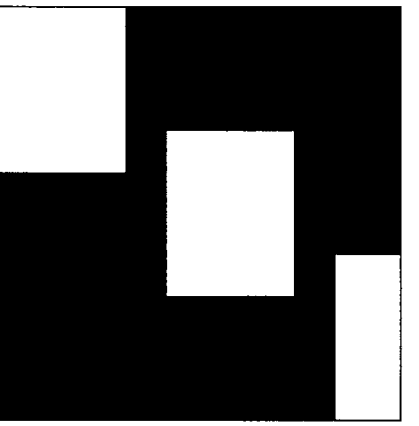

a. Big clumps, high contrast ($\overline{X}$ = 3.56, S = 3.75).

2	2	2	2	2	5	5	5	5	2
5	5	5	5	2	5	5	5	5	2
5	5	5	5	2	5	5	5	5	2
5	5	5	5	2	5	5	5	5	2
2	2	2	2	2	2	2	2	2	2
2	2	2	2	2	2	2	2	2	2
2	5	5	5	5	2	5	5	5	5
2	5	5	5	5	2	5	5	5	5
2	5	5	5	5	2	5	5	5	5
2	2	2	2	2	2	2	2	2	2

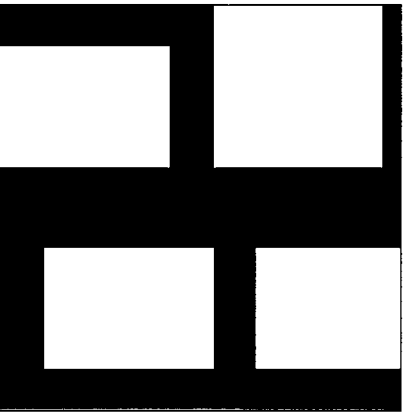

b. Big clumps, medium contrast ($\overline{X}$ = 3.56, S = 1.51).

4	4	4	3	3	3	4	4	4	4
4	4	4	3	3	3	4	4	4	4
4	4	4	3	3	3	4	4	4	4
3	3	3	4	4	4	3	3	3	3
3	3	3	4	4	4	3	3	3	3
3	3	3	4	4	4	3	3	3	3
4	4	4	3	3	3	4	4	4	4
4	4	4	3	3	3	4	4	4	4
4	4	4	3	3	3	4	4	4	4
3	4	3	3	3	3	4	4	4	4

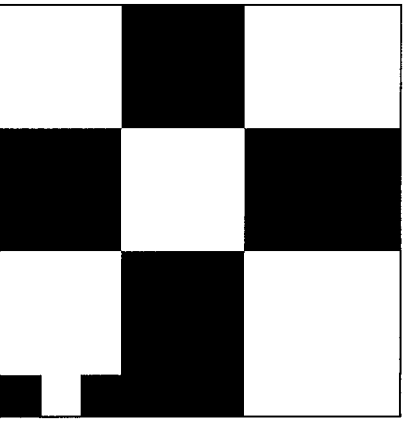

c. Big clumps, low contrast ($\overline{X}$ = 3.56, S = 0.5).

Figure 6.4. Numerical matrices and corresponding simulated digital images. Mean ($\overline{X}$) and standard deviation (S) are shown.

8	1	1	1	1	8	8	1	1	1
1	1	8	8	1	1	1	1	8	8
9	1	1	1	1	8	9	1	1	1
1	1	9	9	1	1	1	1	9	9
8	1	1	1	1	8	8	1	1	1
1	1	8	8	1	1	1	1	8	8
8	1	1	1	1	9	8	1	1	1
1	1	9	9	1	1	1	1	9	9
8	1	1	1	1	8	8	1	1	1
1	1	8	8	1	1	1	1	8	8

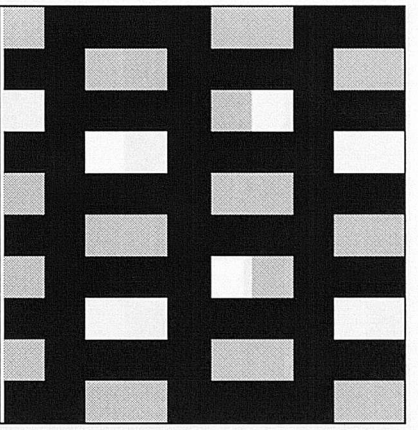

d. Small clumps, high contrast ($\overline{X}$ =3.56, S = 3.52).

5	5	2	2	5	5	2	6	6	2
5	5	2	2	5	5	2	6	6	2
2	2	5	5	2	2	2	2	2	2
2	2	5	5	2	2	2	2	5	5
5	5	2	2	5	5	2	2	5	5
5	5	2	2	5	5	2	2	2	2
2	2	5	5	2	2	5	5	2	2
2	2	5	5	2	2	5	5	2	2
5	5	2	2	6	6	2	2	6	6
5	5	2	2	6	6	2	2	6	6

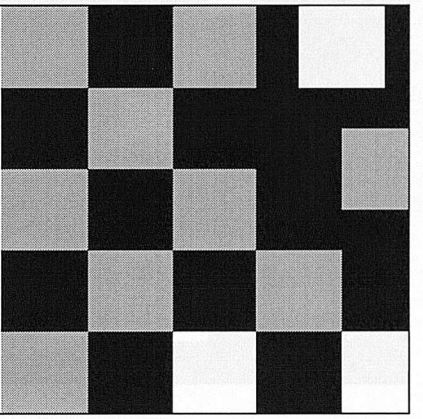

e. Small clumps, medium contrast ($\overline{X}$ =3.56, S = 1.66).

4	4	3	3	4	4	3	3	4	4
4	4	3	3	4	4	3	3	4	4
3	3	5	4	3	3	4	4	3	3
3	3	4	4	3	3	4	4	3	3
4	4	3	3	4	5	3	3	4	4
4	4	3	3	4	4	3	3	5	4
3	3	4	4	3	3	4	4	3	3
3	3	4	4	3	3	4	4	3	3
4	5	3	3	4	4	3	3	4	4
4	4	3	3	4	4	3	3	4	4

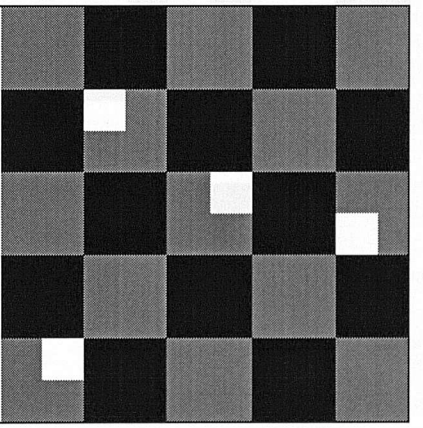

f. Small clumps, low contrast ($\overline{X}$ =3.56, S = 0.57).

Figure 6.4 (cont). Numerical matrices and corresponding simulated digital images. Mean ($\overline{X}$) and standard deviation (S) are shown.

7	1	7	6	1	6	1	1	1	6
6	1	6	1	6	2	6	1	6	1
1	2	1	1	6	1	6	2	2	1
6	7	7	1	6	1	6	7	6	6
1	1	1	6	1	6	1	1	1	7
6	2	1	1	6	1	6	2	6	1
1	7	1	6	1	7	1	7	1	6
7	1	6	1	6	1	1	1	6	1
6	7	7	6	1	6	1	7	1	6
7	1	2	6	1	6	1	1	1	6

g. Random, high contrast ($\overline{X}$ =3.56, S = 2.62).

4	2	4	3	2	7	4	3	4	5
2	3	4	3	3	3	2	3	2	4
2	3	4	3	3	5	2	2	2	3
4	7	2	7	3	3	4	5	4	2
7	5	4	5	5	4	6	3	6	4
4	3	5	5	3	6	4	3	4	5
3	2	3	6	2	5	3	2	3	5
2	3	4	3	3	3	2	3	2	4
2	7	2	3	7	4	2	5	2	2
2	3	4	3	3	3	2	3	2	4

h. Random, medium contrast ($\overline{X}$ =3.56, S = 1.4).

4	4	4	3	4	2	4	4	3	3
4	4	2	4	4	2	4	4	2	4
4	4	3	4	4	4	3	3	4	4
4	4	4	4	3	4	4	4	4	4
3	4	4	4	4	4	4	4	2	2
2	2	4	4	4	2	4	4	4	4
4	3	3	4	4	3	3	2	4	4
4	4	4	4	4	4	4	2	3	2
3	4	4	3	4	4	4	3	4	2
3	4	4	3	4	4	4	4	4	4

i. Random, low contrast ($\overline{X}$ =3.56, S = 0.72).

Figure 6.4 (cont). Numerical matrices and corresponding simulated digital images. Mean ($\overline{X}$) and standard deviation (S) are shown.

In all 22 texture measures derived from the GLCM, SADH (using 3 x 3 pixel window and 256 grey levels) and local statistics were extracted from the simulated images and variograms were computed, fitted with spherical models and used to calculate a further five texture measures.

The texture measures able to differentiate clumpiness levels regardless of contrast, and therefore texture in real data, were selected following analysis of variance (figure 6.5).

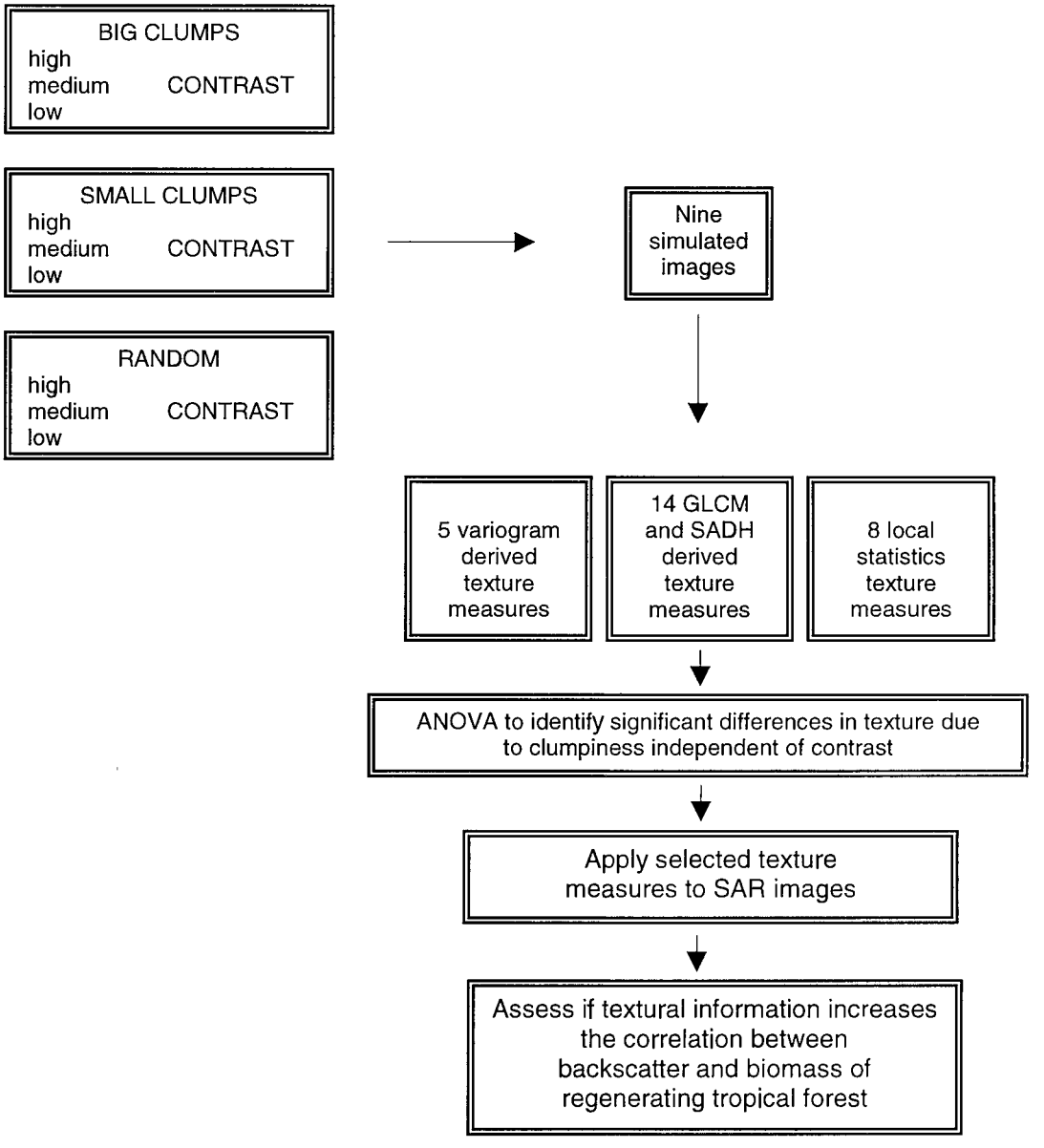

Figure 6.5. An experiment using simulated images.

6.6. Statistical and analytical procedures for evaluating texture measures

An evaluation of the ability of textural information to increase the correlation of backscatter and log of biomass (logbio) was performed using two data sets: first, 27 texture measures derived from simulated images (as described above) and second, selected texture measures derived from "real" SAR images of both study areas.

The evaluation involving simulated images aimed at selecting texture measures that recorded textural information independently of contrast (section 6.5). The mean DN of texture bands created from simulated images and descriptors from the modeled variograms were input to an Analysis of Variance (ANOVA), with differences assessed at 5% (α=0.05) significance levels. ANOVA highlighted the sensitivity of certain texture measures to particular textural features and allowed the selection of measures to be used on "real" SAR images (figure 6.5).

The texture measures selected as described above were derived from SAR data. High image quantisation levels generate sparse GLCM (Dutra and Huber 1999), which may compromise the accuracy of the probability estimates for GLCM and SADH and thus derived texture measures (Bijlsma 1993). The window size used for calculating GLCM texture measures determine the spatial characterisation of the study plots. Therefore, an additional investigation was undertaken using different quantisation levels and window sizes when deriving GLCM and SADH texture measures (table 6.1).

The decision to consider and/or discard a texture measure was based on the correlation between the texture measure and logbio. The procedures were:

(i) Scatterplots between texture measures and logbio were produced to identify trends in these relationships. (ii) These relationships were quantified by correlation analysis with Spearman's rank test. Quantisation levels and window sizes were tested and the ones that provided the strongest correlation with logbio were selected. (iii) All the texture measures that were correlated strongly with logbio were selected. More details of this procedure are provided in section 6.7.5. (iv) Data from the two study areas were combined and backscatter added to the analysis. Logbio was regressed against backscatter and the texture measures in a stepwise multiple

regression procedure. The texture measures that increased the correlation between backscatter and logbio were identified and models relating these three variables were proposed.

6.7. Results

The results were presented in two sections:

- In section 6.7.1. simulated images and the utility of 27 texture measures were explored. The texture measures that maximised the discrimination of textural information independently of image contrast were selected for use in section 6.7.2.

- In section 6.7.2. the measures selected were applied to real SAR data. The textural information was related to the log of biomass of the regenerating forest, mature forest and pasture plots in Manaus and Tapajós study areas.

6.7.1. Texture measures in simulated images

The 27 texture measures derived from the simulated images are discussed here. The main concern was to check the potential utility of those measures in discriminating texture regardless of contrast. The statistical significance of the differences in texture values for levels of clumpiness and contrast were assessed by ANOVA. Intuitive expectations about the performance of each texture measure were not always met, as human perception of texture is subjective.

6.7.1.1. Texture measures derived from the variogram

A summary of the variogram descriptors is presented in table 6.3. The modeled variograms indicated no nugget variance in any of the models as there was neither noise nor sub-pixel spatial variability.

Values of range tended to increase according to clumpiness and were indicative of the size of elements within the images. In *big clumps* images, range corresponded roughly to the size of the clumps (three pixels). For *small clumps* images ranges were smaller than in *big clumps* and were indicative of the average spacing of clumps (one pixel). Random images presented decreasing values of range for increasing contrast levels. Range was the only variogram-derived measure that seemed invariant to contrast (table 6.3)

Table 6.3. Semivariance at lags 1, 2 and 3, sill and range of variograms produced from simulated images and fitted with spherical models.

		lag1	lag2	lag3	sill	range
Big clumps	**High contrast**	4.8	9.34	13.76	15.17	3.62
	Medium contrast	1.2	2.03	2.65	2.34	2.56
	Low contrast	0.12	0.21	0.3	0.26	2.57
Small clumps	**High contrast**	13.96	13.72	13.7	12.38	0.97
	Medium contrast	2.16	3.59	2.47	2.77	1.7
	Low contrast	0.31	0.48	0.29	0.33	1.26
Random	**High contrast**	9.14	5.27	7.55	6.87	0.97
	Medium contrast	1.89	2.02	1.94	2.02	1.27
	Low contrast	0.45	0.58	0.49	0.51	1.42

Semivariance showed increasing values with lag for *big clumps* images. For *small clumps* and *random* images no pattern was found and the semivariance either increased or decreased with lag. Decreasing values of semivariance occurred for decreasing contrast levels.

Sill values were distinct according to contrast levels and operated as indicators of the total variance of the images, which was obviously high for high contrast and decreased for medium and low contrast.

6.7.1.2. Texture measures derived from GLCM and SADH

Although not always statistically significant, the different values of GLCM derived texture measures (x) were normalised ($(x - x_{min}) / (x_{max} - x_{min})$) for comparison. They

are plotted in figures 6.6 and 6.7. As the normalisation process produced values ranging between 0 and 1, data trends must be interpreted with care.

Values of GLCM contrast and entropy were very similar and both increased with decreasing clumpiness (figure 6.6). These measures contain information about DN disorder and scatter, they are, therefore, more likely to differentiate clumpiness than contrast.

GLCM energy and homogeneity values were similar for *big clumps* and *small clumps* images (figures 6.6). In addition, for both measures *random* images exhibited minimum and maximum values for medium and low contrast, respectively, indicating their sensitivity to contrast. The theory underlying these measures is related to uniformity and local similarity of pixel values and therefore these measures are unlikely to be suitable for differentiating clumpiness.

GLCM correlation and chi-square values varied with clumpiness (figure 6.6). Contrast levels were not distinct, as in *big clumps* images correlation mean values were very similar. High correlation values corresponded to low chi-square values and *vice-versa*, denoting the diverse information contained in these two measures.

The first two measures derived from sum of vector technique - mean and variance - varied according to clumpiness and, to a less extent, to contrast (figure 6.7). Entropy of the sum vector values varied with contrast, especially for *small clumps* and *random* images. Energy of the sum vector values, however, did not differentiate either clumpiness or contrast (figure 6.7).

The measures derived from the difference vector – mean and variance - did discriminate clumpiness and contrast (figure 6.7). For entropy and energy of difference vector, the discrimination of clumpiness and contrast was less apparent (figure 6.7). That made those measures less likely to discriminate texture in real SAR data. Values of entropy and energy of sum and difference vectors were similar with basically the same trends and magnitudes.

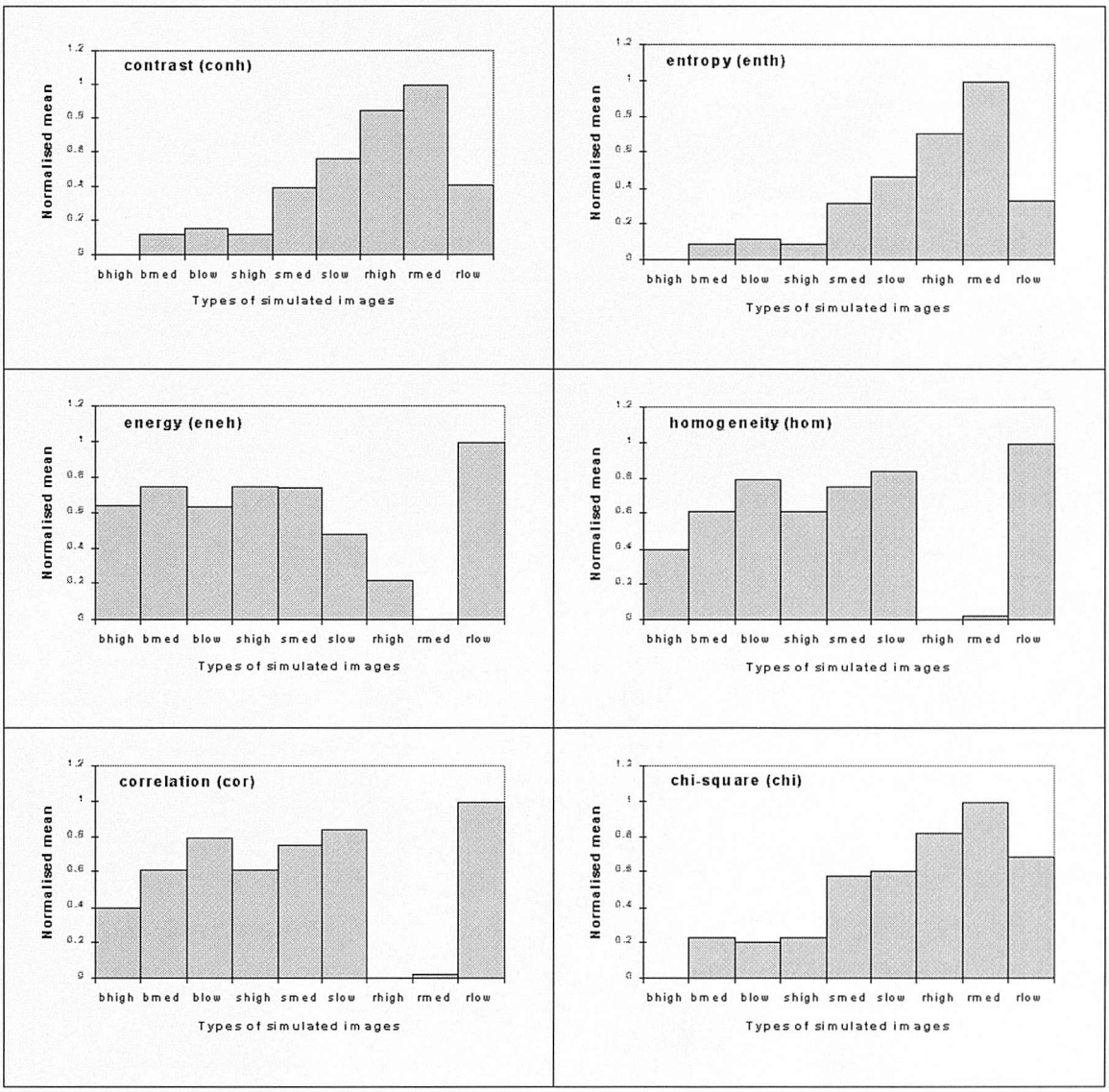

Figure 6.6. Normalised mean values of GLCM derived texture measures from simulated images. Codes for the simulated images are: b for big clumps, s for small clumps and r for random; high, med and low for high, medium and low contrast.

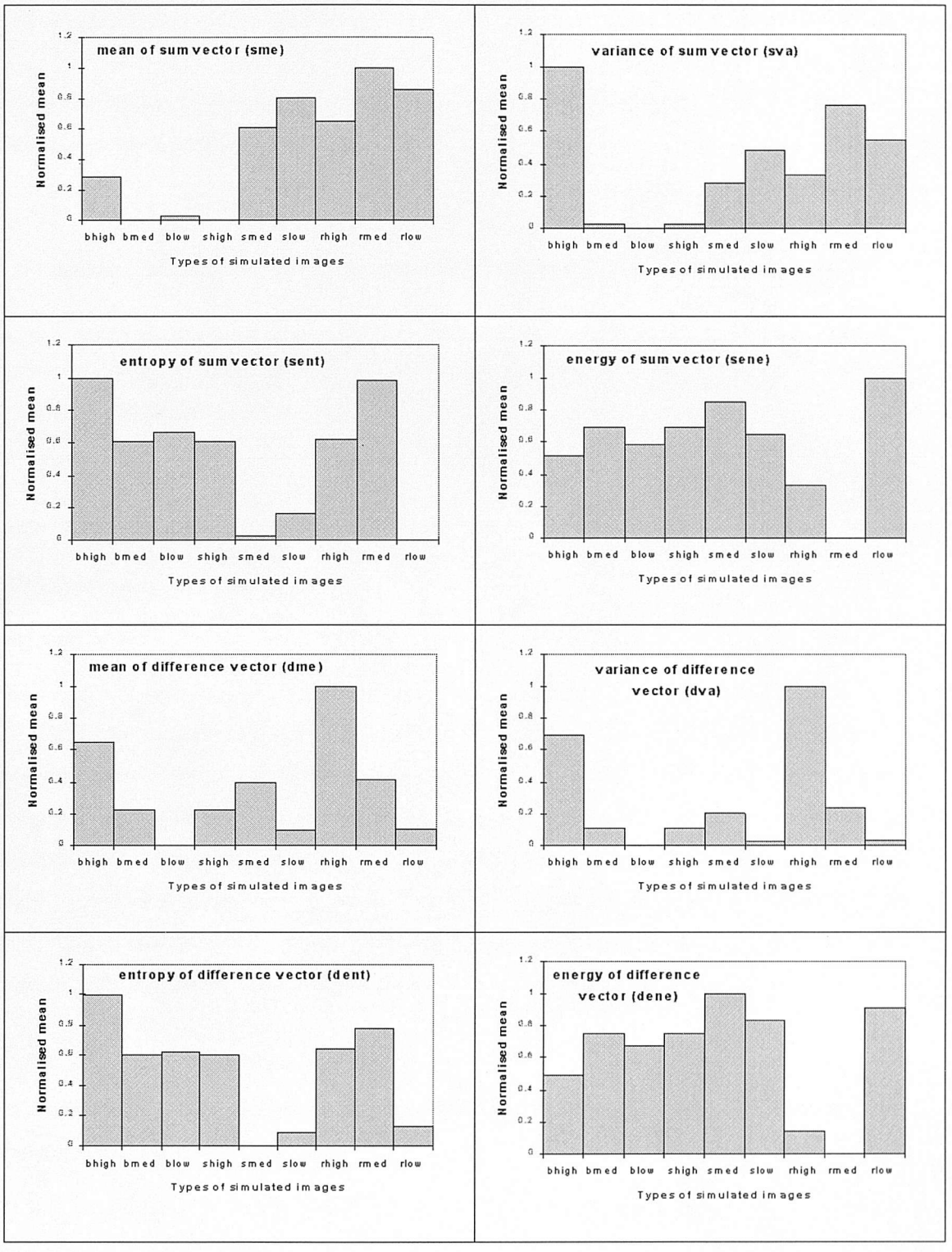

Figure 6.7. Normalised mean values of SADH derived texture measures from simulated images. Codes for the simulated images are: b for big clumps, s for small clumps and r for random; high, med and low for high, medium and low contrast.

6.7.1.3. Texture measures derived from local statistics

The local statistics measures were not normalised due to the negative values for skewness and kurtosis (table 6.4).

Table 6.4. Texture measures derived from local statistics for simulated images.

		mad	med	ent	ene	ske	kur	CV
Big clumps	**High contrast**	1.98	1.53	0.09	0.34	0.12	-0.51	0.34
	Medium contrast	1.83	1.79	0.11	0.31	0.03	-0.69	0.18
	Low contrast	1.72	1.72	0.11	0.30	0	-0.78	0.06
Small clumps	**High contrast**	1.83	1.79	0.11	0.31	0.03	-0.69	0.18
	Medium contrast	1.65	1.52	0.15	0.25	0.11	-0.91	0.23
	Low contrast	1.74	1.72	0.17	0.23	0.13	-0.82	0.08
Random	**High contrast**	1.68	1.31	0.22	0.20	0.10	-0.96	0.39
	Medium contrast	1.83	1.70	0.28	0.15	0.22	-0.50	0.18
	Low contrast	1.76	1.92	0.15	0.28	-0.56	-0.08	0.09

The local statistics entropy was sensitive to clumpiness as it presented low values for *big* and *small clumps* images, opposing to the higher values found for *random* images (i.e., higher heterogeneity). Energy values, however, were less sensitive to clumpiness and contrast. Coefficient of variation decreased with image contrast for each clumpiness level making it unsuitable for quantifying texture in real data. The remaining measures, i.e., mean absolute deviation (mad), median, skewness and kurtosis, did not differentiate clumpiness.

6.7.1.4. Statistically significant differences in texture for different levels of clumpiness and contrast

Analysis of variance (ANOVA) was performed to test if differences in the values of texture measures identified above were statistically significant for different levels of contrast and different levels of clumpiness. The ANOVA results show *p*-values for testing those differences at $\alpha=0.05$ (table 6.5).

None of the texture measures considered was able to discriminate contrast and clumpiness concomitantly. Contrast was differentiated by five texture measures: geostatistical measures such as semivariance at lags 1, 2 and 3 (lag1, lag2 and lag3, respectively), variogram's sill and coefficient of variation (CV). Semivariance estimates have been used as "semivariogram signature" of tropical vegetation types and have been used successfully in their classification (Miranda *et al.* 1996, 1998). Sill is a measure of image contrast and was expected to vary accordingly (Cohen *et al.* 1990). CV was, as already pointed out, a useful measure for discriminating tropical forest regeneration stages (Luckman *et al.* 1997, Yanasse *et al.* 1997) and boreal forest types (Kurvonen and Hallikainen 1999).

Clumpiness (texture) was differentiated by range, a measure of the "coarseness" of the image (Rubin 1990) and also of the size of image elements (Treitz and Howarth 2000).

GLCM derived measures such as contrast (conh), entropy (enth), correlation (cor), chi-square (chi) and mean of the sum vector (sme) also differentiated clumpiness. Contrast, entropy and correlation are some of the more relevant measures that can be derived from the GLCM (Weszka *et al.* 1976, Haralick 1979, Baraldi and Parmigiani 1995). They have been used extensively for texture analysis in forest mapping (Ulaby *et al.* 1986, Kushwaha *et al.* 1994), land cover mapping (van der Sanden and Hoekman 1999, Korusu *et al.* 1999) and crop discrimination (Soares *et al.* 1997) with varied degree of success. The assumption that preceded initial computations of GLCM was that it contains all textural information of an image (Haralick *et al.* 1973) and justifies the inclusion of some of its derived measures for clumpiness differentiation.

Local statistics entropy (ent) also differentiated clumpiness levels, despite the small DN range of the simulated images (1-9).

The remaining 15 measures (out of 27) did not show any sensitivity either to clumpiness or contrast.

Table 6.5. *P*-values for differences in contrast and clumpiness levels. The values statistically significant at α =0.05 were indicated in bold.

	CONTRAST	CLUMPINESS
lag1	**0.013**	0.736
lag2	**0.011**	0.734
lag3	**0.001**	0.886
sill	**0.003**	0.855
range	0.991	**0.005**
conh	0.838	**0.031**
enth	0.974	**0.049**
eneh	0.627	0.664
hom	0.105	0.485
cor	0.904	**0.006**
chi	0.943	**0.012**
sme	0.942	**0.029**
sva	0.546	0.524
sent	0.083	0.314
sene	0.248	0.759
dme	0.070	0.612
dva	0.082	0.617
dent	0.269	0.196
dene	0.519	0.198
mad	0.595	0.462
var	0.065	0.710
ske	0.342	0.688
kur	0.789	0.463
cv	**0.020**	0.865
med	0.300	0.973
ent	0.753	**0.044**
ene	0.733	0.078

In summary, the seven measures identified as sensitive to clumpiness but not contrast were:

- variogram range (range).
- GLCM contrast (conh),
- GLCM entropy (enth),
- GLCM correlation (cor),
- GLCM chi-square (chi),
- SADH mean of sum vector (sme),
- local statistics entropy (ent)

6.7.2. *Texture measures in SAR images*

The above 7 measures derived from JERS-1 SAR images were used to determine the relationship between texture and log of biomass of regenerating forests, mature forests and pasture plots.

6.7.2.1. Texture measure derived from variogram - range

Variograms have been used to characterise the spatial structure of vegetation. These have been calculated using field transect data (Wallace *et al.* 2000) or from combined field and remotely sensed data (Cohen *et al.* 1990, Bijlsma 1993, Lacaze *et al.* 1994, Treitz and Howarth 2000). Resulting trends of range and sill variation as a function of forest type, for example, were observed using variogram and modelled variogram descriptor analyses (Treitz and Howarth 2000). Such empirical studies have demonstrated that range is determined by the size of objects in the image (Woodcock *et al.* 1988b).

Figure 6.8 shows a variogram for 3 selected plots in the Tapajós study area. Semivariance estimates did not provide a unique "signature" for regenerating and mature forest plot. The values shown in figure 6.8 were derived from pixel transects, where only a sample of data values was considered. Pixel transects were not as

representative of the vegetation types in the images as matrices of pixels would have been (Cohen *et al.* 1990). However transects were used here due to software limitations.

The variograms (figure 6.8) had a multifrequency shape (Curran 1988) for the overlapping regenerating and mature forest plots and no pattern was recognised. The remaining plots in both study areas are not presented here as they showed variograms similar to the ones seen in figure 6.8 with no trend apparent. The range of influence was about three lags for the three plots, which can be a sign of the low spatial correlation in the data as a consequence of a random component in pixel DN introduced by speckle noise. The variogram results indicated the need for modelled variogram analysis to assess if the range would act as an indicator of vegetation structure in SAR images.

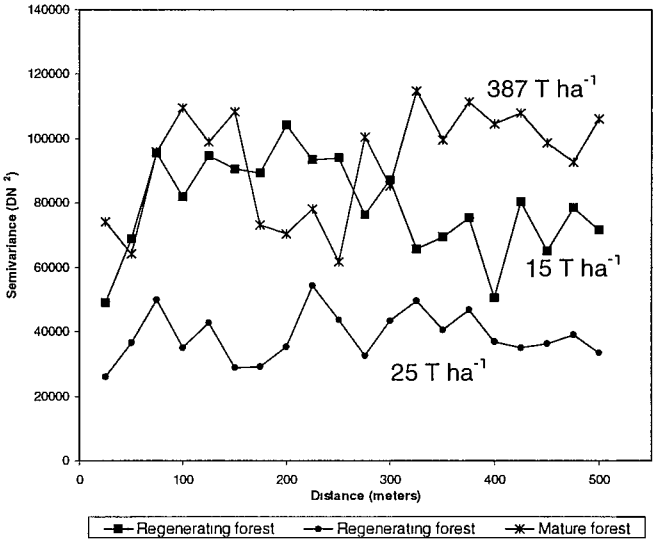

Figure 6.8. Variograms derived from three forest plots (with corresponding biomass estimates) in JERS-1/SAR images of Tapajós study area.

The ranges of the modelled variograms for both study area plots are presented in table 6.6. The variograms for plots 3, 7 and 8 in Manaus study area could not be modelled using a spherical model and were therefore discarded. Biomass estimates and dominant genera for each plot are also included in table 6.6.

Comparison among relative values of range was performed with care, as no indication of goodness of model fit was available for the different variograms produced.

Table 6.6. Range of variograms for pixel transects. Spherical models were fitted to the variograms. Plot number, biomass and dominant genera in Manaus (m) and Tapajós (t) study areas. NA refers to not available.

Plot (biomass – T ha^{-1})	Dominant genera	Range (m)
m1 (144.1)	*Cecropia*	185
m2 (131.3)	*Vismia, Cecropia*	119
m4 (144.8)	*Cecropia, Guatteria*	205
m5 (134.7)	*Vismia, Bellutia*	49
m6 (124.3)	*Vismia, Cecropia*	113
m9 (91)	*Cecropia*	43
m10 (127)	*Cecropia*	164
m11 (126.1)	*Cecropia, Laetia*	93
m12 (131.5)	*Vismia*	181
m13 (156.6)	*Laetia, Vismia*	73
m14 (117.4)	*Vismia, Miconia*	39
m15 (116.3)	*Goupia, Vismia*	156
m16 (32.6)	*Goupia, Vismia*	129
m17 (387)	NA	50
m18 (2)	NA	170
t1 (62)	*Cecropia*	82
t2 (15)	NA	232
t3 (62)	*Poecilanthe, Cecropia*	48
t5 (54)	*Vismia*	165
t6 (82)	*Vismia*	176
t7 (78)	*Mangifera*	45
t8 (104)	*Guatteria*	131
t9 (75)	*Orbignya*	100
t10 (181)	NA	49
t11 (101)	*Sloanea*	93
t12 (42)	*Orbignya, Poecilanthe*	45
t13 (89)	*Vismia, Guatteria*	90
t14 (25)	*Vismia*	106
t15 (387)	NA	188
t16 (387)	NA	144
t17 (387)	NA	93
t18 (387)	NA	93
t19 (2)	NA	49
t20 (2)	NA	79

Dominant genera were included in table 6.6. to indicate upper canopy structure, which was smooth for *Cecropia*-dominated and rougher for *Vismia*-dominated regenerating forest plots (Lucas *et al.* 2000). Shadows of emergent trees provide the roughness of upper canopies of mature forest and older stages of forest regeneration (Grover *et al.* 1999). Range values in table 6.6 varied from 39 to 205 meters suggesting different canopy structure and roughness patterns, although no trend was evident. A relationship between range and logbio was not observable, probably due to the absence of a direct relation between logbio and structure of canopy, at least in the diverse regenerating tropical forests.

Figure 6.9 illustrates variograms for 8 forest plots in Manaus and Tapajós study areas. The upper two variograms (m1 and t1) are for plots dominated by *Cecropia* genera even though range values were distinct. For t1, the variogram suggested periodicity (i.e. a repetitive pattern) in the canopy (Curran 1988) and not the homogeneity of a smooth canopy. M2 and t6 plots were dominated by *Vismia* plus *Cecropia* and only by *Vismia*, respectively. These plots had ranges that varied by around 50 meters. The variograms in figure 6.9 for plots m5 and t13 were both dominated by *Vismia* plus *Bellutia* and *Guatteria* genera, respectively. Because the ranges of both m5 and t13 plots varied by 40 meters, similar canopy structures could have been effectively captured by the variograms. The mature forest plots (m17 and t18) displayed high sills, indicative of rough canopy surfaces and visually contrasted land covers in SAR images (Miranda *et al.* 1998), with ranges of 50 and 93 meters, respectively.

The image spatial resolution (18 meters) and an averaged pixel size of 25 meters prevented the quantification of tree crown diameters. Even though tree crowns are not always individualised in forest formations, the plots could have presented clumps or density patterns detected by variogram range at higher spatial resolutions. The inability to define the spatial characteristics of regenerating vegetation through modelled variogram descriptors could also be linked to the nature of the model used. Although being best suited for the overall set of different regenerating forest plots, the spherical model reaches an absolute sill. That implies that the vegetation has a clumpy canopy structure, which was not always true for the vegetation studied here (Wallace *et al.* 2000).

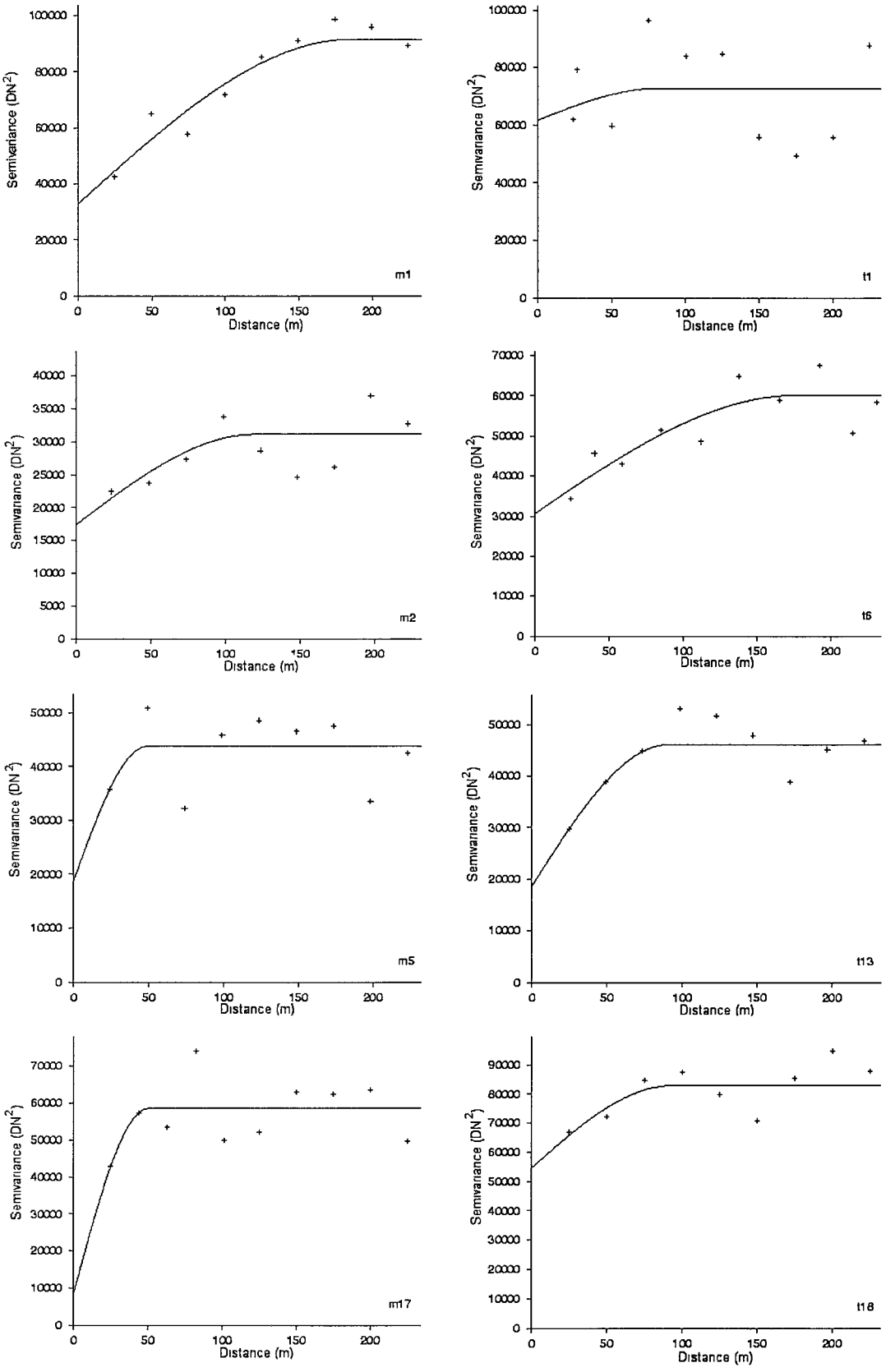

Figure 6.9. Variograms for eight forest plots in the Manaus (m) and Tapajós (t) study areas. Spherical models were fitted to the variograms, their descriptors and plot characteristics are in table 6.6.

The regenerating forest plots in Manaus and Tapajós study areas were located in relatively homogeneous areas that were probably not large enough to allow their spatial structure and physiognomy to be represented by variogram range (Lacaze *et al.* 1994). Detailed vegetation horizontal profiles and, in the case of larger homogeneous areas of regenerating forest plots, regularised variograms would help to reveal spatial variation in the data (Atkinson and Curran 1997). Furthermore, high-spatial resolution sensors would provide more information on vegetation structure and status that could be linked potentially to the features seen in variograms (Wallace *et al.* 2000).

Scatterplots of the range and log of biomass were produced for Manaus and Tapajós study area plots (figures 6.10 and 6.11).

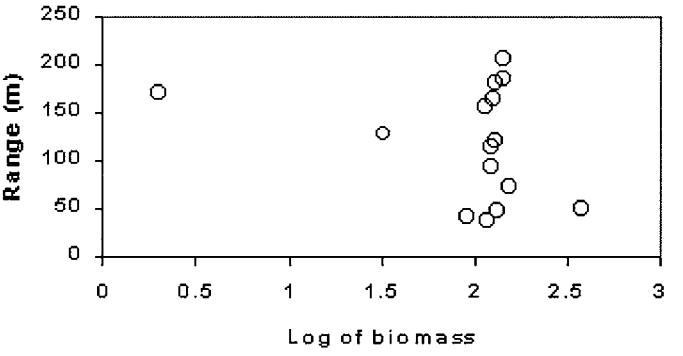

Figure 6.10. Scatterplots for range and log of biomass of Manaus study area plots. Variograms estimated from a SAR image (December 1995).

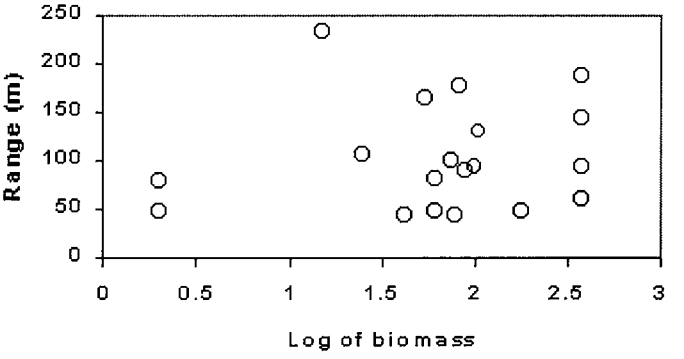

Figure 6.11. Scatterplots for range and log of biomass of Tapajós study area plots. Variograms estimated from a SAR image (July 1994).

6.7.2.2. Texture measures derived from GLCM and SADH – contrast, entropy, correlation, chi-square and mean of sum vector

Before the scatterplots between log of biomass and the five GLCM and SADH derived texture measures is presented, the effect of window size and quantisation level in these texture measures derivation is discussed.

Effect of window size and quantisation level

The choice of an optimal window size and quantisation level of the texture data had a major effect on the correlation analyses performed later. Figure 6.12 shows GLCM contrast values derived from different configurations of window size and quantisation level for the Tapajós study area plots.

Figure 6.12 shows that, for the same window size, contrast values increased according to quantisation level for 4 GL, 16 GL and 64 GL. For 256 GL, contrast values were situated surprisingly between 4 GL and 16 GL. Contrast values carried similar textural information at the different quantisation levels. Increasing and decreasing trends were approximately the same for 16, 64 and 256 grey levels. Similar trends had been noticed in texture measures derived using GLCM for SPOT-1 HRV (high resolution visible) data quantisised in 16 GL and 32 GL (Marceau *et al.* 1990). Contrast values were very similar for 5 x 5 and 3 x 3 pixel windows at all quantisation levels. The range of contrast values for 4 GL was wider and the lower contrast values coincided with the lower biomass plots: plot 2 with 15 T ha^{-1}, plot 14 with 25 T ha^{-1} and plots 19 and 20 with 2 T ha^{-1}. Although the quantisation in only 4 GL will result in information loss (Haralick and Shanmugan 1974), a small number of GL reduces the complexity and sparseness of a GLCM (Dutra and Huber 1999). A smaller GLCM could have improved the spatial characterisation of land covers studied here.

The resulting virtual invariance of contrast values with window size might have been a result of the small range of window sizes used here. Being an image sample from which texture measures were estimated, larger window sizes contain increased textural information (Kurvonen and Hallikainen 1999). *A priori* knowledge about the

Manaus and Tapajós study areas prevented the choice of window sizes larger than 5 x 5 pixels. The expected increase in contrast values with window size (and increase in information content) was not noticeable, also as a result of the small window sizes.

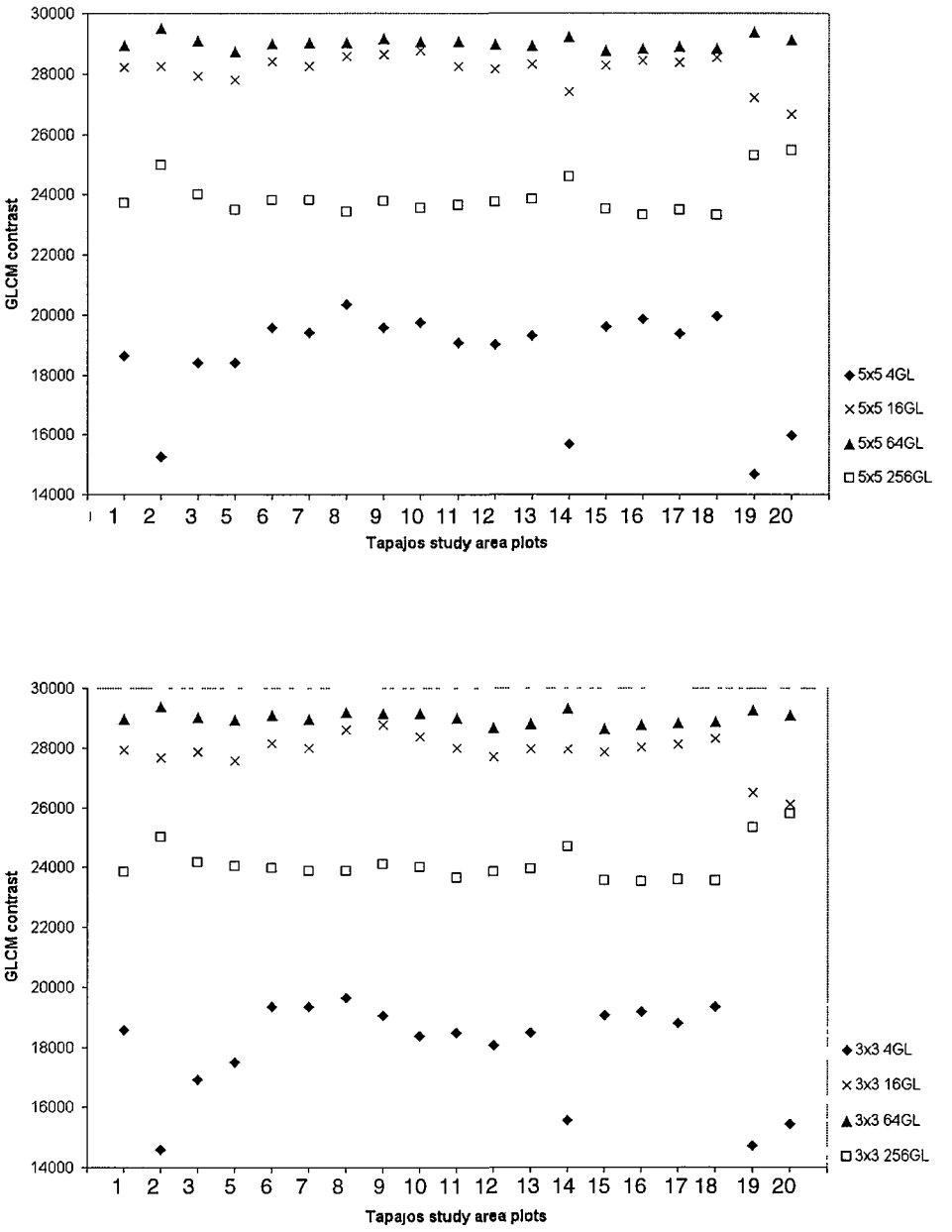

Figure 6.12. GLCM contrast derived from 5x5 pixel window (top), 3x3 pixel window (bottom) and 4, 16, 64 and 256 quantisation levels for Tapajós study area plots. 5x5 and 3x3 are the pixel window sizes and GL refers to grey levels. In X-axis 1 to 14 are regenerating forest plots, 15 to 18 are mature forest plots and 19 to 20 are pasture plots.

Scatterplots of texture measures and log of biomass

Scatterplots of the relationships between texture measures and logbio were produced for Manaus and Tapajós study area data sets (figures 6.13 and 6.14). The first column of the figures shows the relationship between logbio (X-axis) and the 5 texture measures (Y-axis) that were sensitive to clumpiness but not contrast (section 6.7.1). The remaining columns showed the interrelationships between the 5 texture measures.

Figure 6.13 shows a positive near-linear relationship for logbio of Manaus study area plots and GLCM contrast (conh) and entropy (enth). A negative relationship (only noticeable due to the pasture site – lowest biomass value), where an increase in logbio values was paralleled by a decline in Y values, was found for GLCM correlation (cor) and chi-square (chi). SADH mean of sum vector (sme) also showed a near linear-like positive relationship with logbio.

In figure 6.14, where the scatterplots for Tapajós study area are displayed, the relationships between logbio and GLCM contrast and entropy were more pronounced than in Manaus plots. This was due to the wider range of logbio in the Tapajós study area. However, no apparent relationship was found between logbio and GLCM correlation and chi-square. SADH mean of the sum vector (sme) had a positive relationship with logbio (figure 6.14).

When looking for relationships amongst GLCM measures, it was clear that some of them were highly interrelated (Ulaby *et al.* 1986), mainly GLCM contrast and entropy (figure 6.13 and 6.14). For the Manaus data, all GLCM measures were interrelated. That was not true for Tapajós data, where only contrast and entropy were interrelated. In the Manaus data, SADH mean of the sum vector seemed related to the four GLCM measures but for Tapajós data that relationship was present only with contrast and entropy.

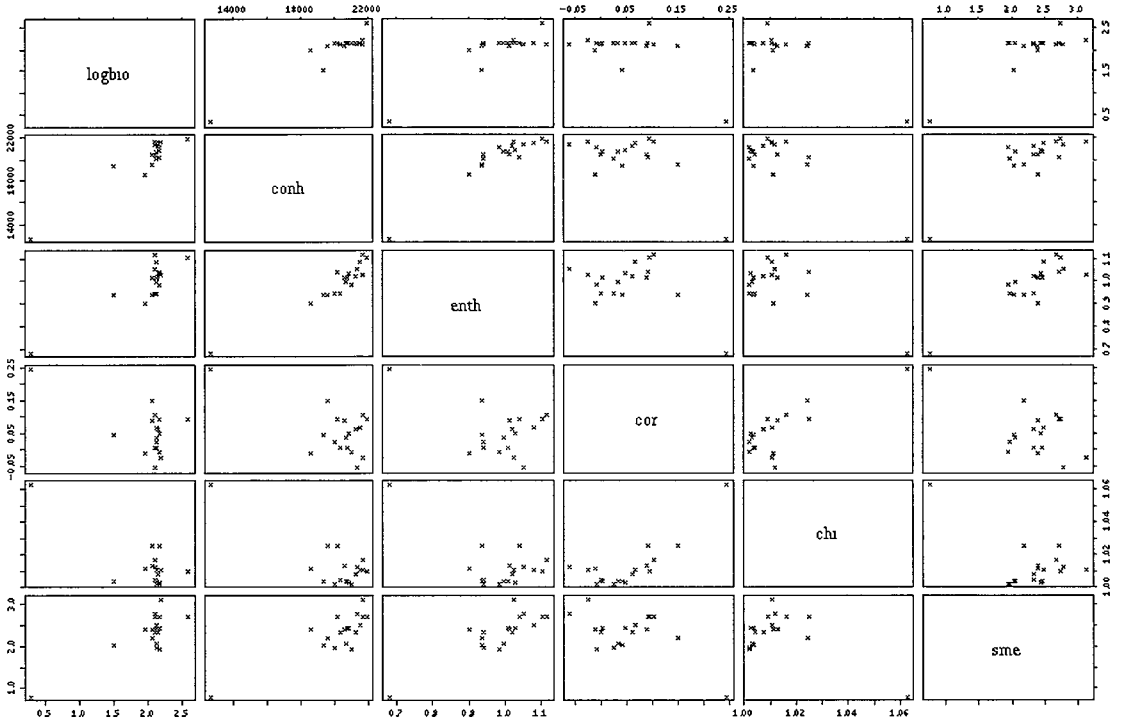

Figure 6.13. Scatterplots for selected texture measures and log of biomass for the Manaus study area. For GLCM derived measures (conh, enth, cor, chi, sme) matrices were estimated using a 5x5 pixel window and a 2-bit (4 GL) SAR image (December 1995).

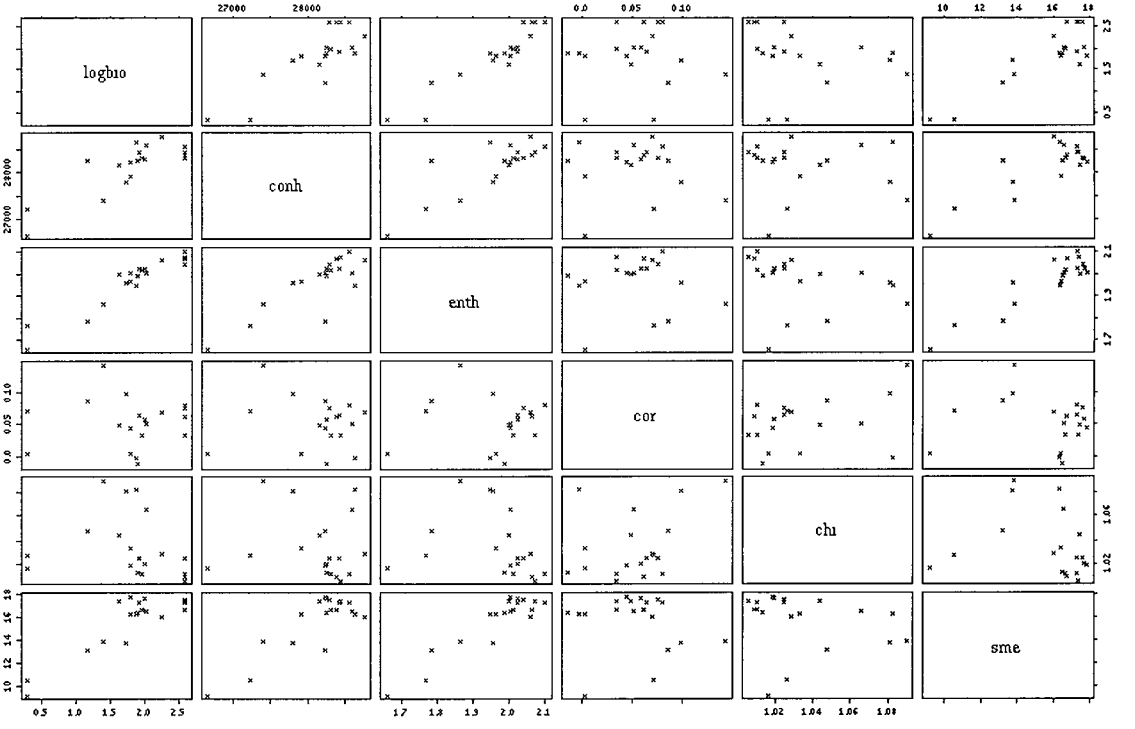

Figure 6.14. Scatterplots for selected texture measures and log of biomass for the Tapajós study area. For GLCM derived measures (conh, enth, cor, chi, sme) matrices were estimated using a 5x5 pixel window and a 4-bit (16 GL) SAR image (July 1994).

The relationship between the GLCM and SADH-derived texture measures and logbio was probably due to the increase in roughness and complexity of forest canopy that follows biomass accumulation during growth and maturation of forests. GLCM contrast and entropy are associated with the degree of spread and disorder of GL. The values of those measures increased with logbio due to increased scattering in a rough canopy/high biomass forest. Similarly, GLCM correlation and chi-square were associated with resemblance and repetition of GL. The values of those measures tended to decrease with biomass, following the lower backscattering (and therefore GL variations) from smoother and less layered young canopy.

6.7.2.3. Texture measure derived from local statistics - entropy

For the Manaus study area, no relationship was found between local statistics entropy and logbio (figure 6.15). For the Tapajós study area, however, some increase of entropy values with logbio was noticeable, although pasture plots and intermediate biomass regenerating forest plots did not follow this trend (figure 6.16).

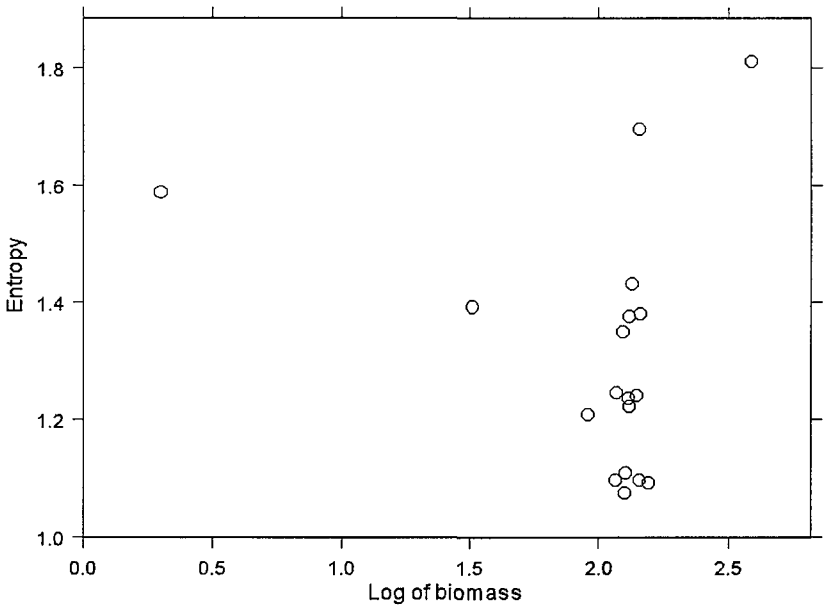

Figure 6.15. Scatterplots for texture measure entropy (estimated from a SAR image of December 1995) and log of biomass of Manaus study area.

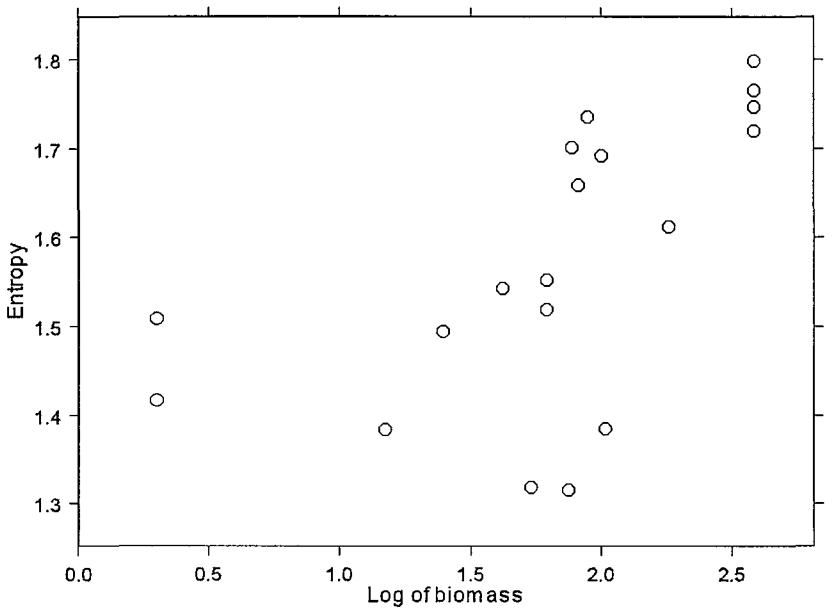

Figure 6.16. Scatterplots for texture measure entropy (estimated from a SAR image of July 1994) and log of biomass of Tapajós study area.

6.7.2.4. Analysis of correlation between texture measures and log of biomass

The strength of the relationships previously observed in the scatterplots was quantified using correlation analysis. In addition, the eight configurations (window sizes and quantisation levels) from which the texture measures derived from GLCM and SADH were computed and statistically assessed.

The scatterplots in section 6.7.2.2 showed that for some measures the relationship between texture and logbio was not linear. Moreover, Kolmogorov-Smirnov goodness-of-fit tests showed that for the texture measures investigated the data were not normally distributed. Therefore a rank correlation coefficient (Spearman's *r*) was calculated, as it does not limit analysis to a particular statistical distribution or parameter (Isaaks and Srivastava 1989).

The logbio and texture relationships with the highest *r* were the basis to further considering some of the texture measures previously studied. This procedure is described below:

i) For each study area, the correlation coefficient (*r*) between logbio and texture was computed. The highest *r* for each GLCM and SADH texture measure derived in eight different configurations was highlighted and then the configuration with the maximum number of highest *r* was selected.

ii) The texture measures that were related most strongly to logbio were selected on the basis of data from both study areas.

According to Spearman's *r* no correlation was found between range and logbio in both study areas. This result was already suggested by the scatterplots in section 6.7.2.2.

Many factors could be contributing to the weak relation between logbio and range. The small size of homogeneous areas and therefore transects used for deriving the variograms can be a limiting factor as the transects represent only a small portion of the regenerating forests plots (Cohen *et al.* 1990). In addition, range is a measure of clumpiness and biomass is a continuous variable related to the spatial structure of vegetation. When these variables are used jointly, they were not suitable for describing the spatial structure of the vegetation studied. Tree crowns and clumps, if present, were probably not detected by range at the spatial resolution of the JERS-1 SAR images.

The entropy was related to logbio for Tapajós study area plots (Spearman's r=0.73) but not for Manaus study area plots. This measure, therefore, was discarded.

The correlation between logbio and the five texture measures extracted in eight different configurations is presented in table 6.7 (Manaus study area) and table 6.8 (Tapajós study area). The distinct configurations (section 6.4.2) refer to window sizes and quantisation levels (GL) used for extracting GLCM and SADH derived texture measures.

The results for the Spearman's correlation between logbio and the GLCM and SADH derived texture measures are presented in table 6.7 and 6.8. A 5 x 5 pixel window and 4 GL was the configuration most strongly related to logbio and therefore was

selected for extracting texture measures for Manaus study area plots. Generally, the *r* values were similar for both study areas.

Table 6.7. Spearman's correlation coefficient between logbio and GLCM derived texture measures for Manaus study area.

Texture measure	5x5, 4 GL	5x5, 16 GL	5x5, 64 GL	5x5, 256 GL	3x3, 4GL	3x3, 16 GL	3x3, 64 GL	3x3, 256 GL
conh	**0.68**	0.24*	-0.15*	-0.47	0.45*	0.02*	-0.34*	-0.61
enth	**0.56**	0.48	0.09*	-0.03*	0.53	0.29*	-0.07*	-0.05*
cor	-0.21*	-0.23*	-0.24*	-0.22*	-0.14*	-0.14*	-0.24*	-0.23*
chi	-0.44*	-0.22*	-0.07*	-0.09*	-0.36*	-0.09*	-0.001*	0.01*
sme	0.48	0.45*	0.45*	0.44*	0.45*	0.46*	**0.49**	0.48

Note: Correlation coefficients not significant at 95% confidence levels are signalled with an asterisk(*). The highest coefficients for each measure are in bold.

Correlation (cor) and chi-square (chi) were not related to logbio in any configuration tested (table 6.7).

The logbio of Tapajós study area plots and GLCM and SADH derived texture measures were highly correlated (table 6.8). Correlation (cor) was not significantly related with logbio.

Table 6.8. Spearman's correlation coefficient between the logbio and GLCM derived texture measures for Tapajós study area.

Texture measure	5x5, 4 GL	5x5, 16 GL	5x5, 64 GL	5x5, 256 GL	3x3, 4GL	3x3, 16 GL	3x3, 64 GL	3x3, 256 GL
conh	**0.87**	0.79	-0.62	-0.79	0.75	0.69	-0.53	-0.81
enth	0.85	**0.94**	0.85	0.76	0.86	0.91	0.78	0.71
cor	-0.06*	0.01*	-0.02*	0.02*	0.13*	-0.24*	0.14*	0.2*
chi	-0.16*	-0.5	-0.49	-0.48	-0.04*	-0.43*	**-0.51**	-0.48
sme	0.6	0.61	0.61	0.61	0.6	**0.62**	0.6	**0.62**

Note: Correlation coefficients not significant at 95% confidence levels are signalled with an asterisk(*). The highest coefficients for each measure are in bold.

On the basis of results in the two previous tables, three GLCM and SADH derived texture measures were selected, based on the results from 5 x 5 pixel window size and quantisation of 4 GL for Manaus study area and of 16 GL for Tapajós study area. The following measures were related significantly to logbio in both study areas: contrast, entropy and mean of sum vector. Measures discarded were correlation and chi-square due to absence of relationship with logbio in Manaus study area.

6.7.2.4. Multiple regression analysis – Log of biomass, backscatter and the texture measures

The association between the texture measures and logbio was assessed. Three texture measures - GLCM contrast, entropy and SADH mean of sum vector – were selected following their strong relation to the log of biomass. As this chapter aims to use textural information to increase the correlation between backscatter and logbio, backscatter was added to the analysis.

The backscatter, log of biomass and texture measures values from Manaus and Tapajós study areas were merged and the analysis performed jointly. This was due to the strong relation of the texture measures to the logbio of both study areas and, additionally, to the stronger relationship between the variables when considering an increased range of biomass. Despite selecting different "suitable" configurations for extracting GLCM and SADH texture measures for each study area (section 6.7.2.2), the multiple regressions were performed using data collected under the same configuration: 5 x 5 pixel window and 4 GL. The magnitude of texture measures values was also a function of configuration settings, so it was not possible to combine values from the two study areas derived under different window sizes and quantisation levels. 5 x 5 pixel window and 4 GL was Manaus' study area most suitable configuration, but for Tapajós study area it still presented a strong correlation between logbio and the texture measures selected.

Stepwise multiple regression was performed as it allowed simultaneous analysis of more than one variable. Regression analysis also allows prediction of one variable from another or others (Neter *et al.* 1996).

Scatterplots - logbio, backscatter and the texture measures

Figure 6.17 shows the scatterplots produced with backscatter, logbio and texture measures GLCM derived contrast, entropy and SADH derived mean of sum vector data from the two study areas.

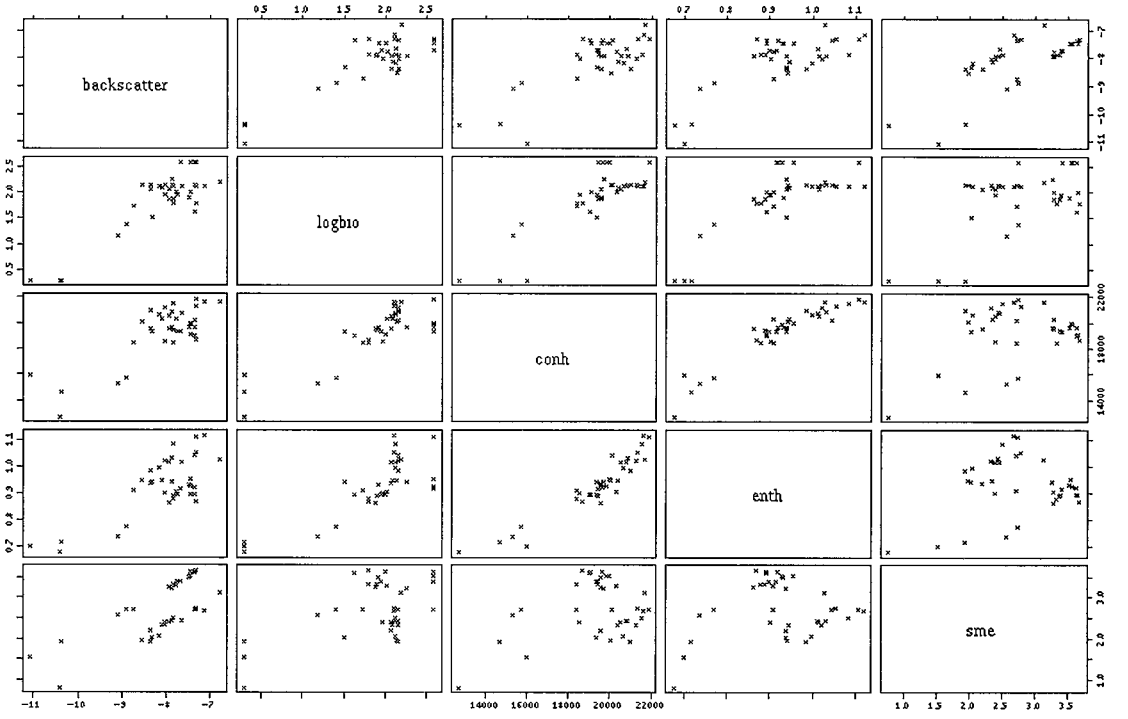

Figure 6.17. Scatterplots for backscatter, logbio and selected texture measures of Manaus and Tapajós study area plots.

The scatterplots (figure 6.17) demonstrated that logbio and the three texture measures were correlated with backscatter. The biomass of the two study area plots combined showed a strong linear relationship with backscatter.

The SADH derived mean of sum vector and backscatter scatterplot appeared to have highlighted DN differences between the two study areas, as they were grouped in two linear clusters. Different weather conditions, sensor settings, etc., were reflected in the images and were captured by sme. Even though SADH derived measures dealt with relationship in a neighbourhood and therefore were less affected by local DN or changing weather conditions, sme was derived following a local statistics measure – the mean - thus being more sensitive to variant scene conditions.

Multiple regression – logbio, backscatter and texture measures

A simple linear regression was performed with backscatter as the independent variable and the log of biomass as the dependent variable. Then, backward stepwise multiple regression was performed with backscatter, GLCM contrast, GLCM entropy and SADH mean of the sum vector as the independent variables and the log of biomass as the dependent variable in the base model. Stepwise regression started with a base model and then variables were added or omitted depending on their ability to increase or decrease the strength of the relationship between the variables and log of biomass. Backward elimination of variables was chosen as there is less risk of omitting important variables in the model.

Partial correlation was used to examine the relationship between two variables after removing the effect of other variables (Johnston 1980, Atkinson and Plummer 1993). The texture measures and backscatter were derived directly from DN values therefore some interrelationship between the variables was present. How much of the relationship between logbio and one variable would remain if the effect of the other variables was removed (controlled)?

Table 6.9. Partial correlation coefficient between log of biomass (logbio) and a variable, after controlling for the effect of the remaining variables.

	Partial correlation coefficient
backscatter	0.6
contrast	0.52
entropy	-0.08*
mean of sum vector	0.13*

Note: Correlation coefficients not significant at 95% confidence levels are signalled with an asterisk (*).

When controlling the effect of the texture measures on the backscatter/logbio relationship, it was clear that this relation was independent of the remaining variables (r = 0.6). Table 6.9 also shows that a significant partial correlation coefficient with

logbio was present when the effect of backscatter and texture measures was removed from the contrast/logbio relationship (r = 0.52). The entropy/logbio relationship however, virtually disappeared when the effect of backscatter, contrast and mean of sum vector was removed (r = -0.08). Similarly, for mean of sum vector/logbio relationship, a partial correlation coefficient of 0.13 showed no correlation remaining after backscatter, contrast and entropy removal. These results were expected following inspection of the scatterplots (figure 6.17).

The correlation between contrast and logbio was independent of backscatter. For mean of sum vector, however, the relationship with backscatter seen in the scatterplot was determinant of its relationship with logbio. For entropy, the relationship with contrast seen in the scatterplot was determinant of its relationship with logbio. These last two measures did not add information on the backscatter/biomass relationship.

Table 6.10 shows the results of simple linear regression and multiple regressions performed on the data. As suggested by the previous analyses, the texture measures derived from GLCM entropy and from SADH mean of sum vector were removed from the model relating logbio, backscatter and the texture measures (model 2). Table 6.10 also presents the adjusted R^2 (R_a^2), which accounts for the inevitable increase in the coefficient of multiple determination (R^2) when another predictor variable X is included in the model (Neter *et al.* 1996).

ANOVA results confirmed the significance of the coefficients to be included in the models.

Table 6.10. Regression models and corresponding adjusted R^2 (R_a^2) and standard error of estimate (s). Y stands for the log of biomass, b for backscatter and c for GLCM contrast.

Model	R_a^2	s
1. $Y = 6.29 + 0.54\ b$	0.74	0.29
2. $Y = 2.24 + 0.33\ b + 0.0001\ c$	0.82	0.25
3. $Y = 0.2\ b + 0.0002\ c$	0.98	0.26

P-values for the different coefficients suggested that model 2 could be built without an intercept ($p>0.05$) therefore model 3 was designed without it. However, comparison between R^2 of the model 3 with R^2 of the two remaining models is not possible.

Comparing models 1 and 2 (table 6.10) the adjusted coefficients of determination R_a^2 increased from 0.74 to 0.82 and the standard errors of the estimates decreased from 0.29 to 0.25 when GLCM contrast information was included in the model. That indicated the potential increase in the accuracy of biomass estimates from SAR data with the inclusion of textural information, in this case GLCM derived contrast.

The analysis of appropriateness of the models was done following the diagnosis steps proposed by Neter *et al.* (1996). The residuals (difference between observed and predicted values) of the regressions were plotted against the different variables. The results of these diagnosis steps are not shown here, but they suggested no systematic variation in the data, particularly in the variance of the error terms (directly related to the residuals). The problems that could have arisen from these initial analyses would probably be related to the gaps in the range of biomass data and therefore gaps in all the plots produced from the variables studied.

Figure 6.18 shows the regression line in the plot of observed versus predicted (fitted) values according to model 3. Although the standard error was slightly higher than when using model 2, model 3 was found more appropriate. The residuals of the model fitting are shown in figure 6.19 and are in accordance with the assumption of residual normality in the linear regression models.

Understanding the association between textural measures of SAR images and the structural properties of vegetation/canopies is not straightforward. The interpretation of texture itself is pursued less often than the increase in classification accuracy provided by using a certain texture measure (Bijlsma 1993). Previous studies, however, showed that spatial patterns such as canopy patchiness (forest areas intermixed with pasture) and large emergent trees were detected by GLCM contrast (Ulaby *et al.* 1986, van der Sanden and Hoekman 1999). Similarly, changes in canopy that occur during the regeneration of tropical forest was also captured by GLCM contrast in a study by Luckman *et al.* (1997), although the local statistics coefficient of variation (CV) discriminated a wider range of regenerating forest age classes.

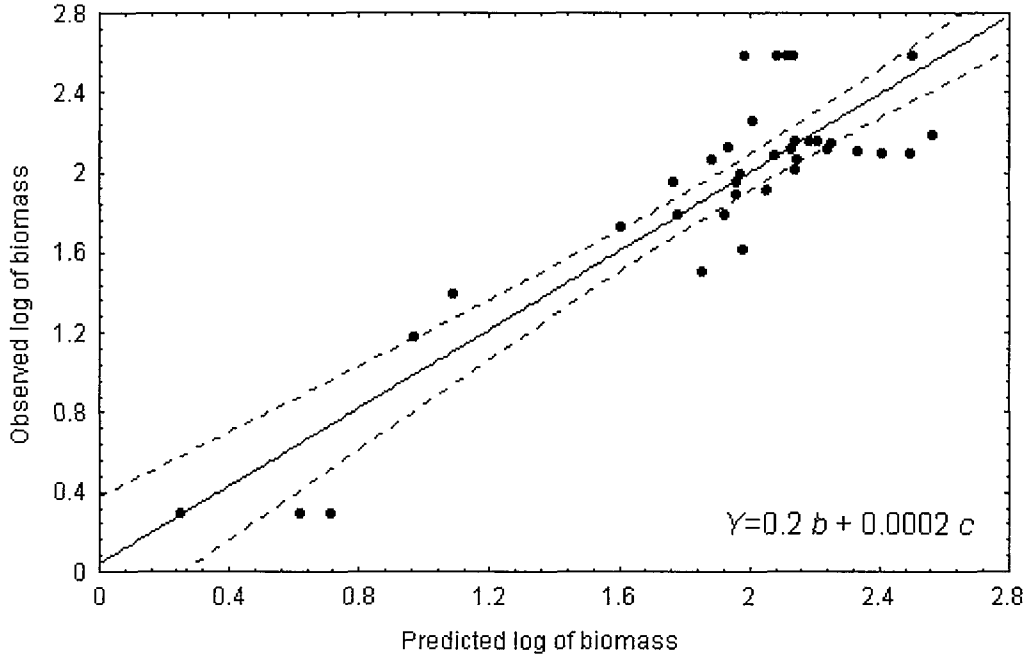

Figure 6.18. Observed x predicted values according to the model where *Y* is the log of biomass, *b* is backscatter and *c* is GLCM contrast. Dashed lines indicate 95% confidence limits.

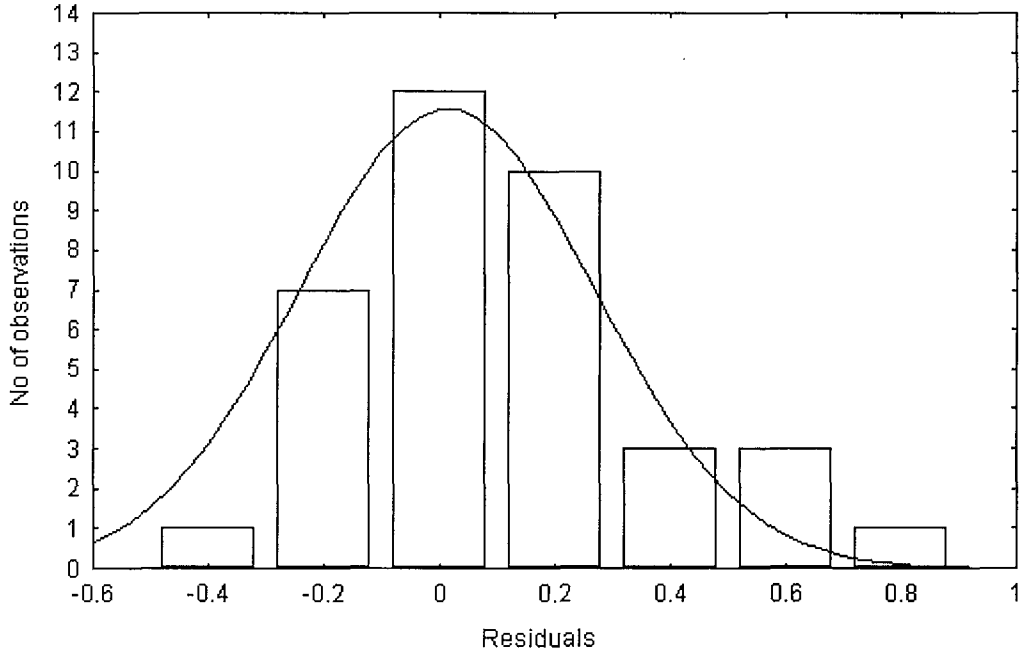

Figure 6.19. Histogram of distribution of the residuals for model relating backscatter and GLCM contrast to the log of biomass (model 3 in table 6.10).

The range of vegetation/canopy structures likely to contribute to different backscattering properties and therefore texture, was certainly high. Tropical vegetation structure is very diverse and in particular, when different ages and successional stages of the forest are involved, their richness in terms of spatial structures is likely to be reflected in the textural information available from SAR images. The relationship between age/successional stage, biomass and canopy structure of the regenerating forest plots could not be established here. Nevertheless, this relationship has been observed by others (Budowski 1965, Brown and Lugo 1990) and could account for the strong relationship between some texture measures and the log of biomass. As a measure of local DN variability, GLCM contrast was the texture measure that best captured the spatial variability of the vegetation/canopy.

6.8. Summary

In this chapter, the use of several texture measures to increase the correlation between backscatter and the log of biomass was investigated. One experiment using simulated images identified seven texture measures capable of discriminating image texture independently of image contrast. They were: GLCM derived *contrast*, *entropy*, *correlation*, *chi-square*, SADH derived *mean of sum vector*, local statistics derived *entropy* and variogram derived *range.*

These seven texture measures were calculated for SAR images and related to the log of biomass. Only GLCM derived *contrast* increased the correlation between backscatter and log of biomass. It was concluded that the addition of GLCM derived *contrast* to backscatter potentially increases the accuracy of biomass prediction and mapping.

Surprisingly, variogram derived range did not show any relationship with the log of biomass and upper canopy structure (as inferred by dominant species composition). This analysis might have been limited by the image spatial resolution, the use of pixel transects to derive the variograms and the bounds imposed by the models used to fit the data.

The information in the σ° spatial domain, as represented by the strong relationship between some texture measures and log of biomass, was due to the increasing roughness of ageing forest canopies.

CHAPTER SEVEN

Classifying regenerating tropical forest stages using multiwavelength and multipolarisation SAR data

Relationships between tropical forest biomass and temporal and spatial characteristics of SAR backscatter were quantified in chapters 5 and 6. It is known that (i) the relationships between SAR data and biomass is dependent upon, among other things, wavelength and polarisation and (ii) older forest regeneration stages tend to have greater biomass than young forest regeneration stages. However, the combined use of both spectral and polarisation characteristics of SAR data for the mapping of forest regeneration stages has yet to be determined. This chapter addresses this issue.

For the Manaus study area, the age of regenerating forests was a viable surrogate for biomass (Lucas *et al.* 2000) and multiwavelength and multipolarisation SAR data were available. Six SAR bands from different sensors with varied parameters, selected by discriminant function analysis, were used as input to a neural network based classifier. The synergy between wavelengths was investigated with the inclusion of visible wavelengths bands from Landsat TM sensor. Eight bands (5 SAR and 3 TM) were selected and classified with a neural network.

The accurate classification of regenerating tropical forest stages is an important step in the estimation of forest biomass and mapping of forest carbon content.

7.1. Data

The data used as input for discriminant analysis and, after feature selection, for the neural network based classifier, are described next.

7.1.1. SIR-C/XSAR images

The Spaceborne Imaging Radar – C/X band Synthetic Aperture Radar (SIR-C/XSAR) flew at an altitude of 225 km onboard the U.S. Space Shuttle Endeavor on April and October 1994. It was the first spaceborne radar system to provide multifrequency data (Jordan *et al.* 1995). The SIR-C was developed by the U.S. National Aeronautics and Space Administration (NASA) in order to obtain the full polarimetric scattering matrix - HH, VV, HV and VH - in L and C bands (Evans *et al.* 1997). The XSAR was the German/Italian space agency instrument that operated at X band and VV polarisation. The SIR-C/XSAR system was the next step in a series of spaceborne imaging radars that started with Seasat (1978) and continued with SIR-A (1981), the Microwave Remote Sensing Experiment (MRSE, 1983) and SIR-B (1984) (Evans *et al.* 1997).

The SIR-C/XSAR data were and still are, applied to issues in ecology, hydrology, geology and oceanography (Evans *et al.* 1997). The SIR-C/XSAR data were downloaded from the Shuttle in near-realtime and the first experimental results were made available in the following year (Dobson *et al.* 1995, Hess *et al.* 1995 and Ranson *et al.* 1995). The SIR-C/XSAR system has proved to be a key milestone in the recent history of imaging radars (Kasischke *et al.* 1997).

The characteristics of the SIR-C/XSAR images used in this work are presented in table 7.1.

Table 7.1. SIR-C/XSAR image characteristics.

Frequency and wavelength	SIR-C: 1.275 GHz, 23.5 cm (L band) SIR-C: 5.3 GHz, 5.8 cm (C band) XSAR: 9.6 GHz, 3.1 cm (X band)
Polarisation	SIR-C: HH, HV and VV XSAR: VV
Incident angle (to the centre of swath)	SIR-C: 33.3° XSAR: 32.1°
Acquisition date	SIR-C/XSAR: 12/04/1994
Spatial resolution	25 m x 25 m

7.1.2. Additional bands

In addition to the SIR-C/XSAR image, a JERS-1 SAR image of the Manaus study area was included in the analysis. The dry season date closest to the SIR-C/XSAR flight was selected (table 7.2).

Cloud-free Landsat TM data were available in bands 3, 4 and 5 but for one year after the SIR-C/XSAR flight (table 7.2). The three TM bands were radiometrically corrected from DN to radiance using calibration coefficients derived from vicarious experiments (Bailey 1997). TM bands 3, 4 and 5 were converted to radiance by dividing the DN by calibration coefficients of 0.9, 1.08 and 7.07 respectively (Bailey 1997). These coefficients were obtained after the shift (offset) in 1995 Landsat TM calibration had been interpolated from the calibration coefficients (1984 – 1994) and applied to the DN (Thome *et al.* 1997).

The SAR data were filtered with a median filter in a 3 x 3 window to reduce speckle.

Table 7.2. Remotely sensed data for Manaus study area.
F in band codes refers to median filtered bands.

Satellite/Sensor	Band-Polarisation	Path/ Row	Date	Band code
JERS-1/SAR	LHH	414/304	05/08/94	JERS and JERSF
Landsat/TM	3,4,5	231/62	20/09/95	TM3,TM4,TM5
SIR-C/SAR	LHH	46_70	12/04/94	LHH and LHHF
	LHV			LHV and LHVF
	LVV			LVV and LVVF
	CHH			CHH and CHHF
	CHV			CHV and CHVF
	CVV			CVV and CVVF
SIR-C/XSAR	XVV	46_70	12/04/94	XVV and XVVF

In addition to this data set (and following the conclusions of chapter 6), a GLCM contrast texture band (called CONT) was derived from the JERS-1 SAR band in a 3 x 3 window and 256 GL. In total, 20 bands were used: 17 SAR bands and 3 TM bands.

7.2. Artificial Neural Networks (ANN)

Artificial Neural Networks (ANN) are an artificial intelligence technique inspired by research on the structure and learning mechanisms of the human brain. ANN are used to enable computers to learn directly from data and thereby assist in tasks such as pattern recognition, classification and data compression (Hammerstrom 1993).

The starting point for the development of an ANN was the work by Rosenblatt (1958), who introduced the concept of perceptron as a processing unit able to receive weighted information and threshold the results according to a rule (Atkinson and Tatnall 1997). One of the requirements for input data in a perceptron was linearity, which sometimes limited its use for classification. Since the 1980s, with increased computer power and network topologies, ANN has been used for the classification of multi-spectral remotely sensed imagery (Atkinson and Tatnall 1997). ANN are an alternative to standard classification methods that require assumptions about the underlying statistics of the data (Paola and Schowengerdt 1995). In addition to the independence of statistical

distribution assumption, ANN (i) are adaptive and able to learn underlying relationships from data, (ii) can generalise and process noisy data and (iii) can be used for near real-time processing (Hammerstrom 1993). Specifically to remote sensing, ANN can incorporate different data types and *a priori* knowledge about the data (Atkinson and Tatnall 1997).

7.2.1. Structure of an ANN

The basic structure of an ANN comprises a number of simple processing units (nodes) arranged in a set of connected layers (Foody 1995). The most commonly used ANN for image classification in remote sensing is based on the multi-layer perceptron (MLP) trained by the back-propagation algorithm (Atkinson and Tatnall 1997, Kanellopoulos and Wilkinson 1997). A typical back-propagation ANN has one input layer, a variable number of intermediate or hidden layers and one output layer (figure 7.1).

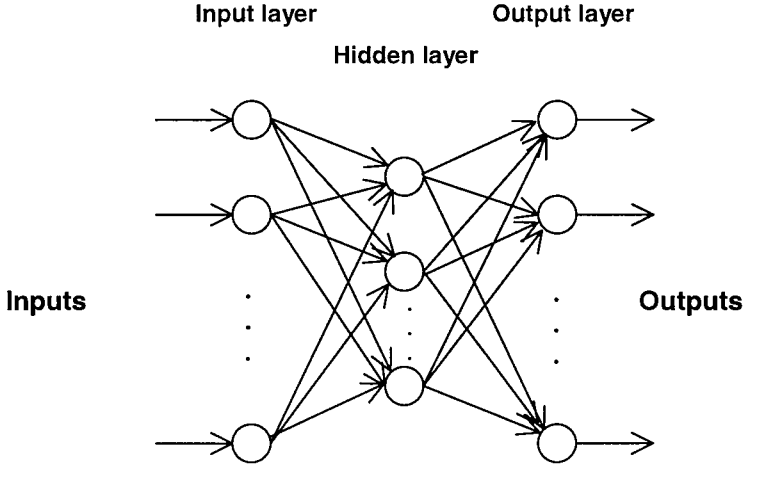

Figure 7.1. Structure of a back-propagation ANN.

The input layer is passive and distributes the data to all nodes in the hidden layer. For remotely sensed data the input layer usually contains DN from spectral bands and the number of nodes equals the number of bands. The hidden nodes calculate a weighted sum of inputs which are then passed through an activation function to produce the node's output value. These adjustable weight values contain the knowledge distribution

of the ANN (Paola and Schowengerdt 1995). The weighted sum of inputs to a node – net_j - is computed from:

$$net_j = \sum_i \omega_{ij} o_i \qquad [7.1]$$

where ω_{ij} are the weights between nodes *i* and *j* and o_i is the output from node *i*. The output from a given node j is then computed from:

$$o_j = f(net_j) \qquad [7.2]$$

where *f* is usually a non-linear sigmoid function which constraint the sums within fixed limits (Atkinson and Tatnall 1997). The output layer presents the network's results e.g., the classes of a classified image. The number of output nodes equals the number of classes.

The input data are passed through the connections to the next layer in a feed-forward manner. The back-propagation algorithm refers to passing the errors back to the hidden layer, after subtraction of output node results from the previously-established results. Subsequently, the hidden nodes calculate the weighted sum of the back-propagated errors to find its contribution to the known output errors. The error values in a hidden node are weighted by a *delta rule* equation, which minimises the network's sum-squared errors (Hammerstrom 1993). The generalised delta rule equation is as follows:

$$\Delta\omega_{ji}(n+1) = \eta(\delta_j o_i) + \alpha\Delta\omega_{ji}(n) \qquad [7.3]$$

where $\Delta\omega_{ji}(n+1)$ and $\Delta\omega_{ji}(n)$ are the weight changes between connecting nodes *i* and *j* at iteration *n*+1 and iteration *n*, respectively, η is the learning rate, δ_j is the rate of change of the error and α is the momentum parameter (Atkinson and Tatnall 1997).

The learning is achieved by iterative weight adjustment (Kanellopoulos and Wilkinson 1997). If the error is still above some predetermined threshold when the training cycle is completed, the weights are adjusted and training continues (Paola and Schowengerdt 1995). The adding of momentum term speeds the reduction in the error. An asymptotic

rate of decrease in the total network error can also be used to terminate the training cycle (Skidmore *et al.* 1997).

7.2.2. Image classification using an ANN

The process described above makes part of the network's training similar to the training for conventional supervised classifiers. The aim of the training phase is to build a model to define the data and this in turn enables the ANN to generalise and predict outputs from different input data (Atkinson and Tatnall 1997). The training data are used to adjust the network weights until the network can identify class membership correctly and allocate DN values to the class associated with the most 'highly activated' output unit (Foody *et al.* 1997).

The most common structure of an ANN for image classification includes three fully interconnected layers (a single hidden layer) (Paola and Schowengerdt 1995).

Many settings influence the ability of an ANN to generalise and classify data including the training time (Paola and Schowengerdt 1995, Atkinson and Tatnall 1997). If an ANN is overtrained it may be unable to generalise and classify new data.

After the overall network structure has been determined (number of nodes and hidden layers, size and selection of training set), some specific settings are selected, usually following experimentation. The learning rate, learning momentum and number of training cycle (iterations) are examples of these settings that affect the accuracy of an ANN classification (Berberoglu *et al.* 2000). The learning rate is related to the distance that the values have to travel in a single iteration to change the network error. The smaller the learning rate, the smaller the changes in the weights at each iteration (Skidmore *et al.* 1997). If the learning rate is too big, the network can become unstable. The learning momentum is added to the learning rate in order to incorporate previous changes in weight with the direction of learning process (Skidmore *et al.* 1997).

Finally, the accuracy of the trained network may be evaluated using testing data set. This is normally done by dividing the available data into a training and a testing data set and using the latter for testing independently the accuracy of the network.

7.3. Methods

The methods for preparing the data set, analysing, selecting, classifying and assessing classification accuracy will be explained next.

7.3.1. Building the data set

7.3.1.1. Ground data – Forest regrowth map

The 1991 forest regrowth map for the Manaus study area (section 4.3.2) included 5 regenerating forest age classes, a mature forest class and a pasture class (Lucas *et al.* 1993). This map was further refined by the addition of dominant species composition to the age classes (Lucas *et al.* 1996) and for the classification of successional pathways as determined by prior land use and forest dominating species (Palubinkas *et al.* 1995, Foody *et. al* 1996).

The original 1991 forest regrowth map was updated with the aid of fieldwork and TM images acquired in 1992, 1994 and 1995 (Bailey 1997). The classes studied here were taken from the updated Manaus forest regrowth map: (1) pasture, (2) regenerating forest <3 years, (3) regenerating forest 3-5 years, (4) regenerating forest 6-10 years, (5) regenerating forest 11-18 years and (6) mature forest. Hereafter they will be called land use classes, as the pasture class prevents calling them age or regrowth classes.

The forest regrowth map was not covered entirely by the images used in this work. As a result, an extract of the forest regrowth map common to all images was selected, making sure that all age classes were represented. The extract covered Fazenda Porto Alegre and Fazenda Esteio, two cattle ranches part of the BDFFP research areas (figure 7.2).

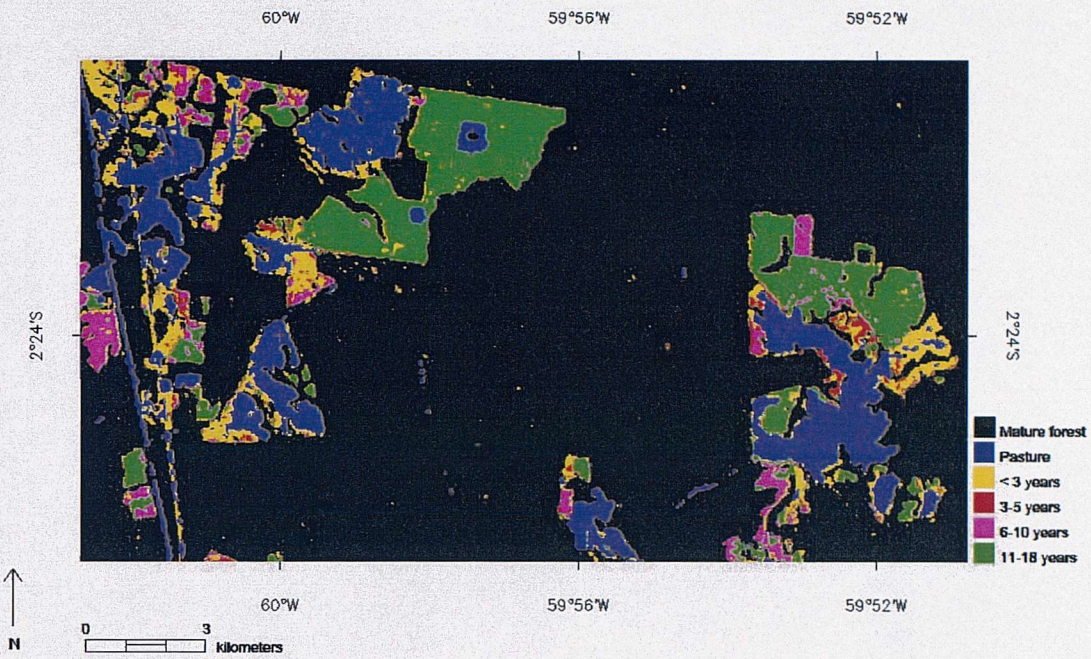

Figure 7.2: Extract from the Manaus forest regrowth map. The production of this map from multitemporal Landsat sensor data is discussed in Bailey (1997).

7.3.1.2. Remotely sensed data - SAR and TM bands

The SIR-C/XSAR images and the 1995 Landsat TM image were registered to the geometrically-corrected 1991 Landsat TM image of the same area (section 5.4.1). The final pixel size of all images was 25 metres.

The extract of the forest regrowth map is shown in SIR-C SAR bands (figure 7.3), Landsat TM bands (figure 7.4) and in bands from both sensors combined (figure 7.5). In addition to the main land covers (mature forest, pasture and regenerating forest at different successional stages), the bands depict the topography of the area. The influence of slope aspect on backscatter and radiance for the discrimination of the land cover classes was out of the scope of this research.

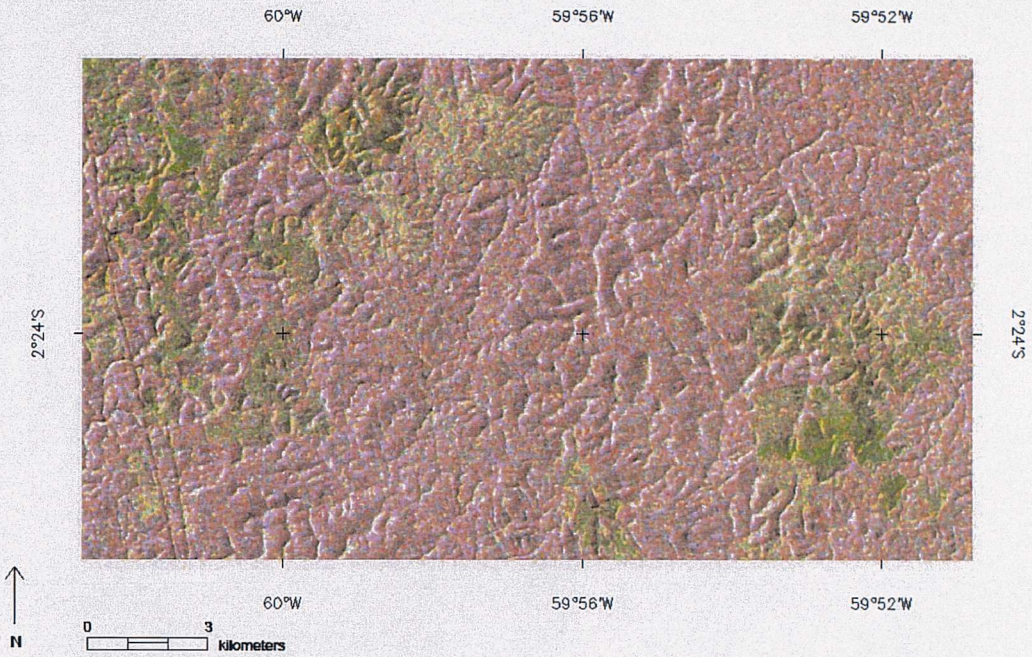

Figure 7.3: SIR-C SAR bands covering Fazenda Porto Alegre and Fazenda Esteio from the Manaus study area. Band LVVF on red, CHVF on green and LHVF on blue.

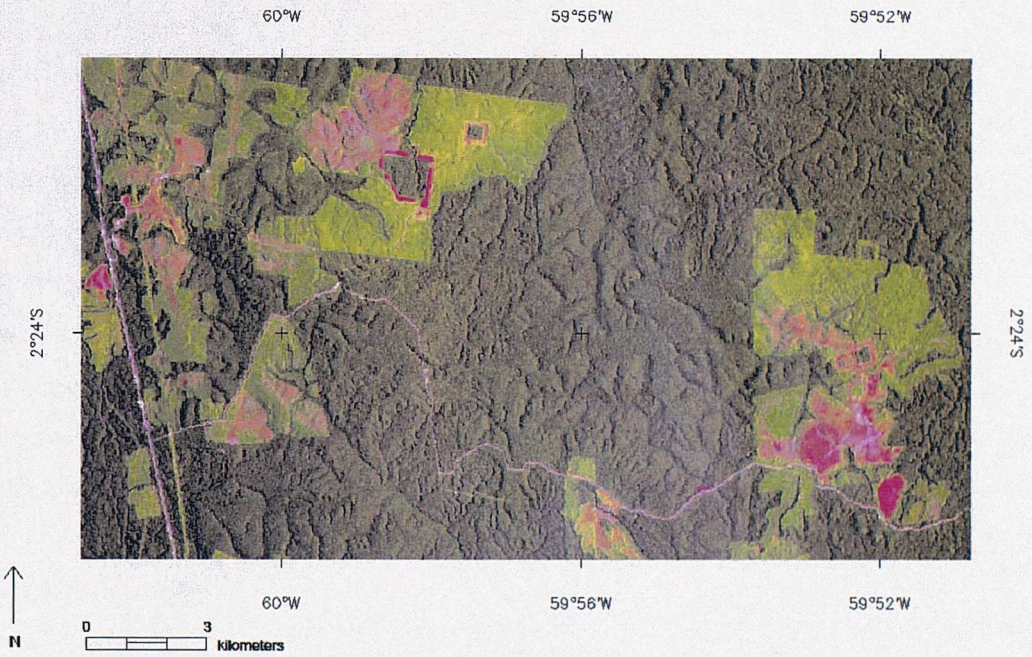

Figure 7.4: Landsat TM bands covering Fazenda Porto Alegre and Fazenda Esteio from the Manaus study area. Band TM5 on red, TM4 on green and TM3 on blue.

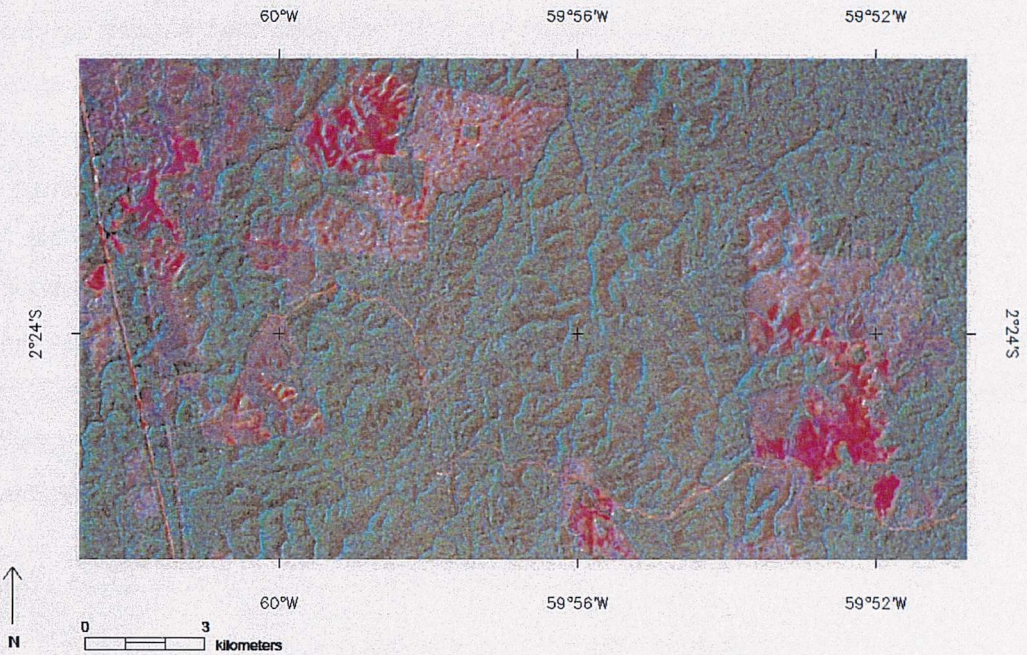

Figure 7.5: SIR-C SAR and Landsat TM bands covering Fazenda Porto Alegre and Fazenda Esteio from the Manaus study area. Band TM5 on red, CHVF on green and LHVF on blue.

All 20 SAR and TM bands were rescaled to the same 256 DN (8-bit format) range. This speeds the convergence of an ANN to a minimal error point as the weights of the nodes have approximately the same range (Skidmore *et al.* 1997). In addition a standardised DN range allowed the performance of discriminant function analysis.

The location of the training and testing sites for the ANN and discriminant function classifications was based on the forest regrowth map. Pixel values were extracted for each class from each band, totalling 113 pixels/class/band. These data was used for DN statistics analysis, discriminant function feature selection and in the first training attempt in an ANN.

7.3.2. Exploratory analysis of the remotely sensed data

Displaying the DN data from the different bands by each land cover class provides a visual summary of the DN distribution. The boxplot is a useful exploratory tool, particularly when plotted and analysed before the classification of DN data. The data are presented as a box whose top and bottom are drawn at the lower and upper quartiles (interquartile range) (Sokal and Rohlf 1995). The median is shown as a line across the box. Additionally, vertical lines are drawn from the top and bottom of the box to the largest and smallest value, respectively, that lie within up to 1.5 times the interquartile range. All values that are further than these lines are plotted individually (outliers) and values more than 3 interquartile ranges away from the box are given proeminence (Sokal and Rohlf 1995).

7.3.3. Discriminant function analysis and feature selection

The different bands were submitted to discriminant analysis (DA), in order to identify those variables able to discriminate the 6 land cover classes (section 7.2.1.1). DA is a technique used to determine which variables discriminate two or more groups. Functions that include the variables being analysed (e.g., bands) are built and predictions as to which class a case (e.g., pixel) belongs are made (Statsoft, Inc. 2001). The Wilks' lambda statistic is used for measuring the discrimination power of each band, based on their variance/covariance matrices. Wilks' lambda values range from 0 (perfect discrimination) to 1 (no discrimination). The bands selected (also called canonical variables) will be given a coefficient in the discriminant functions. These coefficients show the contribution of each band in the discrimination between classes and, when plotted, which classes are discriminated by each function (Statsoft, Inc. 2001).

DA has been used in remote sensing as a feature selection technique to find the optimum input representation for neural network training data (Benediktsson and Sveinsson 1997), to identify bands that optimise discrimination amongst a set of land cover classes (Thomson *et al.* 1998) and to classify SAR data with added prior knowledge (Foody 1995).

Stepwise DA was performed on the data. Within this approach, at each step, the band that minimised the overall Wilks' lambda was entered. Two sets of bands were used: (i) all 17 SAR bands (filtered and non-filtered data) and (ii) all 17 SAR bands plus 3 TM bands, a total of 20 bands.

7.3.4. ANN architecture and classification accuracy assessment

Several trials were made before selecting the settings of the ANN using ENVI 3.4 software that provides ANN training and classification as part of the supervised classification module. The ANN architecture was set as input and output layers plus one or two hidden layers. The number of nodes was the same as the number of input bands for the input layer and hidden layer. For the output layer the number of nodes was equal to the number of classes (6).

Recalling table 3.2 and 3.3, where classification approaches and the use of texture of radar imagery in tropical ecosystems was reviewed, the use of ANN for the classification of tropical land cover types remains new avenue for research.

Several experiments were designed to quantify the influence of each ANN variable in the overall classification accuracy. One setting was varied while holding the other settings constant. The overall classification accuracy was verified in the training data set and independent testing data set.

The selection of training and testing data sets was limited by classes coverage/extent. For instance, mature forest occupied a much larger area than the remaining classes and class 3 (regenerating forest 3-5 years) covered the smallest area. Training and testing data sets were changed following inaccurate results for initial ANN experiments. The results presented in section 7.3 were part of the more accurate achieved hence the training and testing data sets were considered adequate. The final figures for training and testing pixels were (training, testing):

(1) Pasture (325, 172).
(2) Regenerating forest <3 years (121,123).
(3) Regenerating forest 3-5 years (30, 83).
(4) Regenerating forest 6-10 years (100, 137).

(5) Regenerating forest 11-18 years (213, 284).
(6) Mature forest (351, 303).

The ANN was trained until the root mean square (RMS) error reached a constant, which was after approximately 2000 iterations. Experiments on the effect of the number of iterations and training accuracy were also performed.

7.4.Results

The results were presented in three sections:

- In section 7.3.1 the DN statistics of the 6 land cover classes were explored in boxplots.

- In section 7.3.2 the results of Discriminant Analysis were presented, showing 6 bands selected from the 17 SAR bands data set and 8 bands selected from the data set containing the SAR bands plus 3 TM bands.

- In section 7.3.3 the experiments for defining the settings to be used by the ANN were shown. ANN classification and accuracy assessment results were presented after that.

7.4.1. Boxplots

The graphic display of the SAR and TM data in boxplots showed land cover classes with similar DN medians. The range of rescaled intensity SIR-C L and C data values for the 6 land cover classes was narrow, especially for HH and VV polarisations (figure 7.6). All classes overlapped, although in most cases the median for pasture class (class 1) was lower than for the remaining classes. For HV data in both L and C bands the range of DN was wider. The median values for LHV band increased with land cover "age" (as from class 2 to 6 the "age" of regeneration forest increased until reaching maturity). LHV is a key band for discriminating between regenerating forest and mature

forest, because of its sensitivity to biomass and forest structure (Kasischke *et al.* 1997, Saatchi *et al.*1997)

Median-filtered SIR-C data sets showed a slightly narrower DN range and still similar medians leading to a visually low separability between classes. Cross-polarised bands LHVF and to a lesser extent CHVF, demonstrated again a wider dynamic range when compared with non-filtered data. In HH and VV bands the medians were similar for the different land cover classes. For HV bands, however, some differentiation between classes seemed possible (figure 7.7).

XSAR XVV and median-filtered XVVF bands showed a relatively wider DN range and also higher DN values when compared to the SIR-C bands (figure 7.8). Despite that, the discrimination was limited to pasture (class 1) and the remaining 5 forest classes. For JERS and JERSF (LHH bands) some differences in median values were present between pasture and the remaining 5 forest classes. The behavior of median values in JERS and JERSF bands was similar to the HH and VV SIR-C bands, although a relatively wider DN range was present (figure 7.8). GLCM derived contrast (CONT) median values were the higher from the data set, which could be interpreted as highly contrasted classes. Median values for the forest classes were very similar and discrimination between these and pasture class may be possible (figure 7.8).

The TM bands showed distinct median values for the three main land cover classes: pasture (class 1), regenerating forest (classes 2, 3, 4 and 5) and mature forest (class 6) (figure 7.8). That result was expected since these classes were defined after the use of the multitemporal Landsat sensor data to produce the forest regrowth map (Lucas *et al.* 1993, Bailey 1997). In addition, DN values were rescaled from radiance values which have strong spectral meaning. Median values of the land cover classes in TM bands followed the spectral behaviour described for forests and pasture. In TM3 (red channel) values of radiance were low due to pigment absorption of red wavelength (Moran *et al.* 1994). For TM4 (near-infrared channel) radiance increased with forest age as within-leaf scattering was greater due to increased number of leaves (Foody *et al.* 1996). After reaching a peak in near-infrared radiance, shadow of emergent trees in the canopy decreased radiance in both visible and near-infrared bands, and as a result mature forest (class 6) exhibited low radiance values in TM3, TM4 and TM5 (Foody *et al.* 1996). Increased water absorption and shadowing effects associated with canopy development decreased radiance in TM5 (Foody *et al.* 1996). Pasture had higher radiance than mature forest and regenerating forests in TM3 and TM5.

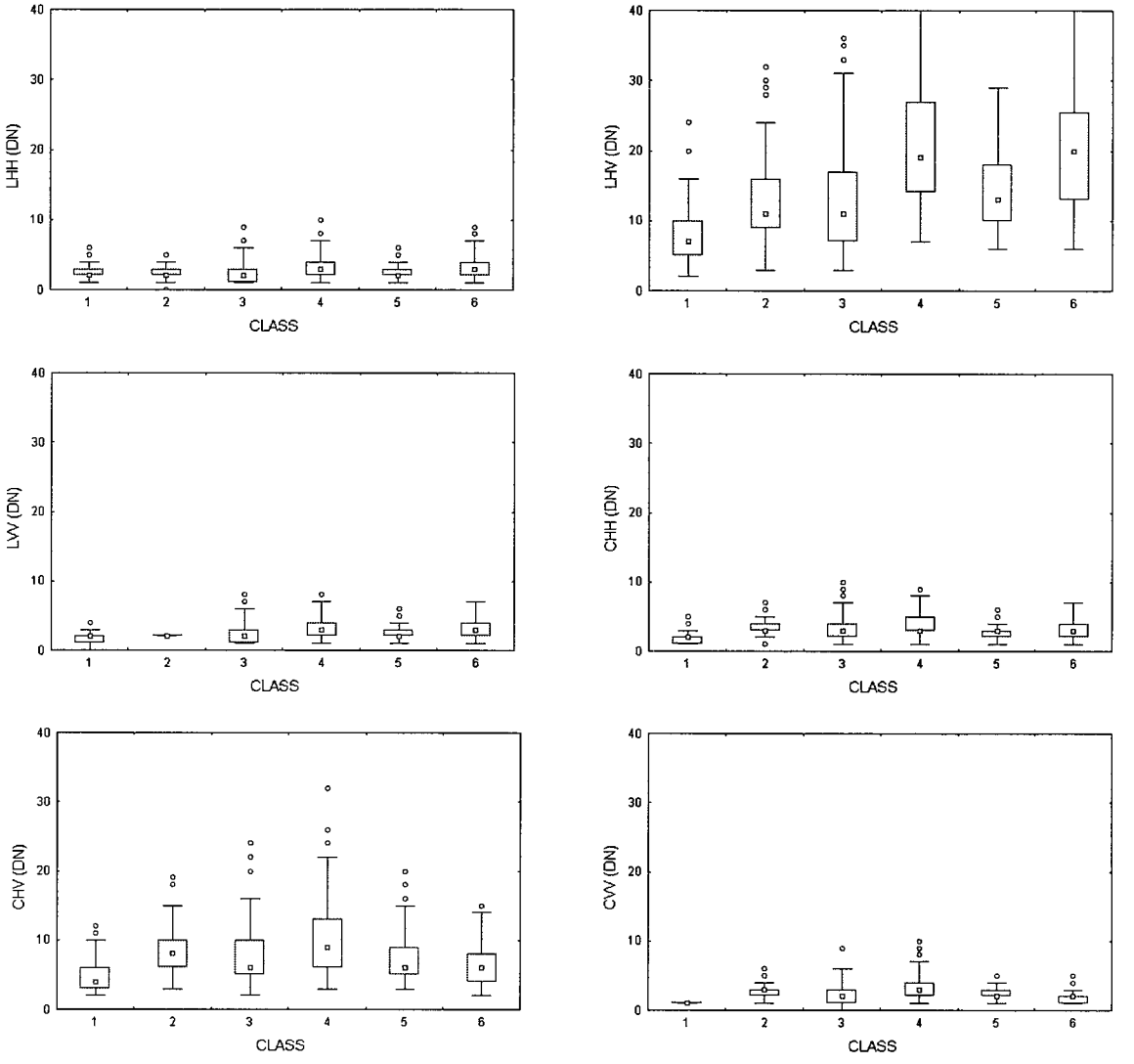

Figure 7.6. Boxplots of DN for pixels in training samples by land cover class in non-filtered and median-filtered XSAR and JERS-1 bands. Upper and lower ends of boxes are upper and lower quartiles, small squares indicate median, 'whiskers' show the interquartile range and values outside - circles - indicate outliers. Classes are: (1) pasture, (2) regenerating forest <3 years, (3) regenerating forest 3-5 years, (4) regenerating forest 6-10 years, (5) regenerating forest 11-18 years and (6) mature forest.

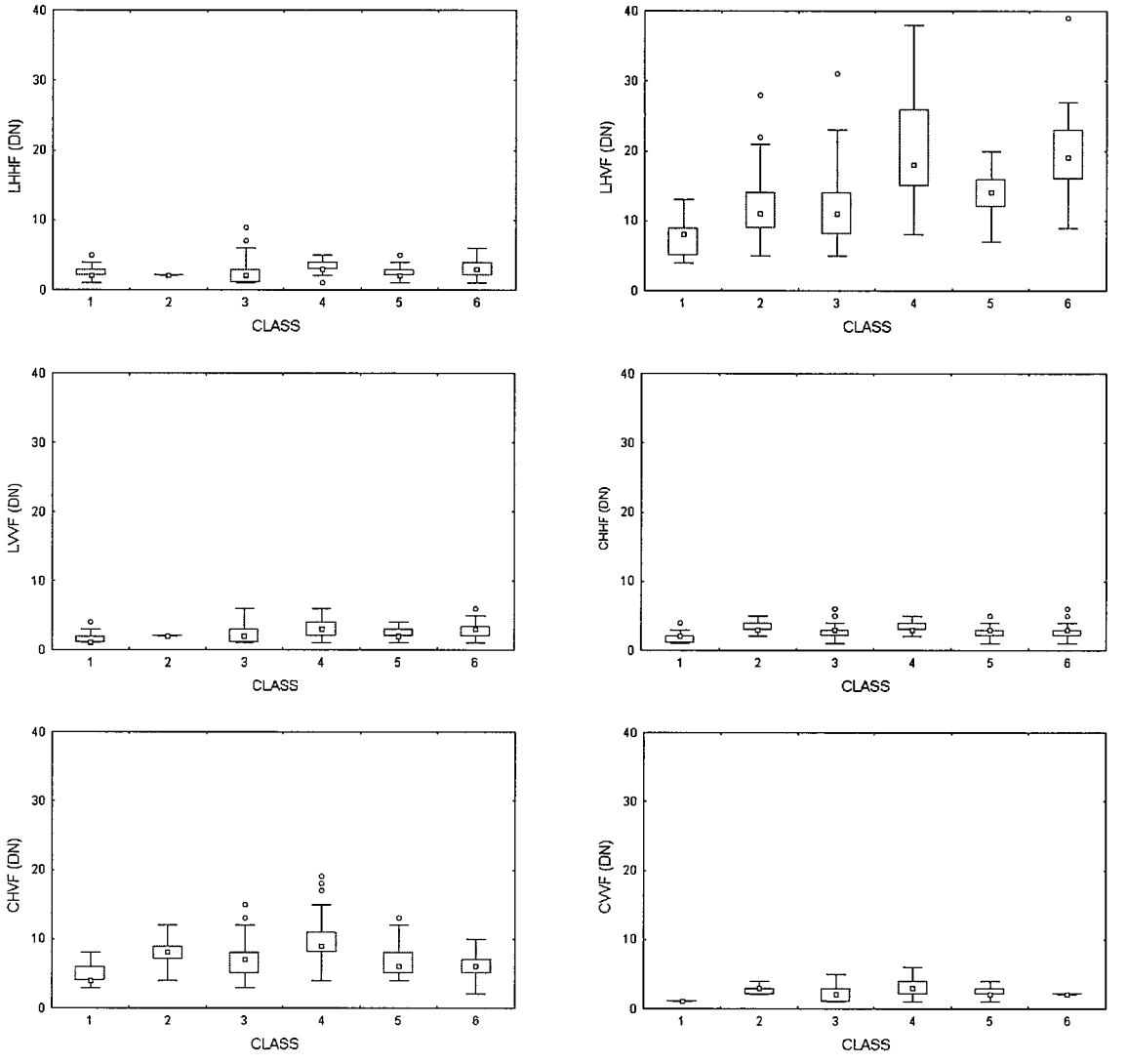

Figure 7.7. Boxplots of DN for pixels in training samples by land cover class in non-filtered and median-filtered XSAR and JERS-1 bands. Upper and lower ends of boxes are upper and lower quartiles, small squares indicate median, 'whiskers' show the interquartile range and values outside - circles - indicate outliers. Classes are: (1) pasture, (2) regenerating forest <3 years, (3) regenerating forest 3-5 years, (4) regenerating forest 6-10 years, (5) regenerating forest 11-18 years and (6) mature forest.

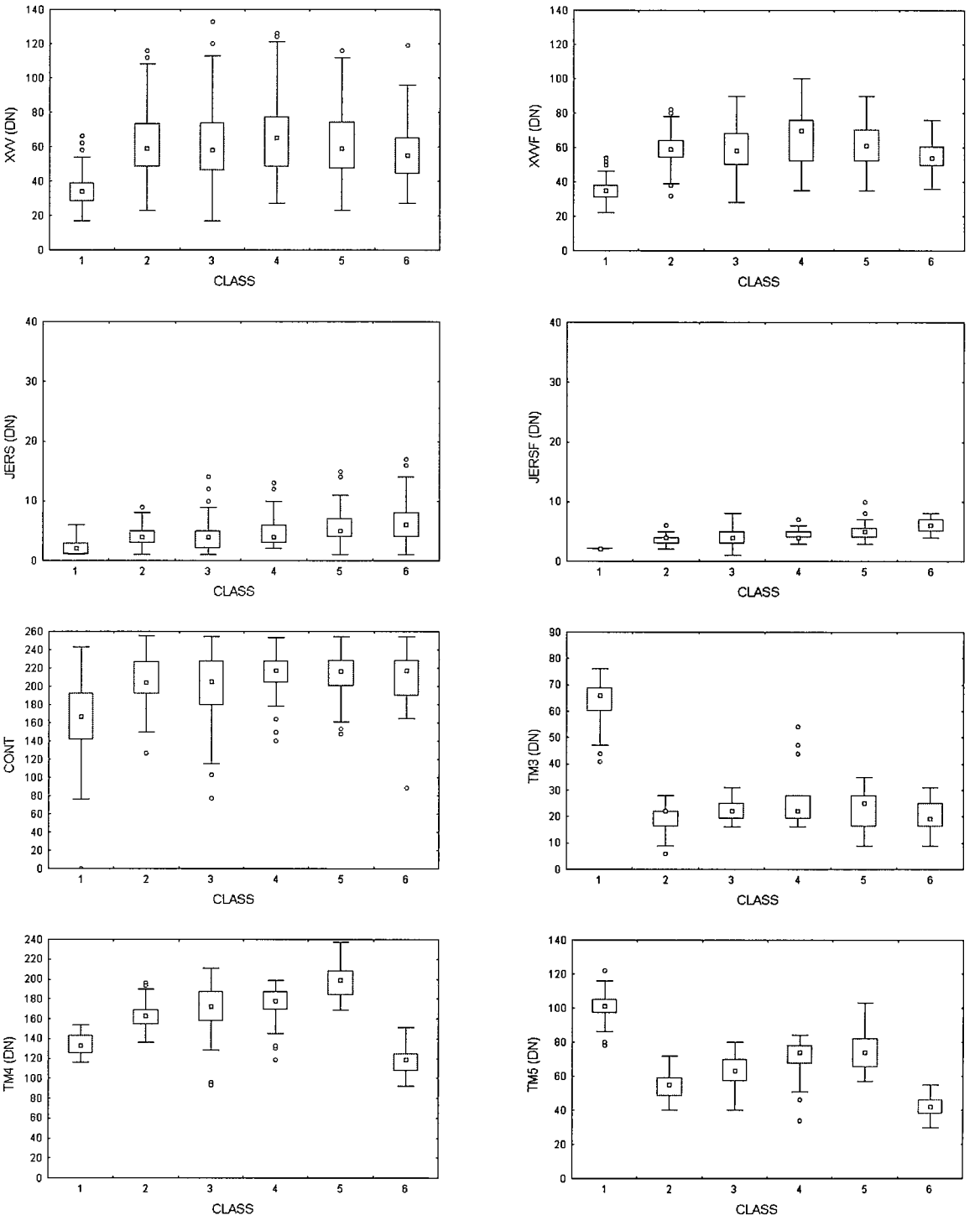

Figure 7.8. Boxplots of DN for pixels in training samples by land cover class in non-filtered and median-filtered XSAR and JERS-1 bands, plus TM bands. Upper and lower ends of boxes are upper and lower quartiles, small squares indicate median, 'whiskers' show the interquartile range and values outside - circles - indicate outliers. Classes are: (1) pasture, (2) regenerating forest <3 years, (3) regenerating forest 3-5 years, (4) regenerating forest 6-10 years, (5) regenerating forest 11-18 years and (6) mature forest.

The boxplots shown in previous 3 figures illustrated the difficulty of mapping the 6 land cover classes using a single band/wavelength and polarisation. The characterisation of land cover classes associated with regenerating tropical forests benefit from multiwavelength and multipolarisation data (Pope *et al.* 1994). The need for a feature selection procedure to reduce the dimensionality of the dataset was also highlighted.

7.4.2. Discriminant analysis

The overall discrimination of the 6 land cover classes in the 20 bands is discussed following presentation of Wilks' lambda for each band in the data set containing only SAR bands (7.3.2.1) and in the data set containing SAR plus TM bands (7.3.2.2).

One drawback of the DA backward elimination procedure used here is that once one band has been removed in the set of discriminant variables, it will not be included again even if it became a class discriminator in a later stage (Sokal and Rohlf 1995). However, DA was used as a feature selection technique, where reduction of data dimensionality without information loss was sought (Mather 1999).

7.4.2.1. SAR bands selected by DA

The stepwise backward DA selected six bands – JERSF, CVVF, LHVF, XVVF, CHVF and LVVF - as discriminant variables for the 6 land cover classes (table 7.3). The selected bands are exhibited sequentially according to overall Wilks' lambda coefficient and their contribution in reducing the ratio within-classes to total class variation (Johnston 1980)

Only SAR-filtered bands were selected, probably due to their smaller range of DN for the land cover classes as seen in the boxplots (table 7.3). Bands discarded include the non-filtered data (JERS, LHH, LHV, LVV, CHH, CHV, CVV and XVV), the median-filtered bands in HH polarisation (LHHF and CHHF) and the GLCM contrast (CONT).

Table 7.3. Bands selected after stepwise discriminant analysis and respective Wilks' lambda. At each step, the band that minimised the overall Wilks' lambda was selected.

	Wilks' Lambda
JERSF	0.467
CVVF	0.286
LHVF	0.204
XVVF	0.151
CHVF	0.135
LVVF	0.124

JERSF band was the first to be selected, demonstrating the importance of LHH data (acquired in a wider incidence angle range than SIR-C data) for discriminating between the 6 land cover classes (table 7.3). Previous researchers have shown that depending on the number of classes and the classification method used, JERS-1 SAR data can achieve accurate discrimination in tropical land cover classification (Saatchi *et al.* 2000, Simard *et al.* 2000). When used in combination with optical and/or SAR bands, ancillary data, multitemporal series or textural information, land cover mapping capabilities of JERS-1 data are usually increased (Rignot *et al.* 1997, Rennó *et al.* 1998, Grover *et al.* 1999).

Discrimination for the 6 land cover classes was also offered by CVVF, the band and polarisation present in ERS-1 SAR. Kuntz and Siegert (1999) suggested the use of ERS-1 SAR CVV band to monitor forest conversion and land cover in tropical forest environments but with additional information derived from texture and multitemporal ERS-1 SAR data.

The VV polarisation was selected in 3 bands: LVVF, CVVF and XVVF. That was probably due to the association of VV polarised backscatter with crown-layer attributes (Dobson *et al.* 1995). These attributes varied greatly from pasture (class 1) to a series of different canopy structures in regenerating forests (class 2 to 5) and mature forest (class 6).

The HV polarised backscatter is related to total biomass which varied with land cover class, justifying the selection of LHVF and CHVF. HV polarised data were key to the differentiation of regenerating forest from mature forest and clearance/pasture in previous works (Rignot *et al.* 1997, Saatchi *et al.* 1997).

X band (selected as XVVF), although not associated with deep canopy penetration length and vegetation type discrimination, was used in the 1970s to map tropical vegetation (RADAM project). However, additional information on topography and drainage was needed to achieve vegetation type discrimination (Leckie and Ranson 1998).

7.4.2.2. SAR and TM bands selected by DA

The stepwise backward DA selected 8 bands – TM5, TM4, JERSF, TM3, LHVF, CONT, CHVF and XVVF - as discriminant variables for the 6 land cover classes (table 7.4).

Although the spectral information was spread over 20 bands, only 8 bands were necessary to define the 6 land cover classes. The selected bands comprised the three TM bands and only SAR median filtered data. Also, the SAR bands selected present no overlap in SAR wavelengths and polarisations, as they cover the range X, C and L bands, with VV, HH (for JERSF) and HV polarisations. Textural information was included with GLCM derived contrast (CONT). Bands discarded include the non-filtered data (JERS, LHH, LHV, LVV, CHH, CHV, CVV and XVV) and some of the median-filtered bands (LHHF, LVVF, CHHF and CVVF).

Table 7.4. Bands selected after stepwise discriminant analysis and respective Wilks' lambda. At each step, the band that minimises the overall Wilks' lambda was selected.

Band	Wilks' Lambda
TM5	0.160
TM4	0.050
JERSF	0.031
TM3	0.021
LHVF	0.015
CONT	0.012
CHVF	0.010
XVVF	0.009

The overall Wilks' lambda coefficients were much lower when compared to the SAR only data set, indicating increased class discrimination (table 7.4). The rank of TM5 as

the band containing the higher discriminant ability of the data set agreed with the findings that middle infrared radiation has a strong relationship with those forest biophysical properties that are related to forest regeneration stage (Boyd *et al.* 1996). TM4 was the second band to be selected, followed by bands JERSF and TM3. The remaining four bands (LHVF, CONT, CHVF and XVVF) had a much lower drop in the overall Wilks' lambda coefficient, indicating less discrimination power.

The inclusion of GLCM contrast textural information (band CONT in table 7.7) agreed with previous works that found that the combination of SAR tonal and textural information can provide increased tropical land use classification accuracy than using tonal information alone (Sant'Anna *et al.* 1998, van der Sanden and Hoekman 1999, Saatchi *et al.* 2000, Simard *et al.* 2000).

The increase is class discrimination with the addition of optical sensor bands to SAR is reported widely (Nezry *et al.* 1993, Rignot *et al.* 1997, Saatchi *et al.* 1997, Kuplich *et al.* 2000). The integration of SAR and optical sensor data in tropical land cover classification works in a synergistic basis with the classification of land covers previously unidentified in optical sensor data (e.g. clearances with residual, woody debris) (Rignot *et al.* 1997).

The results above highlighted the need for multiwavelength and multipolarisation data to discriminate tropical land cover classes. While the bands that presented the greater discriminant ability were selected, the classes that were discriminated most effectively by any particular band were yet to be determined.

7.4.3. ANN experiments

Plots of classification accuracy for training data were produced to define the ANN settings that provide more accurate classifications.

7.4.3.1. ANN experiments with SAR bands

Several experiments were performed in order to define the settings to be used when training and classifying the ANN.

Training accuracy was controlled mainly by the number of land cover classes. Figure 7.6. shows the dramatic decrease in the SAR bands training accuracy when the number of classes increased and comprised the 6 land cover classes of the forest regrowth map. This analysis forecast the problems of discriminating between regenerating forest stages, as these classes were the ones that were merged into a single regenerating forest class for the 3 class example in figure 7.9.

The addition of a second hidden layer did not increase training accuracy. For 6 and 2 land cover classes the accuracy was similar, but for the remaining classes the addition of a second layer decreased the training accuracy (figure 7.9). The final architecture for the SAR bands was set as three (input, hidden, output) layers with six nodes each (6:6:6).

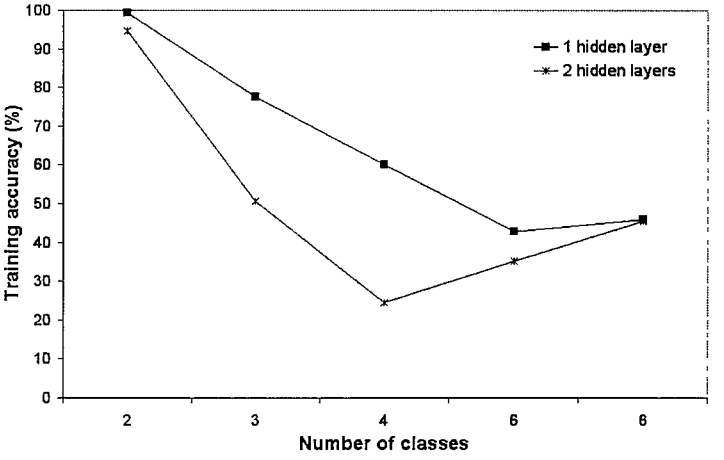

Figure 7.9. The training accuracy of the SAR bands for a varying number of land cover classes and one and two hidden layers. Learning rate, learning momentum and number of iterations were 0.2, 0.2 and 2000, respectively.

The number of iterations changed significantly the training accuracy. The highest training accuracy was achieved around 2500 iterations. Figure 7.10 shows the training accuracy according to the number of iterations.

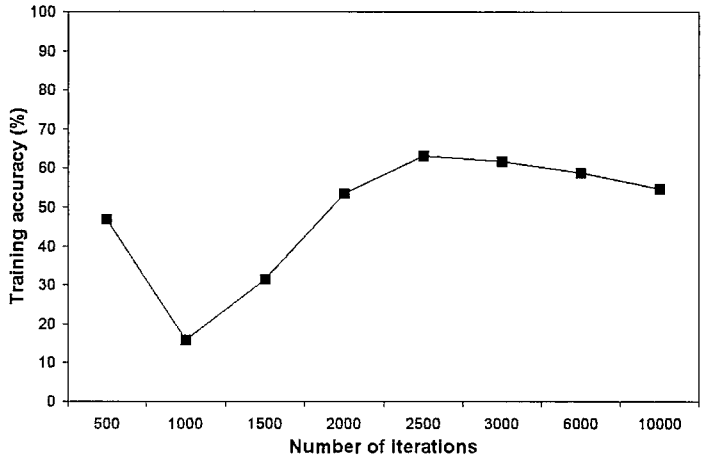

Figure 7.10. SAR bands training accuracy and number of iterations. Learning rate and learning momentum were set at 0.2.

The training accuracy varied with learning rate, until reaching stability at a learning rate of 0.5 (figure 7.11). The peak in training accuracy was reached at a learning rate of 0.4 and this setting was used for the remaining experiments and classifications. The training accuracy also varied with learning momentum and no stability was reached. A peak in training accuracy occurred at a learning momentum of 0.9 (figure 7.11).

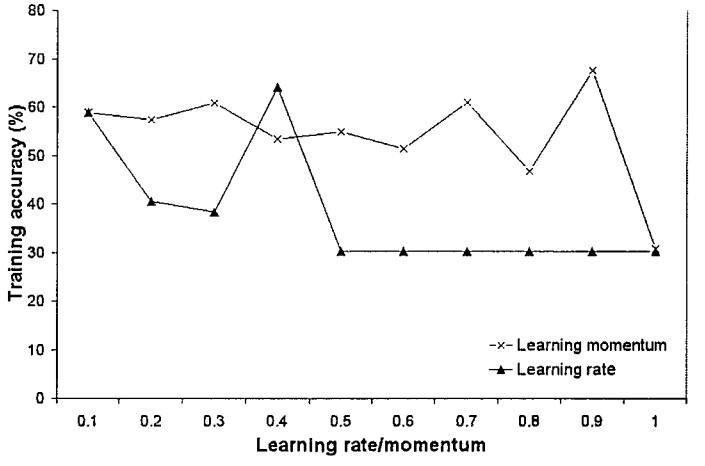

Figure 7.11. SAR bands training accuracy, learning rate and learning momentum. The number of iterations was 2000. Either learning rate or momentum was held at 0.2 while the other varied from 0.1 to 1.

7.4.3.2. ANN experiments with SAR and TM bands

For the experiments with the data set containing SAR and TM bands, the results varied less, due to a more stable training accuracy.

The decrease in training accuracy following an increase in the number of land cover classes was as not marked as for SAR bands only (figure 7.12). The drop in accuracy from 2 to 6 land cover classes was from 100% to around 60%, compared to a decrease from 100 % to 40% with the SAR bands alone.

The addition of a second hidden layer had a variable effect on the training accuracy (with no significant increase or decrease) (figure 7.12). The final architecture for the SAR and TM bands was also set as three (input, hidden, output) layers with six nodes each (6:6:6).

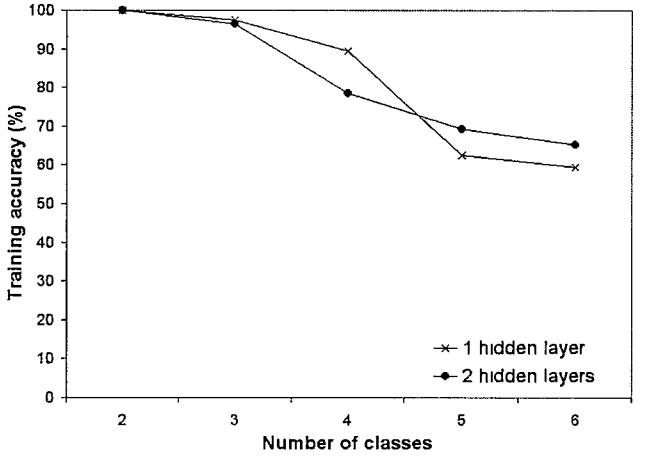

Figure 7.12. SAR and TM bands training accuracy and number of classes for one and two hidden layers. Learning rate, learning momentum and number of iterations were 0.2, 0.2 and 2000, respectively.

The number of iterations did not change significantly the training accuracy (figure 7.13). Although the highest training accuracy was achieved around 10000 iterations, the accuracy was almost as high as 2000 iterations. Therefore, most of the experiments used 2000 iterations.

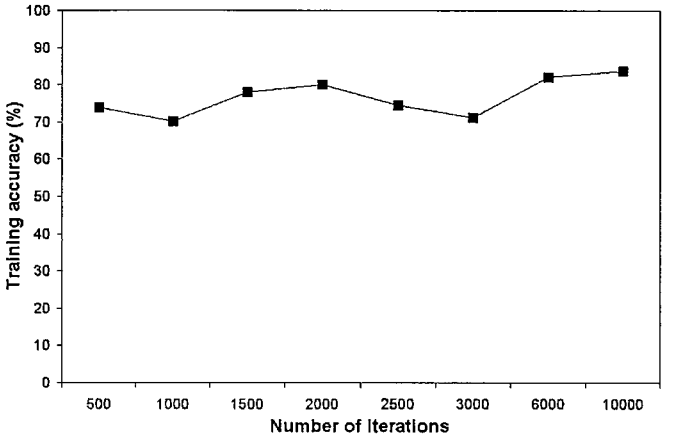

Figure 7.13. SAR and TM bands training accuracy and number of iterations. Learning rate and learning momentum were set at 0.1.

The training accuracy varied with learning rate, reaching stability at a learning rate of 0.7 (figure 7.14). The peak in training accuracy was reached at a learning rate of 0.1 and this setting was used for the remaining experiments and classifications. The training accuracy also varied with learning momentum and no stability was reached. In comparison with the SAR data only, training accuracy oscillated less between the different values for the two rates. A peak in training accuracy occurred at a learning momentum of 0.5 (figure 7.14) and this setting was used for the remaining experiments and classifications.

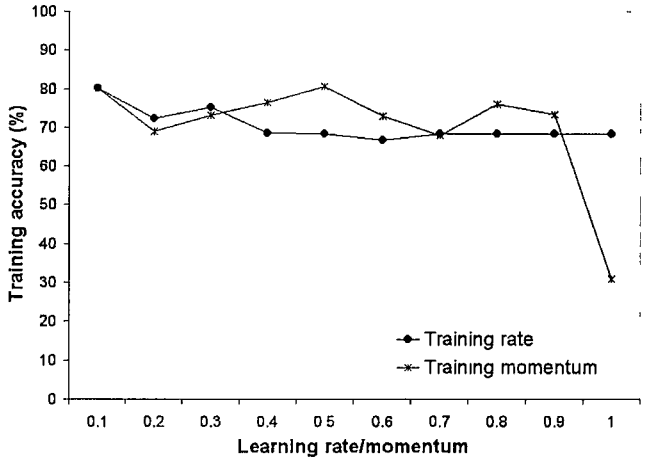

Figure 7.14. SAR and TM bands training accuracy and learning rate and learning momentum. The number of iterations was 2000. Either learning rate or momentum was held at 0.1 while the other varied from 0.1 to 1.

7.4.4. ANN classification and classification accuracy

The experiments above enabled the influence of some ANN settings to be quantified in terms of the training accuracy. This provided a basis on which the settings likely to provide a more accurate classification could be chosen. In addition, the behaviour of the ANN was revealed (through each classification and corresponding confusion matrix), and the ability to discriminate each class was examined in detail. The confusion matrices also display the producer and user's accuracy. Producer's accuracy measures the omission error (error of exclusion) to a certain class and is the probability of a reference site being correctly classified. User's accuracy, on the other hand, is a measure of commission error (error of inclusion) or the probability that a pixel classified on the image actually represents that class on the ground. (Congalton 1991).

In spite of careful analyses of the confusion matrices, the results were still "variable and unpredictable", using the words of Skidmore *et al.* (1997). When trying to understand the results generated by classifying the SAR bands, Principal Components Analysis (PCA), whose fundamentals were given in chapter 5, was performed. The objective was to compute the dimensionality of the SAR data and check their adequacy for such a detailed classification.

7.4.4.1. Classification of SAR bands

The overall training and testing accuracy of SAR band classifications were low. Two key classifications were selected to analyse the behaviour of each class, particularly the regenerating forest classes. These were the full 6 land cover classes and a 3 land cover classes classification, where all regenerating forest stages were merged into a single class. Unless otherwise stated, the settings were a learning rate of 0.4, learning momentum of 0.9 and 2500 iterations.

Table 7.5 displays the confusion matrix for the ANN classification of training SAR data for the 6 land cover classes. The user and producer's accuracies were also shown. The matrix revealed low overall accuracy (46%). Pasture (class 1) and mature forest (class 6) had accuracies of around 63% and 56% respectively, but low commission errors made user's accuracies of around 98% for both classes. Regenerating forests < 3 years

(class 2) although classified correctly in 97% of the reference (training) data, was commissioned to all other classes and only 16% was classified correctly. Classes 3 (3-5 years) and 4 (6-10 years) were ignored on reference data and classified as class 2. Class 5 (11-18 years) also was classified as class 2.

Table 7.5. Confusion matrix for the ANN classification of SAR training data. Kappa coefficient was 0.34. UA and PA refer to user and producer's accuracies.

		Reference data							
	Class	**1**	**2**	**3**	**4**	**5**	**6**	**Total**	**UA(%)**
Classified data	**1**	206	1	0	0	0	3	210	98.1
	2	119	118	30	100	209	142	718	16.43
	3	0	0	0	0	0	0	0	0
	4	0	0	0	0	0	0	0	0
	5	0	0	0	0	2	9	11	18.18
	6	0	2	0	0	2	197	201	98.01
	Total	325	121	30	100	213	351	1140	**Overall accuracy 45.88%**
	PA(%)	63.38	97.52	0	0	0.94	56.13		

Classes:
(1) Pasture
(2) Regenerating forest <3 years
(3) Regenerating forest 3-5 years
(4) Regenerating forest 6-10 years
(5) Regenerating forest 11-18 years
(6) Mature forest.

For the testing data (table 7.6), the results were very similar to the training data, although the overall accuracy was lower (31.4%). Pasture and regenerating forest <3 years presented less omission, unlike mature forest class, that presented more omission errors than in the training data. Around 80% of the testing pixels were classified as regenerating forest <3 years, with commission to all classes, which made its classification inaccurate (around 14%). The classes regenerating forest 3-5 years and 6-10 years were omitted completely.

Table 7.6. Confusion matrix for the ANN classification of SAR testing data. Kappa coefficient was 0.21. UA and PA refer to user and producer's accuracies.

		Reference data							
	Class	1	2	3	4	5	6	Total	UA(%)
Classified data	1	128	0	2	0	0	0	130	98.46
	2	44	123	79	137	281	209	873	14.09
	3	0	0	0	0	0	0	0	0
	4	0	0	0	0	0	0	0	0
	5	0	0	1	0	2	1	4	50
	6	0	0	1	0	1	93	95	97.89
	Total	172	123	83	137	284	303	1102	Overall 31.4%
	PA(%)	74.42	100	0	0	0.7	30.69		

Classes:

(1) Pasture

(2) Regenerating forest <3 years

(3) Regenerating forest 3-5 years

(4) Regenerating forest 6-10 years

(5) Regenerating forest 11-18 years

(6) Mature forest.

Many factors could be behind these inaccurate classification results. The size and characteristics of training data were among the factors found by Foody and Arora (1997) to affect ANN classification results, although small training data sizes were satisfactory for the ANN used by Paola and Schowengerdt (1995). The size of training data sets was defined following the average class coverage and accuracy results.

The characteristics of the training data, however, could have limited classification accuracy. Ideally, training data would have discriminatory characteristics shared with the classes in the Manaus regrowth map (based on multitemporal Landsat sensor data); however, this might not be true. Figure 7.3 showed SAR bands and the poor discrimination of forest regenerating stages within them.

The number of bands or discriminatory variables also affects ANN classification accuracy. Class separability usually increases with increase in number of bands until the addition of new bands has no effect or even reduces the classification accuracy (Bishop 1995, Foody and Arora 1997). Although redundancy on the SAR data was avoided theoretically when selecting bands by discriminant analysis, the question of the intrinsic dimensionality of the bands selected still remained.

Principal components analysis provides information on data set dimensionality (Mather 1999) and was performed on the SAR data. The first two components presented eigenvalues greater than 1 (Kaiser criterion, Statsoft, Inc. 2001) therefore the dimensionality of the data was defined as two. Table 7.7. shows the eigenvalues and the percentage of variance from the SAR data set.

Table 7.7. Eigenvalues and percentage of variance for principal components extracted from SAR bands.

Component	Eigenvalues	
	Total	% of variance
1	2.953	49.21
2	1.012	16.83
3	0.771	12.85
4	0.592	9.86
5	0.352	5.87
6	0.320	5.34

The implications of using a data set with only two dimensions were poor discrimination of classes and low classification accuracy. Despite the availability of 6 SAR bands selected by its discriminatory properties, the data were still inadequate for the representation of the land cover classes. The difficulties of discriminating forest regenerating stages with SAR data, has been documented elsewhere (Rignot *et al.* 1997, Saatchi *et al.* 1997, Sant'Anna *et al.* 1998).

Following that, the regenerating forest stages were merged into a single class and the data were classified into pasture, regenerating forest and mature forest.

Table 7.8 shows the confusion matrix for training SAR data with only three classes and there was a high overall accuracy (81%). Pasture class was classified accurately in reference and classified data. However, 42% of reference data on regenerating forest was classified as mature forest while around 30% of classified mature forest were erroneously committed to regenerating forest.

Table 7.8. Confusion matrix for the ANN classification of training data in SAR bands. Kappa coefficient was 0. 7. UA and PA refer to user and producer's accuracies.

		Reference data				
	Class	Pasture	Regenerating forest	Mature forest	Total	UA (%)
Classified data	Pasture	303	0	0	303	100
	Regenerating forest	0	151	0	151	100
	Mature forest	2	202	394	598	65.89
	Total	305	353	394	1052	Overall 80.61%
	PA (%)	99.34	42.78	100		

In table 7.9 the usual lower overall accuracy for testing data was shown, but the remaining classes behaved similarly as in table 7.22. Pasture class was classified accurately. Mature forest and regenerating forest were not separated completely.

Table 7.9. Confusion matrix for the ANN classification of testing data in SAR bands. Kappa coefficient was 0. 57. UA and PA refer to user and producer's accuracies.

		Reference data				
	Class	Pasture	Regenerating forest	Mature forest	Total	UA (%)
Classified data	Pasture	239	0	0	239	100
	Regenerating forest	0	87	9	96	90.63
	Mature forest	6	244	326	576	56.6
	Total	245	331	335	911	Overall 71.57%
	PA (%)	97.55	26.28	97.31		

Saatchi *et al.* (1997) achieved an accuracy of 87% when classifying the same three land cover classes in Amazonia with SIR-C LHH, LHV, CHH and CHV data. They used a Maximum a Posteriori (MAP) classifier, which provided a highly accurate classification of land cover. A similar result was reported by Rignot *et al.* (1997).

The discrimination of land cover classes in SAR images is related to the type of class being considered. Saatchi *et al.* (2001) achieved an overall accuracy of 89% when

classifying 13 land cover classes in SIR-C SAR data. The classes included several types of crops and natural forest fragments, such as mature, flooded and regenerating forests in the Atlantic Forest in Brazil. Certainly the mapping of regenerating forest stages requires a very subtle discrimination of classes within the data based on a precise understanding of class characterisation on the part of the classifier. As the classes studied were defined following interpretation of multitemporal TM data a synergy of optical and SAR data with TM bands complementing the gaps left by the SAR discrimination of the classes is likely to be successful.

7.4.4.2. Classification of SAR and TM bands

The use of combined TM and SAR data provided higher classification accuracy for training and testing data than for SAR data alone. Figures 7.4 and 7.5 showed the higher discrimination of land cover classes in TM bands and in combined SAR and TM bands, respectively, in relation to SAR bands alone (figure 7.3). The two key classifications analysed were 6 and 4 land cover classes. On the 4 land cover classes the stages were grouped into a young (0-5 years) and an old (6-18 years) regenerating forest class. These classes were suggested also by the results below.

Accuracy results of training and test data shared the same characteristics, although training data provided higher accuracy than testing data (table 7.10 and 7.11). Pasture and mature forest were classified successfully in both training and testing data. For the regenerating forest classes (class 2, 3, 4 and 5) the accuracy varied.

Classes 2 and 5 were well discriminated in reference data and few omission errors were reported. Class 3 in training and testing data was ignored and its reference data was spread in other regenerating forest stage classes. That was not a surprise due to the small coverage of class 2 in the forest regrowth map, leading to a poor spectral characterisation of regenerating forest 3-5 years. Class 3 was mixed mainly with class 2 and class 4 was mixed mainly with class 5 (table 7.10 and 7.11).

Table 7.10. Confusion matrix for the ANN classification of training data in SAR and TM bands. Kappa coefficient was 0.75. UA and PA refer to user and producer's accuracies.

		Reference data							
	Class	1	2	3	4	5	6	Total	UA(%)
Classified data	1	323	2	0	0	0	0	325	99.38
	2	1	91	25	60	67	0	244	37.3
	3	0	1	0	0	0	0	1	0
	4	0	16	0	7	0	0	23	30.43
	5	1	4	5	31	146	0	187	78.07
	6	0	7	0	2	0	351	360	97.5
	Total	325	121	30	100	213	351	1140	Overall 80.52%
	PA(%)	99.38	75.21	0	7	68.54	100		

Classes:

(1) Pasture

(2) Regenerating forest <3 years

(3) Regenerating forest 3-5 years

(4) Regenerating forest 6-10 years

(5) Regenerating forest 11-18 years

(6) Mature forest.

Table 7.11. Confusion matrix for the ANN classification of testing data in SAR and TM bands. Kappa coefficient was 0.63. UA and PA refer to user and producer's accuracies.

		Reference data							
	Class	1	2	3	4	5	6	Total	UA(%)
Classified data	1	172	0	0	6	3	0	181	95.03
	2	0	111	56	43	91	3	304	36.51
	3	0	0	1	4	0	0	5	20
	4	0	2	5	6	4	0	17	35.29
	5	0	10	17	62	185	0	274	67.52
	6	0	0	4	16	1	300	321	93.46
	Total	172	123	83	137	284	303	1102	Overall 70.33%
	PA(%)	100	90.24	1.2	4.38	65.14	99.01		

Classes:

(1) Pasture

(2) Regenerating forest <3 years

(3) Regenerating forest 3-5 years

(4) Regenerating forest 6-10 years

(5) Regenerating forest 11-18 years

(6) Mature forest

The analysis below relates to the classification of SAR and TM bands trained for 4 land cover classes. As with 6 land cover classes, the characteristics of training and test data were similar (table 7.12 and 7.13). The overall classification accuracies were high (both

around 87%). Pasture and mature forest were well discriminated with few omission and commission errors (figure 7.15).

For the training data, class 2 (regenerating forest 0-5 years) was omitted on the reference data, indicating, perhaps, a poor training (table 7.12). On the testing data most of the reference data for class 2 were omitted and misclassified as class 3 (regenerating forest 6-18 years). Figure 7.15 shows the classified image with high omission for class 2 and high commission for class 3. Discrimination between mature forest (class 4) and regenerating forest 6-18 years (class 3) was achieved as a result of combined use of SAR and TM data.

Table 7.12. Confusion matrix for the ANN classification of training data in SAR and TM bands. Kappa coefficient was 0.82. UA and PA refer to user and producer's accuracies.

		Reference data					
	Class	**1**	**2**	**3**	**4**	**Total**	**UA(%)**
Classified data	**1**	304	0	0	0	304	100
	2	0	0	0	0	0	0
	3	1	144	210	0	355	59.15
	4	0	0	0	350	350	100
	Total	305	144	210	350	1009	**Overall**
	PA(%)	99.67	0	100	100		**87.49%**

Classes:

(1) Pasture

(2) Regenerating forest 0-5 years

(3) Regenerating forest 6-18 years

(4) Mature forest

Wilkinson *et al.* (1995) achieved around 80% accuracy when classifying 8 forest classes in a complex Mediterranean landscape using ANN and ERS-1 SAR and Landsat TM images. These authors considered the synergistic SAR-optical approach essential for the discrimination of highly-mixed forest classes.

Regenerating forest up to 15 years old was discriminated from mature forest in TM bands (Steininger 1996). A limit of up to 10 years old was reported for the detection of regenerating forests in L band SAR data alone (Saatchi *et al.* 1997). The use of TM bands, coupled with SAR texture band (GLCM contrast) and different SAR bands and

polarisations made it possible to extend this age range up to 18 years and perhaps beyond.

Table 7.13. Confusion matrix for the ANN classification of testing data in SAR and TM bands. Kappa coefficient was 0.82. UA and PA refer to user and producer's accuracies.

		Reference data					
	Class	**1**	**2**	**3**	**4**	**Total**	**UA(%)**
Classified data	**1**	244	0	0	1	245	99.59
	2	0	33	0	11	44	75
	3	1	108	239	1	348	68.68
	4	1	6	0	322	329	97.87
	Total	245	147	239	335	966	**Overall**
	PA(%)	99.59	22.45	100	96.12		**86.75%**

Classes:

(1) Pasture

(2) Regenerating forest 0-5 years

(3) Regenerating forest 6-18 years

(4) Mature forest

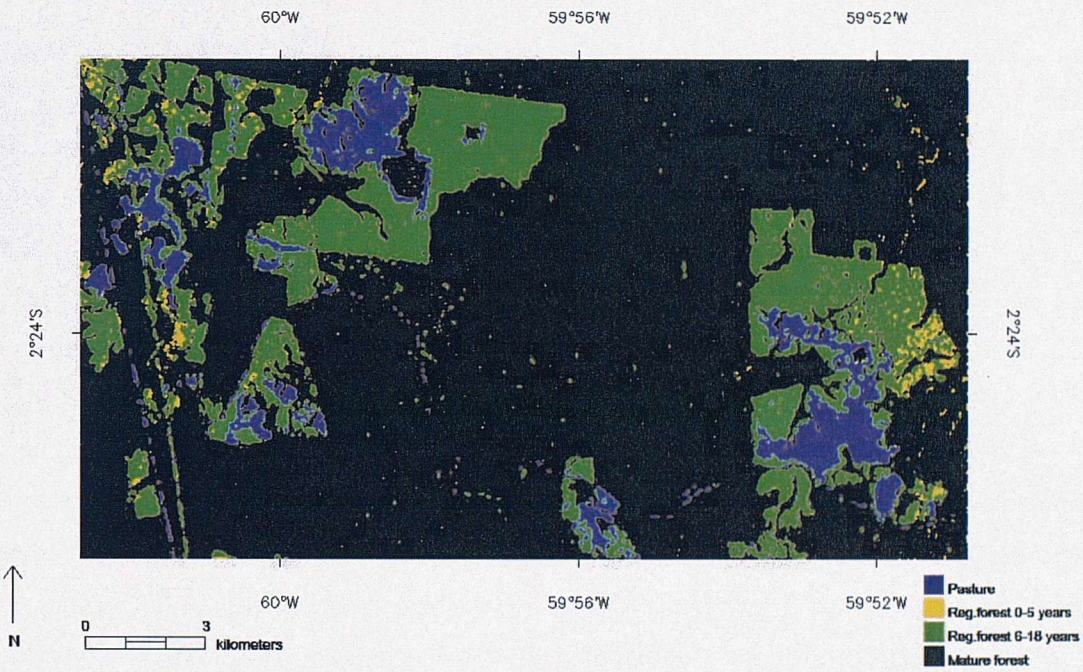

Figure 7.15. ANN classification using SAR and TM bands. Accuracy results were reported in tables 7.12 and 7.13.

7.4. Summary

In this chapter multiwavelength and multipolarisation SAR bands and optical TM bands were used to classify regenerating forest stages. The six land cover classes used for training and testing the overall accuracy of the classification were from a forest regrowth map produced by the classification of a multitemporal series of Landsat TM bands.

The remotely sensed data comprised 20 bands (SAR bands from JERS-1, SIR-C and XSAR and optical bands from TM) upon which a feature selection technique – Discriminant Analysis (DA) - was used. The whole data set was submitted to an exploratory statistical analysis to investigate the discriminating ability of each band. The land cover classes were not discriminated clearly in most of the bands. However, (i) the discrimination between land cover classes was slightly higher for cross-polarised data (SIR-C bands HV and HVF), (ii) TM bands had greater discriminating ability than SAR bands and (iii) median-filtered SAR bands had greater discriminating ability than non-filtered bands. Following DA, 6 out of 17 bands were selected in the set containing SAR bands only and 8 out of the 20 bands were selected in the set containing 7 SAR plus 3 TM bands. A lower overall Wilks' lambda pointed to increased class discrimination for the set containing SAR and TM data in relation to SAR data only.

Classification accuracy using SAR bands alone was around 30% for the 6 land cover classes. When regenerating forest stage classes were merged into a single class, the classification accuracy increased to around 80%. SAR data alone was unable to discriminate regenerating forest stages and PCA results demonstrated that the dimensionality of the 6 SAR bands was 2, limiting their ability to discriminate between the subtle tonal/textural characteristics of each regenerating stage. A data set comprising TM and SAR bands showed increased classification accuracy in relation to SAR data alone, although some confusion between regenerating forest stages was still present. Following merging of regenerating forest stages into young (0-5 years) and intermediate (6-18 years), the overall accuracy was around 87%. The combination of SAR and TM bands were essential for the discrimination between regenerating forest stages, however, pasture and mature forest were discriminated accurately in both SAR data alone and in the combined SAR and TM data.

CHAPTER EIGHT

Conclusions

This thesis has investigated the potential of temporal, spatial, spectral and polarisation characteristics of SAR backscatter for the study of biomass and land cover class of tropical forests in two study areas in Brazilian Amazonia. To conclude, the main findings are divided by subject and summarised, starting by underlining the answers to the questions posed within the objectives (section 1.4). Finally, the significance of findings and future work directions are suggested.

8.1. Temporal analysis

No biomass change was detectable with temporal JERS-1 LHH backscatter.

- A positive backscatter/biomass relationship was found (r = 0.87) and indicated saturation in σ° at biomass levels of around 90 T ha^{-1}.
- A cyclical pattern in σ° for young regenerating forest plots was detected. The pattern was seasonal with the dry season corresponding to lower σ° and the wet season corresponding to higher σ°. This result indicated the influence of vegetation and soil water content on σ°.
- The behaviour of σ° was more strongly time-dependent for plots below the σ° asymptote (e.g., young regenerating forest plots). Although less temporally dynamic than these young regenerating forest plots, intermediate regenerating and mature forest plots presented a similar σ° behaviour.

- The influence of rainfall was assessed and was found to be an important source of variation in σ°. The influence was clearer for young regenerating forest plots, where the change in the water content of vegetation and soil moisture were probably detected.
- To eliminate the influence of varying vegetation and soil water content on backscatter, the use of SAR data from the dry season was recommended.

8.2. Spatial analysis

The addition of GLCM derived *contrast* to backscatter potentially increases the accuracy of biomass prediction and mapping.

- Seven texture measures showed, in simulated images, discrimination of image texture independently of image contrast. They were: GLCM derived *contrast*, *entropy*, *correlation*, *chi-square*, SADH derived *mean of sum vector*, local statistics derived *entropy* and variogram derived *range.*
- These seven texture measures were calculated for real SAR images and the correlation between them and the log of biomass estimated. Only GLCM derived *contrast* increased the correlation between backscatter and log of biomass.
- Values of variogram derived range highlighted the diversity of vegetation/canopy structures found in the field. However, no relationship was found between range, log of biomass and dominant species (and therefore upper canopy structure). Image spatial resolution (18 m), pixel transects (as opposed to pixel matrices) used to derive the variograms and the models used to fit the data could have limited the analysis.
- GLCM and SADH derived texture measures extracted using different window sizes and quantisation levels indicated that textural information was dependent on quantisation levels. Both window sizes contained the same amount of textural information.
- The strong relationships between some texture measures, particularly the ones derived from the GLCM and log of biomass were related to the age-related roughness of the vegetation canopy.

8.3. Spectral and polarisation analysis

Multiwavelength and multipolarisation SAR data only had limited utility for the classification of a surrogate for biomass in regenerating tropical forests.

- Exploratory statistics and discriminant analysis showed that median-filtered SAR bands had increased discrimination ability of land cover classes (as compared to non-filtered SAR bands).
- Cross-polarised HV and HVF (median-filtered) bands presented increased discrimination of land cover classes as compared to the other SAR bands.
- Neural networks can be used for the classification of land cover in tropical forest.
- The reduction of speckle was essential for land cover classification using SAR data, even if the data were previously averaged by multi-look processing.
- Higher overall training and testing accuracies were achieved with SAR and TM bands in combination, as compared with SAR bands only.
- Regenerating forest stages were discriminated in SAR and TM bands when merged into young (0-5 years) and intermediate (6-18 years) regenerating forest classes.
- The use of TM bands, coupled with SAR texture band (GLCM contrast) and different SAR bands and polarisations made it possible to discriminate regenerating forest up to around 13 years old.
- The overall accuracy for classification of mature forest, pasture, young (0-5 years) and intermediate (6-18 years) regenerating forest classes was around 87%.
- Pasture and mature forest were discriminated accurately in both SAR data and combined SAR and TM data.

8.3. Summary

The main findings of this thesis are:

- The σ° temporal characteristics were not related to biomass accumulation. Water content of vegetation and soil were the main cause of temporal σ° change.

- The σ° spectral and polarisation characteristics had some utility for the mapping of regenerating forest stages, but require the combination with optical sensor data.
- The spatial characteristics of σ° have shown a strong relationship with the biomass of tropical forests. The addition of GLCM contrast information to σ° potentially increased the accuracy of biomass estimation from SAR data.

The temporal, spatial, spectral and polarisation characteristics of σ° present great potential for the study of regenerating tropical forests. However, this research is still hindered by the lack of specific knowledge about σ° mechanisms in tropical forests. For example, the σ° asymptote at biomass levels of around 90 T ha^{-1} (for LHH band) is a real limitation that encourages future research into the use of other tropical forest biophysical properties as biomass surrogates when trying to estimate biomass and biomass change from SAR data.

8.4. Significance of results and future directions

The findings of this research supported the use of SAR data, particularly their spatial domain, for the study of regenerating tropical forests. However, to move further and achieve more accurate biomass estimates and mapping with SAR data, some avenues have yet to be fully explored.

Analysis of temporal backscatter would benefit from knowledge of land cover changes, rainfall intensity and biomass accumulation rates of regenerating tropical forests. A change detection approach (as used by Quegan *et al.* 2000) could isolate sources of backscatter variation and allow their quantification. The quantification of all sources of backscatter variation is far from complete, but in this research the importance of water content in regenerating tropical forests and soils was revealed.

A measure that best captured the spatial variability of vegetation/canopy structure was GLCM contrast calculated on a LHH band. The assessment of the use of GLCM contrast (and other texture measures) needs to be done using different SAR bands and polarisations, particularly LHV. The strong relationship between some texture measures and the log of biomass means that textural information is required if biomass is to be estimated accurately from SAR data.

Research is needed to assess the performance of neural networks and fuzzy classifiers in the classification of regenerating forest stages (as defined by the biophysical properties of vegetation). The successional paths proposed by Foody *et al.* (1996) and Lucas *et al.* (2000) could provide the land cover classes whose characteristics might be more related to backscatter than stage/age of regenerating forests.

The synergy between SAR and optical sensor data stands to enhance the discrimination of regenerating forest stages and ultimately tropical forest biomass and carbon content estimation. Further studies using combined SAR and optical sensor data for the study of regenerating tropical forests are needed.

An operational biomass mapping scheme for Amazonia would require the production of high-spatial resolution SAR image mosaics and the derivation of texture measures. To refine the Amazon basin land cover map produced by Saatchi *et al.* (2000) with regenerating forest stage classes, optical sensor images could be integrated with the SAR data, at least on the critical deforestation and regrowth areas defined by PRODES (Deforestation Project - INPE 2000). Monitoring and mapping of regenerating tropical forest stages using such a methodology could be operational, using for example multipolarisation L band SAR data from ALOS (Advanced Land Observing Satellite) once it has been launched.

Earth observation with SAR systems is a valuable tool for increasing our understanding of environmental processes and the management of human activities that result in environmental disturbance. This thesis has provided an insight into the possibilities offered by SAR data for helping to fill some of the gaps in specific areas of knowledge about tropical forest ecosystems and their local scale assessment.

REFERENCES

Ab'Sáber, A.N. (1996). *Amazônia: Do Discurso a Práxis.* Editora da Universidade de São Paulo, São Paulo. 320 p.

Aber, J.D. and Melillo, J.M. (2001). *Terrestrial ecosystems.* Academic Press, San Diego. 556 p.

Adams, J.B., Sabol, D.E., Kapos, V., Almeida Filho, R., Roberts, D.A., Smith, M.O. and Gillespie, A.R. (1995). Classification of multispectral images based on fractions of endmembers: application to land-cover change in the Brazilian Amazon. *Remote Sensing of Environment,* 52: 137-154.

Ahern, F.J., Leckie, D.J. and Drieman, J.A. (1993). Seasonal changes in relative C-band backscatter of northern forest cover types. *IEEE Transactions on Geoscience and Remote Sensing,* 31: 668-680.

Alsdorf, D.E., Melack, J.M., Dunne, T., Mertes, L.A.K., Hess, L. and Smith, L.C. (2000). Interferometric radar measurements of water level changes on the Amazon flood plain. *Nature,* 404: 174-176.

Alves, D.S., Soares, J.V., Amaral, S., Mello, E.M.K., Almeida, S.A.S., Silva, O.F. and Silveira, A.M. (1997). Biomass of primary and secondary vegetation in Rondonia, Western Brazilian Amazon. *Global Change Biology,* 3: 451-461.

Alves, D.S., Pereira, J.L.G., Souza, C.L., Soares, J.V. and Yamaguchi, F. (1999). Characterizing landscape changes in central Rondonia using Landsat TM imagery. *International Journal of Remote Sensing,* 20: 2877-2882.

Anderson, A.B. (1990). Deforestation in Amazonia: Dynamics, Causes and Alternatives. *In:* A. B. Anderson (Ed.). *Alternatives to Deforestation in Amazonia*, Columbia University Press, New York, pp. 3-23.

Araújo, L.S., Santos, J.R., Freitas, C.C. and Xaud, H.A.M. (1999). The use of microwave and optical data for estimating aerial biomass of the savanna and forest formations at Roraima State, Brazil. In: *IGARSS'99*, IEEE Piscataway, Hamburg, CDROM.

Atkinson, P.M. and Plummer, S.E. (1993). The influence of percentage cover and biomass of clover on the reflectance of mixed pasture. *International Journal of Remote Sensing,* 14: 1439-1444.

Atkinson, P.M. and Curran, P.J. (1997). Choosing an appropriate spatial resolution for remote sensing investigation. *Photogrammetric Engineering and Remote Sensing,* 63: 1345-1351.

Atkinson, P.M. and Tatnall, A.R.L. (1997). Neural networks in remote sensing. *International Journal of Remote Sensing,* 18: 699-709.

Atkinson, P.M. (1999). Spatial Statistics. *In:* A. Stein, F. van der Meer and B. Gorte (Eds.). *Spatial Statistics for Remote Sensing*, Kluwer Academic, Dordrecht, pp. 57-81.

Atkinson, P.M. and Lewis, P. (2000). Geostatistical classification for remote sensing: an introduction. *Computers and Geosciences,* 26: 361-371.

Attema, E.P.W. and Ulaby, F.T. (1978). Vegetation modeled as a water cloud. *Radio Science,* 13: 357-364.

Azevedo, L.H.A. (1971). Radar in the Amazon. In: *International Symposium on Remote Sensing of Environment*, Environmental Research Institute of Michigan, Ann Arbor, Michigan, pp. 2303-2306.

Bailey, P. (1997). *Exploring remotely sensed shadow in Amazonian regrowth forests.* Unpublished PhD. Thesis, University of Southampton, Southampton. 226 p. p.

Baillie, I.C. (1996). Soils of the humid tropics. *In:* P. W. Richards (Ed.). *The Tropical Rain Forest - An Ecological Study*, Cambridge University Press, Cambridge, pp. 256-285.

Baltzer, H. (2001). Forest mapping and monitoring with interferometric synthetic aperture radar (InSAR). *Progress in Physical Geography,* 25: 159-177.

Baraldi, A. and Parmiggiani, F. (1995). An investigation of the textural characteristics associated with gray level cooccurrence matrix statistical parameters. *IEEE Transactions on Geoscience and Remote Sensing,* 33: 293-304.

Batista, G.T. (1999). Resultados do projeto seqüestro e emissões de carbono em função de mudanças no uso e cobertura da terra amazônica. In: *Seminário de Avaliação dos Resultados do Programa Piloto para a Proteção das Florestas Tropicais do Brasil*, Secretaria Técnica do Ministério da Ciência e Tecnologia, Manaus, Brazil, pp. 127-156.

Beaudoin, A., Le Toan, T., Goze, S., Nezry, E., Lopes, A., Mougin, E., Hsu, C.C., han, H.C., Kong, J.A. and Shin, R.T. (1994). Retrieval of forest biomass from SAR data. *International Journal of Remote Sensing,* 14: 2777-2796.

Benediktsson, J.A. and Sveinsson, J.R. (1997). Feature extraction for multisource data classification with artificial neural networks. *International Journal of Remote Sensing,* 18: 727-740.

Benjamini, Y. (1988). Opening the box of a boxplot. *The American Statistician,* 42: 257-262.

Berberoglu, S., Lloyd, C.D., Atkinson, P.M. and Curran, P.J. (2000). The integration of spectral and textural information using neural networks for land cover mapping in the Mediterranean. *Computers and Geoscience,* 26: 385-396.

Bergen, K.M., Dobson, M.C., Pierce, L.E. and Ulaby, F.T. (1998). Characterizing carbon in a northern forest by using SIR-C/X-SAR imagery. *Remote Sensing of Environment,* 63: 24-39.

Bierregaard, J., R.O. and Stouffer, P.C. (1997). Understory birds and dynamic habitat mosaics in Amazonian Rainforests. *In:* W. F. Laurance and J. Bierregaard, R.O. (Eds.). *Tropical Forest Remnants- Ecology, Management and Conservation of Fragmented Communities*, The University of Chicago Press, Chicago, pp. 138-155.

Bijlsma, R.J. (1993). The characterisation of natural vegetation using first-order and texture measurements in digitized, color-infrared photography. *International Journal of Remote Sensing,* 14: 1547-1562.

Bishop, C.M. (1995). *Neural Networks for Pattern Recognition.* Clarendon Press, Oxford. 482 p.

Boyd, D.S., Foody, G.M., Curran, P.J., Lucas, R.M. and Honzak, M. (1996). An assessment of radiance in Landsat TM middle and thermal infrared wavebands for the detection of tropical forest regeneration. *International Journal of Remote Sensing,* 17: 249-261.

Brown, S., Gillespie, A.J.R. and Lugo, A.E. (1989). Biomass estimation methods for tropical forests with application to forest inventory data. *Forest Science,* 24: 881-902.

Brown, S. and Lugo, A.E. (1990). Tropical secondary forests. *Journal of Tropical Forestry,* 6: 1-32.

Brown, S. and Lugo, A.E. (1992). Aboveground biomass estimates for tropical moist forests of the Brazilian Amazon. *Interciencia,* 17: 8-18.

Brown, I.F., Nepstad, D.C., Pires, I.O., Luz, L.M. and Alechandre, A.S. (1992). Carbon storage and land use in extractive reserves, Acre, Brazil. *Environmental Conservation,* 19: 307-315.

Budowski, G. (1965). Distribution of tropical American rain forest species in the light of

Burrough, P.A. (1996). Methods of Spatial Interpolation. *In: Principles of Geographical Information Systems for Land Resources Assessment*, Clarendon Press, Oxford, pp. 147-166.

Buschbacher, R., Uhl, C. and Serrão, E.A.S. (1988). Abandoned pastures in eastern Amazonia. II. Nutrient stocks in the soils and vegetation. *Journal of Ecology,* 76: 682-699.

Castel, T., Beaudoin, A., Floury, N., Le Toan, T., Caraglio, Y. and Barczi, J.F. (2001). Deriving forest canopy parameters for backscatter models using the AMAP architectural plant model. *IEEE Transactions on Geoscience and Remote Sensing,* 39: 571-583.

Ceccon, E. and Miramontes, O. (1999). Mecanismos y actores sociales de la deforestation en la Amazonia Brasilena. *Interciencia,* 24: 112-119.

Chambers, J.Q., Higuchi, N., Tribuzy, E.S. and Trumbore, S.E. (2001). Carbon sink for a century. *Nature,* 410 p. 429.

Chapman, B., Freeman, A. and Siqueira, P. (1999). JERS-1 SAR Global Rain Forest Mapping (GRFM) project - data quality for multi-temporal studies. *In:* M. Shimada (Ed.). *JERS-1 Science Program'99 - PI reports*, EORC/NASDA, Tokyo, pp. 13-17.

Chapman, C.A. and Chapman, L.J. (1999). Forest restoration in abandoned agricultural land: a case study from East Africa. *Conservation Biology,* 13: 1301-1311.

Chen, K.S., Huang, W.P., Tsay, D.H. and Amar, F. (1996). Classification of multifrequency polarimetric SAR imagery using a dynamic learning neural network. *IEEE Transactions on Geoscience and Remote Sensing,* 34: 814-820.

Chica-Olmo, M. and Abarca-Hernandez, F. (2000). Computing geostatistical image texture for remotely sensed data classification. *Computers and Geoscience,* 26: 373-383.

Cochrane, M.A., Alencar, A., Schulze, M.D., Souza Jr., C.M., Nepstad, D.C., Lefebvre, P. and Davidson, E.A. (1999). Positive feedbacks in the fire dynamic of closed canopy tropical forests. *Science,* 284: 1832-1835.

Cohen, W.B., Spies, T.A. and Bradshaw, G.A. (1990). Semivariograms of digital imagery for analysis of conifer canopy structure. *Remote Sensing of Environment,* 34: 167-178.

Congalton, R.G. (1991). A review of assessing the accuracy of classifications of remotely sensed data. *Remote Sensing of Environment,* 37: 35-46.

Curran, P.J. (1988). The semi-variogram in remote sensing: an introduction. *Remote Sensing of Environment,* 3: 493-507.

Curran, P.J. and Foody, G.M. (1994). the use of remote sensing to characterise the regenerative states of tropical forests. *In:* G. Foody and P. J. Curran (Eds.). *Environmental Remote Sensing from Regional to Global Scales*, Wiley & Sons, Chichester, pp. 44-83.

Curran, P.J., Foody, G.M., Lucas, R.M. and Honzak, M. (1995). A methodology for remotely sensing the stage of regeneration in tropical forests. *In:* P. M. Mather (Ed.). *TERRA 2 - Understanding the Terrestrial Environment. Remote Sensing Systems and Network*, John Wiley and Sons, London, pp. 189-202.

Curran, P.J. and Atkinson, P.M. (1998). Geostatistics and remote sensing. *Progress in Physical Geography,* 22: 61-78.

Curran, P.J., Milton, E.J., Atkinson, P.M. and Foody, G.M. (1998). Remote sensing: from data to understanding. *In:* P. A. Longley, S. M. Brooks, R. McDonnell and B. Macmillan (Eds.). *Geocomputation: A Primer*, John Wiley and Sons, London, pp. 33-59.

Davis, J.C. (1986). Analysis of Sequences of Data. *In: Statistical and Data Analysis in Geology*, John Wiley, New York, pp. 239-248.

Deans, J.D., Moran, J. and Grace, J. (1996). Biomass relationships for tree species in regenerating semi-decidous tropical moist forest in Cameroon. *Forest Ecology and Management,* 88: 215-225.

Delire, C., Calvet, J.C., Noilhan, J., Wright, I., Manzi, A. and Nobre, C. (1997). Physical properties of Amazonian soils: a modeling study using the Anglo-Brazilian Amazonian Climate Observation Study area. *Journal of Geophysical Research,* 102: 119-133.

Detwiller, R.P. and Hall, C.A.S. (1988). Tropical forests and the global carbon cycle. *Science,* 239: 42-47.

Diegues, A.C. (1992). The social dynamics of deforestation in the Brazilian Amazon: an overview. http://www.unsrid.org/engindex/publ/list/dp/dp36/toc.html.

Dixon, R.K., brown, S., Houghton, R.A., Solomon, A.M., Trexler, M.C. and Wisniewski, J. (1994). Carbon pools and flux of global forest ecosystems. *Science,* 263: 185-190.

DNM (Departamento Nacional de Meteorologia) (1992). *Normais Climatológicas (1961-1990).* Ministério da Agricultura e Reforma Agrária, Brasília.

Dobson, M.C., Ulaby, F.T., Le Toan, T., Beaudoin, A., Kasischke, E.S. and Christensen, N. (1992). Dependence of radar backscatter on coniferous forest biomass. *IEEE Transactions on Geoscience and Remote Sensing,* 30: 412-415.

Dobson, M.C., Ulaby, F.T., Pierce, L.E., Sharik, T.L., Bergen, K.M., Kellndorfer, J., Kendra, J.R., Li, E., Lin, Y.C., Nashashibi, A., Sarabandi, K. and Siqueira, P. (1995). Estimation of forest biophysical characteristics in northern Michigan with SIR-C/X-SAR. *IEEE Transactions on Geoscience and Remote Sensing,* 33: 877-894.

Dutra, L.V. and Huber, R. (1999). Feature extraction and selection for ERS-1/2 InSAR classification. *International Journal of Remote Sensing,* 20: 993-1016.

Eastman, J.R. and Fulk, M. (1993). Long sequence time series evaluation using standardized principal components. *Photogrammetric Engineering & Remote Sensing,* 59: 1307-1312.

Eden, M.J. (1990). *Ecology and land management in Amazonia.* Belhaven Press, UK. 257 p.

Elachi, C. (1988). *Spaceborne radar remote sensing: applications and techniques.* IEEE Press, New York. 255 p.

Eggers, L. (1999). Pontifície Universidade Católica (PUC), Porto Alegre, Brazil.

Evans, D.L., Plaut, J.J. and Stofan, E.R. (1997). Overview of the spaceborne imaging radar-C/X-band synthetic aperture radar (SIR-C/X-SAR) missions. *Remote Sensing of Environment,* 59: 135-140.

Ewel, J. (1971). Biomass changes in early tropical succession. *Turrialba,* 21: 110-112.

FAO. (1971). *FAO/UNESCO Soil Map of the World. Volume 4. South America.* United Nations Educational, Scientific and Cultural Organisation, Paris.

FAO. (1971). *FAO-UNESCO Soil Map of the World: 1:5 000 000.* Volume 4, South America. United Nations Educational, Scientific and Cultural Organisation, Paris. 193 p.

Fearnside, P.M. and Guimarães, W.M. (1996). Carbon uptake by secondary forests in Brazilian Amazonia. *Forest Ecology and Management,* 80: 35-46.

Fearnside, P.M. (2000). Global warming and tropical land use change: greenhouse gas emissions from biomass burning, decomposition and soils in forest conversion, shifting cultivation and secondary vegetation. *Climatic Change,* 46: 115-158.

Ferrazzoli, P., Paloscia, S., Pampaloni, P., Schiavon, G., Sigismondi, S. and Solimini, D. (1997). The potential of multifrequency polarimetric SAR in assessing agricultural and arboreous biomass. *IEEE Transactions on Geoscience and Remote Sensing,* 35: 5-17.

Foody, G.M. (1995). Using prior knowledge in artificial neural network classification with a minimal training set. *International Journal of Remote Sensing,* 16: 301-312.

Foody, G.M. and Hill, R.A. (1996). Classification of tropical forest classes from Landsat TM data. *International Journal of Remote Sensing,* 17: 2353-2367.

Foody, G.M., Green, R., Lucas, R.M., Curran, P.J., Honzak, M. and Amaral, I. (1997). Observations on the relationship between SIR-C radar backscatter and the biomass of regenerating tropical forests. *International Journal of Remote Sensing,* 18: 687-694.

Foody, G.M. and Arora, M.K. (1997). An evaluation of some factors affecting the accuracy of classification by an artificial neural network. *International Journal of Remote Sensing,* 18: 799-810.

Foody, G.M., Green, R.M., Lucas, R.M., Curran, P.J., Honzak, M. and Do Amaral, I. (1997a). Observations on the relationship between SIR-C radar backscatter and the biomass of regenerating tropical forests. *International Journal of Remote Sensing,* 18: 687-694.

Foody, G.M., Lucas, R.M., Curran, P.J. and Honzak, M. (1997b). Non-linear mixture modelling without end-members using an artificial neural network. *International Journal of Remote Sensing,* 18: 937-953.

Fransson, J.E.S. and Israelsson, H. (1999). Estimation of stem volume in boreal forests using ERS-1 C- and JERS-1 L-band SAR data. *International Journal of Remote Sensing,* 20: 123-137.

Freitas, C.C., Sant'Anna, S.J.S. and Renno, C.D. (1999). The use of JERS-1 and RADARSAT images for land user classification in the Amazon region. In: *IGARSS'99*, IEEE Piscataway, Hamburg, CDROM.

Gash, J.H.C., Nobre, C.A., Roberts, J.M. and Victoria, R.L. (1996). An overview of ABRACOS. *In:* J. H. C. Gash, C. A. Nobre, J. M. Roberts and R. L. Victoria (Eds.). *Amazonian Deforestation and Climate*, Jonh Wiley, Chichester, pp. 1-14.

Gates, D.M. (1991). Water relations of forest trees. *IEEE Transactions on Geoscience and Remote Sensing,* 29: 836-842.

Gheerbrant, A. (1992). *The Amazon.* Thames and Hudson, London. 192 p.

Grace, J. and Malhi, Y. (1999). The role of rain forests in the global carbon cycle. *Progress in Environmental Science,* 1: 177-193.

Grover, K., Quegan, S. and Freitas, C.C. (1999). Quantitative estimation of tropical forest cover by SAR. *IEEE Transactions on Geoscience and Remote Sensing,* 37: 479-490.

Haack, B. and Bechdol, M. (2000). Integrating multisensor data and radar texture measures for land cover mapping. *Computers and Geosciences,* 26: 411-421.

Hammerstrom, D. (1993). Neural networks at work. *IEEE Spectrum,* 30: 26-32.

Haralick, R.M., Shaunmugam, K. and Dinstein, I. (1973). Textural features for image classification. *IEEE Transactions on Systems, Man and Cybernetics,* 3: 610-621.

Haralick, R.M. and Shanmugam, K.S. (1974). Combined spectral and spatial processing of ERTS imagery data. *Remote Sensing of Environment,* 3: 3-13.

Haralick, R.M. (1979). Statistical and structural approaches to texture. *Proceedings of the IEEE,* 67: 786-804.

Hartshorn, G.S. (1980). Neotropical forest dynamics. *Biotropica,* 12: 23-30.

Hashimoto, Y., Tsuchiya, K. and Iijima, T. (1996). Normalized backscattering radar cross section of tropical rain forest in Rondonia, northern Brazil. *Advances in Space Research,* 19: 1425-1428.

He, D. and Wang, L. (1990). Texture unit, texture spectrum and texture analysis. *IEEE Transactions on Geoscience and Remote Sensing,* 28: 509-512.

Hernandez Filho, P., Shimabukuro, Y.E., Lee, D.C.L., Santos Filho, C.P. and Almeida, R.R. (1993). *Final report on the forest inventory project at the Tapajós National Forest.* Internal Report. INPE, São José dos Campos, SP, Brazil. 120 p.

Hess, L.L., Melack, J.M., Filoso, S. and Yong, W. (1995). Delineation of inundated area and vegetation along the Amazon floodplain with the SIR-C Synthetic Aperture Radar. *IEEE Transactions on Geoscience and Remote Sensing,* 33: 896-904.

Hoekman, D.H. and Quinones, M.J. (2000). Land cover type and biomass classification using AirSAR data for evaluation of monitoring scenarios in the Colombian Amazon. *IEEE Transactions on Geoscience and Remote Sensing,* 38: 685-696.

Honzák, M., Lucas, R.M., Amaral, I., Curran, P.J., Foody, G., M. and Amaral, S. (1996). Estimation of the leaf area index and total biomass of tropical regenerating forests: comparison of methodologies. *In:* J. H. C. Gash, C. A. Nobre, J. M. Roberts and R. L. Victoria (Eds.). *Amazonian Deforestation and Climate*, John Wiley and Sons Ltd., Chichester, pp. 365-381.

Honzák, M., (1997). *Mapping carbon pools in the regenerating forests of Brazil and Cameroon using remote sensing techniques*. Unpublished PhD. Thesis. University of Wales, Swansea. 212 p.

Houghton, R.A., Skole, D.L., Nobre, C.A., Hackler, J.L., Lawrence, K.T. and Chomentowski, W.H. (2000). Annual fluxes of carbon from deforestation and regrowth in the Brazilian Amazon. *Nature,* 403: 301-304.

Ii, F. A. M. (2000). Department of Geography, University of Reading, UK.

Imhoff, M.L. (1995a). A theoretical analysis of the effect of forest structure on Synthetic Aperture Radar backscatter and the remote sensing of biomass. *IEEE Transactions on Geoscience and Remote Sensing,* 33: 341-352.

Imhoff, M.L. (1995b). Radar backscatter and biomass saturation: ramifications for the global biomass inventory. *IEEE Transactions on Geoscience and Remote Sensing,* 33: 511-518.

INPE (Instituto Nacional de Pesquisas Espaciais) (2000). Monitoring of the Brazilian Amazonian forest by satellite: 1999-2000. INPE, São Jose dos Campos. http://www.inpe.br/informacoes_Eventos/amz1999_2000/Prodes.

IPCC. (2001). *Climate Change 2001: The Scientific Basis. Contribution of Working Group I to the Third Assessment Report of the Intergovernmental Panel on Climate Change*. J. T. Houghton, Y. Ding, D. J. Griggset. Cambridge University Press, Cambridge. http://www.ipcc.ch/pub/spm22-01.pdf.

Isaacks, E.H. and Srivastava, R.M. (1989). Univariate Description. *In: An Introduction to Applied Geostatistics*, Oxford University Press, New York, pp. 10-39.

Jacobs, M. (1988). Primary and secondary forest. *In:* R. Kruk (Ed.). *The Tropical Rain Forest: A First Encounter*, Springer-Verlag, Berlin, pp. 89-100.

Jensen, J.R. (1996). *Introductory Digital Image Processing: A Remote Sensing perspective*. 2nd. Prentice-Hall, Saddle River, NJ.

Jensen, J.R. (2000). *Remote Sensing of the Environment: An Earth Resource Perspective*. Prentice Hall, Saddle River. 544 p.

Johnston, R.J. (1980). *Multivariate statistical analysis in geography*. Longman, London. 280 p.

Jordan, R.L., Huneycutt, B.L. and Werner, M. (1995). The SIR-C/X-SAR Synthetic Aperture Radar System. *IEEE Transactions on Geoscience and Remote Sensing,* 33: 829-839.

Kanellopoulos, I. and Wilkinson, G.G. (1997). Strategies and best practice for neural network image classification. *International Journal of Remote Sensing,* 18: 711-725.

Kasischke, E.S. and Christensen, N. (1990). Connecting forest ecosystem and backscatter models. *International Journal of Remote Sensing,* 11: 1277-1298.

Kasischke, E.S., Melack, J.M. and Dobson, M.C. (1997). The use of imaging radars for ecological applications - a review. *Remote Sensing of Environment,* 59: 141:156.

Kingsley, S. and Quegan, S. (1992). *Understanding Radar Systems*. McGraw-Hill Book Company, London. 375 p.

Krebs, C.J. (1978). *Ecology - The Experimental Analysis of Distribution and Abundance*. 2nd. Harper & Row, New York. 678 p.

Kuntz, S. and Siegert, F. (1999). Monitoring of deforestation and land use in Indonesia with multitemporal ERS data. *International Journal of Remote Sensing,* 20: 2835-2853.

Kuplich, T.M. and Curran, P.J. (1999). Temporal analysis of JERS-1/SAR images over regenerating forests in Brazilian Amazonia. In: *IGARSS'99*, IEEE Piscataway, Hamburg, CDROM.

Kuplich, T.M., Freitas, C.C. and Soares, J.V. (2000a). The study of ERS-1 SAR and Landsat TM synergism for land use classification. *International Journal of Remote Sensing,* 21: 2101-2111.

Kuplich, T.M., Salvatori, V. and Curran, P.J. (2000b). JERS-1/SAR backscatter and its relationship with biomass of regenerating forests. *International Journal of Remote Sensing,* 21: 2513-2518.

Kurosu, T., Uratsuka, S., Maeno, H. and Kozu, T. (1999). Texture statistics for classification of land use with multitemporal JERS-1 SAR single-look imagery. *IEEE Transactions on Geoscience and Remote Sensing,* 37: 227-235.

Kurvonen, L. and Hallikainen, M.T. (1999). Textural information of multitemporal ERS-1 and JERS-1 SAR images for land and forest type classification in boreal zone. *IEEE Transactions on Geoscience and Remote Sensing,* 37: 680-689.

Kushwaha, S.P.S., Kuntz, S. and Oesten, G. (1994). Applications of image texture in forest classification. *International Journal of Remote Sensing,* 15: 2273-2284.

Lacaze, B., Rambal, S. and Winkel, T. (1994). Identifying spatial patterns of Mediterranean landscapes from geostatistical analysis of remotely-sensed data. *International Journal of Remote Sensing,* 15: 2437-2450.

Lane, D.M. (2000). *HyperStat Online Textbook*. Rice University, Houston, TX. http://www.ruf.rice.edu/~lane/rvls.html.

Le Toan, T., Beaudoin, A., Riom, J. and Guyon, D. (1992). Relating forest biomass to SAR data. *IEEE Transactions on Geoscience and Remote Sensing,* 30: 403-411.

Leckie, D.G. and Ranson, K.J. (1998). *Forestry applications using imaging radar*. Principles and Applications of Imaging Radar. *In:* F. M. Henderson and A. J. Lewis (Eds.). *Principles and Applications of Imaging Radar*, John Wiley, New York, pp. 435-509.

Leysen, M. (1998). Flemish Institute for Technological Research, Belgium.

Lewis, A.J. and Henderson, F.M. (1998). Radar fundamentals: the geoscience perspective. *In:* F. M. a. Henderson and A. J. Lewis (Eds.). *Principles and Applications of Imaging Radar*, John Wiley, New York, pp. 131-181.

Lillesand, T.M. and Kiefer, R.W. (2000). *Remote Sensing and Image Interpretation*. Fourth Edition. John Wiley, New York. 750 p.

Lucas, R.M., Honzák, M., Foody, G.M., Curran, P.J. and Corves, C. (1993). Characterizing tropical secondary forests using multi-temporal Landsat sensor imagery. *International Journal of Remote Sensing,* 14: 3061-3067.

Lucas, R.M., Curran, P.J., Honzák, M., Foody, G.M., Amaral, I. and Amaral, S. (1996). Disturbance and recovery of tropical forests: balancing the carbon account. *In:* J. H. C. Gash, C. A. Nobre, J. M. Roberts and R. L. Victoria (Eds.). *Amazonian Deforestation and Climate*, John Wiley, Chichester, pp. 383-398.

Lucas, R.M., Honzák, M., Curran, P.J., Foody, G.M., Milne, R., Brown, T. and Amaral, S. (2000). Mapping the regional extent of tropical forest regeneration in the Brazilian Legal Amazon using NOAA AVHRR data. *International Journal of Remote Sensing,* 21: 2855-2881.

Luckman, A., Baker, J. and Groom, G., (1994). Radar remote sensing for tropical forest inventory and carbon balance investigation (TIGER 1.4.3). No. 94/1, Remote Sensing Applications Development Unit (RSADU) - British National Space Centre, Monks Wood.

Luckman, A.J., Baker, J., Lucas, R. and Kuplich, T.M. (1995). Retrieval of the biomass of regenerating tropical forest in Amazonia using spaceborne SAR data. In: *International Symposium on Retrieval of Bio- and Geophysical Parametres from SAR Data for Land Applications,* Toulouse, France, pp. 107-118.

Luckman, A., Baker, J., Kuplich, T.M., Yanasse, C.C.F. and Frery, A. (1997a). A study of the relationship between radar backscatter and regenerating tropical forest biomass for spaceborne SAR instruments. *Remote Sensing of Environment,* 60: 1-13.

Luckman, A.J., Frery, A.C., Yanasse, C.C.F. and Groom, G.B. (1997b). Texture in airborne SAR imagery of tropical forest and its relationship to forest regeneration stage. *International Journal of Remote Sensing,* 18: 1333-1349.

Luckman, A., Baker, J., Honzák, M. and Lucas, R. (1998). Tropical forest biomass density estimation using JERS-1/SAR: seasonal variation, confidence limits and application to image mosaics. *Remote Sensing of Environment,* 63: 126-139.

Luckman, A., Baker, J. and Wegmuller, U. (2000). Repeat-pass interferometric coherence measurements of disturbed tropical forest from JERS and ERS satellites. *Remote Sensing of Environment,* 73: 350-360.

Lugo, A.E. and Brown, S. (1992). Tropical forests as sinks of atmospheric carbon. *Forest Ecology and Management,* 54: 239-255.

Marceau, D.J., Howarth, P.J., Dubois, J.M. and Gratton, D.J. (1990). Evaluation of the grey-level co-occurrence matrix method for land-cover classification using SPOT imagery. *IEEE Transactions on Geoscience and Remote Sensing,* 28: 513-519.

Mather, P.M. (1999). *Computer Processing of Remotely-Sensed Images.* Second edition. Jonh Wiley and Sons, Chichester. 292 p.

Matheron, G. (1965). *Les Variables Regionalisées et Leur Estimation.* Masson, Paris.

McDonald, K.C., Dobson, M.C. and Ulaby, F.T. (1990). Using MIMICS to model L-band multiangle and multitemporal backscatter from a walnut orchard. *IEEE Transactions on Geoscience and Remote Sensing,* 28: 477-491.

McDonald, K.C., Dobson, M.C. and Ulaby, F.T. (1991). Modeling multi-frequency diurnal backscatter from a walnut orchard. *IEEE Transactions on Geoscience and Remote Sensing,* 29: 852-863.

Miranda, F.P., Fonseca, L.E.N., Carr, J.R. and Taranik, J.V. (1996). Analysis of JERS-1 (Fuyo-1) SAR data for vegetation discrimination in northwestern Brazil using the semivariogram textural classifier (STC). *International Journal of Remote Sensing,* 17: 3523-3529.

Miranda, F.P., Fonseca, L.E.N. and Carr, J.R. (1998). Semivariogram textural classification of JERS-1 (Fuyo-1) SAR data obtained over a flooded area of Amazon rainforest. *International Journal of Remote Sensing,* 19: 549-556.

Moran, E.F., Brondizio, E., Mausel, P. and Wu, Y. (1994). Integrating Amazonian vegetation, land-use, and satellite data. *BioScience,* 44: 329-338.

Myers, N. (1984). *The Primary Source: Tropical Forests and Our Future.* W.W.Norton, New York.

Nelson, B.W. (1996). Caracterizacão da flora Amazonica por satelite. *In:* C. Pavan (Ed.). *Uma Estratégia Latino-Americana para a Amazônia*, 2, Memorial, UNESP, São Paulo, pp. 127-148.

Nepstad, D.C., Veríssimo, A., Alencar, A., Nobre, C., Lima, E., Lefebvre, P., Schlesinger, P., Potter, C., Moutinho, P., Mendoza, E., Cochrane, M. and Brooks, V. (1999). Large-scale impoverishment of Amazonian forests by logging and fire. *Nature,* 398: 505-508.

Neter, J., Wasserman, W. and Kutner, M.H. (1996). *Applied Linear Statistical Models.* Irwin, Chicago.

Nezry, E., Mougin, E., Lopes, A. and Gastellu-Etchegorry, J.P. (1993). Tropical vegetation mapping with combined visible and SAR spaceborne data. *International Journal of Remote Sensing,* 14: 2165-2184.

Oliver, C. and Quegan, S. (1998). *Understanding Synthetic Aperture Radar Images.* Artech House, London. 464 p.

Oliver, C. (1998). The application of texture measures to classifying the rain forest. In: *IX SBSR: Brazilian Remote Sensing Symposium,* Santos, Brazil, CDROM.

Palubinkas, G., Lucas, R.M., Foody, G.M. and Curran, P.J. (1995). An evaluation of fuzzy and texture-based classification approaches for mapping regenerating tropical forest classes from Landsat-TM data. *International Journal of Remote Sensing,* 16: 747-759.

Paola, J.D. and Schowengerdt, R.A. (1995). A review and analysis of backpropagation neural networks for classification of remotely-sensed multi-spectral imagery. *International Journal of Remote Sensing,* 16: 3033-3058.

Pearce, E.A. and Smith, C.G. (1993). Brazil. *In: The World Weather Guide*, Helicon Publishing Ltd., Oxford, pp. 173-180.

Pebesma, E.J. and Wesseling, C.G. (1998). GSTAT: a program for geostatistical modelling, prediction and simulation. *Computers and Geosciences,* 24: 17-31.

Podest, E. and Saatchi, S. (1999). Application of texture to JERS-1 SAR imagery for tropical forest land cover classification. In: *IGARSS'99*, IEEE, Hamburg, CDROM.

Pope, K.O., Rey-Benayas, J.M. and Paris, J.F. (1994). Radar remote sensing of forest and wetland ecosystems in the Central American Tropics. *Remote Sensing of Environment,* 48: 205-219.

Prance, G.T. (1987). Vegetation. *In:* T. C. Whitmore and G. T. Prance (Eds.). *Biogeography and Quaternary History in Tropical America*, Clarendon Press, Oxford, pp. 46-65.

Pulliainen, J.T., Kurvonen, L. and Hallikainen, M.T. (1999). Mutltitemporal behaviour of L- and C-band SAR observations of boreal forests. *IEEE Transactions on Geoscience and Remote Sensing,* 37: 927-937.

Quegan, S., Le Toan, T., Yu, J.J., Ribbes, F. and Floury, N. (2000). Multitemporal ERS SAR analysis applied to forest mapping. *IEEE Transactions on Geoscience and Remote Sensing,* 38: 741-753.

RADAMBRASIL, (1976). Levantamento de Recursos Naturais. Folha SA.21 - Santarém, Vol. 10, DNPM/Projeto RADAMBRASIL, Rio de Janeiro, Brazil.

Raney, R.K. (1998). Radar Fundamentals: Technical Perspective. *In:* F. M. Henderson and A. J. Lewis (Eds.). *Principles and Applications of Imaging Radar*, John Wiley, New York, pp. 9-130.

Ranson, K.J. and Sun, G. (1994). Mapping biomass of a northern forest using multifrequency SAR data. *IEEE Transactions on Geoscience and Remote Sensing,* 32: 388-395.

Ranson, K.J., Saatchi, S. and Sun, G. (1995). Boreal forest ecosystem characterization with SIR-C/XSAR. *IEEE Transactions on Geoscience and Remote Sensing,* 33: 867-876.

Ranson, K.J., Sun, G., Lang, R.H., Chauhan, S., Cacciola, R.J. and Kilic, O. (1997a). Mapping of boreal forest biomass from spaceborne synthetic aperture radar. *Journal of Geophysical Research,* 102: 29599-29610.

Ranson, K.J., Sun, G., J.F., W. and Knox, R.G. (1997b). Forest biomass from combined ecosystem and radar backscatter modeling. *Remote Sensing of Environment,* 59: 118-133.

Rauste, Y., Hame, T., Pulliainen, J., Heiska, K. and Hallikainen, M. (1994). Radar-based forest biomass estimation. *International Journal of Remote Sensing,* 15: 2797-2808.

Rennó, C.D., Freitas, C.C. and Sant'Anna, S.J.S. (1998). A system for region image classification based on textural measures. In: *2nd Latino-American Seminar on Radar Remote Sensing*, ESA, Santos, Brazil, ESA SP-434, pp. 159-164.

Reyes, G., Brown, S., Chapman, J. and Lugo, A.E., (1992). Wood Densities of Tropical Tree Species. SO-88, Department of Agriculture, Forest serrvice, New Orleans.

Ribbes, F., Le Toan, T., Bruniquel, J. and Floury, N. (1997). Deforestation monitoring in tropical regions using multitemporal ERS/JERS SAR and INSAR data. In: *IGARSS'97,* Singapore, IV, pp. 1560-1562.

Richards, J.A. (1990). Radar backscatter modelling of forests: a review of current trends. *International Journal of Remote Sensing,* 11: 1299-1312.

Richards, P.W. (1996). *The Tropical Rain Forest: an Ecological Study*. 2nd. Cambridge University Press, Cambridge. 575 p.

Rignot, E., Salas, W.A. and Skole, D.L. (1997). Mapping deforestation and secondary growth in Rondonia, Brazil, using imaging radar and Thematic Mapper data. *Remote Sensing of Environment,* 59: 167-179.

Rosenblatt, F. (1958). The perceptron: a probabilistic model for information storage and organisation in the brain. *Psychological Review,* 65: 386-408.

Rosenqvist, A. (1996a). Evaluation of JERS-1/SAR and Alamaz/SAR backscatter for rubber and oil palm stands in West Malaysia. *International Journal of Remote Sensing,* 17: 191-202.

Rosenqvist, A. (1996b). The Global Rain Forest Project by JERS-1 SAR. In: *International Society for Photogrammetry and Remote Sensing – ISPRS,* Vienna, Austria.

Rosenqvist, A., Shimada, M., Chapman, B., Freeman, A., De Grandi, G., Saatchi, S. and Rauste, Y. (2000). The Global Rain Forest Mapping project - a review. *International Journal of Remote Sensing,* 21: 1375-1387.

Royal Society, The (2001). The role of land carbon sinks in mitigating global climate change. Policy document 10/01, The Royal Society, London.

Rubin, T. (1990). Analysis of radar texture with variograms and other simplified descriptors. In: *Image Processing'89*, American Society for Photogrammetry and Remote Sensing, Falls Church, pp. 185-195.

Saatchi, S.S., Soares, J.V. and Alves, D.S. (1997). Mapping deforestation and land use in Amazon rainforest by using SIR-C imagery. *Remote Sensing of Environment,* 59: 191-202.

Saatchi, S.S. and Rignot, E. (1997). Classification of boreal forest cover types using SAR images. *Remote Sensing of Environment,* 60: 270-281.

Saatchi, S.S. and McDonald, K.C. (1997). Coherent effects in microwave backscattering models for forest canopies. *IEEE Transactions on Geoscience and Remote Sensing,* 35: 1032-1044.

Saatchi, S.S., Nelson, B., Podest, E. and Holt, J. (2000). Mapping land cover types in the Amazon Basin using 1 km JERS-1. *International Journal of Remote Sensing,* 21: 1201-1234.

Saatchi, S., Agosti, D., Alger, K., Delabie, J. and Musinsky, J. (2001). Examining fragmentation and loss of primary forest in the Southern Bahian Atlantic Forest of Brazil with radar imagery. *Conservation Biology,* 15: 867-875.

Sader, S.A. (1987). Forest biomass, canopy structure and species composition relationships with mutlipolarization L-band Synthetic Aperture Radar data. *Photogrammetric Engineering and Remote Sensing,* 53: 193-202.

Salas, W. and Skole, D. (1998). Remote sensing of land cover change: secondary growth dynamics in Rondonia, Brazil. In: *IGARSS'98*, IEEE Geoscience and Remote Sensing Society, Seattle, CDROM.

Salati, E. and Vose, P.B. (1984). Amazon Basin: a system in equilibrium. *Science,* 225: 129-225.

Saldarriaga, J.G., West, D.C., Tharp, M.L. and Uhl, C. (1988). Long-term chronosequence of forest succession in the upper Rio Negro of Colombia and Venezuela. *Journal of Ecology,* 76: 938-958.

Sanchez, P.A., Bandy, D.E., Villachica, J.H. and Nicholaides, J.J. (1982). Amazon Basin soils: management for continuos crop production. *Science,* 216: 821-827.

Sant'Anna, S.J.S., Yanasse, C.C.F., Hernandez Filho, P., Kuplich, T.M., Dutra, L.V., Frery, A.C. and Santos, P.P. (1995). Secondary forest age mapping in Amazonia using multitemporal Landsat TM imagery. In: *IGARSS'95,* Firenze, Italy, 1, pp. 323-325.

Sant'Anna, S.J.S., Freitas, C.C. and Rennó, C.D. (1998). The use of textural features on the polarimetric SAR image classification. In: *IX SBSR: Brazilian Remote Sensing Symposium,* Santos, Brazil, CD-ROM.

Schiermeier, Q. (2001). Accord in Morocco breathes fresh life into Kyoto Protocol. *Nature,* 414 p. 238.

Schimel, D.S. et al. (2001). Recent patterns and mechanisms of carbon exchange by terrestrial ecosystems. *Nature,* 414: 169-172.

Shimabukuro, Y.E., Amaral, S., Ahern, F.J. and Pietsch, R.W. (1997). Classification and monitoring the Tapajós National Forest region using SAR (RADARSAT-Standard mode and SAREX-Wide swath mode) and Landsat Thematic Mapper data. In: *GER'97 Geomatics in the era of RADARSAT*, CCRS, Ottawa, pp. 103-115.

Shimada, M. (1996). Radiometric and geometric calibration of JERS-1 SAR. *Adv. Space Res.,* 17: 79-88.

Shimada, M. (Ed.) (1999). *JERS-1 Science Program.* PI Reports. Tokyo, National Space Development Agency of Japan/Earth Observation Research Center. 189 p.

Shukla, J., Nobre, C. and Sellers, P. (1990). Amazonian deforestation and climate change. *Science,* 247: 1322-1325.

Simard, M., Saatchi, S. and de Grandi, G. (2000). The use of decision tree and multiscale texture for classification of JERS-1 SAR data over tropical forest. *IEEE Transactions on Geoscience and Remote Sensing,* 38: 2310-2321.

Skidmore, A.K., Turner, B.J., Brinkhof, W. and Knowles, E. (1997). Performance of a neural network: mapping forests using GIS and remotely sensed data. *Photogrammetric Engineering and Remote Sensing,* 63: 501-514.

Soares, J.V., Rennó, C.D., Formaggio, A.R., Yanasse, C.C.F. and Frery, A.C. (1997). An investigation of the selection of texture features for crop discrimination using SAR imagery. *Remote Sensing Environment,* 59: 234-247.

Sokal, R.R. and Rohlf, F.J. (1995). *Biometry.* 3rd. W.H.Freeman and Company, New York. 887 p.

Statsoft, I. (2001). *Electronic Statistics Textbook.* Statsoft, Tulsa, OK. http://www.statsoft.com/textbook/stathome.html

Steininger, M.K. (1996). Tropical secondary forest regrowth in the Amazon: age, area and change estimation with Thematic Mapper data. *International Journal of Remote Sensing,* 17: 9-27.

Steininger, M.K. (2000). Satellite estimation of tropical secondary forest above-ground biomass: data from Brazil and Bolivia. *International Journal of Remote Sensing,* 21: 1139-1157.

Tardin, A.T., Lee, D.C.L., Santos, J.R., Assis, O.R., Barbosa, M.P.S., Moreira, M.L., Pereira, M.T., Silva, D. and Santos Filho, C.P., (1980). Subprojeto desmatamento: convenio IBDF/CNPq-INPE. INPE-1649-RPE/103, Instituto Nacional de Pesquisas Espaciais, São José dos Campos, Brazil.

Thome, K., Markham, B., Barker, J., Slater, P. and Biggar, S. (1997). Radiomatric calibration of Landsat. *Photogrammetric Engineering and Remote Sensing,* 63: 853-858.

Thomson, A.G., Fuller, R.M., Sparks, T.H., Yates, M.G. and Eastwood, J.A. (1998). Ground and airborne radiometry over intertidal surfaces: waveband selection for cover classification. *International Journal of Remote Sensing,* 19: 1189-1205.

Treitz, P. and Howarth, P. (2000). High spatial resolution remote sensing data for forest ecosystem classification: an examination of spatial scale. *Remote Sensing of Environment,* 72: 268-289.

Tremberth, K.E., Houghton, J.T. and Meira Filho, L.G. (1996). The climate system: an overview. *In:* J. T. Houghton, L. G. Meira Filho, N. Callenderet (Eds.). *Climate Change 1995*, Cambridge University Press, Cambridge, pp. 1-59.

Trevett, J.W. (1986). *Imaging Radar for Resources Surveys*. Chapman and Hall, London. 313 p.

Uhl, C. (1987). Factors controlling succession following slash and burn agriculture in Amazonia. *Journal of Ecology,* 75: 377-407.

Uhl, C., Busbacher, R. and Serrão, A.S. (1988). Abandoned pastures in eastern Amazonia. I. Patterns of plant succession. *Journal of Ecology,* 76: 663-681.

Ulaby, F.T., Cihlar, J. and Moore, R.K. (1974). Active microwave measurement of soil water content. *Remote Sensing of Environment,* 31: 185-205.

Ulaby, F.T., Kouyate, F., Brisco, B. and Williams, T.H.L. (1986). Textural information in SAR images. *IEEE Transactions on Geoscience and Remote Sensing,* GE-24: 235-245.

Ulaby, F.T., Sarabandi, K., McDonald, K., Whitt, M. and Dobson, M.C. (1990). Michigan microwave canopy scattering model. *International Journal of Remote Sensing,* 11: 1223-1253.

USDA. (1975). *Soil Taxonomy: A Basic System of Soil Classification for Making and Interpreting Soil Surveys.* U.S. Department of Agriculture, Washington, 754 p.

van der Sanden, J.J. and Hoekman, D.H. (1999). Potential of airborne radar to support the assessment of land cover in a tropical rain forest environment. *Remote Sensing of Environment,* 68: 26-40.

Viana, V. (1998). Introducão. *In:* C. Gascon and P. Moutinho (Eds.). *Floresta Amazonica: Dinâmica, Regeneracão e Manejo*, Ministério da Ciência e Tecnologia, Instituto Nacional de Pesquisas da Amazônia, Manaus, pp. 15-24.

Wallace, C.S.A., Watts, J.M. and Yool, S.R. (2000). Characterizing the spatial structure of vegetation communities in the Mojave Desert using geostatistical techniques. *Computers and Geoscience,* 26: 397-410.

Walsh, R.P.D. (1996). Climate. *In:* P. W. Richards (Ed.). *The Tropical Rain Forest - An Ecological Study*, Cambridge University Press, Cambridge, pp. 159-202.

Wang, Y., Davis, F.W., Melack, J.M., Kasischke, E.S. and Christensen, N.L. (1995). The effects of changes in forest biomass on radar backscatter from tree canopies. *International Journal of Remote Sensing,* 16: 503-513.

Waring, R.H., Way, J., Hunt Jr., E.R., Morrissey, L., Ranson, K.J., Weishampel, J.F., Orem, R. and Franklin, S.E. (1995). Imaging radar for ecosystems studies. *BioScience,* 45: 715-723.

Wegmuller, U. and Werner, C.L. (1995). SAR interferometric signatures of forest. *IEEE Transactions on Geoscience and Remote Sensing,* 33: 1153-1161.

Weishampel, J.F., Sun, G., Ranson, K.J., Lejeune, K.D. and Shugart, H.H. (1994). Forest textural properties from simulated microwave backscatter: the influence of spatial resolution. *Remote Sensing of Environment,* 47: 120-131.

Weszka, J.S., Dyer, C.R. and Rosenfeld, A. (1976). A comparative study of texture measures for terrain classification. *IEEE Transactions on Systems, Man, and Cybernetics,* SMC-6: 269-285.

Whitmore, T.C. (1997). *An Introduction to Tropical Rain Forests.* Oxford University Press, Oxford. 226 p.

Wilkinson, G.G., Folving, S., Kannelopoulos, I. and McCormick, N. (1995). Forest mapping from multisource satellite data using neural network classifiers - an experiment in Portugal. *Remote Sensing Reviews,* 12: 83-106.

Williams, C.L., McDonald, K. and Chapman, B. (1999). Global boreal forest mapping with JERS-1: North America. In: *IGARSS'99*, IEEE, Hamburg, CDROM.

Williamson, G.B., Mesquita, R.C.G., Ickes, K. and Ganade, G. (1998). Estratégias de colonização de árvores pioneiras nos Neotrópicos. *In:* C. Gascon and P. Moutinho (Eds.). *Floresta Amazônica: Dinamica, Regeneração e Manejo*, INPA Press, Manaus, pp. 131-144

Woodcock, C.E., Strahler, A.H. and Jupp, D.L.B. (1988a). The use of variograms in remote sensing: I. Scene models and simulated images. *Remote Sensing of Environment,* 25: 323-348.

Woodcock, C.E., Strahler, A.H. and Jupp, D.L.B. (1988b). The use of variograms in remote sensing: II. Real digital images. *Remote Sensing of Environment,* 25: 349-379.

Wu, D. and Linders, J. (1999). A new texture approach to discrimination of forest clearcut, canopy and burned area using airborne C-band SAR. *IEEE Transactions on Geoscience and Remote Sensing,* 37: 555-563.

Yanasse, C.C.F., Sant'Anna, S.J.S., Frery, A., Rennó, C.D., Soares, J.V. and Luckman, A. (1997). Exploratory study of the relationship between tropical forest regeneration stages and SIR-C L- and C-data. *Remote Sensing of Environment,* 59: 180-190.